

THERMALLY STABILISED, CROSSLINKER-FREE POLY(VINYL  
ALCOHOL) NANOFIBERS PRODUCED BY ELECTROSPINNING:  
APPLICATIONS IN CELL PROCESSING AND TISSUE ENGINEERING

WILLIAM JOSEPH ASHLEY HOMER

Doctor of Philosophy

ASTON UNIVERSITY

March, 2023

©William Joseph Ashley Homer, 2023.

William Joseph Ashley Homer asserts their moral right to be identified as the author of this thesis.

This copy of the thesis has been supplied on condition that anyone who consults it is understood to recognise that its copyright belongs to its author and that no quotation from the thesis and no information derived from it may be published without appropriate permission or acknowledgement.



**Abstract: *Thermally stabilised, crosslinker-free poly(vinyl alcohol) nanofibers produced by electrospinning: Applications in cell processing and tissue engineering***

William Joseph Ashley Homer

Thesis presented for the degree of  
Doctor of Philosophy

2023

Electrospun poly(vinyl alcohol) (PVA) nanofibers are used extensively in biomedical applications, but many production methods rely heavily on the use of chemical crosslinkers to stabilise the fibrous morphology against dissolution in aqueous environments. A crosslinker-free approach, based on heat treatment at 180 °C for up to 16 hours, was used to stabilise nanofibers produced by cutting edge needleless direct current (DC) and alternating current (AC) electrospinning platforms. Characterisation of these materials showed that heat treatment preserved fibre morphology and prevented their dissolution, and that neither production method nor treatment duration had a negative impact on cytocompatibility.

Application of the nanofibrous membranes for cell processing in the context of blood salvage during oncological surgeries, involved challenging them with various suspensions of different cell populations (sheep's blood, neural blastoma cells as a cancer model and human erythrocytes). The thermally stabilised PVA nanofibers allowed the unhindered passage of cells under convective flow, with the loose structure of AC spun materials giving the highest recovery. The absence of flow channelling was further confirmed using the DigiDEM computational fluid dynamics software, and some early prototype designs of a prospective housing for the above nanofibers were also explored.

The final part of this study investigated the potential use of the thermally stabilised, needleless DC electrospun supports from 98% and 99% hydrolysed PVA, in tissue engineering. A battery of bio- and haemocompatibility assays indicated that the 4 hours heat treated fibrous mats resulted in optimal cell proliferation, whilst maintaining minimum levels of thermal degradation, the latter agreeing with results obtained during the cell processing work.

*Keywords: Electrospinning; nanofibers; poly(vinyl alcohol); biomaterials; membrane chromatography; blood salvage; tissue engineering; medical devices.*

## Acknowledgements

Firstly, I would like to thank my supervisory team, especially my main supervisor: Eirini Theodosiou. Her unfaltering availability for guidance, relentless positive attitude, and exceptional support throughout every step of the PhD have undoubtedly saved me from madness at some point or another, and I am grateful for her continued support and personal guidance above and beyond my PhD. I would also like to thank Paul Topham, for his role as associate supervisor and for opening avenues to collaboration outside of my main research, as well as always being a good laugh and a top bloke.

My sanity is also owed to my PhD office colleagues at Aston University and I would like to thank them all for the much needed (and frequently unneeded) distractions. Firstly, a sincere thank you to those who I began my journey with: Jakub, Sian, Kinana, Manuela, and especially Helena – your guidance and support at a daunting time were of tremendous value to me. I would also like to express equal gratitude to those who I finished that journey with: Georgia, Bridget, and Bawan; but a special thanks to Ben (the chess master and my travel companion to Liberec) and most of all my personal confidants Lauren and Anisha, who helped me when I did not have the courage to help myself. From the bottom of my heart, thank you.

My PhD afforded me the opportunity to spend a substantial amount of time at the Technical University of Liberec, Czechia, working in their wonderful facilities thanks to funding from The Royal Society. I would like to thank the PhD Students there: Maxim Lisnenko, Šárka Hauzerová, and Kristýna Havlíčková for making me feel welcome in their office and labs, as well as the academic staff, Věra Jenčová, Eva Košťáková, Jan Valtera, and Prof. David Lukáš, for their hospitality, and for sharing their experience and knowledge with me.

I would also like to acknowledge Adrian Gardner from the Royal Orthopaedic Hospital who inspired the application behind the project, the staff who assisted me in the Dubrowsky lab, and the Birmingham Orthopaedic Charity for their partial funding of the project.

Finally, I would like to thank my dad and step-mum, Mark and Karen Homer for their on-going support from the beginning of my undergrad and throughout my entire time at university. Thank you for everything.

If I have missed anyone, I apologise, but know that I am thankful.

## Collaborator acknowledgements

The author would like to acknowledge the following collaborations from which work has been included within this thesis.

### **Supervision of final year MEng research projects**

Work presented in **Chapter 4** was carried out as part of two different final year MEng projects: one Chemical engineering; and one Mechanical engineering. For both projects, the author was a direct supervisor, remaining actively involved in planning, design, and analysis at all stages of the work.

The chemical engineering masters project, carried out by Ryan Kainth, pertained to flow simulation studies presented in the first half of the chapter. The student was advised and directed closely on methodological approaches and decisions throughout, and all final simulations carried out on the student's personal computer due to a combinations of hardware compatibility issues and limited software licenses. As such, all rendered images depicted were provided by the student.

The mechanical engineering project was carried out by Sukhbinder Singh, Rachel Lau, and Libby Pincher, relating to device to design which in included in the second half of the chapter. The information and images presented formed part of a larger body of work which is largely omitted from this thesis. The author was directly involved intellectually in the design and iteration process, with final renders being produced by the students.

### **Collaboration with the Technical University of Liberec, Czechia (TUL)**

Though most Nanospider™ and AC electrospinning samples presented in this work were produced by the author during several research trips to TUL, where necessary collaborators at TUL would manufacture some additional samples on request. This was especially critical during periods of restricted travel due to the COVID-19 pandemic. Furthermore, some experiments were agreed collaboratively and carried out on the authors behalf within laboratories at TUL and Liberec regional hospital. Specifically, the 98% DH PVA Nanospider™ samples used in **Chapter 5** were produced to specification by Maxim Lisnenko at TUL. These samples were heat treated, along with 99% DH PVA counterparts provided by the author, and were assessed for bio- and haemocompatibility as per previous agreement by Šárka Hauzerová in laboratories at Liberec regional hospital (Both students being PhD candidates under supervision of Dr. Věra Jenčová). SEM images presented in this chapter were also provided as part of this work.

## List of Publications

HOMER, W. J. A., LISNENKO, M., GARDNER, A. C., KOSTAKOVA, E. K., VALTERA, J., WALL, I. B., JENCOVA, V., TOPHAM, P. D. & THEODOSIOU, E. 2023. Assessment of thermally stabilized electrospun poly(vinyl alcohol) materials as cell permeable membranes for a novel blood salvage device. *Biomaterials Advances*, 144

DIEZ, B., HOMER, W. J. A., LESLIE, L. J., KYRIAKOU, G., ROSAL, R., TOPHAM, P. D. & THEODOSIOU, E. 2022. Chemically cross-linked poly(vinyl alcohol) electrospun fibrous mats as wound dressing materials. *Journal of Chemical Technology and Biotechnology*, 97, 620-632.

THOMSON, L., MCDOWALL, D., MARSHALL, L., MARSHALL, O., NG, H., HOMER, W. J. A., GHOSH, D., LIU, W. L., SQUIRES, A. M., THEODOSIOU, E., TOPHAM, P. D., SERPELL, L. C., POOLE, R. J., SEDDON, A. & ADAMS, D. J. 2022. Transferring Micellar Changes to Bulk Properties via Tunable Self-Assembly and Hierarchical Ordering. *Acs Nano*, 16, 20497-20509.

## Table of contents

Abstract .....	iii
Acknowledgements .....	iv
Collaborator acknowledgements .....	v
List of Publications .....	vi
Table of Contents .....	vii
List of Abbreviations .....	xiv
Nomenclature .....	xv
List of Figures .....	xvi
List of Tables .....	xxi
<b>Chapter 1. Introduction and background .....</b>	<b>1</b>
1.1 Introduction to biomaterials .....	1
1.2 Electrospinning .....	2
1.2.1 What and when? .....	2
1.2.2 Description of the electrospinning process .....	3
1.2.3 Material classes in electrospinning .....	5
1.2.3.1 Polymers .....	6
1.2.3.2 Composite materials .....	6
1.2.3.3 Molecular self-assembly materials .....	6
1.2.4 Factors affecting electrospinning .....	7
1.2.4.1 Solution parameters .....	8
1.2.4.2 Process setup .....	9
1.2.4.3 Ambient conditions .....	11
1.2.5 Electrospinning emitters and platforms .....	12
1.2.5.1 DC Electrospinning .....	12
1.2.5.1.1 Needle based emitters .....	12

1.2.5.1.2	Needleless emitters .....	13
1.2.5.1.3	AC electrospinning setups .....	14
<b>1.3</b>	<b>Electrospun materials .....</b>	<b>16</b>
1.3.1	Applications of electrospun materials .....	16
1.3.2	Common electrospun polymers as biomaterials .....	18
<b>1.4</b>	<b>Poly(vinyl alcohol).....</b>	<b>20</b>
1.4.1	Production of PVA .....	20
1.4.2	Properties of PVA .....	20
1.4.3	Enhancement of water stability .....	22
1.4.3.1	Chemical crosslinking .....	22
1.4.3.2	Physical crosslinking.....	23
<b>1.5</b>	<b>Biomedical applications of electrospun PVA nanofibers.....</b>	<b>25</b>
1.5.1	Drug delivery.....	25
1.5.2	Wound dressings .....	26
1.5.3	Tissue engineering .....	26
<b>1.6</b>	<b>Blood salvage .....</b>	<b>28</b>
1.6.1	Cell separation of whole blood .....	28
1.6.1.1	Filtration.....	29
1.6.1.2	Centrifugation .....	30
1.6.1.3	Fluorescence-activated cell sorting .....	31
1.6.1.4	Magnetic-activated cell sorting.....	32
1.6.1.5	Comparison of various cell separation methods.....	34
1.6.2	Chromatography for cell separations .....	34
1.6.3	Existing blood salvage platforms.....	35
<b>1.7</b>	<b>Conclusion.....</b>	<b>37</b>
<b>1.8</b>	<b>Aims of this work.....</b>	<b>38</b>



Chapter 2. Manufacture and characterisation of thermally stabilised poly(vinyl alcohol) membranes produced by electrospinning .....	40
2.1 Introduction.....	40
2.2 Materials and Methods .....	41
2.2.1 Materials .....	41
2.2.2 Production methods .....	42
2.2.2.1 Solution preparation.....	42
2.2.2.2 Electrospinning .....	42
2.2.2.2.1 Needle DC electrospinning .....	42
2.2.2.2.2 Needleless DC electrospinning.....	43
2.2.2.2.3 AC electrospinning.....	44
2.2.2.3 Heat treatment.....	45
2.2.3 Analytical methods.....	45
2.2.3.1 Scanning electron microscopy .....	45
2.2.3.2 Fourier transform - Infrared spectroscopy .....	46
2.2.3.3 Gel permeation chromatography.....	46
2.2.3.4 Nitrogen sorption porosimetry .....	46
2.2.3.5 Proton nuclear magnetic resonance.....	47
2.2.3.6 Environmental scanning electron microscopy .....	47
2.2.3.7 X-ray diffraction.....	47
2.2.3.8 Tensile testing.....	47
2.2.3.9 In vitro cytotoxicity testing .....	48
2.3 Results and Discussion .....	48
2.3.1 Needle-based electrospinning of 88% hydrolysed PVA and the effects of extended thermal stabilisation.....	48
2.3.1.1 Thermal stabilisation of non-woven mats produced from 88% PVA .....	48
2.3.2 Production of electrospun mats from 99% hydrolysed PVA.....	52

2.3.2.1	Needle-based DC electrospinning.....	52
2.3.2.2	Needleless DC electrospinning .....	54
2.3.2.3	AC electrospinning.....	54
2.3.3	Comparison of electrospinning platforms for nanofiber production .....	55
2.3.3.1	Morphological analysis.....	56
2.3.3.2	Chemical analysis.....	58
2.3.3.3	Method of Production analysis .....	61
2.3.4	Effects of extended heat treatment on 99% hydrolysed PVA .....	63
2.3.5	Characterisation of thermally stabilised nanofibrous samples produced by and needleless DC and AC electrospinning.....	66
2.3.5.1	In-situ swelling behaviour.....	66
2.3.5.2	Chemical analysis.....	69
2.3.5.3	Mechanical analysis.....	71
2.3.5.4	Biological analysis .....	75
2.4	Conclusion.....	76
<b>Chapter 3. Cell flowthrough studies using thermally stabilised non-functionalised PVA nanofiber membranes.....</b>		<b>77</b>
3.1	Introduction.....	77
3.2	Materials and Methods .....	79
3.2.1	Materials.....	79
3.2.2	Preparation of cell suspensions .....	80
3.2.2.1	SH-SY5Y .....	80
3.2.2.2	Dilute defibrinated sheep's blood .....	80
3.2.2.3	Human erythrocytes.....	80
3.2.2.4	Flowthrough experimental set up.....	80
3.3	Results and Discussion .....	81

3.3.1	Cell flowthrough studies using membranes produced by needleless DC electrospinning.....	81
3.3.1.1	SH-SY5Y cell suspension of fixed concentration.....	82
3.3.1.2	Undiluted cell suspensions of defibrinated sheep's blood .....	83
3.3.1.3	Dilute cell suspensions of defibrinated sheep's blood .....	84
3.3.1.4	Dilute suspensions of human erythrocytes.....	87
3.3.2	Cell flowthrough studies using membranes produced by AC electrospinning.	89
3.4	Conclusion.....	91
Chapter 4. Validation of flow behaviour through nanofibrous networks, and device design and prototyping .....		92
4.1	Introduction.....	92
4.2	Materials and Methods .....	93
4.2.1	Materials.....	93
4.2.2	DigiDEM - Investigation of flow through nanofibrous supports .....	93
4.2.2.1	Generating pseudo-3D nanofibrous membranes.....	93
4.2.2.2	Generation of the packed bed.....	94
4.2.2.3	Flow simulation.....	94
4.2.3	Device design and prototyping.....	94
4.3	Results and Discussion .....	95
4.3.1	Flow simulation.....	97
4.3.2	Device design .....	98
4.4	Conclusion.....	102
Chapter 5. Poly(vinyl alcohol) non-woven mats for tissue engineering applications .....		104
5.1	Introduction.....	104
5.2	Materials and Methods .....	105

5.2.1	Materials .....	105
5.2.2	Production and stabilisation of electrospun materials.....	106
5.2.3	Analytical methods.....	106
5.2.3.1	Scanning electron microscopy .....	106
5.2.3.2	Fourier transform-infrared spectroscopy .....	106
5.2.3.3	X-ray diffraction.....	106
5.2.3.4	Tensile testing.....	107
5.2.3.5	Contact angle testing and film preparation .....	107
5.2.3.6	Biocompatibility testing .....	107
5.2.3.7	Haemocompatibility – Collection and preparation of blood product solutions .....	108
5.2.3.8	Thrombogenicity .....	108
5.2.3.9	Coagulation .....	108
5.2.3.10	Haemolysis .....	109
<b>5.3</b>	<b>Results and Discussion .....</b>	<b>109</b>
5.3.1	Morphological comparison of nanofibers produced from 98% and 99% hydrolysed PVA .....	109
5.3.2	Physicochemical comparison of nanofibers produced from 98% and 99% hydrolysed PVA .....	112
5.3.2.1	Fourier transform infrared spectroscopy.....	112
5.3.2.2	X-ray diffraction.....	113
5.3.2.3	Tensile testing.....	114
5.3.2.4	Contact angle .....	116
5.3.3	Biological assessment and comparison of nanofibers produced from 98% and 99% hydrolysed PVA .....	118
5.3.3.1	Biocompatibility.....	118
5.3.3.2	Thrombogenicity .....	120
5.3.3.3	Coagulation .....	122
5.3.3.4	Haemolysis .....	123

5.4 Conclusion.....	125
Chapter 6. Conclusions and Future work.....	126
6.1 Conclusions.....	126
6.2 Future work.....	130
References.....	133
Appendices .....	156
Appendix A – Nitrogen porosimetry.....	156
Appendix B - FT-IR of 99% hydrolysed PVA produced by needle electrospinning.....	158
Appendix C - Flowthrough of hMSCs using PVA non-woven membranes created by needleless DC electrospinning.....	159
Appendix D - Velocity profile during flow simulation through nanofiber packed beds .....	159

## List of Abbreviations

<b>ABTs</b>	Allogeneic blood transfusions
<b>AC</b>	Alternating current
<b>AgNPs</b>	Silver nanoparticles
<b>APTT</b>	Activated partial thromboplastin time
<b>ATR</b>	Attenuated total reflectance
<b>BET</b>	Brunauer-Emmett-Teller
<b>CAD</b>	Computer aided design
<b>CCK-8</b>	Cell counting kit - 8
<b>CFD</b>	Computational fluid dynamics
<b>CNF</b>	Cellulose nanofibers
<b>CTCs</b>	Circulating tumour cells
<b>DC</b>	Direct current
<b>DEM</b>	Discreet element modelling
<b>DH</b>	Degree of hydrolysis
<b>DMEM</b>	Dulbecco's modified eagle medium
<b>ECM</b>	Extracellular matrix
<b>ESEM</b>	Environmental scanning electron microscopy
<b>FACS</b>	Fluorescence assisted cell sorting
<b>FBS</b>	Fetal bovine serum
<b>FDA</b>	Food and drug administration
<b>FDM</b>	Fused deposition modelling
<b>FT-IR</b>	Fourier transform – infrared spectroscopy
<b>GA</b>	Glutaraldehyde
<b>GMP</b>	Good manufacturing practice
<b>GPC</b>	Gel permeation chromatography
<b>HAp</b>	Hydroxy apatite
<b>hMSCs</b>	Human mesenchymal stem cells
<b>HPLC</b>	High performance liquid chromatography
<b>ICS</b>	Intraoperative cell salvage
<b>LBM</b>	Lattice Boltzmann method
<b>LDF</b>	Leukodepletion filter
<b>MACS</b>	Magnet assisted cell sorting
<b>Mw</b>	Molecular weight
<b>NC</b>	Negative control
<b>NMR</b>	Nuclear magnetic resonance

<b>PBM</b>	Patient blood management
<b>PBS</b>	Phosphate buffered saline
<b>PC</b>	Positive control
<b>PCL</b>	Poly(caprolactone)
<b>PLA</b>	Poly(lactic acid)
<b>PPP</b>	Platelet poor plasma
<b>PT</b>	Prothrombin time
<b>PU</b>	Polyurethane
<b>PVA</b>	Poly(vinyl alcohol)
<b>PVAc</b>	Poly(vinyl acetate)
<b>RBC</b>	Red blood cell
<b>RH</b>	Relative humidity
<b>SA</b>	Sodium alginate
<b>SEC</b>	Size exclusion chromatography
<b>SEM</b>	Scanning electron microscopy
<b>SF</b>	Silk fibroin
<b>SLA</b>	Stereolithography
<b>SLS</b>	Selective laser sintering
<b>TE</b>	Tissue Engineering
<b>TRS</b>	Thrombocyte rich solution
<b>TUL</b>	Technical University of Liberec
<b>UTS</b>	Ultimate tensile strength
<b>WBC</b>	White blood cell
<b>XRD</b>	X-ray diffraction

## Nomenclature

<b><math>A_x</math></b>	Absorbance at wavenumber $x$	$(\text{cm}^{-1})$
<b><math>g</math></b>	Gravitational force	$(\text{m}\cdot\text{s}^{-2})$
<b><math>I_a</math></b>	Sum of the intensity of the amorphous regions	-
<b><math>I_c</math></b>	Sum of the intensity of the crystalline regions	-
<b><math>p</math></b>	Equilibrium pressure applied	$(\text{Pa})$
<b><math>p_0</math></b>	Saturation vapour pressure of $\text{N}_2$	$(\text{Pa})$
<b><math>r</math></b>	Average fibre radius	$(\text{nm})$
<b><math>\alpha</math></b>	Degree of crystallinity	$(\%)$
<b><math>\rho</math></b>	Density of PVA	$(\text{g}\cdot\text{cm}^3)$

## List of Figures

<b>Figure 1.1.</b> A simple, needle-based, electrospinning setup.....	3
<b>Figure 1.2.</b> Diagram of Taylor cone formation following application of DC voltage to the conductive needle .....	4
<b>Figure 1.3.</b> Depiction of the needle electrospinning process with DC voltage, indicating the various stages of jet formation .....	5
<b>Figure 1.4.</b> Depiction of common fibre morphologies produced by electrospinning.....	9
<b>Figure 1.5.</b> Common collector geometries used in electrospinning.....	11
<b>Figure 1.6.</b> Examples of needle-based emitters used in DC electrospinning .....	13
<b>Figure 1.7.</b> Examples of needleless emitters used in DC electrospinning .....	14
<b>Figure 1.8.</b> Types of emitter used in AC electrospinning.....	15
<b>Figure 1.9.</b> Chemical structure of PVA .....	20
<b>Figure 1.10.</b> Schematic representation of the hydrogen bonding between macromolecules of PVA in a solid, water-free state .....	21
<b>Figure 1.11.</b> Schematic representation of the reaction between two PVA chains and glutaraldehyde in the presence of hydrochloric acid (HCl).....	222
<b>Figure 1.12.</b> Fringed micelle model of a semi-crystalline polymer.....	23
<b>Figure 1.13.</b> Illustration of PVA polymer with internally bound water molecules forming hydrogen bonds with the hydroxyl groups. ....	24
<b>Figure 1.14.</b> Common filtration methods with flow direction indicated by the red arrow .....	29
<b>Figure 1.15.</b> Diagram of a sample before and after density gradient centrifugation (discontinuous gradient).....	30
<b>Figure 1.16.</b> Diagram illustrating cell separation based on FACS .....	32
<b>Figure 1.17.</b> Diagram of positive selection of a target cell population using MACS.....	33
<b>Figure 1.18.</b> Diagram of an immunoaffinity separation process .....	35
<b>Figure 1.19.</b> Centrifugal separation diagram of a Latham bowl device.....	36
<b>Figure 1.20.</b> Diagram of the HemoSep ICS system .....	36
<b>Figure 2.1.</b> Illustrative drawing of needle-based electrospinning setup and process.....	43



<b>Figure 2.2.</b> Illustrative drawing of wire-based configuration of needleless DC electrospinning used in the Elmarco Nanospider™ .....	44
<b>Figure 2.3.</b> Illustrative drawing of AC electrospinning with rod-like electrode and rotating drum collector. ....	45
<b>Figure 2.4.</b> SEM Images of heat treated 88% hydrolysed PVA nanofibers, after 24 h immersion in water .....	49
<b>Figure 2.5.</b> FT-IR spectra of sample needle spun 88% hydrolysed samples following heat treatment.....	50
<b>Figure 2.6.</b> Crystallinity (%) vs heat treatment duration graph for samples of needle spun 88% hydrolysed PVA .....	51
<b>Figure 2.7.</b> Optical microscopy image of nanofibers following electrospinning of 99% hydrolysed PVA .....	53
<b>Figure 2.8.</b> SEM image of nanofibers produced by needle-based electrospinning of 99% hydrolysed PVA .....	53
<b>Figure 2.9.</b> SEM images of samples produced using the Nanospider™ with variable PVA concentration .....	54
<b>Figure 2.10.</b> Photograph of nanofiber plume of PVA produced by AC electrospinning.....	55
<b>Figure 2.11.</b> SEM image of nanofibers produced by AC electrospinning .....	55
<b>Figure 2.12.</b> Histograms of untreated 99% hydrolysed PVA nanofibers by needle, needleless and AC electrospinning .....	57
<b>Figure 2.13.</b> FT-IR spectra of samples of 99% hydrolysed PVA produced by three methods of electrospinning.....	59
<b>Figure 2.14.</b> Calculated crystallinity from FT-IR data for samples produced from 99% hydrolysed PVA by each method of electrospinning.....	59
<b>Figure 2.15.</b> GPC traces of 99% hydrolysed PVA samples series produced by each method of electrospinning.....	59
<b>Figure 2.16.</b> <sup>1</sup> H NMR spectra comparing electrospun samples of 99% hydrolysed PVA.....	61
<b>Figure 2.17</b> Photographs of PVA electrospun onto their respective substrates.....	61
<b>Figure 2.18.</b> SEM images of heat treated samples of 99% hydrolysed PVA nanofibers before and after water immersion for 24 h.....	64

<b>Figure 2.19.</b> FT-IR spectra of 99% hydrolysed PVA nanofibers produced by needleless DC electrospinning following heat treatment at 180 °C.....	65
<b>Figure 2.20.</b> ESEM images showing swelling of electrospun PVA produced by needleless DC electrospinning.....	67
<b>Figure 2.21.</b> ESEM images showing swelling of electrospun PVA produced by AC electrospinning.....	68
<b>Figure 2.22.</b> FT-IR Spectra of two sample series of 99% DH PVA produced by needleless DC and AC electrospinning .....	70
<b>Figure 2.23.</b> XRD spectra of PVA nanofibers produced by DC and AC electrospinning.....	71
<b>Figure 2.24.</b> Tensile performance of PVA mats produced by DC and AC electrospinning ..	72
<b>Figure 2.25.</b> Stress-strain graphs of PVA mats produced by AC and DC electrospinning under tensile load.....	74
<b>Figure 2.26.</b> Cytotoxicity of PVA materials produced by DC and AC electrospinning following heat treatment.....	75
<b>Figure 3.1.</b> Overview of the proposed cell salvage process .....	79
<b>Figure 3.2.</b> (a): Illustrated setup of the flowthrough experiment. (b): Cross-section of the exploded filter holder assembly including the nanofiber membrane support.....	81
<b>Figure 3.3.</b> Percentage of SH-SY5Y cells recovered per fraction following flowthrough experiments using heat treated 99% DH PVA materials produced by needleless DC electrospinning.....	82
<b>Figure 3.4.</b> Left hand side: Recovery of defibrinated sheep's blood following flowthrough experiments through heat treated 99% DH PVA materials produced by needleless DC electrospinning. Right hand side: SEM image of a membrane treated for 4 h after flowthrough experiments and cell fixing.....	84
<b>Figure 3.5.</b> Total sheep blood cell recovery after passing through 4 h heat treated 99% DH PVA materials produced by needleless DC electrospinning. ....	85
<b>Figure 3.6.</b> Percentage of the defibrinated sheep's bloodcells recovered following flowthrough experiments using 4 h heat treated PVA materials produced by DC electrospinning.....	86
<b>Figure 3.7.</b> Total human erythrocyte recovery after passing through 4 h heat treated 99% DH PVA materials produced by needleless DC electrospinning. ....	87
<b>Figure 3.8.</b> Percentage of human erythrocytes recovered following flowthrough experiments using 4 h heat treated 99% DH PVA materials produced by DC electrospinning.....	88

<b>Figure 3.9.</b> Total erythrocyte recovery after passing through 4 h heat treated 99% DH PVA materials produced by AC electrospinning. ....	89
<b>Figure 3.10.</b> Percentage of the human erythrocytes recovered following flowthrough experiments using 4 h heat treated 99% DH PVA materials produced by AC electrospinning .....	90
<b>Figure 4.1.</b> 2D bitmap traces of nanofibers produced by needleless DC and AC electrospinning and their corresponding extruded volumes. ....	95
<b>Figure 4.2.</b> Stacks of extruded volumes produced from traces of needleless DC and AC electrospinning, an extracted core of the initial stack, and final packed bed. ....	96
<b>Figure 4.3.</b> Heat graphs indicating flow within the packed bed based on needleless DC electrospun nanofibers.....	97
<b>Figure 4.4.</b> Heat graphs indicating flow within the packed bed based on AC electrospun nanofibers.....	98
<b>Figure 4.5.</b> Filter holder from Cole Parmer .....	99
<b>Figure 4.6.</b> CAD generated sample models of filter holders with 5 mL fixed bed volume and varying diameters.....	100
<b>Figure 4.7.</b> Provisional flow distributor designs.....	100
<b>Figure 4.8.</b> Initial design concepts and iterations for the 3D printed filter holder .....	101
<b>Figure 4.9.</b> 3D printed prototypes of the third design iteration produced by SLA printing ..	102
<b>Figure 5.1.</b> SEM images of 98% and 99% hydrolysed electrospun PVA following heat treatment at 180 °C.....	110
<b>Figure 5.2.</b> Box and whisker plot of fibre diameters for 98% and 99% DH PVA needleless electrospun mats.....	111
<b>Figure 5.3.</b> FT-IR Spectra of two sample series of 98% and 99% DH PVA produced by needleless electrospinning.....	113
<b>Figure 5.4.</b> XRD spectra of 98% and 99% DH PVA materials produced by needleless DC electrospinning.....	114
<b>Figure 5.5.</b> Tensile performance of samples produced from 98% and 99% hydrolysed PVA electrospun mats after thermal stabilisation .....	116
<b>Figure 5.6.</b> Sessile drop contact angle data for films produced from 98% and 99% hydrolysed PVA after thermal stabilisation .....	117

<b>Figure 5.7.</b> Representative images from sessile drop contact angle testing of films produced from 98% and 99% hydrolysed PVA .....	118
<b>Figure 5.8.</b> Cell viability results of 98% and 99% PVA nanofibrous mats after heat treatment at time points of 1, 3 and 7 days .....	119
<b>Figure 5.9.</b> Representative SEM images of 3T3 cells on 98% and 99% DH PVA mats produced by electrospinning 7 days after cell seeding .....	120
<b>Figure 5.10.</b> Cell viability results of thrombocyte activity on 98% and 99% DH PVA mats following heat treatment and 2 h exposure to TRS.....	121
<b>Figure 5.11.</b> Representative SEM images of activated platelets on 98% and 99% DH PVA mats produced by needleless DC electrospinning.....	122
<b>Figure 5.12.</b> Box and whisker plots of APTT and PT coagulation tests of nanofibrous mats produced from 98% and 99% hydrolysed PVA after heat treatment.....	123
<b>Figure 5.13.</b> Haemolysis percentage of red blood cells after incubation in the presence of nanofibrous materials.....	124
<b>Figure 5.14.</b> SEM images of nanofibrous materials produced by needleless DC electrospinning after fixing of red blood cells.....	125
<b>Figure 6.1.</b> Reaction pathway for the modification of hydroxyl containing supports with proteins as a route for functionalisation.....	125
<b>Figure A.1.</b> SEM and Histogram for needleless DC and AC spun PVA nanofibers analysed by N <sub>2</sub> Porosimetry .....	156
<b>Figure A.2.</b> Porosimetry adsorption graph for 99% DH PVA produced by AC and needleless DC electrospinning.....	157
<b>Figure B.1.</b> Calculated crystallinity (%) vs heat treatment duration graph for samples of needleless DC spun 99% DH PVA.....	158
<b>Figure C.1.</b> Setup for hMSC flowthrough experiment.....	158
<b>Figure C.2.</b> Optical microscope images of fractions collected during the hMSC flowthrough experiments .....	158
<b>Figure D.1.</b> Velocity vs step graph for simulated flow through untreated nanofiber beds produced by Nanospider™ .....	158
<b>Figure D.2.</b> Velocity vs step graph for simulated flow through untreated nanofiber beds produced by AC electrospinning .....	1587

## List of Tables

<b>Table 1.1.</b> Variables effecting the electrospinning process and their influence on fibre generation.....	7
<b>Table 1.2.</b> Summary of literature reviews on topic-specific electrospinning applications found on Web of Science (as per 21/03/2023) .....	17
<b>Table 1.3.</b> List of the most common electrospun polymers used in biomedical applications, such as drug delivery, wound dressings, and TE .....	19
<b>Table 1.4.</b> Recent literature on the use of PVA nanofibers in TE .....	27
<b>Table 2.1.</b> Optical images of PVA (88% DH) samples following heat treatment between 1 and 32 h at 180 °C.....	49
<b>Table 2.2.</b> Comparison of the material configurations and manufacturing considerations when needleless DC and AC platforms are used for the electrospinning of the PVA supports.....	63
<b>Table 5.1.</b> Summary of peaks commonly associated with FT-IR spectrum of PVA .....	112
<b>Table 5.2.</b> Crystallinity of nanofibre samples after treatment calculated from XRD data....	114

# Chapter 1

## Introduction and background

### 1.1 Introduction to biomaterials

Biomaterials are materials which are designed or selected to interact with a biological system to restore or improve its natural function and span a wide range of applications, including medical devices and implants, biosensors, and drug delivery vectors. Today, the field of biomaterials hinges upon interdisciplinary research, with expertise from biology, chemistry, materials engineering, and medicine all being drawn together to develop new and innovative materials for cutting edge treatments and devices, however the use of biomaterials is far more ancient than the recent advent of scientific enquiry.

Early examples of biomaterials include the use of gold sutures and animal teeth for dental repairs or the metal implant which was famously discovered fused to the skull of a 2000 year old Peruvian warrior (Migonney, 2014, Oli, 2022). Much progress has been made since these humble beginnings, with a plethora of materials being used routinely in many areas of modern medicine, and without a doubt saving millions of lives and enhancing and restoring the quality of life to millions more. From dental fillings to contact lenses and pacemakers, biomaterials are ubiquitous, a fact which is unlikely to change any time soon. It is therefore no surprise that behind these life changing and/or lifesaving materials is a booming industry, with a global market size of \$135.4 billion in 2021, which is expected to grow to almost half a trillion by 2030 (Grand View Research, 2022).

Biomaterials can be broadly categorised into three major classes: **metallic**, such as metal alloys deployed in orthopaedic surgery; **ceramics**, such as bioinert materials for dental implants, or bioactive glasses for bone regeneration; and **polymers**, used in wound healing and joint replacements.

**Polymer** biomaterials are commonly utilised as large, moulded components, films, and hydrogels, but more recent developments within the field have seen an increase in the

utilisation of polymer nanofibers made from a broad range of materials and as composites, with one option for scalable production of such fibres being achievable by a process known as electrospinning. Electrospinning technology offers an economically viable platform for mass production of highly customisable biomaterials and is explored in more depth in the following section.

## 1.2 Electrospinning

### 1.2.1 What and when?

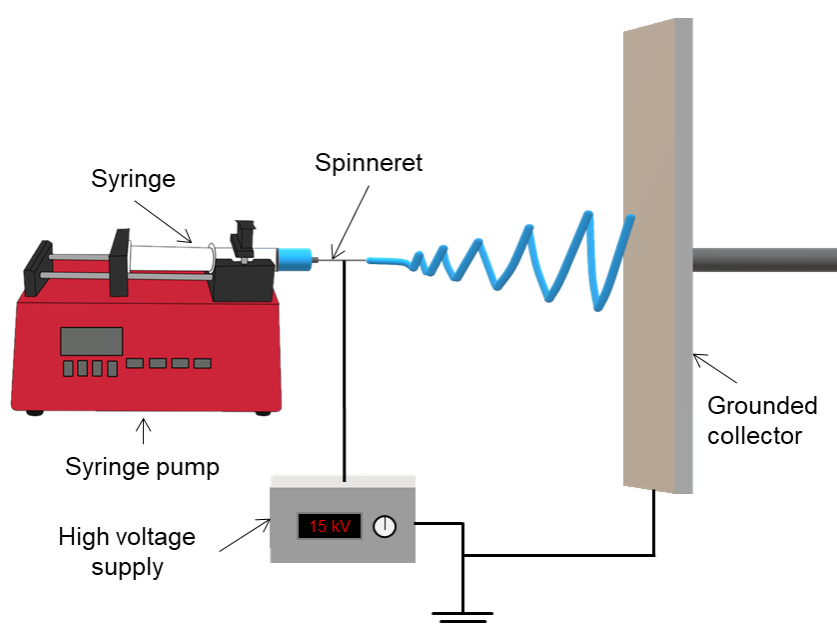
Electrospinning is a process by which nanofibers are drawn from a viscoelastic solution through the application of a strong electric field. Though a lot of foundational science underpins electrospinning and is much of a precursor, the first explicit report of this process was published in 1887, when Charles Boys described the act of applying voltage to an insulated conductive dish, filled with various viscous solutions, and generating almost imperceptible fibres which were readily drawn to any conducting body placed along their path. Boys referred to the process as “*the old, but now apparently little-known experiment of electrical spinning*”, suggesting that electrospinning may predate this work, though by how much is uncertain (Boys, 1887). A little more than a decade later, the first patent for electrospinning was filed by John Cooley in 1900, with many other reports and patents following over the proceeding half century, including the first practical application for electrospun materials as air filters (Spurny, 1996, Tucker et al., 2012). In the 1960s, Geoffrey Taylor offered insight into the underlying theory through mathematical description of the liquid cone, which acts as an origin for the produced nanofibers (now known as the ‘Taylor cone’), thus laying the first stones on the road to the modern understanding of electrospinning (Taylor, 1964).

Since these early beginnings, electrospinning has increased in popularity and demand, with many commercial manufacturers producing scalable electrospinning equipment and thousands of research articles published each year on the topic (Zhang et al., 2021). It has been anticipated that the commercial market for nanofibers in general will reach an estimated market cap of \$3.35 billion by 2030, with electrospinning set to represent a substantial portion of this (Straits Research, 2021). With this in mind, it is clear that electrospinning still offers fertile ground for research and development of nanofibrous materials in a continuously expanding area.

### 1.2.2 Description of the electrospinning process

Numerous methods exist for producing small, synthetic fibres from solutions, melts, gels and emulsions, but most of these techniques depend on external shear forces (*i.e.* through centrifugation) and mechanical drawing to form the liquids into elongated threads, which then dry or otherwise solidify into fibres (Luo et al., 2012). Electrospinning is distinct from these methods in its use of an electric field to form said fibres, and it is well established that it produces much finer materials than these common counterparts. Early observations by microscope suggested electrospinning had the ability to produce fibres within the nano-scale, a fact which was later confirmed by scanning electron microscopy (SEM) (Boys, 1887, Doshi and Reneker, 1995). These fibres are orders of magnitude smaller than those produced by conventional methods, which typically lie within the range of 10-100  $\mu\text{m}$  (Xue et al., 2019).

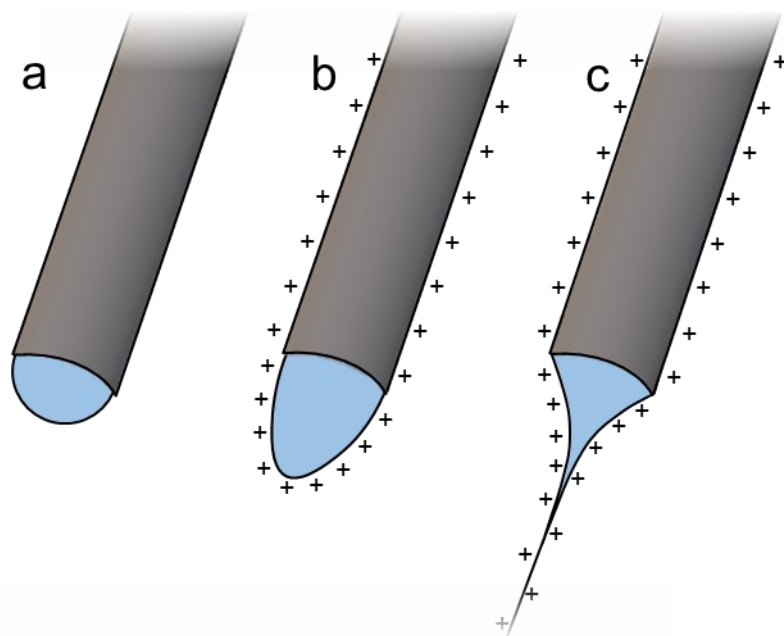
The simplest form of modern electrospinning setup is commonly known as needle-based electrospinning. The equipment for this type of electrospinning comprises only a syringe, a syringe pump, a conductive needle (acting as a spinneret), a high voltage power supply, and a conductive collector. Though factors such as collector geometry, needle quantity and needle orientation may vary, these are typically arranged as shown in **Figure 1.1**, and can be found most frequently in research environments, where scale of production is not of primary interest. This setup generally uses a direct current (DC) power supply to apply a voltage to the conductive needle and syringe containing the electrospinning liquid, the latter most commonly being a polymer solution.



**Figure 1.1.** A simple, needle-based, electrospinning setup.



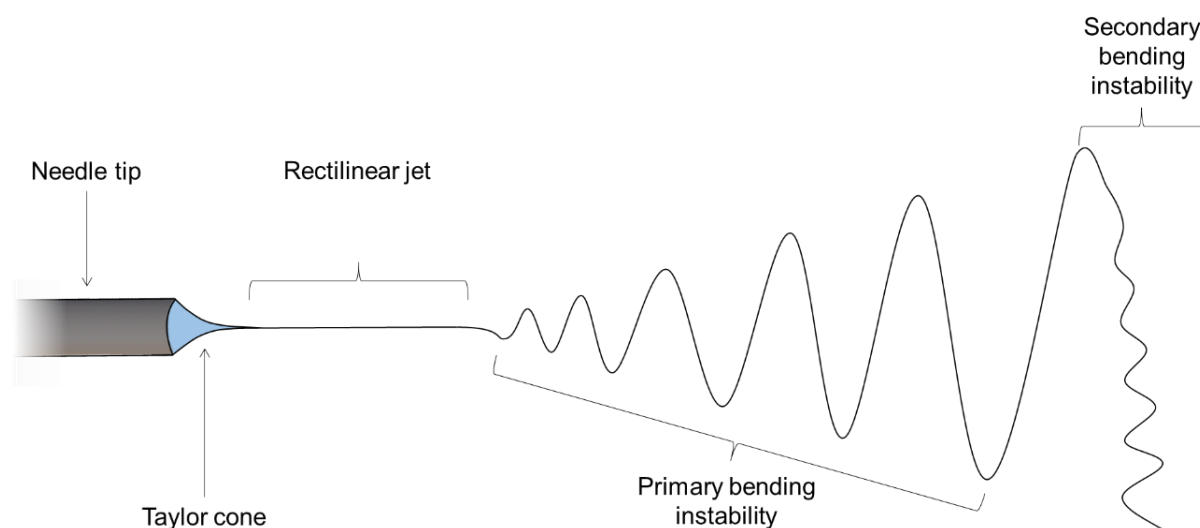
In order to form nanofibers by this method, electric current must be applied to a spinning solution at or above the critical voltage, which is solution specific. Prior to application of the current, the syringe pump begins flowing the spinning solution down the needle until a droplet is formed, as in **Figure 1.2.a**, at which point the high voltage current is then supplied. Below the critical voltage, charge is created on the surface of the droplet causing it to distort, approaching a conical shape drawn towards the grounded collector, but is insufficient to overcome the surface tension and viscosity of the solution and begin transferring solution material (**Figure 1.2.b**). As voltage increases further, the droplet will continue to distort until eventually the critical voltage for the solution is surpassed, the Taylor cone is formed, and the electrospinning jet is initiated (**Figure 1.2.c**).



**Figure 1.2.** Taylor cone formation following application of DC voltage to the conductive needle. (a) Formation of a droplet at the needle tip in the absence of an applied voltage. (b) Distortion of the liquid under the applied voltage into the beginning of a Taylor cone shape. (c) Supercritical voltage causes generation of a jet to form from the Taylor cone, which is rapidly drawn towards a grounded, or counter-charged, collector.

The formed jet is accelerated towards the collector firstly as a stable, linear jet which remains as solution with a constantly decreasing diameter as it gets further away from the emitter. The jet then becomes unstable and begins a primary phase of whipping and bending, followed by further bending instability, and coiling of the fibres commences before being deposited upon the collector (**Figure 1.3**). At all phases of the process, the jet is drawn ever thinner, allowing the formation of very fine fibres, with diameters which have been recorded as small as the sub

nanometre scale (Jian et al., 2018). During the instable jet phase, in the case of solution spinning, much of the solvent is evaporated and the drying (or in the case of melt electrospinning: solidification) of the fibre occurs rapidly.



**Figure 1.3.** Depiction of the needle electrospinning process with DC voltage, indicating the various stages of jet formation: from the formation of the rectilinear jet (often known as the stable region); proceeding into the instable (or whipping) region, where primary, secondary, and even tertiary (not depicted) bending instability rapidly elongates and narrows the jet; before the final fibre formation on the collector.

In order to remain as a continuous jet and not be pulled into small droplets (as with the process of electro spraying<sup>1</sup>), it is necessary to carefully balance the electrospinning parameters, as many factors can significantly influence electrospinning behaviour and the morphology of the produced nanofibers (described in section 1.2.4).

### 1.2.3 Material classes in electrospinning

Through the process of electrospinning, it is possible to produce fibres composed of many different materials and material blends, ranging from single polymer species to ceramics, and magnetic materials in the form of composites. A brief overview of the most common electrospinning processes employed for differing material classes is presented in the following sections.

<sup>1</sup> Electro spraying is a similar process to electrospinning, which creates discrete spheres rather than continuous fibres.

### 1.2.3.1 Polymers

Polymers are large molecules (sometimes termed macromolecules) composed of many repeating monomer units. They can be broadly categorised as synthetic polymers, such as poly(caprolactone) (PCL) or poly(lactic acid) (PLA), and natural polymers, such as cellulose or silk fibroin (SF). Through dissolution in an appropriate solvent, many of these polymers have been electrospun by the standard electrospinning process already described. Thermoplastic polymers (which can be heated to soften and melting point and re-set with no change to material properties) with moderate melting temperatures are often used in a different version of electrospinning known as melt electrospinning, in which no solvent is required, but rather molten polymer forms the electrospinning jet. Fibres produced by this method are often in the micrometre rather than nanometre range, and typically at least one order of magnitude larger than those spun via 'conventional' electrospinning. This is largely due to the high viscosity of the polymer melt, differences in charge density of the liquid, and the rapid solidification of the jet (Morikawa et al., 2019, Bachs-Herrera et al., 2021). Polymer electrospinning can feature single species liquids, polymer blends, and the addition of chemical crosslinkers as well as specific additives to form composite fibres.

### 1.2.3.2 Composite materials

Composite fibrous materials produced by electrospinning represents a substantial portion of modern electrospinning research. Major areas of research include biomaterials produced with bio-additives, such as platelet lysate or bioactive glass (Filova et al., 2021, Ghorbani et al., 2023), creation of ceramic nanofibers for catalysis and energy storage through incorporation of inorganic precursors to the spinning solution (Wu et al., 2012), and incorporation of magnetic nanoparticles for applications including data storage, nanogenerators and electromagnetic shielding (Jia et al., 2021).

### 1.2.3.3 Molecular self-assembly materials

The combination of molecular self-assembly species with polymers in a single solution has been used to produce materials with core-shell structures and materials with dual fibre and web (Gharraei et al., 2016, Liu et al., 2019a). Self-assembly molecules have also been used in a melt-electrospinning configuration at high temperatures (Luo et al., 2012), whereas Thomson and co-workers employed electrospun fibres within the micro- and nano-regions to study the behaviour of dipeptide self-assembling into worm-like micelles conceptualised as polymer chains (Thomson et al., 2022).

### 1.2.4 Factors affecting electrospinning

The many variables affecting electrospinning and the produced nanofibers (in terms of fibre uniformity, diameter, and orientation) can be broken down into the following categories: solution parameters<sup>1</sup>, process setup, and ambient factors. For simplicity, these factors are described in the context of polymer solutions and are summarised in **Table 1.1**.

*Table 1.1. Variables effecting the electrospinning process and their influence on fibre generation.*

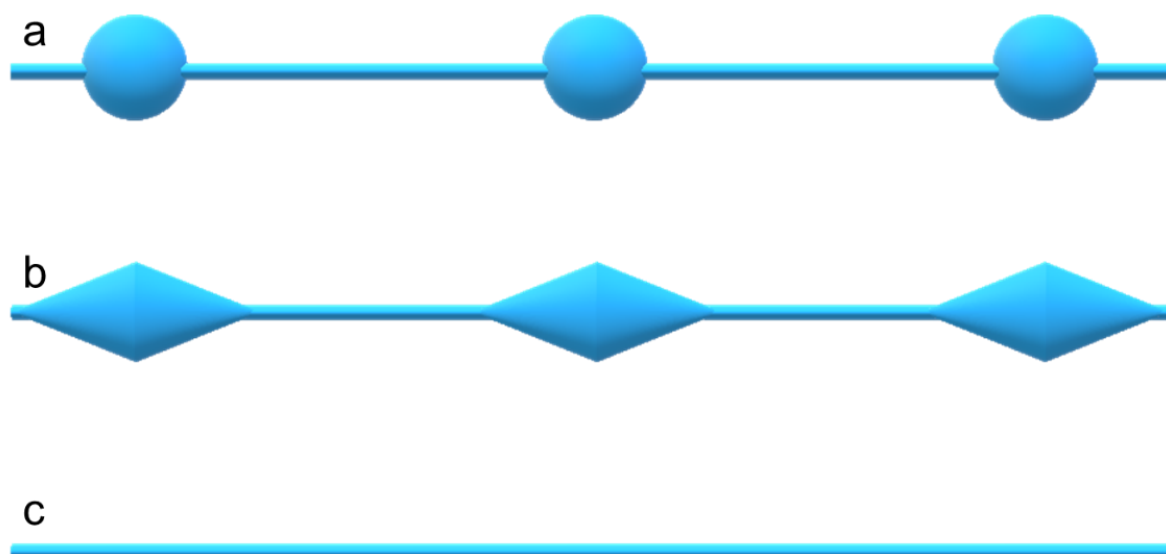
Category	Variable	Influence on Nanofibres
Solution parameters	Viscosity	Rate of morphological defects
	Surface tension	Rate of morphological defects
	Solvent	Surface morphology
	Conductivity	Fibre diameter
Process setup	Voltage	Morphological defects and fibre diameter
	Flow rate	Morphological defects and fibre diameter
	Solution temperature	Fibre diameter
	Collector geometry	Fibre alignment
	Tip-collector distance	Fibre diameter
	Needle diameter	Fibre diameter and individuation
Ambient factors	Humidity	Fibre diameter and surface morphology
	Temperature	Fibre diameter
	Pressure	Fibre uniformity
	Atmospheric composition	Fibre diameter

<sup>1</sup> It should be noted that by selecting poly(vinyl alcohol) as a base polymer in section 1.3.2, degree of hydrolysis is introduced as an additional variable to the electrospinning process which is not included here, however increasing degree of hydrolysis is known to result in increased fibre diameter (Park et al., 2010).

### 1.2.4.1 Solution parameters

The role of viscosity in electrospinning is well established, following extensive research with solutions prepared from many polymers. The primary affect is on the uniformity of the nanofibers produced, with lower viscosity solutions tending to produce fibres with a greater number of defects, such as the formation of beads and spindles shown in **Figure 1.4**. The entanglement of polymer chains within the solution allows the jet to elongate, while maintaining a continuous stream of solution which does not retract into droplets under the surface tension of the fluid, and among other things, viscosity is reflected by this process. Both polymer concentration and molecular weight (Mw) affect the process of chain entanglement, as well as the solvent system used and temperature of solution. (Ramakrishna et al., 2005, Henriques et al., 2009, Haider et al., 2018b, Zhang et al., 2018a). Solutions with too low a viscosity tend to be unsuitable for electrospinning and result in electro spraying, while highly viscous solutions make polymer extrusion into a jet impossible (Amariei et al., 2017). Similar to viscosity, the effect of surface tension is responsible for the possibility for jet formation, and subsequent morphology and uniformity of the nanofibers produced. Charges aggregating on the polymer surface must overcome surface tension at the boundary of the solution in order to form the extruded jet, which results in solutions of lower surface tensions being capable of jet formation at lower applied voltages. As well as requiring higher voltage, solutions with high surface tension typically result in the formation of beads or other imperfections, or a total absence of jet initiation (Amariei et al., 2017, Kailasa et al., 2021). Surface tensions can be influenced by polymer concentration, but also through the introduction of surfactants or by modifying the solvent composition (Xue et al., 2019). Though the ideal ranges for viscosity and surface tension are highly dependent upon factors such as polymer used, apparatus setup, and voltage applied, a proposed heuristic has been given as 1-20 poise for viscosity and 35-55 dyn·cm<sup>-2</sup> (Amariei et al., 2017).

The conductivity of the solution has been found to impact fibre diameter, with increasing solution conductivity resulting in the formation of fibres with smaller diameter (Kim et al., 2005, Angamma and Jayaram, 2011). The low ion concentration in normal solvents results in few charge carrying particles, and therefore greater applied voltages are required to initiate jets. To a much lesser degree, solvent composition can influence conductivity, but most notably a substantial effect on fibre surface morphology has been demonstrated by varying solvent ratios, arising from differences in evaporation rates of the constituent solvents (Cay et al., 2015, Liu et al., 2015).



**Figure 1.0.1.** Visual representation of common fibre morphologies produced by electrospinning: (a) bead formations; (b) spindle formations; (c) uniform and defect free fibres.

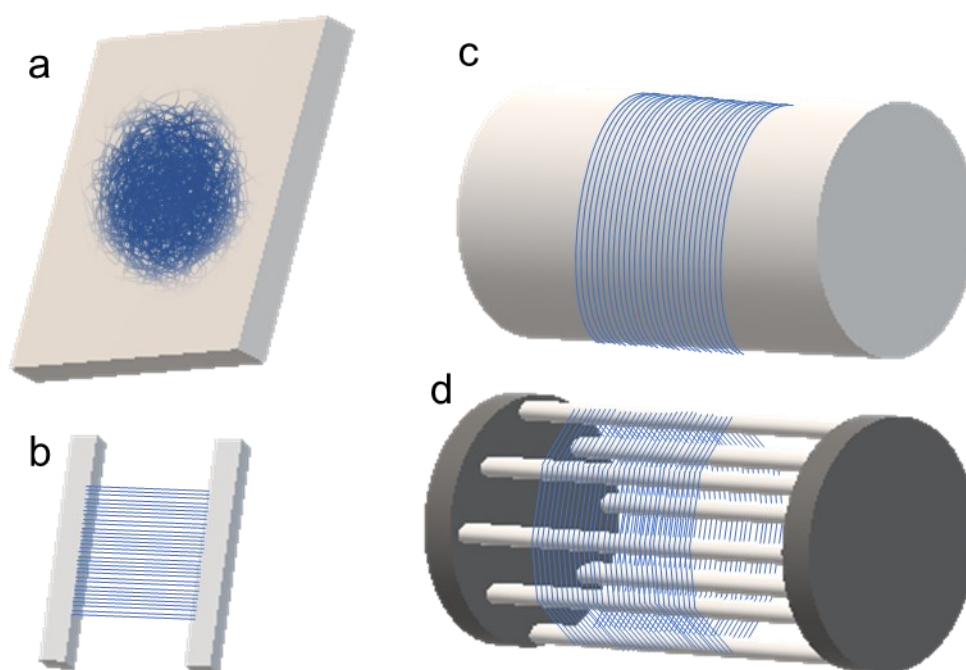
#### 1.2.4.2 Process setup

Among the variables relating to process setup, applied voltage relates most closely to the solution parameters, as it is chiefly viscosity and surface tension that dictate the so-called critical voltage of the solution. At this critical voltage, bead-free nanofibers are typically produced, whilst exceeding it has been found to cause the Taylor cone to recede within the needle, having negative effects on fibre morphology and resulting in the production of beads/beaded fibres (Deitzel et al., 2001, Zong et al., 2002), although some sources report increases in fibre diameter associated with increased applied voltage (Can-Herrera et al., 2021). On one hand, increased charge and subsequent application of the electrical field could result in a more accelerated jet, which at constant flow rates could cause breaking of the continuous stream and therefore bead formation, but this greater acceleration could also reduce flight time of the jet and therefore decrease the time available for elongation to occur, thus resulting in thicker fibres. It is likely that the observed behaviour may be dependent upon polymer species and Mw, since long linear polymers would be expected to remain sufficiently entangled to minimise the probability of bead formation. It has also been observed that the polarity of the applied voltage has some possible effect on thickness and morphology of electrospun fibres produced, but the results are inconsistent and occasionally conflicting. However, polarity was found to produce a consistent and reproducible effect on surface chemistry of materials, and particularly those with significant electronegative moieties (Ura and Stachewicz, 2022). Directly related to applied voltage is the solution flow rate. When flow rate is reduced, it can cause withdrawal of the Taylor cone into the needle, whereas when it

is increased, it results in more solution extruded to the needle tip, producing fibres of thicker diameter, as well as ribbon-like defects arising from inadequate evaporation of solvents (Megelski et al., 2002, Zong et al., 2002)

The temperature of the solution influences both surface tension and viscosity, which can lead to changes in uniformity and rate of defects associated with each of those parameters. On top of this, Demir et al. (2002) found that electrospinning at increased solution temperature created fibres with narrower fibre diameter distribution, whilst other researchers suggest there may be a reduction in fibre diameter associated with electrospinning up to certain temperatures, before fibre diameter increases again (Yang et al., 2017). This is explained theoretically *via* the competing mechanisms of reduced viscosity, which allows for greater flow and shearing of the fluid into thinner fibres, followed by a more rapid onset of solvent evaporation at the most elevated temperatures, which leads to a reduced window of elongation.

Collector geometry is the primary consideration when attempting to influence the alignment of fibres produced by electrospinning. Several common collector geometries are shown in **Figure 1.5**, including flat plate collectors which generate fibres with random orientation, and parallel electrodes which catch suspended fibres in a bridging pattern. The drum and wire drum collectors depicted in **Figure 1.5.c & d** respectively, are combined with high RPMs in order to collect aligned fibres – this is achieved by matching the external velocity of the drum with final velocity of the jet (Ramakrishna et al., 2005, Zander, 2013, Xue et al., 2019). The distance between the collector and the tip/spinneret is also very important, because it influences the flight time of the jet. Shorter distances result in a stronger electric field and therefore higher potential jet velocity from the tip. In general, small distances tend to produce fibres with poor uniformity and large diameter with poor jet stability, whilst larger distances create finer fibres, enabled by the enhanced time for elongation (Matabola and Moutloali, 2013).



**Figure 1.5.** Common collector geometries used in electrospinning: (a) flat plate; (b) two parallel collectors; (c) rotating drum collector; (d) rotating wire drum collector.

#### 1.2.4.3 Ambient conditions

Relative humidity (RH) can play a significant role in both fibre diameter and surface morphology. Having established common behaviours arising from already discussed process conditions, it is possible to intuit that high RH might influence the rate of solvent evaporation and increase the time of elongation, a trend which has been observed in literature (Park and Lee, 2010, Pelipenko et al., 2013). As well as this more predictable behaviour, it is also possible through RH control to generate a significant variance in surface morphology of nanofibers produced from a range of polymers in different solvents (Mailley et al., 2021). At constant humidity, there is an inverse relationship between the temperature of the surrounding environment and fibre diameter, as long as the RH varies between 30% and 70% (Icoglu and Ogulata, 2017).

Pressure and atmospheric composition can also affect nanofiber formation, though they are less frequently explored. Low pressure causes faster flow behaviour from the needle during electrospinning, which leads to unstable jets. Continuing to lower the pressure results in boiling of the spinning solvents (Ramakrishna et al., 2005), while high pressure CO<sub>2</sub> setup has been used to reduce defects and increase fibre diameters of poly(vinylpyrrolidone) spun in dimethylformamide (Wahyudiono et al., 2012). The use of gases with high breakdown voltage



(e.g. freon) can also result in fibre diameters much greater than those produced in air with all other conditions being kept unchanged (Baumgarten, 1971).

### 1.2.5 *Electrospinning emitters and platforms*

As previously mentioned, the typical emitter employed in electrospinning research laboratories is broadly known as needle electrospinning and consists of a single needle spinneret connected to a DC power supply as shown in **Figure 1.1**. For the sake of clarity, this setup will be referred to as ‘needle DC’ in this work. While this emitter is a reliable staple within literature and for most of the history of electrospinning, there has been extensive innovation in this area. This section provides an overview of some common methods within the categories of needle DC, needleless DC, and alternating current (AC) electrospinning, though the list of DC based systems is far from exhaustive, and numerous review articles provide a more extensive summary (Niu and Lin, 2012, Xue et al., 2019, Subrahmanya et al., 2021, Ravandi et al., 2022, Tan et al., 2022).

#### 1.2.5.1 DC Electrospinning

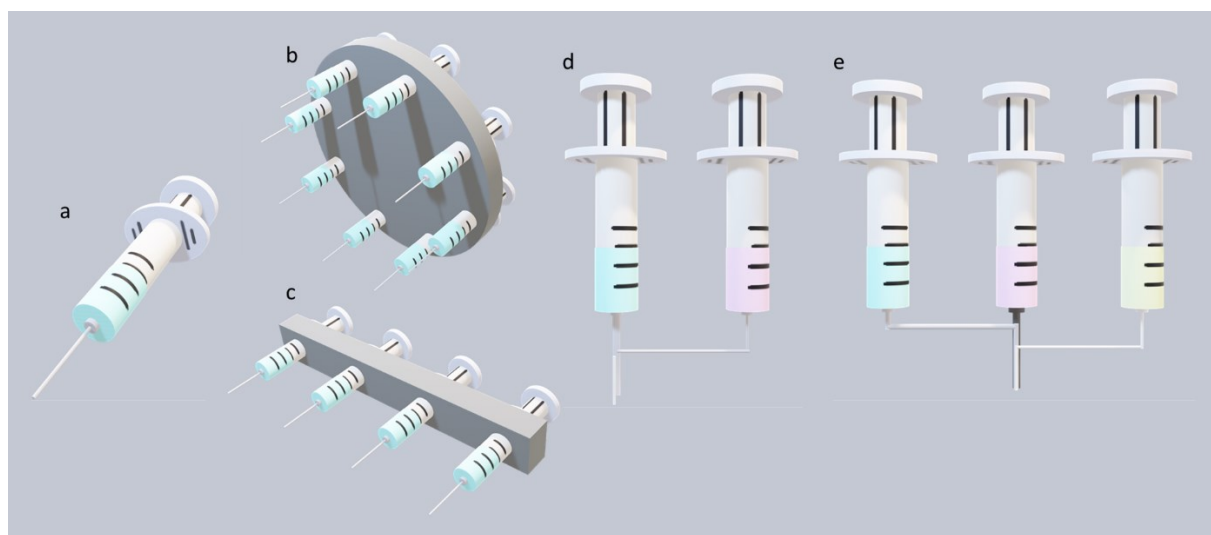
The overwhelming majority of all electrospinning research to date has been carried out using DC voltage, and the different systems can be categorised as ‘needle’ (sometimes called nozzle) and ‘needleless’.

##### 1.2.5.1.1 *Needle based emitters*

The first patent for electrospinning was based on a nozzle setup (Cooley, 1902). Following from this, syringes loaded with polymer solutions (**Figure 1.6.a.**) and mounted into syringe pumps to drive flow to a conductive needle tip where jet formation occurs, became the norm. This concept has been extended to different forms of coaxial spinning (with bi- and tri-axial spinning setups shown in **Figure 1.6.d & e**, respectively), which facilitates the formation of core-shell structures and allows the design of fibres with mix-and-matchable properties (Han et al., 2019). Some notable examples include: drug delivery systems by the encapsulation of pharmaceuticals within biocompatible sheaths, for delayed and sustained drug release by multi-layered fibres (Han and Steckl, 2013, Zhang et al., 2020, Reise et al., 2023); and, filtration systems (Haloui et al., 2017).

A major flaw experienced by single needle emitter systems is the limited productivity (Ravandi et al., 2022). One way to resolve this issue is the development of multi-needle systems, which can enhance productivity significantly while being easy to implement and retrofit into existing

*ad-hoc* electrospinning setups found in many research laboratories. Some possible arrangements for multi-needle emitters are shown in **Figure 1.6.b & c**, however a drawback of these setups is interference and warping of the electric field by proximity of each electrode, which can be resolved by optimising needle arrangement and combining additional irregular electrodes to dampen the electric field as required (Kim et al., 2006).

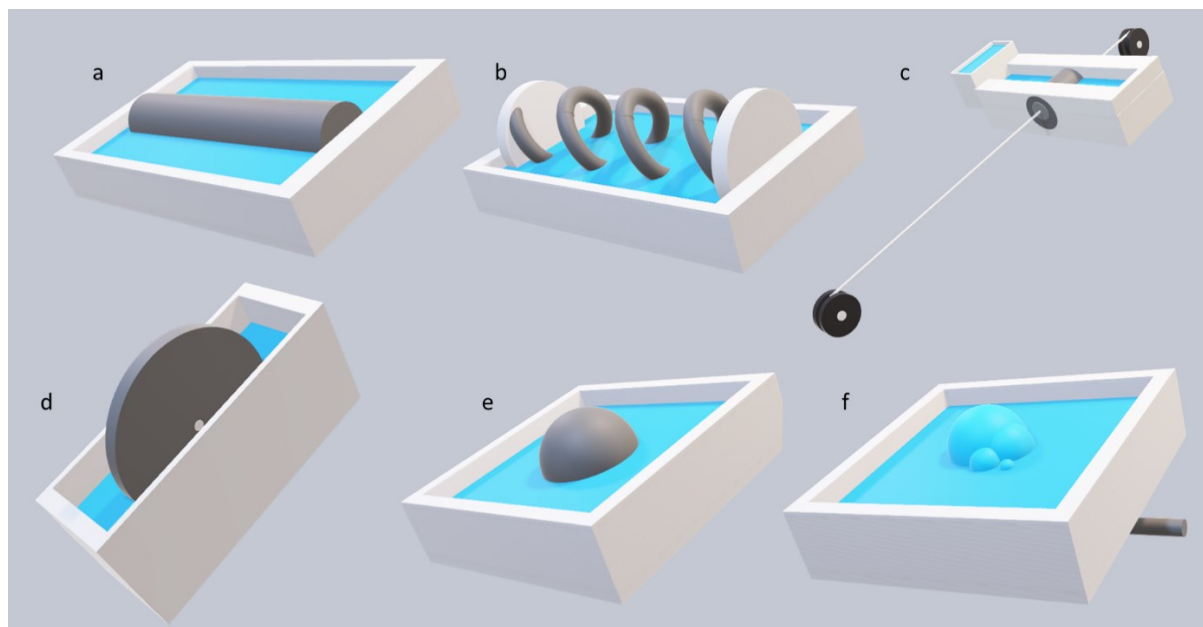


**Figure 1.6.** Examples of needle-based emitters used in DC electrospinning: (a) single needle spinneret; (b & c) multi-needle spinneret in cylindrical and linear arrangements, respectively; (d & e) coaxial needle representations for production of bi- and tri-axial fibres, respectively.

#### 1.2.5.1.2 Needleless emitters

Despite the fact that the first account of the electrospinning process was a needleless configuration, needle became the accepted norm until the need for scale up, brought the attention back to needleless systems (Boys, 1887, Ravandi et al., 2022). The scalability of these emitters comes from the principle that a highly charged, free liquid surface is capable of forming multiple jets across a large area, rather than being limited to the number of nozzles. **Figure 1.7.a-d** shows spinnerets designed to rotate continuously through a polymer solution, applying a constant liquid coating to its surface from which jets can be formed. Rather than passing the electrode through solution, alternative instruments sometimes use a delivery system to deposit solution upon an electrode, such as the mechanisms shown in **Figure 1.7.c**, where a wire based spinneret with a traversing cartridge deposits solution from a solution sump via capillary action under gravity (Elmarco, 2020). Furthermore, it is possible to produce fibres without the use of any solid spinneret, but instead utilising the stretched, thin surface formed by bubbles, also known as bubble electrospinning (Liu et al., 2007). A number of these

methods have been utilised to produce scalable commercial platforms, with potential throughputs as high as  $1 \text{ kg}\cdot\text{h}^{-1}$ , though it should be noted that needle based systems are not unscalable, with extremely high productivity reported up to  $6.5 \text{ kg}\cdot\text{h}^{-1}$  in systems featuring as many as 5000 needles (Ravandi et al., 2022, Bionicia, 2023).



**Figure 1.7.** Examples of needleless emitters used in DC electrospinning: (a) cylindrical spinneret; (b) spiral spinneret; (c) traversing cartridge with wire spinneret; (d) rotating disc spinneret; (e) ball spinneret; (f) bubble electrospinning (emitter-free/self-emitting).

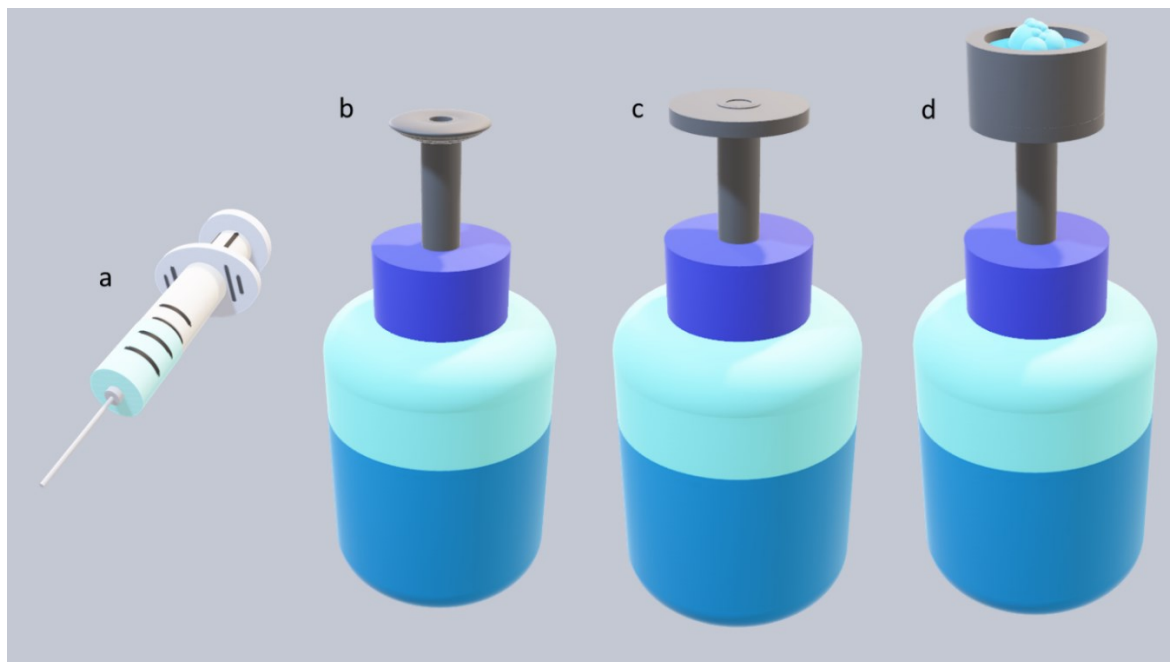
### 1.2.5.1.3 AC electrospinning setups

AC electrospinning has emerged in the 21<sup>st</sup> century as a novel research area within nanofiber production, with early literature coming from Richmond (Virginia, USA) under Prof. Gary Tepper (Kessick et al., 2004, Sarkar et al., 2007), and most of the current research originating at the Technical University of Liberec (TUL; Czechia) and Budapest University of Technology and Economics (Hungary). As the name suggests, it relies on AC, rather than DC, voltage to excite the fluid surface sufficiently to form Taylor cones and subsequent jets. Unlike DC electrospinning, this method produces fibres with a distribution of charges, since 50% of the fibres are produced during the positive phase of the waveform, whilst 50% are generated during the negative phase. Because of this, each proceeding pulse of fibres acts as a collector to the subsequent, oppositely charged, pulse of fibres (Sivan et al., 2022). For this reason, the attraction towards any collector, charged or grounded, is reduced substantially and therefore the collector plays a much less critical role in the process with respect to the electric field (Kalous et al., 2021). This distinctly different process provides interesting research

W. J. A. Homer, PhD Thesis, Aston University, 2023

opportunities as it can produce markedly different macroscopic morphologies when compared to many DC spun materials (Farkas et al., 2019, Kalous et al., 2021).

Some early uses of AC electrospinning relied on needles or nozzles to supply solution to a charged tip (**Figure 1.8.a**) and observed different behaviours in the fibre plume produced (Kessick et al., 2004). However, as all solution material is not properly drawn from the needle by the strong electric field as per DC electrospinning, prolonged production results in issues arising from the drying of the solution at the tip, thereby negatively impacting the region in which the plume is generated, and the ability to properly collect the nanofibers is impeded. Subsequently, an inverted cone spinneret with cascading polymer solution in constant flow was developed as seen in **Figure 1.8.b**, in which jets initiate from the rim of the cone (Kocis et al., 2018). More advanced configurations of this emitter have been made, to facilitate the spinning of two solution simultaneously and form internal and external plumes (Soucek et al., 2018). Other types of AC electrospinning include the use of flat plate spinnerets and bubble electrospinning, as shown in **Figure 1.8.c & d**, respectively.



**Figure 1.8.** Types of emitter used in AC electrospinning: (a) needle based spinnerets; (b) cone geometry; (c) flat disc; (d) bubble electrospinning.

AC electrospinning introduces new variables alongside those previously discussed in section 1.2.4, most notably frequency and waveform. Manipulation of the waveform (for example, from sinusoidal to rectangular) optimises productivity in theory, as less time is spent with sub-critical voltage applied to the emitter (Sivan et al., 2022). This can also have effects on fibre

morphology and diameters, because it influences the duration of jet formation, due to changes in proximity of each subsequent pulse of fibres. This means that low frequency spinning struggles to form stable jets/plumes, which even when formed, may be dominated by fibres of a single polarity, thereby explaining any reduction in productivity (Sivan et al., 2022). In terms of fibre morphology, mixed results have been reported depending on the polymer system used. Farkas and co-workers examined the effect of these variables on a solution of Kollidon® VA64 and reported no notable impact on fibre diameter or morphology observed with varying voltage or waveform (Farkas et al., 2020). In comparison, the morphology of fibres produced by AC spinning of PCL was found to be heavily influenced by waveform, with a triangle wave producing significantly thinner fibres than those generated using a square or sinusoidal waveform, whereas increasing frequency resulted in larger average fibre diameters (Sivan et al., 2022). Some research which compared the productivity of these platforms, evidenced that AC bubble electrospinning is significantly more productive than its DC counterpart and needle spinning (Erben et al., 2020). Overall, this form of electrospinning is still in its infancy, with no commercial devices yet available.

## 1.3 Electrospun materials

### *1.3.1 Applications of electrospun materials*

Electrospun fibres seem to continuously find new applications and many review articles have been written detailing extensive research in a number of fields. A search for reviews entitled 'Electrospinning applications' on Web of Science returned 137 articles from the last 20 years, for which a breakdown based on key topic titles has been included in **Table 1.2**. While many base polymers are common to all these fields, the frequency of any given polymer varies depending on use, and typically, within the niche of a specific application, is being tailored accordingly by adjusting the fibre composition with additives or post electrospinning treatments. The distribution of the number of review articles between topics presented in **Table 1.2** indicates that a significant majority of the research on applications of electrospun materials is as biomaterials, with sub-topics such as drug delivery and tissue engineering (TE), representing substantive bodies of research on their own.

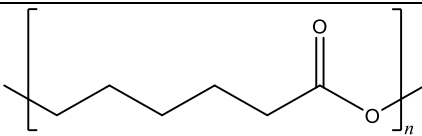
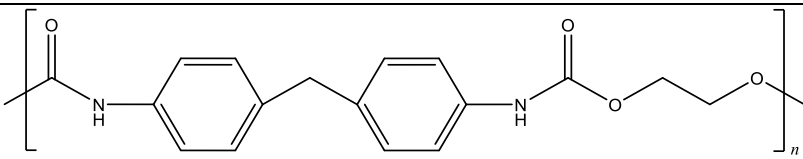
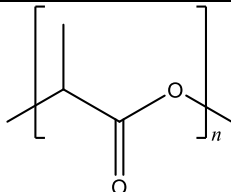
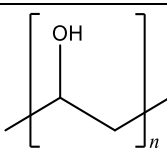
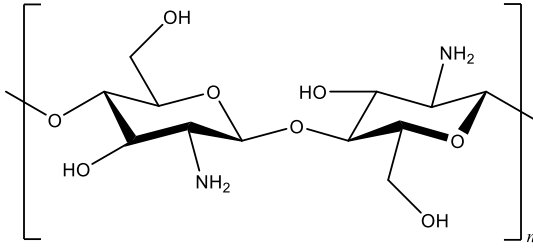
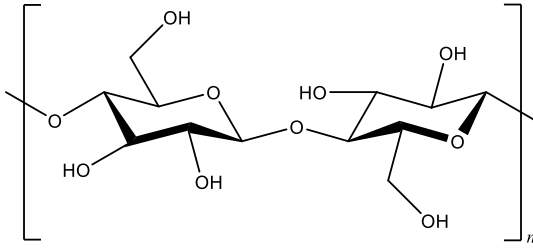
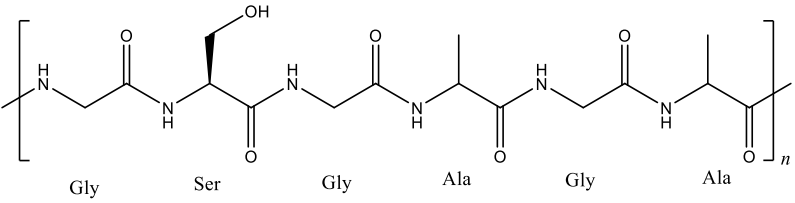
**Table 1.2.** Summary of literature reviews on topic-specific electrospinning applications found on Web of Science (as per 21/03/2023).

<b>Application topic</b>	<b>Reference</b>
Biomedical & biotechnology	(Agarwal et al., 2008, Supaphol et al., 2012, Wade and Burdick, 2014, Zhao et al., 2015, Repanas et al., 2016, Cheng et al., 2017, Haider et al., 2018a, Hemamalini and Dev, 2018, Ashraf et al., 2019, Wroblewska-Krepsztul et al., 2019, Partheniadis et al., 2020, Garkal et al., 2021, Zhang et al., 2021, Golba et al., 2022, Kumar and Rajan, 2022, Wang et al., 2022b, Zhong et al., 2022)
Tissue engineering	(Pham et al., 2006, Liu et al., 2013, Sakina and Ali, 2014, McClellan and Landis, 2016, Kishan and Cosgriff-Hernandez, 2017, Mortimer and Wright, 2017, Chen et al., 2018, Liu et al., 2018, Hong et al., 2019, Dejob et al., 2021, Ghaderpour et al., 2021, Heilingoetter et al., 2021, Rahmati et al., 2021, Yang et al., 2021, Zhao et al., 2021, Muthukrishnan, 2022)
Biosensors	(Vellayappan et al., 2016, Zhang et al., 2017)
Pharmaceuticals	(Wroblewska-Krepsztul et al., 2019, Nangare et al., 2020, Partheniadis et al., 2020, Vass et al., 2020)
Drug delivery	(Hu et al., 2014, Esenturk et al., 2016, Repanas et al., 2016, Pant et al., 2019, Topuz and Uyar, 2019, Ghaderpour et al., 2021, Luraghi et al., 2021)
Energy & energy storage	(Dai et al., 2011, Dong et al., 2011, Gong et al., 2014, Liu et al., 2019b, Dou et al., 2020, Waldrop et al., 2020, Wang et al., 2020b, Wang et al., 2020a, Nguyen and Lee, 2022, Sun et al., 2022)
Data storage	(Dopke et al., 2019)
Food processing & storage	(Bhushani and Anandharamakrishnan, 2014, Rezaei et al., 2015, Drosou et al., 2017, Mercante et al., 2017, Zhang et al., 2018b, Wroblewska-Krepsztul et al., 2019, Mohammadi et al., 2020, Munteanu and Vasile, 2021, Coelho et al., 2022, Yao et al., 2023)
Antibacterial	(Antaby et al., 2021, Li et al., 2021b)
Electrical components	(Miao et al., 2010)
Sensors	(Su et al., 2014, Zhang et al., 2017, Veeramuthu et al., 2020, Nguyen and Lee, 2022)
Agriculture	(Schiffman and Diep, 2023, Mercante et al., 2017)
Water and air filtration	(Ray et al., 2016, Sarbatly et al., 2016, Wang et al., 2016, Perea et al., 2017, Agrawal et al., 2021, Lyu et al., 2021, Madalosso et al., 2021, Coelho et al., 2022)

### *1.3.2 Common electrospun polymers as biomaterials*

A wide variety of polymers have been used in electrospinning, with many of these often applied to the production of biomaterials for a range of biomedical applications. **Table 1.3** summarises the most common synthetic and natural polymers employed for the creation of electrospun nanofibers for drug delivery, wound dressings, and TE. Within the context of this thesis, it was also necessary to identify a suitable material for use within a biomedical device suitable for blood processing. While all the materials identified in **Table 1.3** have established biocompatibility both as pure polymer fibres and as blends/composites and have been researched extensively as biomaterials across many applications, some are more suitable than others for the work presented here. To ensure good wettability and allow for the blood to pass through the material without high resistances to flow, the base material should ideally be hydrophilic. Furthermore, it would be preferable that the material can be produced using 'green' solvents, to minimise the potential risk of contamination when considering its clinical use. PCL, PLA and polyurethane (PU), all require organic solvents for electrospinning and are typically hydrophobic. Concentrated formic acid is a common electrospinning solvent for SF (Belbeoch et al., 2021), and is also utilised in the spinning of chitosan nanofibers, alongside other concentrated acids and organic solvents (Salazar-Brann et al., 2021). Though it appears the solvent used for electrospinning of cellulose may vary depending on its precise form, species such as cellulose acetate use organic solvents (e.g. hexafluoroisopropanol; (Li et al., 2021a). By comparison, poly(vinyl alcohol) (PVA) is a hydrophilic polymer which is readily dissolved in and can be spun from pure aqueous solvents and was therefore chosen as the starting material within this research.

**Table 1.3.** List of the most common electrospun polymers used in biomedical applications, such as drug delivery, wound dressings, and TE. The list is based on recent literature reviews and notable texts and is reduced to include only the most common polymers (Patel and Gundloori, 2023, Muthukrishnan, 2022, Ramakrishna et al., 2005).

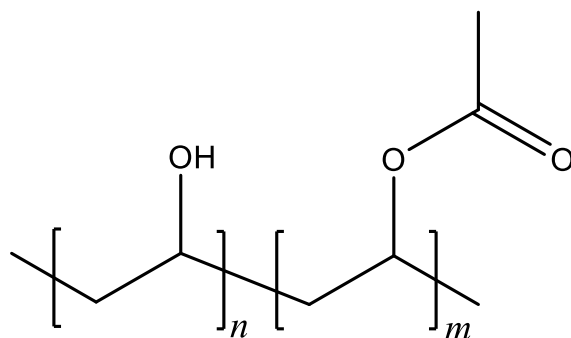
Polymer	Structure	References
<b>Synthetic polymers</b>		
PCL		(Azari et al., 2022)
PU		(Joseph et al., 2018)
PLA		(Kanmaz et al., 2018)
PVA		(Teixeira et al., 2020, Kumar and Rajan, 2022)
<b>Natural polymers</b>		
Chitosan		(Al-Jbour et al., 2019, Kalantari et al., 2019)
Cellulose		(Surendran and Sherje, 2022)
SF		(Farokhi et al., 2018, Farokhi et al., 2020, Chen et al., 2023)



## 1.4 Poly(vinyl alcohol)

### 1.4.1 Production of PVA

PVA is a semi-crystalline, water-soluble polymer for which the monomer unit is composed of a two-carbon backbone with a single hydroxyl functional group. It was first prepared by (Herrmann, 1924) by hydrolysis of poly(vinyl acetate) (PVAc) in the presence of ethanol and potassium hydroxide. As it is not produced from two independent monomers, but rather through modification of an existing polymer, PVA has been classified by Wiley and co-workers as a pseudo-copolymer (Wiley, 2016). Through this process, the partially hydrolysed PVA has a chemical structure as shown in **Figure 1.9**, with  $n\%$  hydroxyl containing groups, and  $m\%$  residual acetate groups. Though PVA has been synthesised from a number of monomers (Nawaz and Hummelgen, 2019), the preferred industrial scale production is a two-step production process, first by polymerisation of PVAc, followed by its transesterification using methanol in the presence of alkali catalyst, such as sodium methoxide (Sapalidis, 2020, Hallensleben et al., 2015, Saxena, 2003). The percentage of hydroxyl (%mol) containing groups within the final product is commonly known as the degree of hydrolysis (DH) and plays a significant role in the properties of PVA, along with the tacticity and Mw.

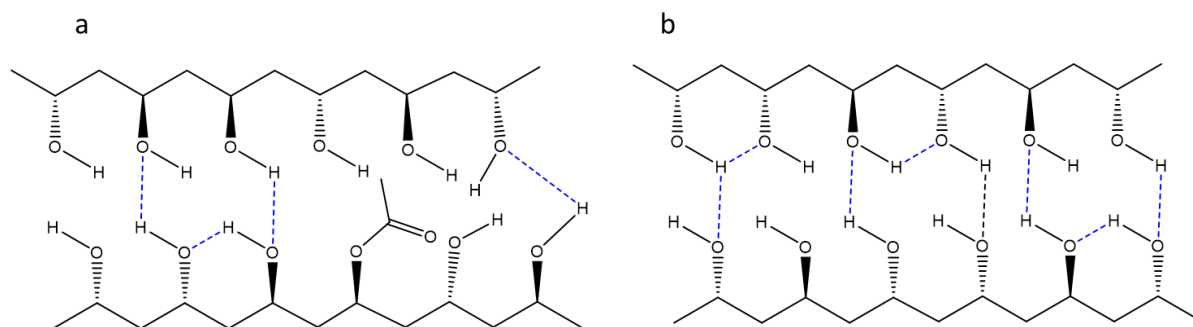


**Figure 1.9.** Chemical structure of PVA, where the left monomer unit is PVA, at a relative molar abundance of  $n\%$ , and the right monomer unit showing a residual acetate group of relative molar abundance of  $m\%$ .

### 1.4.2 Properties of PVA

Tacticity is affected by the method used to produce PVA, as hydrolysis or transesterification of PVAc results in atactic polymers, whilst it is possible to produce syndiotactic species via other polymerisation methods (Muppalaneni, 2013). Tacticity can influence glass transition

temperature and melting point, but this is rarely considered in literature as practically all research is conducted with off-the-shelf PVA which, as has been already acknowledged, is generally produced at scale by transesterification of PVAc. The DH and Mw, on the other hand, are discussed more frequently, as both of these influence the inter- and intramolecular forces of the polymer and subsequently its bulk and solution properties such as viscosity, ease of solubility and tensile strength (Muppalaneni, 2013). In the case of the DH, more hydrolysed polymers experience less steric hindrance from the residual acetate groups and therefore the polymer chains are able to pack together more tightly, whereas higher Mw increases the total number of molecular interactions per polymer chain. This concept has been further substantiated using PVA films of differing DH and Mw, where differential scanning calorimetry was employed to confirm that, increasing either of these factors resulted in diminished chain mobility. Furthermore, this trend was also associated with increased crystallinity, shown by X-ray diffraction (Hdidar et al., 2017). **Figure 1.10** illustrates an example of the effect of DH on intermolecular forces between neighbouring PVA chains, with **Figure 1.10.a** showing the steric interference caused by residual acetate groups, resulting in a disruption to local hydrogen bond formation and reducing chain proximity, whilst **Figure 1.10.b** shows two sections of acetate-free PVA (more frequent in species with high DH) with close packing and undisrupted hydrogen bonding.



**Figure 1.10.** Schematic representation of the hydrogen bonding (dashed blue lines) within macromolecules of PVA in a solid, water-free state, showing (a) a section of chain with an acetate group present, which results in changes to chain conformation and forces, whilst (b) is pure PVA units with consistent hydrogen bonding and tight chain packing.

Other important properties of PVA include a melting point between 180-230 °C (depending on DH), density of 1.19-1.31 g·cm<sup>-3</sup> (depending on crystallinity) and good chemical stability (Sapalidis, 2020, Wypych, 2022). Though it is thermally stable at temperatures below 100 °C, polymer degradation of PVA begins around 120 °C with slight colour changes, followed by accelerated darkening around 150 °C, and rapid degradation between 200-240 °C (Yan and W. J. A. Homer, PhD Thesis, Aston University, 2023

Kellie, 2016, Wypych, 2022). Additionally, PVA has been found to be at least partially biodegradable via enzymatic and microbial pathways (Halima, 2016).

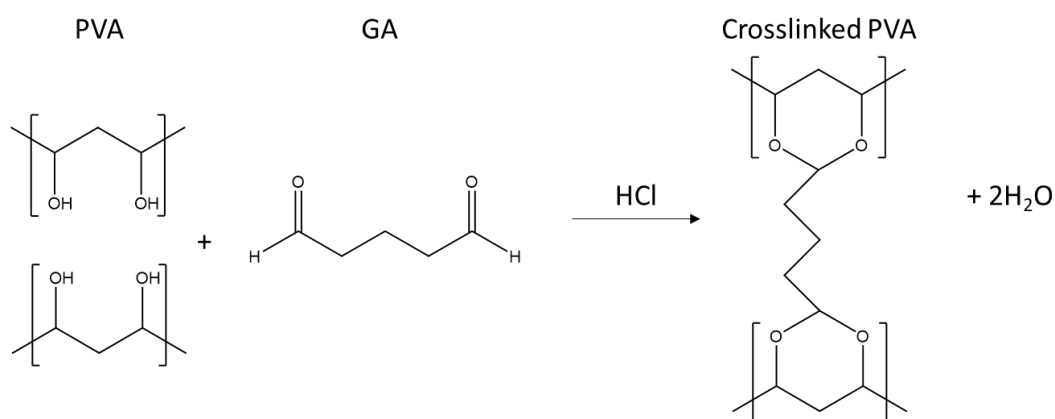
In relation to the biomedical field, PVA has some other important characteristics: it is inexpensive; its solubility in water affords it greener and more bio-friendly credentials; it is considered non-toxic and biocompatible; and, it has received food and drug administration (FDA) approval for food packaging and biomedical applications (Baker *et al.*, 2012, Chong *et al.*, 2013, Hassan and Peppas, 2000).

### 1.4.3 Enhancement of water stability

When in contact with water, even PVA with high DH and Mw can readily form hydrogels and dissolve at various rates depending on environment conditions. In order to slow down this process or mitigate it entirely, many different treatment methods have been applied to PVA, in the form crosslinking. Broadly speaking, these can be categorised as either chemical crosslinking or physical crosslinking (Golba *et al.*, 2022, Kamoun *et al.*, 2015).

#### 1.4.3.1 Chemical crosslinking

Chemical crosslinking of PVA is used to enhance water stability of the material through the addition of a crosslinking agent which covalently bonds two neighbouring chains of the polymer. The compounds often employed in chemical crosslinking of PVA are dialdehydes, aliphatic and aromatic di/tricarboxylic acids and isocyanates, among which, glutaraldehyde (GA) is the most popular (see schematic illustration in **Figure 1.11**; (Teixeira *et al.*, 2020, Golba *et al.*, 2022).

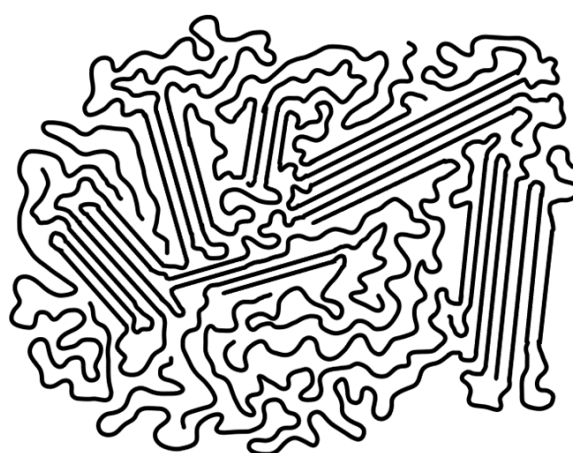


**Figure 1.11.** Schematic representation of the reaction between two PVA chains and GA in the presence of HCl.

Crosslinking of PVA with dialdehydes is commonly carried out in the presence of acid (Choudhury et al., 2006, Plieva et al., 2006), which, combined with the presence of the residual highly toxic crosslinking agent, results in a need for extensive post-treatment to ensure full removal of unreacted products. Chemical crosslinking with dialdehydes has been carried out with varied concentration both in solution prior to electrospinning and as a post-spinning treatment, demonstrating a good ability to render fibres highly stable in water (Roy et al., 2017, Tang et al., 2010). Work has been carried out to utilise 'greener' crosslinking agents for stabilisation of PVA fibres, such as citric acid (Nataraj et al., 2020, Diez et al., 2022), however despite it being more ecologically friendly, it is still found to be a cytotoxic species (Amaral et al., 2007), so within the biomedical field, there is a preference for water-stable PVA nanofibers, free of potential toxic agents.

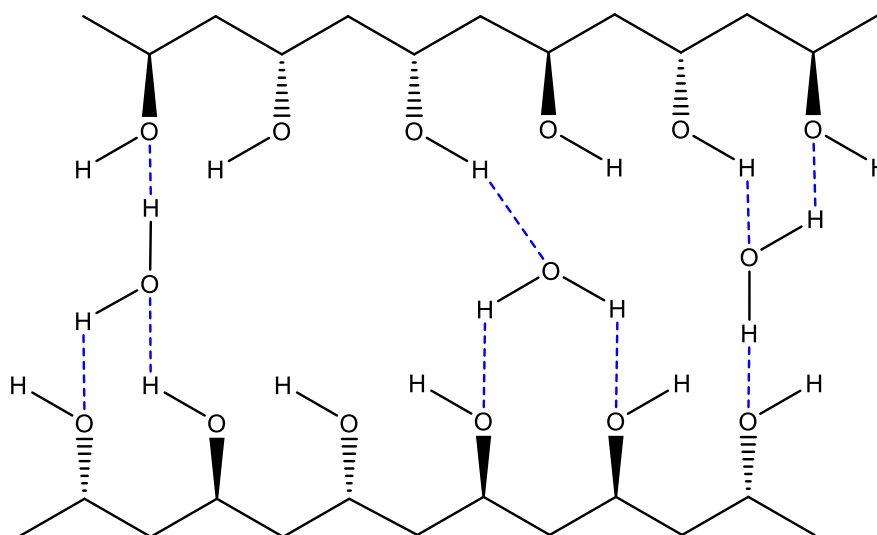
#### 1.4.3.2 Physical crosslinking

Physical crosslinking of polymers is a process by which the material's ability to absorb water is inhibited by modifying the weak intermolecular bonds of the polymer, thus increasing the crystalline regions of the structure. **Figure 1.12** shows a fringed micelle model of a semi-crystalline polymer. During physical crosslinking, external forces are manipulated to expand the crystal nuclei and increase the packing density of the chains, thus reducing its solubility in water.



*Figure 1.12. Fringed micelle model of a semi-crystalline polymer.*

Improving the crystallinity within the bulk of the material, and thereby enhancing the physical crosslinking, can also require displacement of internally bound moisture, (illustrated in **Figure 1.13**). The primary methods of physical crosslinking are freeze thawing and heat treatment, though methanol treatments have also been tested (Miraftab et al., 2014).



**Figure 1.13.** Illustration of PVA polymer with internally bound water molecules forming hydrogen bonds (dashed blue lines) with the hydroxyl groups.

As well as creating strong intermolecular bonds, the hydroxyl groups may also form hydrogen bonds with water, resulting in internally bound moisture. This property contributes to swelling behaviour of hydrogels and in part makes PVA very desirable for some biomedical applications. Displacing these molecules and allowing for energetic conditions, which facilitate expansion of the crystal nuclei, are achieved by freeze thawing or heat treatment (Cowie and Arrighi, 2008, Kudo et al., 2014).

Freeze thawing was described for crosslinking of PVA as early as 1975 and has since been used in conjunction with other methods, such as irradiation crosslinking (Yang et al., 2008, Peppas, 1975). When carried out on hydrogels, this process occurs simultaneously with cryogelation, as the mechanisms are intrinsically linked (Trudicova et al., 2021). The change in mechanical properties, therefore, is attributed to both morphological properties as well as crystallinity. Both rate of freezing and number of freeze-thaw cycles play a role in the crosslinking process, with increasing cycle duration and freezing time, resulting in higher crystallinity at lower temperatures (Adelnia et al., 2022).

Heat treatments have been used at a range of temperatures to enhance physical crosslinking of PVA, and in particular with electrospun materials. Heat treatment is also commonly

W. J. A. Homer, PhD Thesis, Aston University, 2023

combined as a secondary treatment, to complete chemical crosslinking processes (Nataraj et al., 2020, Diez et al., 2022), and has shown excellent promise in stabilising pure PVA nanofibers. Tretinnikov and Zagorskaya (2012) demonstrated increasing crystallinity in PVA films with increasing treatment temperature up to 150 °C after 1 h of heating. Electrospun nanofibers of PVA were also found to have improved water stability, with greater preservation of morphology at temperatures up to 180 °C after as long as 8 h of treatment. (Miraftab et al., 2014, Enayati et al., 2016, Wijanarko et al., 2016, Diez et al., 2022). Central to these processing methods, is the key benefit of a total absence of toxic additives, such as the commonly used GA, which has led to the increasing popularity of physical crosslinking for biomedical research applications (Muppalaneni, 2013, Teixeira et al., 2020, Golba et al., 2022).

### 1.5 Biomedical applications of electrospun PVA nanofibers

PVA nanofibers produced by electrospinning have been used within the major biomedical domains of wound dressings, drug delivery, and TE, due to their tuneable characteristics (such as hydrophilicity, mechanical strength, and porosity), and their capacity for loading with nanoparticles, pharmaceuticals, or formation of blends/composites (Rasouli et al., 2019, Garkal et al., 2021). Each of these application areas look to exploit different properties or features of electrospun nanofibers, thereby highlighting the versatile nature of these materials.

#### 1.5.1 Drug delivery

The use of electrospun nanofibers in drug delivery applications is favoured chiefly for tuneable release properties, with drugs loaded in one of four ways: as blends mixed directly with the polymer; added into a secondary nanocarrier, which is then spun into the fibres; surface loading of the drug to the nanofiber post-spinning; and in core shell configurations via coaxial electrospinning (Torres-Martinez et al., 2018).

Recent applications of PVA nanofibers include cancer treatment, via the combination of gold nanoparticles (Yan et al., 2016, Serio et al., 2021), and formation of a core-shell nanofiber for the tuneable delivery of anti-cancer agent doxorubicin within a PVA core and PCL outer shell (Yan et al., 2020). Drug-loaded membranes are not just used as delivery vehicles, but are often combined with other biomedical applications, such as wound dressings and TE. Some examples include the incorporation of antibiotics together with anti-microbial metal

nanoparticles for wound healing (El-Okaily et al., 2021), as well as the delivery of proteins, growth factors, and bioactive glass in TE contexts (Darbasizadeh et al., 2019, Mohammadi et al., 2019).

### *1.5.2 Wound dressings*

Chronic wounds, such as pressure ulcers, venous ulcers and diabetic foot ulcers, affect a large proportion of the world population, with an estimated 1 in 50 patients in developed countries likely to experience this silent epidemic during their lifetime (Jarbrink et al., 2016). Electrospun materials, especially as composites, are finding increasing use as chronic wound dressings, due to their capacity to reduce scarring (Mulholland, 2020). Preferred properties for wound dressings found in electrospun materials include their ability to act as a bacterial barrier, whilst allowing good gas exchange, and enabling high absorbance of exudates (Kumar and Rajan, 2022).

Much of the research on PVA nanofibers for wound dressings is focused on antibacterial agents of one kind or another. Recent examples include: polymer blends that also feature antibiotics, such as ciprofloxacin (Shankhwar et al., 2016, Yerra and Dadala, 2022); green antimicrobial alternatives in the form of plant mucilage extracts (Jafari et al., 2021, Sen et al., 2022); and formation of a bi-layer wound dressing containing copper nanoparticles within the outward facing layer of nanofibers (Lemraski et al., 2021). PVA has also been reported to have been combined with casein, so as to improve the haemostatic properties of the dressings (Biranje et al., 2019).

### *1.5.3 Tissue engineering*

Utilisation of electrospun materials in TE is extensive, not only for their properties as drug delivery vehicles and high diffusivity that have already been discussed, but also because of the near biomimetic quality of the fibres themselves and their resemblance to the extracellular matrix (ECM) (Teixeira et al., 2020). The ability to control the orientation, porosity, and 3D structure of electrospun materials through simple process adjustments provides a highly promising tissue scaffolding technology, to be applied across a wide range of TE applications.

**Table 1.4** summarises some modern applications of PVA electrospun materials in TE providing a summary of some recent uses, including any blended polymers and bioactive components. Due to the extremely complex nature of human tissues, there is no one-size-fits-all ideal blueprint or specific set of properties a scaffold must possess, and the desired parameters will rather vary from tissue to tissue. For example, (Shankhwar et al., 2016)

created materials for bone TE with ultimate tensile strength (UTS) in the range of 5.5-26 MPa, which is approximately an order of magnitude less than that of cortical bone, (~93-135 MPa; (Morgan et al., 2018)). By comparison, human corneal tissue has significantly different design requirements, with a UTS of 3-5 MPa (Kong and Mi, 2016). Factors such as fibre alignment, can also be extremely cell specific, and dependent upon the potential need to orientate cells (e.g. in the case of nerve or muscle cells), compared to skin cells which have more random arrangements.

**Table 1.4.** Recent literature on the use of PVA nanofibers in TE.

Tissue type	Polymer composition	Bioactive component	Notable morphology/production method	Reference
Bone	PVA-Gelatine	Biphasic calcium phosphate	-	(Nguyen et al., 2018)
	PVA	SiO <sub>2</sub>	-	(Xia et al., 2018)
	PVA	HAp	-	(Hartatiek et al., 2019)
	PVA	CNF and HAp	-	(Enayati et al., 2018a)
	PVA-SF	AgNPs	-	(Mejia et al., 2021)
Vascular	PVA	-	-	(Thomas and Nair, 2019)
	PVA + PCL-Gelatin	-	Co-electrospun	(Tan et al., 2016)
Nerve	PVA-Chitosan	Nerve growth factor	-	(Mottaghitalab et al., 2011)
Cartilage	PVA-Chitosan	CaCO <sub>3</sub>	Visible encapsulated particles	(Sambudi et al., 2015)
	PVA-SF	-	-	(Pillai et al., 2016)
Skin	PVA-SA	-	-	(Jadbabaei et al., 2021)
	PVA + PCL	Aloe Vera (PCL fibre)	Co-electrospun	(Shabannejad et al., 2020)
	PVA	Graphene oxide	-	(Narayanan et al., 2020)
Cardiac	PVA-SF	-	-	(Sayed et al., 2019)
Muscle	PVA	Eumelanin*	-	(Srisuk et al., 2018)

\*Eumelanin is a conductive nanoparticle, and not bioactive *per se*.



Simple needle-based lab scale electrospinning setups were employed for the production of all the materials listed in **Table 1.4**, and though many of these example materials were created without any secondary polymer, in the majority of cases, crosslinkers, such as GA or citric acid, were used to stabilise the fibres. The process of chemical crosslinking of PVA appears to be an accepted practice within TE research, with some instances of no crosslinking being used where gelation is desirable. Nevertheless, and taking into account the arguments against the use of chemical crosslinking presented in section 1.4.3.1, the potential for crosslinker-free PVA scaffolds within the field of TE is worth exploring.

## 1.6 Blood salvage

Allogeneic blood transfusions (ABTs), though overwhelmingly lifesaving, are not without risk, and suffer from high cost and supply issues. Patient autotransfusion in the form of blood salvage, on the other hand, can be viewed as a low cost, low risk alternative, and involves the return of blood shed intraoperatively back to the patient. Blood salvage [sometimes known as intraoperative cell salvage(ICS)] is used routinely across a range of surgeries, but its use in oncological applications remains limited due to concerns of re-introduction of circulating tumour cells (CTCs) to the patient (Sikorski et al., 2017). While some existing guidelines encourage its use in certain oncological contexts (Klein et al., 2018), evidence suggests that recurrence rates of cancer may still be higher in patients that receive autotransfusions intraoperatively from blood salvage, compared to those that donate blood pre-operatively for autotransfusion during surgery (Murtha-Lemekhova et al., 2022). Oncological surgeons, therefore, lack confidence in the use of current blood salvage platforms, and further innovation is needed for their routine adoption in the oncological setting, and especially in the instances of primary tumour surgery.

### *1.6.1 Cell separation of whole blood*

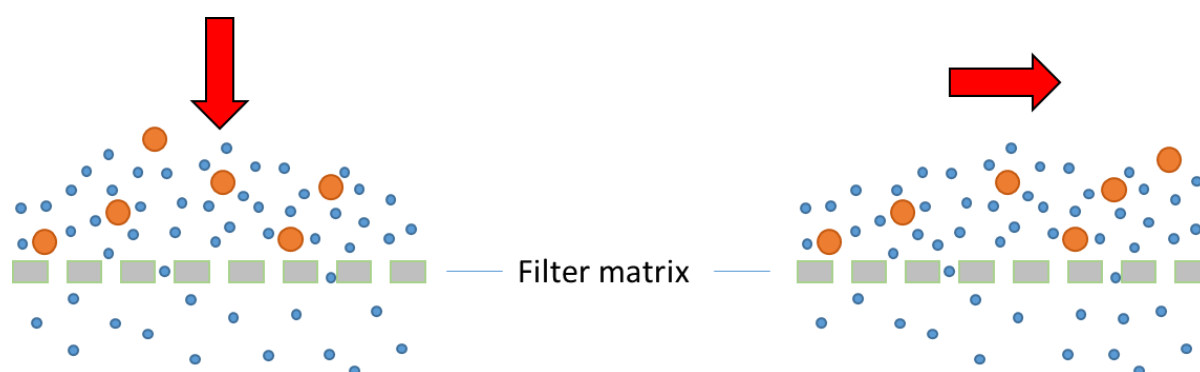
Whole human blood is a complex heterogenous mixture containing numerous distinct cell populations. Cell separations from blood are often carried out for various reasons, with examples being the isolation of rare cell types (such as eosinophils and basophils), for the study of inflammatory and allergic responses, the purification of erythrocytes for cell salvage, the extraction of leukocytes for immunotherapies, and the capture of CTCs for research. Due to the differences in morphology, size, density, and physiology of these populations, the best

separation method is typically dependent on the target cell, its characteristics, and the specifications of the final product. The optimal isolation method is also dictated by factors such as the size of the sample to be processed and processing time or rate.

Cell separation, *i.e.*, the removal of unwanted cells from a target population, is based on their physical or surface properties. Physical properties generally include size and density, whilst surface properties are factors such as antigen expression and adherence interactions (Kumar and Lykke, 1984). There are four major categories of cell separation explored here, namely filtration, centrifugation, fluorescence-activated cell sorting (FACS), and magnetic-activated cell sorting (MACS).

### 1.6.1.1 Filtration

Filtration separates cells based on size and can be used as a standalone method or, more commonly, as a pre-treatment step to other methods (Niazi, 2016). Based on the direction of flow, filtration can be classified as dead-end (alternatively known as conventional) or tangential flow (also known as cross flow; see **Figure 1.14**). Cells (shown in orange) are too large to penetrate the pores and therefore are retained by the filter and separated from the remaining components (represented in blue) present in the feedstocks.



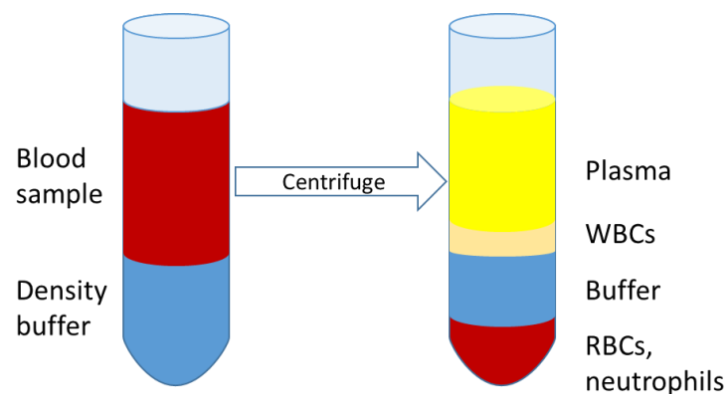
**Figure 1.14.** Common filtration methods with flow direction indicated by the red arrow. Left hand side: conventional or dead-end flow filtration. Right hand side: Tangential or cross flow filtration.

Dead-end filtration can suffer from the limitation of the pores becoming clogged quickly, in a process known as caking (Calabrò *et al.*, 2011). This behaviour has however been utilised such as in one early documented method of filtration, which employed the use of adhesive tape as a dead-end filter for the isolation of cancer cells from whole blood, by facilitating their retention and subsequent adhesion to the filter while other products were able to pass through to the filtrate (Seal, 1964). Tangential flow filters are less susceptible to pore fouling and can

maintain a constant membrane flux, which makes them more suitable for continuous processing. The downside of this, however, is the need for recycling in order to maximise recovery, which leads to increased energy consumption (Van der Bruggen and Luis, 2018).

### 1.6.1.2 Centrifugation

Centrifugation separates cells based on their relative densities in bulk quantities. Density gradient filtration is shown in **Figure 1.15**, where blood is layered upon density buffer solutions, in order to fractionate cells into either continuous or discontinuous gradients. The sample is then centrifuged and forms a discontinuous gradient, with denser components, such as red blood cells (RBCs) and neutrophils, at the bottom, through to the least dense components, such as plasma, at the top.



**Figure 1.15.** Diagram of a sample before and after density gradient centrifugation (discontinuous gradient).

Density gradient centrifugation is a well-established process and used routinely for cell pelletisation or for isolation/enrichment of various components from whole blood (Dagur and McCoy, 2015). Over 40 years ago, separation of lymphocytes from whole blood was achieved through a two-step centrifugation, involving first the separation of blood mononuclear cells, followed by a second centrifugation step using an alternative density buffer, to give a leukocyte yield of ~75% at ~63% purity (Brandslund *et al.*, 1982). Around the same time, a similar two-step method for the isolation of basophils (one of the rarest cells in whole blood) was devised, although with low efficiency (~20%) (Raghuprasad, 1982).

The apparent lack of specificity during gradient centrifugation (since cells of sufficiently similar density are likely to occupy the same fraction within the sample or form a continuous gradient) introduces the need for multiple centrifugation steps, as well as additional separations based

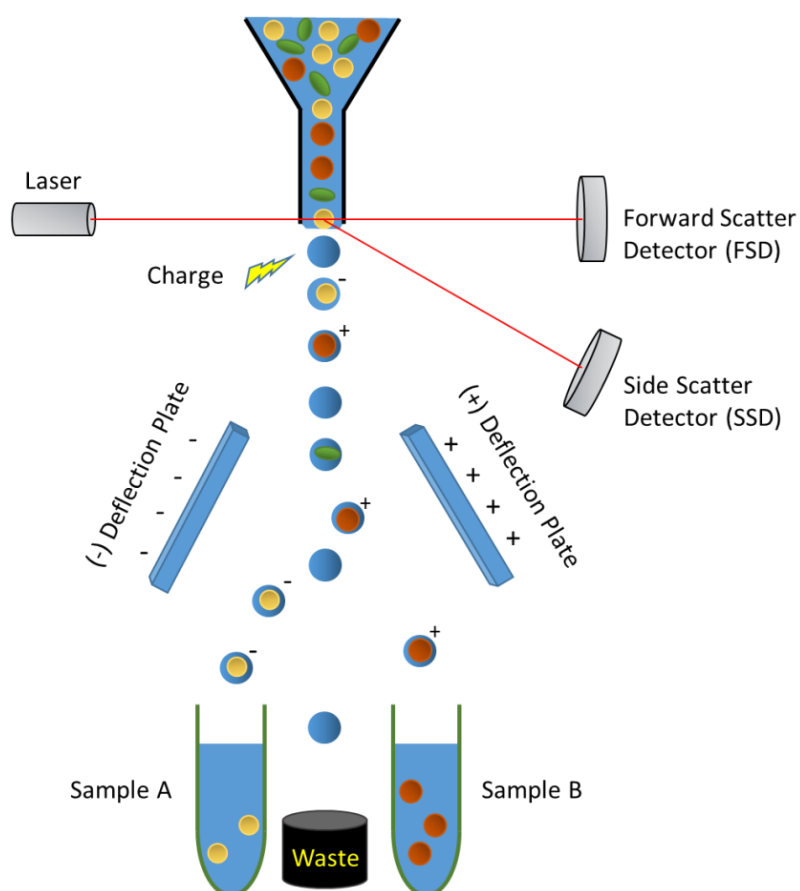
on more specific interactions. Therefore, current protocols for basophil and eosinophil isolation employ density gradient centrifugation, followed by MACS (discussed in section 1.6.1.4), resulting in the desirable high overall cell purities (~99%) (Schroeder and Bieneman, 2016).

An extension of density gradient centrifugation is ultracentrifugation (centrifugation carried out at speeds up to 150,000 RPM and 1,000,000 *g*), which is already being used to separate nanoscale membrane bound vesicles called exosomes from stem cell culture supernatant and directly from whole blood (Gupta *et al.*, 2018, Wu *et al.*, 2017).

### 1.6.1.3 Fluorescence-activated cell sorting

FACS separates cells individually by organising them into a single line by a process known as hydrodynamic focussing. Each cell is then deposited with its own droplet, analysed spectroscopically, charged according to those properties, and then sorted by directing plates into target receptacles. The principle of the separation is illustrated in **Figure 1.16**. Modern FACS is based on flow cytometry, which was created in the mid-60s and sorted cells based on volume and complexity. A laser and single detector setup (forward scatter only) would direct cells based on the degree of light scattering. The limiting factor of this meant that any complex suspensions containing similarly sized but functionally distinct cells could not be isolated effectively. This, however, paved the way for current FACS devices, which have since become a core tool in biological and biomedical research and are often described as the 'gold standard' of cell sorting (Faraghat *et al.*, 2017, Sutermeister and Darling, 2019).

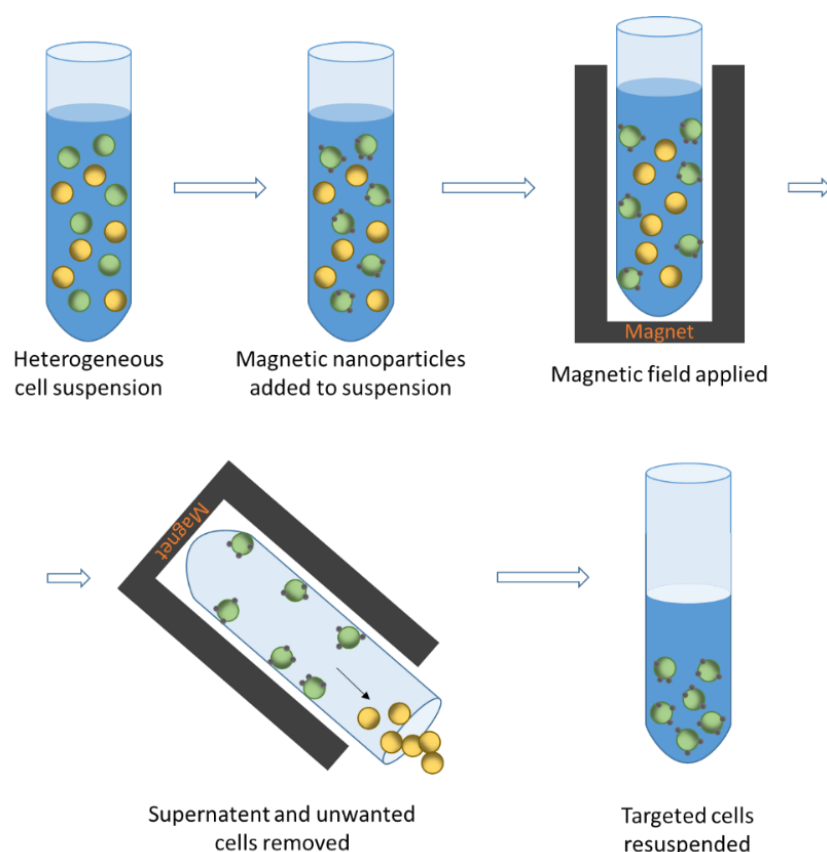
FACS uses conjugated fluorochromes bound to specific surface markers of the cell, typically via immunoaffinity interaction. This results in fluorescent light scattering across a range of wavelengths, which can be analysed by relative intensity, in order to calculate the extent of protein expression and subsequently identify and sort cells into homogenous samples. Reported sorting rates are typically 5,000-50,000 cells·s<sup>-1</sup>, with the highest throughput device boasting 100,000 events analysed per second, and 70,000 sorting actions (Beckman Coulter, 2017). While FACS can create a very pure and homogenous sample, it suffers from a relatively poor cell yield (as low as 30%) and lack of scalability (Sutermeister and Darling, 2019).



**Figure 1.16.** Diagram illustrating cell separation based on FACS. Cells are analysed and deposited in individual droplets which are charged based on the droplet's combined optical properties. The charge droplet passes through the electric field generated by the deflecting plates and is funnelled into sample collection tubes.

#### 1.6.1.4 Magnetic-activated cell sorting

MACS is underpinned by the same immuno-physiological principles and methods as FACS, meaning that it utilises antibody labelling to select for specific cells. The difference between MACS and FACS however, is that MACS employs magnetic nanoparticles to carry out the separation. These particles are tagged with cell specific antibodies, which bind to the cells of interest, allowing both the particle and cells to be retained from the bulk mixture through the aid of a magnetic field, while all other components are removed from the mixing chamber. **Figure 1.17** illustrates the separation principle of MACS, where antibody-conjugated magnetic nanoparticles are added to a heterogeneous cell mixture, and selectively bind to a target cell population expressing specific antigens. Cells bound to the nanoparticles are then separated from the mixture using a magnetic field, whereas the none bound cells are discarded. Target cells are subsequently recovered by removal of the magnetic field.



**Figure 1.17.** Diagram of positive selection of a target cell population using MACS.

Early magnetic separation technology did not feature antibody labelled nanoparticles to form magnetic complex, as with modern MACS, but rather depended on the innate paramagnetic properties of deoxygenated haemoglobin in erythrocytes (Bren *et al.*, 2015, Melville *et al.*, 1975, Owen, 1978, Pauling and Coryell, 1936), and this principle has also been demonstrated as a continuous process (Han *et al.*, 2003, Jung and Han, 2008, Takayasu *et al.*, 2000). MACS has applications as an alternative to FACS (with conjugated superparamagnetic nanoparticles to enrich large samples of cells), as well as the routine isolation of leukocyte subpopulations (Miltenyi *et al.*, 1990, Molday *et al.*, 1977).

MACS is often considered as a bulk processing method, in contrast to FACS, as it processes numerous cells into subpopulations in parallel, rather than in series. High volume MACS handles around  $10^9$  cells (Faraghat *et al.*, 2017) with processing times of 5-30 min (Sutermaster and Darling, 2019). To contextualise this, one unit of blood contains approximately  $2.5 \times 10^{12}$  cells (Downey, 2017, Osei-Bimpong *et al.*, 2012, Stemcell Technologies, 2017), making this the equivalent of 0.21 mL of blood per cycle.

### 1.6.1.5 Comparison of various cell separation methods

Although they are extremely selective compared to filtration and centrifugation, MACS and FACS suffer from low throughputs. Looking at their relative performance, FACS and MACS can achieve processing rates of  $3.2 \times 10^5$  and  $1.6 \times 10^6$  cells·min<sup>-1</sup>, respectively (Sutermaster and Darling, 2019). When compared with devices employed for ICS (based on filtration and centrifugation, discussed in section 1.6.3), this translates into 94 days for FACS and 19 days for MACS, to process a single unit of blood. Furthermore, FACS has high capital cost, is only designed for analytics purposes, and separations must be performed in series. MACS can be carried out more easily in parallel with multiple devices, so has greater scale out potential (Sutermaster and Darling, 2019), but the handling requirements would also increase, rendering it impractical in its current state.

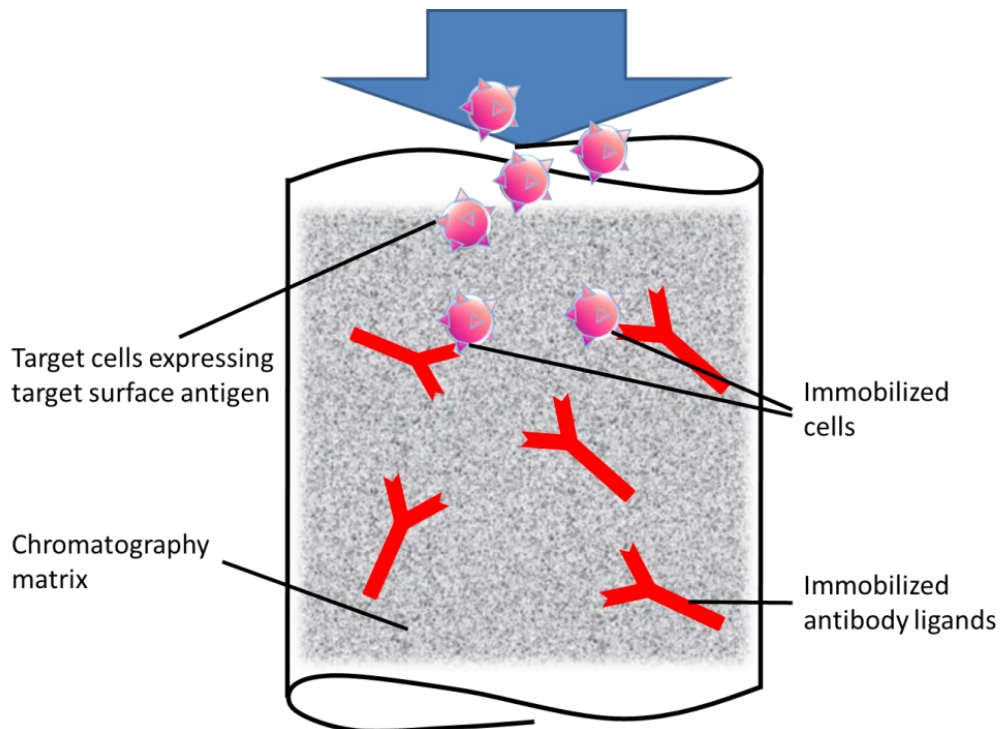
The common theme within FACS and MACS is the use of antibody-antigen binding as part of the isolation process, which removes target cells with high selectivity. However, it should be considered that the saturation of surface-markers during the initial labelling phase may make identification of the target cells difficult post-process. If the epitopes become saturated, they will most likely be unable to bind with the signal or sensor antibodies, resulting in false negatives (Tomlinson *et al.*, 2013).

### 1.6.2 Chromatography for cell separations

Chromatography is a highly popular separation technique in which complex solutions are separated according to the affinity of each species within the solution for the chromatography matrix (also known as a stationary phase or chromatography media) *versus* the mobile phase (*i.e.* solvent). Chromatography can achieve high resolution separation, and based on the principle of the interaction it can be classified into ion-exchange, size exclusion (or gel permeation or gel filtration), affinity, reverse phase and hydrophobic interaction (Coskun, 2016). Typically, cell chromatography is performed using some variant of affinity chromatography, because of the advantages it offers in selectivity.

There are different types of affinity chromatography depending on the ligands which are immobilised on the stationary phase. In the case of immobilized metal affinity chromatography, for example, cells are passed through a column in suspension and adsorb with a high degree of specificity to the metal-ion ligands on the surface of the material, followed by their desorption. This positive selection through a 'bind-elute' process has been used in purification of *E.coli* on a cryogel matrix (Dainiak *et al.*, 2005). A more recent development is the use of antibodies as immobilised ligands and is known as immunoaffinity chromatography (see W. J. A. Homer, PhD Thesis, Aston University, 2023

**Figure 1.18).** In this process, a high degree of specificity can be achieved if the surface antigens of the cells in solution to be separated are well understood. This technique has been employed successfully for the removal of lymphocytes directly from whole blood (Mohr *et al.*, 2018).

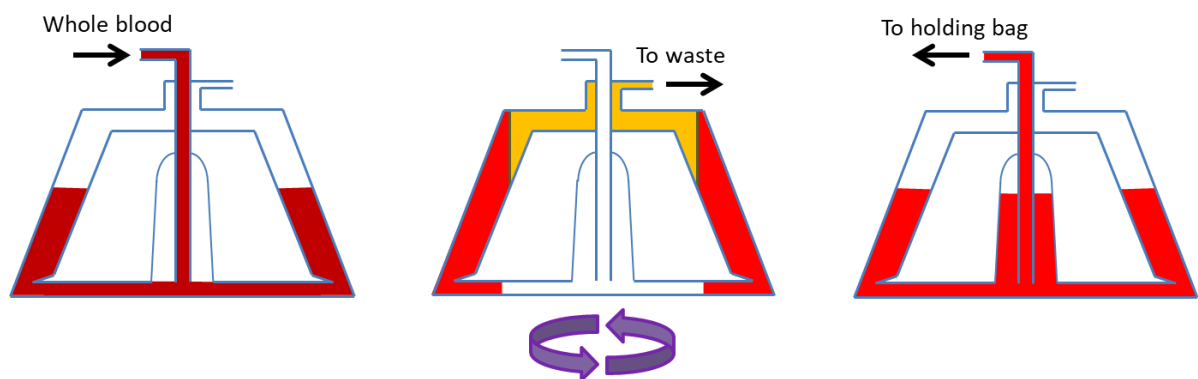


**Figure 1.18.** Diagram of an immunoaffinity separation process. Antibodies immobilized on the substrate bind with a high degree of selectivity to the expressed surface marker antigen on the target cells.

### 1.6.3 Existing blood salvage platforms

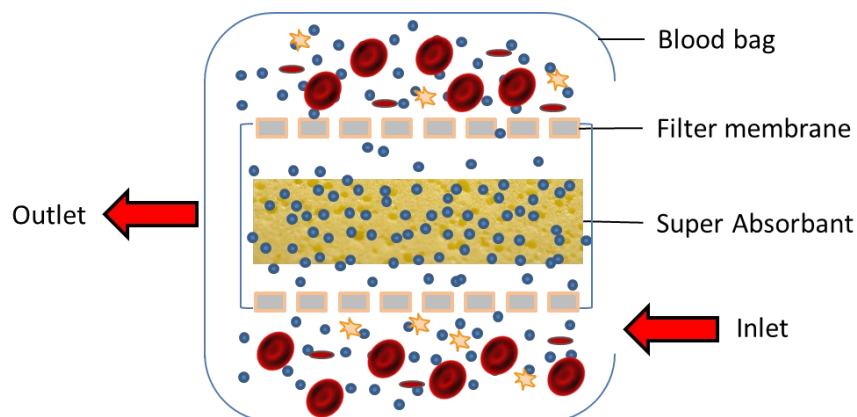
The current commercially available products for ICS which are based on centrifugation, include the Cell Saver (Haemonetics, Boston, USA), Sorin XTRA Autotransfusion System (LivaNova, Gloucester, UK), and the CATSmart (Fresenius Kabi, Cheshire, UK) (Haemonetics, 2019, JPAC, 2020). The first two are discontinuous flow systems, in which the blood is centrifuged using equipment known as ‘bowls’ (**Figure 1.19** shows a diagram of a Latham bowl operating sequence). According to the manufacturer, Haemonetics Cell Saver can process up to  $800 \text{ mL} \cdot \text{min}^{-1}$  in ‘emergent situations’, with typical cycle times between 3 and 7 min. This maximum processing rate equates to roughly  $6.1 \times 10^{10}$  cells per second (Haemonetics, 2019). In operation the Cell Saver retains predominantly RBCs, and depletes other large biological molecules from the shed blood (Boyle *et al.*, 2019).





**Figure 1.19.** Centrifugal separation diagram of a Latham bowl device. The device is filled with whole blood, centrifuged to achieve separation whilst extracting waste, and then concentrated RBCs are pumped into a holding bag for reinfusion.

The Sorin XTRA system is capable of processing a 225 mL bowl in approximately 5 min, or in approximately 3 min in emergency situations (Sorin Group, 2013). This translates to 45-75 mL·min<sup>-1</sup> processing rate. The CATsmart utilises a continuous rotary system (classed as a continuous flow device), and is able to produce RBC output rates ranging from 20-100 mL·min<sup>-1</sup> (Fresenius Kabi, 2020), which is estimated to be equivalent to 40-200 mL·min<sup>-1</sup> whole blood processing rate.



**Figure 1.20.** Diagram of the HemoSep ICS system. Whole blood is collected in the outer layer of the blood bag, where plasma is depleted through osmosis across the filter membrane towards the super-absorbent in the internal layer.

The HemoSep (Advancis Surgical, Kirkby-in-Ashfield, UK; illustrated in **Figure 1.20**), a commercial blood processing unit employed in ICS, uses filtration and osmotic pressure, combined with a super-adsorbent membrane material, to achieve haemoconcentration in

excess of a single transfusion unit of blood per bag through plasma extraction (Advancis Surgical, 2017, Boyle et al., 2019). It is capable of processing an average of 775 mL of blood during surgery, which can then be reinfused to the patient within 60 min following collection (Gunaydin and Gourlay, 2013, Hogan et al., 2015). This haemoconcentration process also reduces instances of post-operative ABTs through retention of other blood components including fibrinogen and platelets (Gunaydin et al., 2018, Advancis Surgical, 2017).

### 1.7 Conclusion

The technology of electrospinning continues to develop and expand year upon year, both in terms of academic research and commercial use. Scalable production is of particular importance for biomedical applications but is seldomly discussed in the relevant literature, compared to the more specialist electrospinning research. Given the overwhelming use of needle-based systems, there is a need to translate existing ideas to larger scale systems, so that their scale-up potential can be explored, as well as to introduce novel platforms, such as the AC systems outlined at the beginning of this chapter.

PVA was identified as a suitable polymer for biomedical applications, due to its notable biocredentials and an established track record in both electrospinning and biomedical literature. Nevertheless, it is posited that there may exist an over dependence on toxic crosslinkers to stabilise the highly hydrophilic PVA against dissolution in aqueous environments. Employing physical crosslinking methods, can overcome this limitation and may yield promising results when biomaterials need to be created from electrospun PVA. This can be very useful in TE and in particular wound dressings, where prolonged water stability of the nanofibers is favourable.

Finally, discussions with clinicians drew attention to the problem that exists with respect to blood salvage and its use, or lack thereof, in cancer surgeries. Examination of the existing platforms quickly reveals that the issue resides within the method of cell separation deployed, as it lacks specificity. One potential solution to this problem is to combine immunoaffinity cell chromatography with the concept of blood salvage. The ability to tune the morphology of the electrospun material, in conjunction with 'physical' stabilisation of the electrospun PVA nanofibers, can produce biocompatible membranes, which will allow the processing of blood cells, and thus further expand the application for electrospun nanofibers within the clinical setting.

## 1.8 Aims and structure of this thesis

The aim of the research presented within this thesis is to explore potential biomedical applications of crosslinker-free, thermally stabilised, pure PVA nanofibers produced by different electrospinning platforms, with specific interest in cell processing and TE applications. Each subsequent chapter is presented in self-contained, manuscript format, with a brief introduction section recapping key details relating from this chapter, followed by methods, results and conclusion. The topics and aims are broken down into the following chapters.

Chapter 2 characterises the effect of extended duration heat treatments, beyond those found in literature, on a range of materials produced from low (88%) to high (99%) DH PVA. The heat treatments are explored via standard needle electrospinning and subsequently using cutting edge needleless platforms based on both DC and AC voltage. This chapter aims to:

- Establish appropriate, application specific, duration limits for the heat treatment process.
- Apply treatments within these limits to materials produced on advanced electrospinning platforms and explore the role of these platforms and their effect on chemical structure and fibrous morphology.
- Examine the effect of heat treatment duration on preservation of fibre morphology in aqueous environments.

In the context of a prospective blood salvage platform, Chapter 3 progresses potential candidates identified in Chapter 2 as supports for cell processing. The primary objective of this chapter was to explore what effect, if any, heat treatment duration and electrospinning platform has on cell flowthrough behaviour in a convective flow system, and investigate this with a range of cell populations.

Chapter 4 follows on with a more detailed examination of the flow behaviour through electrospun membranes using computational fluid dynamic (CFD) modelling tools. The aim of the CFD work was to identify possible issues such as flow channelling during the operation of a nanofibrous blood salvage device. This chapter also contains some cursory designs for the prospective housing for nanofibrous materials for use in blood salvage and provide some initial insights and considerations for further development.

Finally, chapter 5 revisits needleless DC electrospinning and introduces the use of 98% DH PVA. The scope of this chapter is to demonstrate another potential application of the heat

treated electrospun membranes, this time within the TE field. The objective was to compare heat treated materials with differing DH produced on the same platform for their suitability in TE applications. This was done through extensive chemical and biological characterisation which included bio- and haemocompatibility assays.

## Chapter 2

# Manufacture and characterisation of thermally stabilised poly(vinyl alcohol) membranes produced by electrospinning

### 2.1 Introduction

As previously described, PVA is a hydrophilic polymer used commonly in a broad array of biomedical applications and has the benefit of Food and Drug Administration (FDA) approval. It is typically produced by the hydrolysis of PVAc in the presence of an alkali catalyst and alkanol solvent, such as methanol (Hedayati et al., 2022, Hallensleben et al., 2015). The degree to which acetate groups are converted to alcohol groups is known as the degree of hydrolysis (DH), and is influenced by the time of reaction, temperature, and catalyst ratio (Aruldass et al., 2019). The resultant polymer is commercially available in various of degrees of hydrolysis (80%-99%), with a degree of polymerisation typically between 200 and 3000 (Sato, 2021).

PVA is a popular choice of starting material for biomedical applications due to its biocompatibility and lack of cytotoxicity, along with its tendency to form hydrogels with bioadhesive properties (Gaaz et al., 2015). In its hydrogel form it has been used for medical implants and devices, such as synthetic blood vessels, and as part of bone and cartilage tissue replacements (Kumar and Han, 2017), as well as biosensors, drug delivery vectors and supercapacitors (Wang et al., 2021). PVA is also a common polymer for the creation of non-woven nanofibers via electrospinning, with common biomedical applications in TE, such as wound dressings and vascular scaffolds (de Castro et al., 2022, Jatoi et al., 2019, Teixeira et al., 2020). One of the biggest challenges with PVA electrospun supports, however, is the highly hydrophilic character of the polymer and therefore its tendency to form gels upon contact with aqueous solutions and subsequent loss of the fibrous morphology. It has been

shown that the degree of hydrolysis can impact water stability of nanofibers alone, but the effect is limited (Park et al., 2010). There is therefore a need to preserve against the swelling and dissolution of the nanofibers formed during electrospinning by treatment or otherwise modification of the materials. Chemical crosslinking using glyoxal, citric acid, succinic acid and GA, is a method commonly employed to stabilise the nanofibers (do Nascimento et al., 2021, Diez et al., 2022, Plieva et al., 2006). While this method can be highly effective, many crosslinkers can be cytotoxic and therefore prohibitive for medical applications.

Chemical-free crosslinking of PVA nanofibers is typically described as physical crosslinking. Given that PVA is a semi-crystalline polymer, the goal of this process is generally to enhance its crystallinity and thereby improve the water stability of the fibres. These methods include: the use of alternative solvents, such as methanol, which displace residual water within the material and result in enhanced degree of ordering of the polymer chain; and, freeze thawing and heat treatments, which aim to liberate internally bound water without a displacing species (Miraftab et al., 2014, Yao et al., 2003, Yang et al., 2008, Enayati et al., 2016, Tretinnikov and Zagorskaya, 2012).

Herein we present the production of a series of non-woven PVA supports employing different electrospinning methods, *i.e.* needle DC, needleless DC, and AC. We then investigate ways to increase their water stability and preserve their fibrous morphology without the use of chemicals. We opt for the use of heat treatment at 180 °C as this temperature has been found to more effectively preserve the morphology of the PVA nanofibers after water immersion compared to lower temperatures, and investigate the effect of heating durations on the physical and chemical characteristics of the final materials (Miraftab et al., 2014, Chee et al., 2021, Enayati et al., 2016, Diez et al., 2022).

## 2.2 Materials and Methods

### 2.2.1 Materials

PVA 'Mowiol 18-88' (88% hydrolysed, 130,000 Mw); PVA 'Mowiol 28-99' (99% hydrolysed, 145,000 Mw); and sodium azide [ $\geq 99.5\%$  for gel permeation chromatography (GPC)] were purchased from Sigma-Aldrich Company Ltd. (Missouri, USA). Ethanol (AR, purity  $\geq 99.8\%$ ); deuterium oxide [ $D_2O$ , 99.8% for nuclear magnetic resonance (NMR)]; and water (HPLC water for GPC) were acquired from Fischer Scientific UK Ltd. (Zurich, Switzerland). Water for

electrospinning solutions All purchased chemicals were of analytical grade and used without further purification (unless stated otherwise).

## 2.2.2 Production methods

### 2.2.2.1 Solution preparation

Solutions were prepared by mixing solvent systems (either pure de-ionised (DI) water [Resistivity > 15 MΩ] or DI Water combined with 10% ethanol) with PVA and heating at 90 °C for 4 h while stirring intermittently. After fully dissolving the PVA, solutions were allowed to cool to room temperature and left to settle overnight before final stirring to ensure homogeneity.

### 2.2.2.2 Electrospinning

Three different methods of electrospinning were employed during this work, two using DC power, namely needle-based and needleless, and one using AC power. Please note that 'needleless' and 'Nanospider' may be used interchangeably in this chapter.

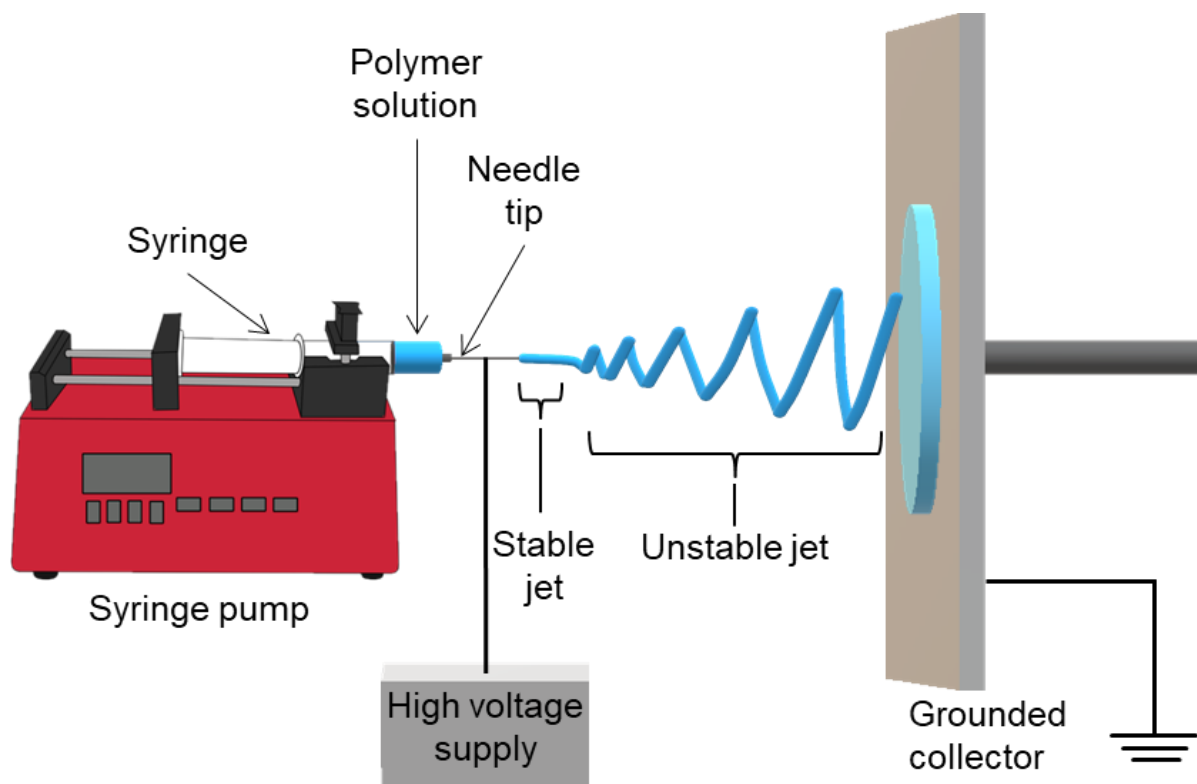
#### 2.2.2.2.1 Needle DC electrospinning

Solutions were loaded into a disposable polypropylene syringe combined with a 20G blunt point needle (Hamilton Kel-F Hub Blunt Point Needle; Fischer Scientific UK Ltd., Loughborough, UK) and mounted to a syringe pump (Alladin-8000, World Precision Instruments, UK). Aluminium foil was attached to a collector plate and positive voltage clip was applied to the needle tip directly, whilst the grounding clip was applied to the collector foil (see **Figure 2.1**). Climate control was not possible in this setup, but humidity and temperature were recorded using a humidity meter (Fisherbrand Traceable Humidity/Temperature Meter/Recorder, Fisher Scientific UK Ltd., Loughborough, UK) with all utilised samples being spun within the ranges of 19-20 °C and 27.5-35.3% RH.

Samples produced from 88% hydrolysed PVA were based on work carried out previously at Aston University using 14% (w/w) PVA in water, solution flow rate of 0.6 mL·h<sup>-1</sup>, 22 kV applied voltage and a tip-collector distance of 15 cm (Diez et al., 2022).

Production of samples from 99% hydrolysed PVA required some optimisation (briefly discussed in section 2.3.1.1), following on from starting operating conditions as described in literature (Koski et al., 2004, Park et al., 2010, Mirafteb et al., 2014, Supaphol and Chuangchote, 2008). Final electrospinning parameters were identified as: 8% (w/w) PVA in a

9:1 water: ethanol (w/w) solvent; solution flowrate of  $0.3 \text{ mL}\cdot\text{h}^{-1}$ ; 9 kV applied voltage; and tip-collector distance of 15 cm.

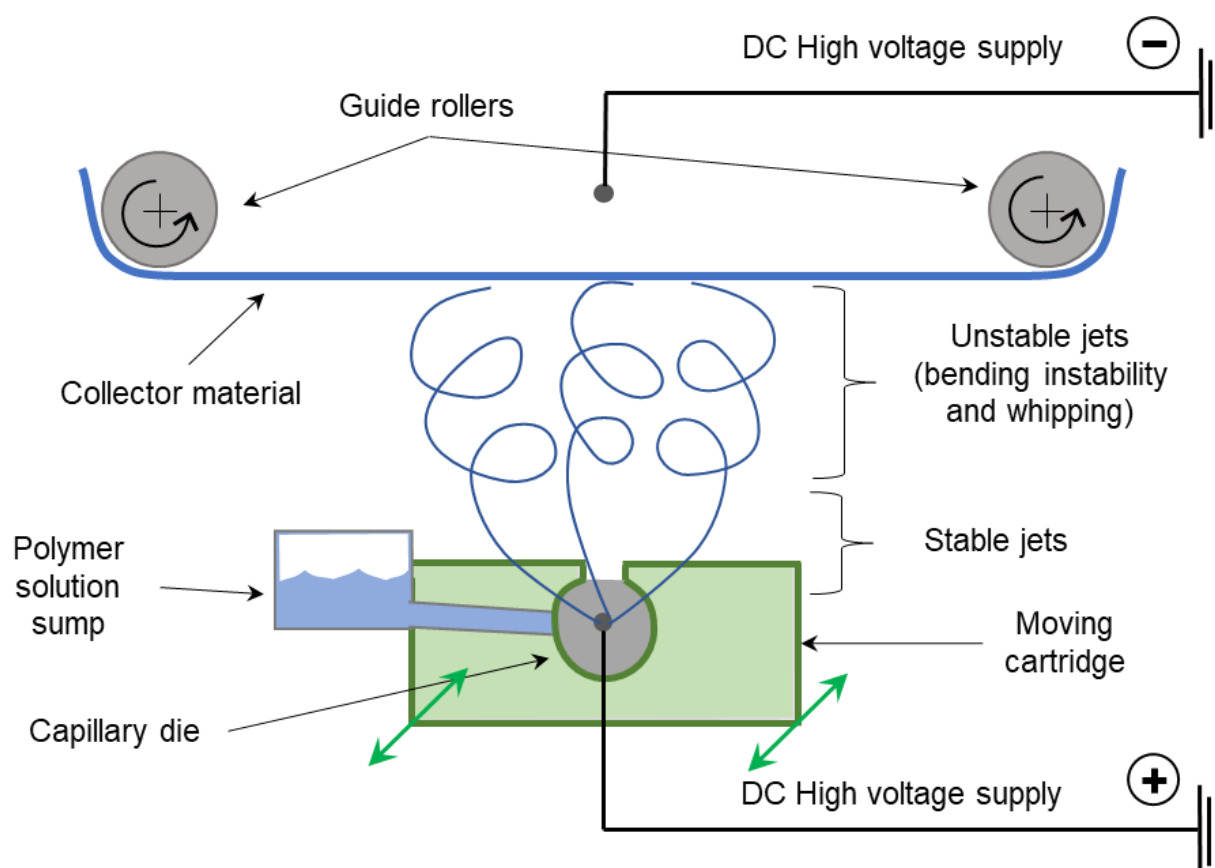


**Figure 2.1.** Illustrative drawing of needle-based electrospinning setup and process. A syringe pump flows polymer solution through a needle tip, to which a high voltage power supply is connected. Polymer just is then formed and propelled towards the grounded collected, forming a non-woven mat of nanofibers.

#### 2.2.2.2.2 Needleless DC electrospinning

Samples produced by needleless DC electrospinning technology with static wire spinning electrode (Nanospider™, Elmarco NS 1S500U; Librec, Czech Republic), used a 50 kV voltage differential (+40 kV and -10 kV) with an electrode separation distance of 16 cm (**Figure 2.2**). Spinning solution was applied to the positively charged electrode (wire with diameter 0.25 mm) by traversing cartridge with a capillary die diameter of 0.7 mm. Climate parameters were fixed at 22 °C and 30% RH by precision air conditioning unit (NS AC150, Elmarco; Librec, Czech Republic), and solution system used was a 9:1 (w/w) water: ethanol solvent ratio with 99% hydrolysed PVA at a concentration of 8% (w/w).

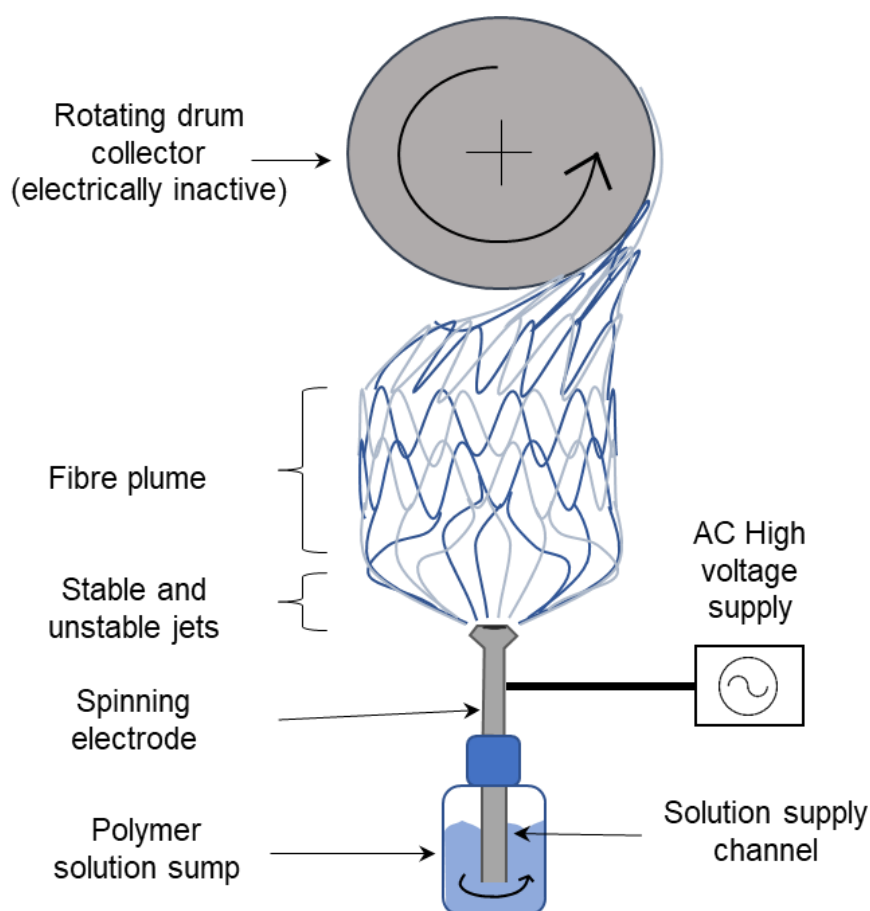




**Figure 2.2.** Illustrative drawing of wire-based configuration of needleless DC electrospinning used in the Elmarco Nanospider™.

#### 2.2.2.2.3 AC electrospinning

Samples produced by AC electrospinning employed a rod-like spinning electrode with emitter diameter of 22 mm [developed by TUL, (Kocis et al., 2018)], as illustrated in **Figure 2.3**. The electrically inactive drum had a diameter of 30 cm, rotated at 10 RPM and the emitter-drum surface distance was 17 cm. High voltage supply applied an effective voltage of 35 kV with a 30 Hz sinusoidal waveform to the emitter. The spunbond nonwoven fabric ( $30 \text{ g} \cdot \text{m}^{-2}$ ) that was used as collector material in DC spinning, was also applied to the drum of the AC equipment. AC samples were produced using pure water as a solvent.



**Figure 2.3.** Illustrative drawing of AC electrospinning with rod-like electrode and rotating drum collector.

### 2.2.2.3 Heat treatment

Electrospun samples were placed in open foil pouches and heat treated at 180 °C for a range of durations (0, 1, 2, 4, 8, 16, 24 and 32 h) in a forced convection drying oven (SciQuip Oven-80 HT; Newtown, UK), followed by cooling at ambient temperature (18-20 °C) for ~15 min.

## 2.2.3 Analytical methods

### 2.2.3.1 Scanning electron microscopy

Morphological analysis was carried out by SEM. Samples were prepared for analysis by sputter-coating with gold on a Quorum (Q150R ES) sputter coater and subsequently analysed with a Tescan Vega3 SB Easy Probe (Tescan, Brno, Czech Republic). SEM images analysed in ImageJ 1.52a software (NIH, USA) in order to assess average fibre diameter by taking at least 100 (with the exception of needle electrospinning) measurements from at least two images per sample.

### 2.2.3.2 Fourier transform - Infrared spectroscopy

Fourier transform infrared spectroscopy (FT-IR) was conducted with a Frontier Spectrometer (PerkinElmer Ltd., Waltham, MA, USA) combined with an attenuated total reflectance (ATR) accessory (GladiATR; Pike Technologies, Madison, WI, USA). Each scan was performed from 4000  $\text{cm}^{-1}$  to 700  $\text{cm}^{-1}$  with a resolution of 4  $\text{cm}^{-1}$  for a total of 16 scans per measurement.

### 2.2.3.3 Gel permeation chromatography

Aqueous GPC was employed to analyse changes in Mw distribution following electrospinning. Samples were prepared in 1.5 mL Eppendorf tubes by dissolving material in HPLC water with 0.02% sodium azide, to achieve a final concentration of  $\sim 4 \text{ mg} \cdot \text{mL}^{-1}$ . The samples were subsequently heated to 90 °C in a silicon oil bath, mixed with a vortex mixer, and left to cool before they were filtered through a nylon syringe filter with a pore size of 0.45  $\mu\text{m}$  (Fisher Scientific UK Ltd., Loughborough, UK). GPC runs were performed on a 1269 Infinity II (Agilent Technologies, Inc., Santa Clara, CA, USA) comprised of two PL aquagel-OH 8  $\mu\text{m}$  columns with Mw range limits of 100-10,000,000  $\text{g} \cdot \text{mol}^{-1}$ . Each column was calibrated using near monodisperse polyethylene glycol/polyethylene oxide standard. The data was analysed using Agilent GPC/SEC software (Agilent Technologies Inc., Santa Clara, CA, USA). Data normalisation for the purposes of proportional peak comparison was done with Microsoft Excel.

### 2.2.3.4 Nitrogen sorption porosimetry

Surface areas and pore volumes of the electrospun mats were determined by  $\text{N}_2$  porosimetry using a Quantasorb Nova 4000 e porosimeter and Novawin 11.03 software (Quantachrome, Boynton Beach, Florida, USA). Samples were outgassed in vacuo at 80 °C for 18 h prior to analysis, with specific surface areas calculated by applying the Brunauer–Emmet–Teller (BET) model over the relative pressure range  $p/p_0 = 0.04\text{--}0.16$  (where  $p$  = equilibrium pressure applied, and  $p_0$  = saturation vapour pressure of  $\text{N}_2$ ) of the adsorption isotherm where a linear relationship was maintained. These were then compared to theoretical specific surface areas calculated by the relationship of fibre diameter to surface area shown in equation 1, where  $r$  = average fibre radius and  $\rho$  = density of PVA.

$$\frac{2}{r\rho} = \text{specific surface area (Eq. 1)}$$

### 2.2.3.5 Proton nuclear magnetic resonance

$^1\text{H}$  NMR was used to examine chemical changes arising specifically from electrospinning. Samples were dissolved in  $\text{D}_2\text{O}$  at a concentration of  $\sim 4 \text{ mg} \cdot \text{mL}^{-1}$ . Testing was carried out on an Avance 300 spectrometer and visualised using TopSpin software (Bruker, Billerica, MA, USA).

### 2.2.3.6 Environmental scanning electron microscopy

To assess fibre morphology and swelling behaviour *in situ*, environmental scanning electron microscopy (ESEM) images were taken with a Quattro S environmental scanning electron microscope (Thermo Fisher Scientific, Waltham, MA, USA). Examination of swelling behaviour was done using initial conditions of 400 Pa with a stage temperature of  $2^\circ\text{C}$ . Pressure was increased gradually to 800 Pa to saturate the samples, and steadily reduced again, resulting in evaporation of surface moisture, and thereby allowing observation of morphological changes.

### 2.2.3.7 X-ray diffraction

The crystallinity of the materials was evaluated by X-ray diffraction (XRD) on a Bruker D8 Advance diffractometer, equipped with a LynxeyePSD detector (Bruker, Billerica, MA, USA) and with  $\text{Cu K}_{\alpha 1,2}$  radiation (40 kV and 40 mA), 0.02 mm  $\text{Ni K}_{\beta}$  absorber,  $5\text{--}50^\circ$   $2\theta$  range, a step scan of  $0.02^\circ$  with a sample rotation speed of 30 RPM. The degree of crystallinity was calculated using equation 2, where  $\alpha$  is the degree of crystallinity,  $I_c$  is the sum of the intensity under the crystalline peaks, and  $I_a$  is the sum of the intensity under the amorphous sections of the spectra.

$$\alpha (\%) = \frac{I_c}{I_c + I_a} * 100 \quad (\text{Eq. 2})$$

### 2.2.3.8 Tensile testing

The mechanical properties of the mats were measured by means of uniaxial tensile tests using an Instron 5965 (Instron, High Wycombe, Buckinghamshire, UK), equipped with a 50 N load cell, at a rate of  $10 \text{ mm} \cdot \text{min}^{-1}$ , with samples prepared using a punch tool in a dumb bell shape ( $21 \mu\text{m}$  average thickness,  $n=3$ ) and loaded until failure (defined as a 50% reduction from peak force). Stress-strain curves were obtained and mean averages of the UTS and strain at UTS were calculated.

### 2.2.3.9 *In vitro* cytotoxicity testing

The effect of potential leachables from the electrospun materials on metabolic activity was assessed using the extract cytotoxicity test (Baek et al., 2005, Diez et al., 2022). Human mesenchymal stem cells (hMSCs) were seeded at  $6 \times 10^3$  cells  $\cdot$  cm<sup>-2</sup> in a 96 well plate (tissue culture plastic) and cultured in cell growth medium comprising of Dulbecco's modified eagle medium (DMEM), 10% fetal bovine serum (FBS), 2 mM UltraGlutamine and 1 ng  $\cdot$  mL<sup>-1</sup> bFGF, at 37 °C and 5% CO<sub>2</sub> for 3 days. In parallel, electrospun mats (4 mg  $\cdot$  mL<sup>-1</sup>) were added to fresh culture medium and left in the incubator for 24 h in order to produce 'conditioned media'. After 3 days, the cell growth medium was replaced with the conditioned media and incubated for another 24 h. Cell counting kit-8 (CCK-8) was then added to all wells and allowed to develop for 4 h as per manufacturer's protocol, before measuring the absorbance at 450 nm using a Multiskan EX plate reader (Thermo Fisher Scientific, Waltham, MA, USA). Cells cultured in the presence of 10% (v/v) ethanol from day 3 were used as positive controls.

## 2.3 Results and Discussion

### *2.3.1 Needle-based electrospinning of 88% hydrolysed PVA and the effects of extended thermal stabilisation*






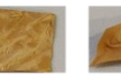


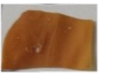




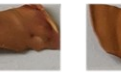

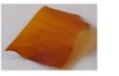
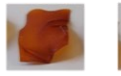



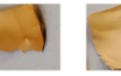

#### *2.3.1.1 Thermal stabilisation of non-woven mats produced from 88% PVA*

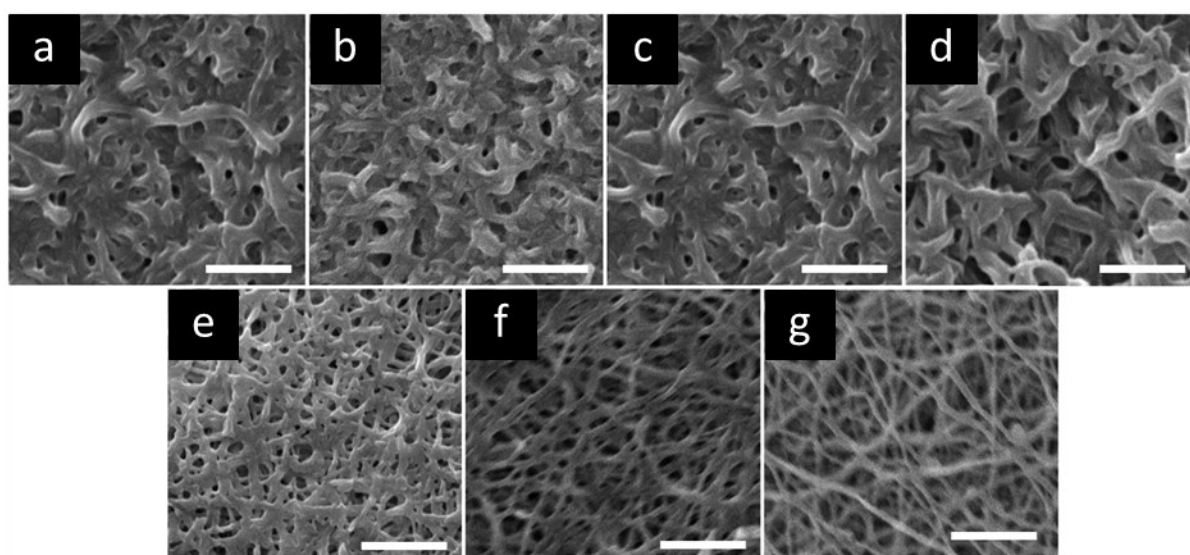
Initial work sought to explore previous research which examined nanofibrous mats produced from 88% hydrolysed PVA, created by needle electrospinning and thermally stabilised to preserve fibre morphology (Diez et al., 2022). This work, along with other studies found in the literature, showed that PVA mats electrospun without the use of chemical crosslinkers could be morphologically preserved against dissolution when in contact with water, by heat treatment at 180 °C. The duration of heat treatment in this work was extended beyond the limit of 8 h found in literature (Miraftab et al., 2014, Enayati et al., 2016), to identify the optimum stabilisation conditions for subsequent studies. Materials were produced by electrospinning of 88% hydrolysed PVA and thermally stabilised at 180 °C for 0, 1, 2, 4, 8, 16, 24 and 32 h.

**Table 2.1** summarises the full sample series and the visual impact on the samples pre and post water immersion. Immediately following treatment, the samples exhibited a degree of

discolouration and yellowing, which generally became increasingly pronounced with exposure duration, and could be attributed to some extent of thermolysis (supported by FT-IR results in **Figure 2.5**). The samples were then immersed in water for 24 h to assess their solubility. Following immersion, the untreated sample dissolved, whilst all others remained intact. Upon drying, the samples from 1, 2, 4 and 8 h of heat treatment acquired a visually translucent quality, suggesting they may have formed films rather than maintaining their fibrous morphology. Samples treated for more than 8 h (*i.e.* 16, 24 and 32 h) showed no translucence, but became increasingly brittle.

**Table 2.1.** Optical images of PVA (88% DH) samples following heat treatment between 1 and 32 h at 180 °C. Untreated sample (0 h) is included as control. 'Post immersion' refers to following immersion in water for 24 h, and 'Final (re-dried)' refers to the same samples following drying at room temperature for 3 days.

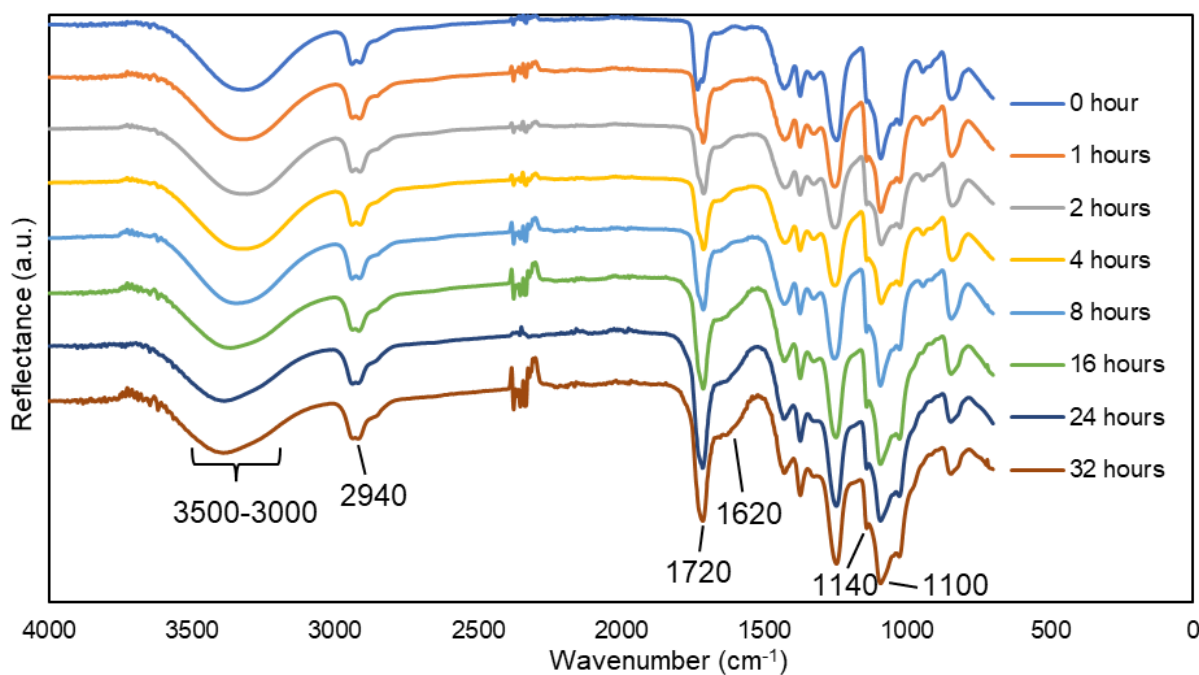
	0 h	1 h	2 h	4 h	8 h	16 h	24 h	32 h
Pre-immersion								
Post-immersion (wet)	Dissolved							
Post-immersion (dry)	Dissolved							



**Figure 2.4.** SEM Images of 88% hydrolysed PVA with 1, 2, 4, 8, 16, 24 and 32 h (a-g respectively) of heat treatment after 24 h immersion in water, and air drying for 3 days. Scale bar: 5  $\mu\text{m}$ .

The visual observations were further confirmed by SEM (**Figure 2.4**). After 16 h of heat treatment the non-woven mat still exhibited a heavily fused structure with proportionally very small pores, whereas the more prolonged thermal treatments of 24 and 32 h led to greater morphological preservation and maintained the fibrous structure.

Possible chemical changes induced by the heat treatment were investigated using FT-IR, and the spectra for 0-32 h treatments at 180 °C are shown in **Figure 2.5**. The broad band at 3000-3500  $\text{cm}^{-1}$  is commonly associated with a combination of O-H stretching in the polymer chain and hydrogen bonding with any residual, bound water molecules, stretching in the range of 2900-2950  $\text{cm}^{-1}$ , is linked with C-H in methyl, methylene and methine groups. The band at 1710-1750  $\text{cm}^{-1}$  is associated with stretching in the C=O of the carbonyl group present in the 12% residual acetate groups of PVA with lower degrees of hydrolysis (Ping et al., 2001, Yang et al., 2012). This band was found to increase in intensity with increasing treatment duration, as well as the development of a shoulder to the right of the peak around 1650-1600  $\text{cm}^{-1}$ , commonly associated with conjugated alkenes (Fleming and Williams, 2019). There appears to be a reduction, and slight shift, in the peak associated with O-H groups in the samples treated for 16, 24 and 32 h, indicating some loss of hydroxyl function groups, mostly likely via dehydration degradation pathways, and potential reduction in molecular size due chain scission (Akhter et al., 1988, Peng and Kong, 2007, Okada et al., 2011).

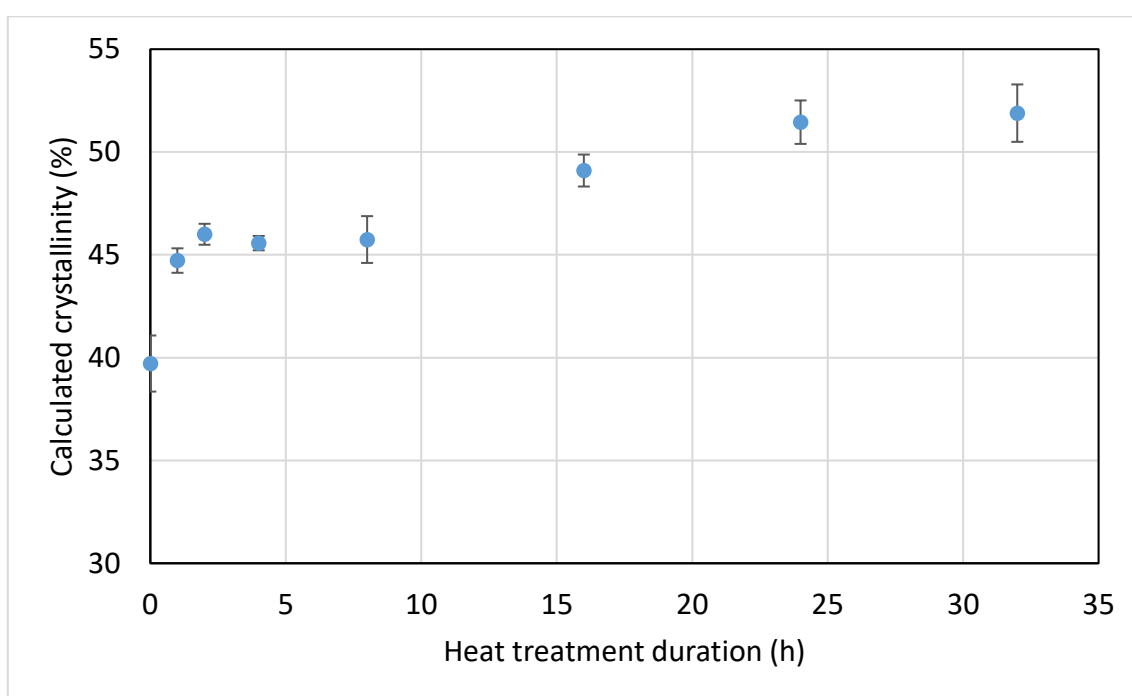


**Figure 2.5.** Representative FT-IR spectra of samples produced by needle electrospinning of 88% hydrolysed samples at a concentration of 14% (w/w), at a flow rate of 0.6  $\text{mL}\cdot\text{h}^{-1}$ , applied voltage of 22 kV and tip-collector distance of 15 cm following 0-32 h of heat treatment at 180 °C ( $n=3$ ).

The band at  $1140\text{ cm}^{-1}$  is commonly linked with C-C stretching (Yang *et al.*, 2008). This band can be seen to be closely adjacent to the band around  $1100\text{ cm}^{-1}$ , and work carried out by Tretinnikov and Zagorskaya (2012) demonstrated that the absorbance at the bands of  $1144\text{ cm}^{-1}$  and  $1094\text{ cm}^{-1}$  can be used to describe the crystallinity of 98.7% hydrolysed PVA in solid samples within 0.3% correlation with XRD calibration data. The numerical method derived is shown in equation 3, where  $A_x$  corresponds to the absorbance value at wavenumber  $x$ .

$$\text{Crystallinity (\%)} = -13.1 + 89.5 * \left( \frac{A_{1144}}{A_{1094}} \right) \quad \text{Eq. (3)}$$

This correlation has been previously used to describe crystallinity of PVA nanofibers, with increases in crystallinity being related to enhanced water stability resulting from heat treatments (Enayati *et al.*, 2016, Mirafteb *et al.*, 2014).



**Figure 2.6.** Calculated crystallinity (%) ( $n=3$ ) vs heat treatment duration graph for samples of needle spun 88% hydrolysed PVA calculated using Eq. 3 and absorbance values derived from **Figure 2.5**.

Equation 3 was therefore employed in an attempt to quantify changes in crystallinity of the heat treated samples, and the results are shown in **Figure 2.6**. This method of quantification suggests an initial increase in crystallinity (from 39.8% to 44.8%) following the first hour of heat treatment. Beyond this, and though there is a general trend of slightly increasing

W. J. A. Homer, PhD Thesis, Aston University, 2023



crystallinity, the percentage change per hour of treatment is reduced. According to **Figure 2.6**, the highest degree of crystallinity was found in the sample treated for 32 h with a calculated value of 52.0%.

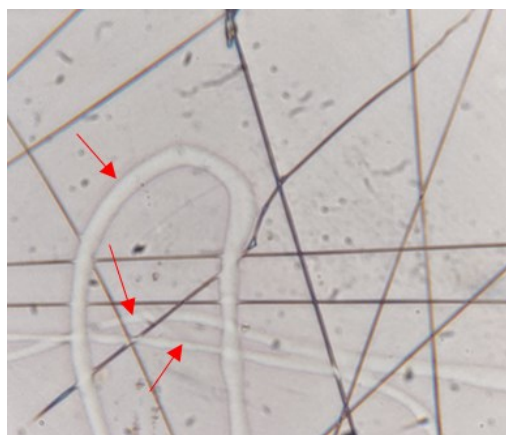
Though the sample with the highest calculated crystallinity is also the sample which retained the most fibre-like morphology, it should be noted that Tretinnikov and Zagorskaya (2012) identified that this method becomes less reliable when heat treatment exceeds 150 °C (which is the case in this work). Furthermore, their method was developed for PVA with a higher degree of hydrolysis (98.7% *c.f.* 88%), which according to the literature produces more morphologically stable fibres in aqueous environments and therefore would be a closer match for the intended biomedical applications presented in this work (Park et al., 2010).

### *2.3.2 Production of electrospun mats from 99% hydrolysed PVA*

Work was carried out to identify solution parameters which could be used with a range of electrospinning equipment, in order to aid comparison between the produced samples. Optimum conditions were established on a needle-based electrospinning machine at Aston University, and they were subsequently trialled at the TUL on their needleless DC and AC electrospinning systems.

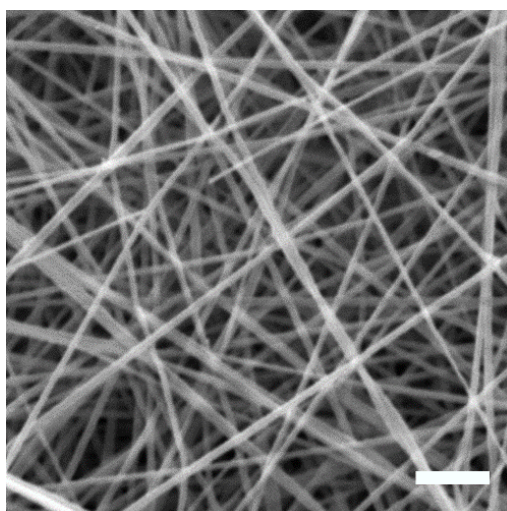
#### *2.3.2.1 Needle-based DC electrospinning*

Initial optimisation of electrospinning conditions was carried out by varying the polymer concentration (6-12%), flow rate (0.1-1 mL·h<sup>-1</sup>), applied voltage (6-30 kV) and tip-collector distance (8-15 cm). Visual observation of a stable jet and reviewing microscope slides placed on the collector using optical microscopy, were chosen as preliminary methods of assessment. In all cases only an intermittently stable jet was produced, with the best result obtained from a PVA concentration of 8% (**Figure 2.7**). The sample was a mixture of small fibres and splashes/streaks, the latter being a result of initiation/termination of the spinning jet, where the stream breaks in the stable region near to the Taylor cone in the electrospinning process.



**Figure 2.7.** Optical microscopy image of nanofibers showing defects formed (highlighted with red arrows) following electrospinning of 99% hydrolysed PVA in pure water solvent at a concentration of 8% (w/w), with applied voltage of 12 kV, flow rate of  $0.5 \text{ mL} \cdot \text{h}^{-1}$  and tip-collector distance of 15 cm. (100x magnification).

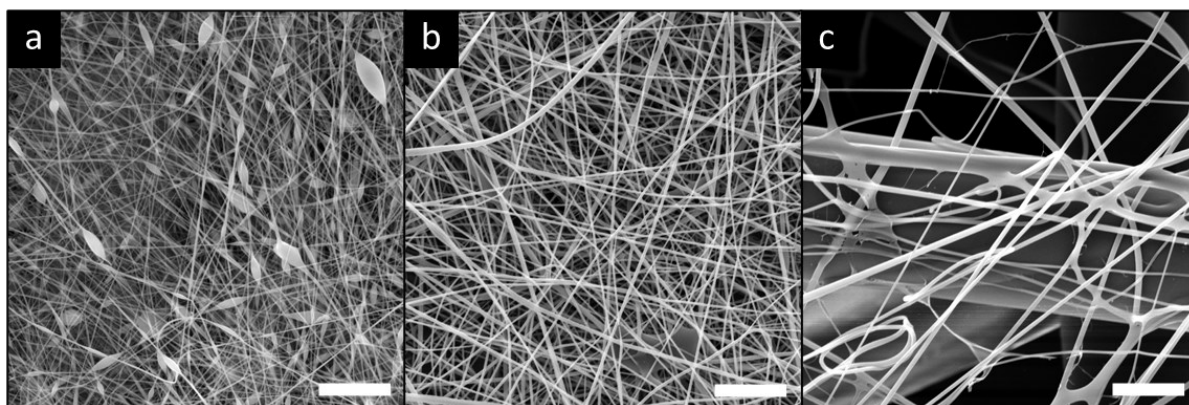
Reduced surface tension has been shown to enhance the electrospinnability of polymer solution, and improve formation of stable jets (Park et al., 2010, Yao et al., 2003), and therefore the pure water solvent was replaced by a ratio of 9:1 water: ethanol (Vazquez *et al.*, 1995). A second round of optimisation of electrospinning with the new solvent system involved varying the flow rate between  $0.15$  and  $1 \text{ mL} \cdot \text{h}^{-1}$  and applied voltage from 7.5 to 17 kV, but maintained the PVA solution concentration to 8%. A visually stable jet was formed at a flow rate of  $0.3 \text{ mL} \cdot \text{h}^{-1}$ , applied voltage of 9 kV and tip-collector distance of 15 cm, and defect-free fibres were produced as shown in **Figure 2.8**. These solution parameters for electrospinning were then transferred to the other platforms *i.e.* needleless DC and AC.



**Figure 2.8.** SEM image of nanofibers produced by needle-based electrospinning of 99% hydrolysed PVA in 9:1 water/ethanol solvent at a concentration of 8% (w/w), with applied voltage of 9 kV, flow rate of  $0.3 \text{ mL} \cdot \text{h}^{-1}$  and tip-collector distance of 15 cm. Scale bar:  $2 \mu\text{m}$ .

### 2.3.2.2 Needleless DC electrospinning

Having successfully identified solution parameters for electrospinning 99% hydrolysed PVA in needle electrospinning, attempts to reproduce the results with the Nanospider device at TUL were then carried out. Since the Nanospider equipment is substantially different in operation to the needle laboratory set-up used previously, certain operating parameters had to be changed, such as applied voltage, and factors such as cartridge speed, electrode distance, and wire electrode rewind speed were set based the advice of our Czech collaborators, with extensive experience on the device (Personal communications). Furthermore, and to verify that 8% was the preferred PVA solution concentration for the Nanospider experiments, three different concentrations (6, 8 and 10%) were tested. The SEMs shown in **Figure 2.9a** indicate that at 6%, the fibres are extremely thin with many spindle defects. Increasing the concentration to 10% (**Figure 2.9c**) resulted in jets which struggled to initiate, and the very few fibres that reached the collector material were of low quality and had variable fibre diameters. By comparison, the 8% concentration solution (produced many and largely defect-free nanofibers, thereby confirming the suitability of the previously identified solution parameters for direct transfer between the two forms of DC electrospinning (needle and needleless).



**Figure 2.9.** SEM images of samples produced using the Nanospider™ with variable PVA concentration of (a) 6%; (b) 8%; and (c) 10%. Scale bar: 10  $\mu\text{m}$ .

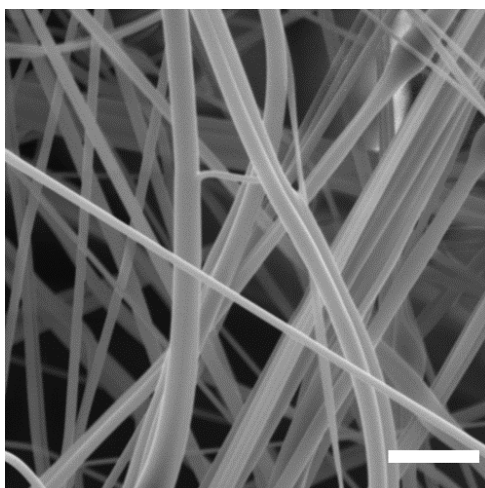
### 2.3.2.3 AC electrospinning

Though ideally all three systems employed in this work should use the same solvent for electrospinning, AC electrospinning is a lot more sensitive to solution conditions than the more traditional DC methods, and therefore spinning of PVA was not possible with ethanol in the

solvent system. Samples of 6, 8 and 10% concentration of 99% hydrolysed PVA using DI water as the solvent, were therefore prepared for some further optimisation for this equipment. Both the 6% and 10% samples did not initiate formation of jets and subsequent plume, whilst the 8% sample was able to form a stable stream of nanofibers (**Figure 2.10**) with the desired morphology (**Figure 2.11**).



**Figure 2.10.** Photograph of nanofiber plume of 99% DH PVA (8% w/w concentration in water) produced by AC electrospinning.



**Figure 2.11.** SEM image of nanofibers produced by AC electrospinning of 99% DH PVA (8% w/w concentration in water). Scale bar: 5  $\mu$ m

### 2.3.3 Comparison of electrospinning platforms for nanofiber production

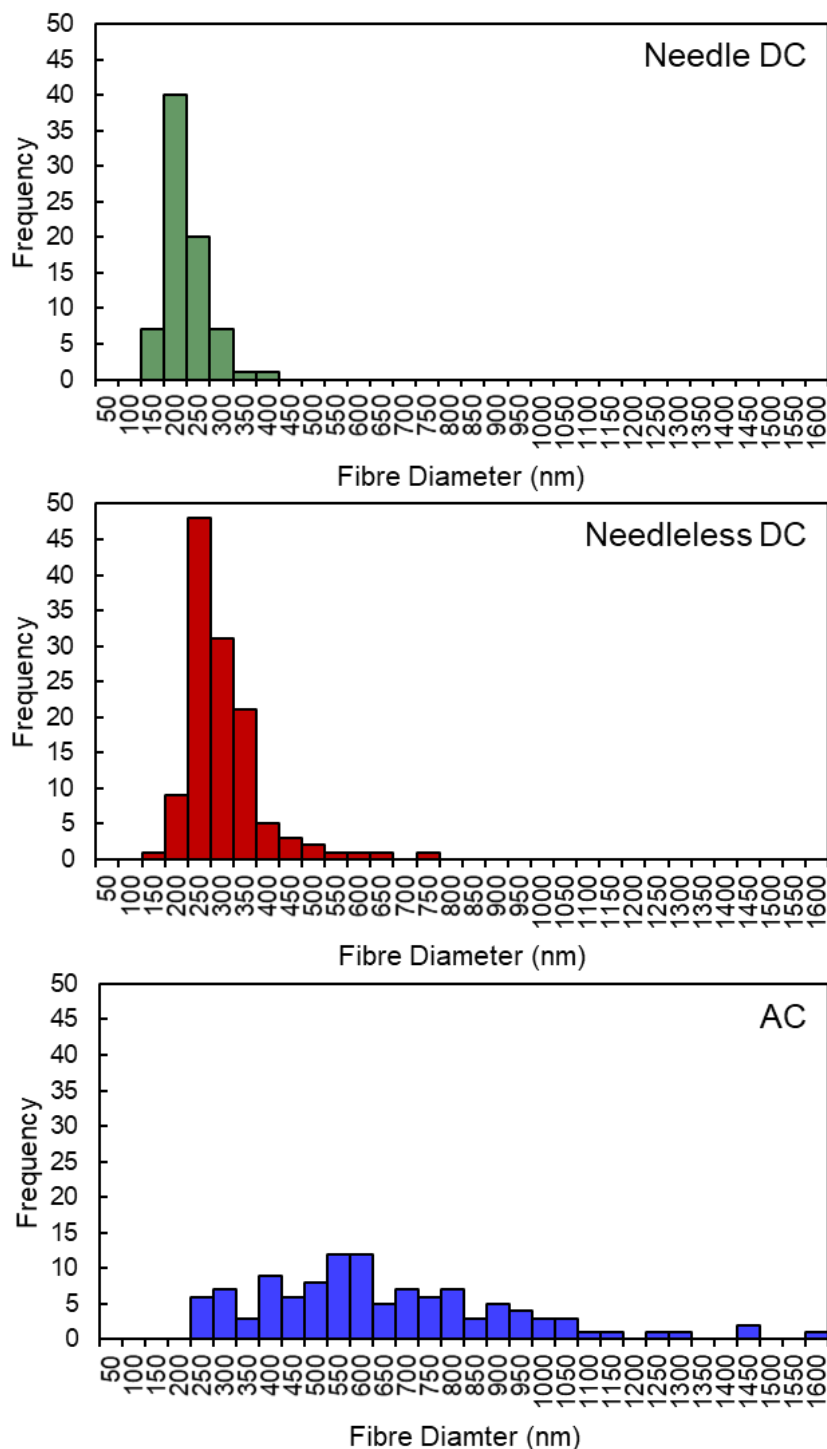
Having established parameters for the successful production of nanofibers from 8% PVA with 99% degree of hydrolysis across all 3 electrospinning platforms, morphological, chemical and production analyses were carried out for each method.

### 2.3.3.1 Morphological analysis

Average nanofiber diameters were calculated following measurement of the fibres visible in the SEMs (as described in section 2.2.3.1) from the different electrospinning methods as they are presented in the previous sections, i.e. needle (**Figure 2.8**), needleless (**Figure 2.9.b**) and AC (**Figure 2.11**). Needle electrospinning produced the smallest average diameter fibres (199 nm  $\pm$ 10 nm, CI=95%, n=76), followed by needleless spinning (280 nm  $\pm$ 15 nm, CI=95%, n=124) and finally AC spinning (624 nm  $\pm$ 51 nm, CI=95%, n=113). All histograms (**Figure 2.12**) had a slightly positive/left modal skew towards smaller fibres (skewness of 0.8102, 2.2078 and 0.9717 for needle, needleless and AC respectively), indicating that the needleless sample has the greatest skew. Furthermore, the AC sample had a much broader fibre diameter range, with an overall flatter distribution when compared to both DC methods.

Based on the average fibre diameters, it is possible to calculate theoretical specific surface area for nanofibrous materials using equation 1 described in section 2.2.3.4 on the assumptions that fibre size distributions are normal, or near normal, with minimal skewness; contribution to surface area from fibre termination is negligible (*i.e.* material is composed of long, continuous fibres); material density is constant within the sample; and nanofibers are smooth. Though it is clear these assumptions are not 100% true, the method can be considered useful to understand the relationship between fibre size and surface area intrinsic to fibrous materials (Ko and Yang, 2008). This theoretical value was then compared with measured surface area by nitrogen sorption porosimetry and calculated using the BET method. Due to the low productivity of the needle DC electrospinning, discussed later on in section 2.3.3.3, and the relatively large sample size required for N<sub>2</sub> porosimetry, it was not feasible to make enough sample for this test, so comparison was limited to needleless DC and AC spinning methods. Samples of nanofibers produced by each method were prepared and analysed for surface area determination, as well as being imaged using SEM, with sample specific average fibre diameters calculated from these images in order to account for any possible sample to sample variation (**Appendix A**). Theoretical specific surface areas for needleless DC and AC spun samples were calculated to be 11.818 m<sup>2</sup>·g<sup>-1</sup> and 5.775 m<sup>2</sup>·g<sup>-1</sup> respectively, whilst experimentally derived values were much lower at 4.060 m<sup>2</sup>·g<sup>-1</sup> and 1.151 m<sup>2</sup>·g<sup>-1</sup>. Although this suggests that the theoretical calculation is overestimating the surface area by a factor of 2.91 and 5.02 respectively, it confirms that these materials maintain surface areas in the order of m<sup>2</sup>·g<sup>-1</sup> despite the absence of diffusive pores. These values can offer a good initial estimation of the available surface area for binding for large biological molecules

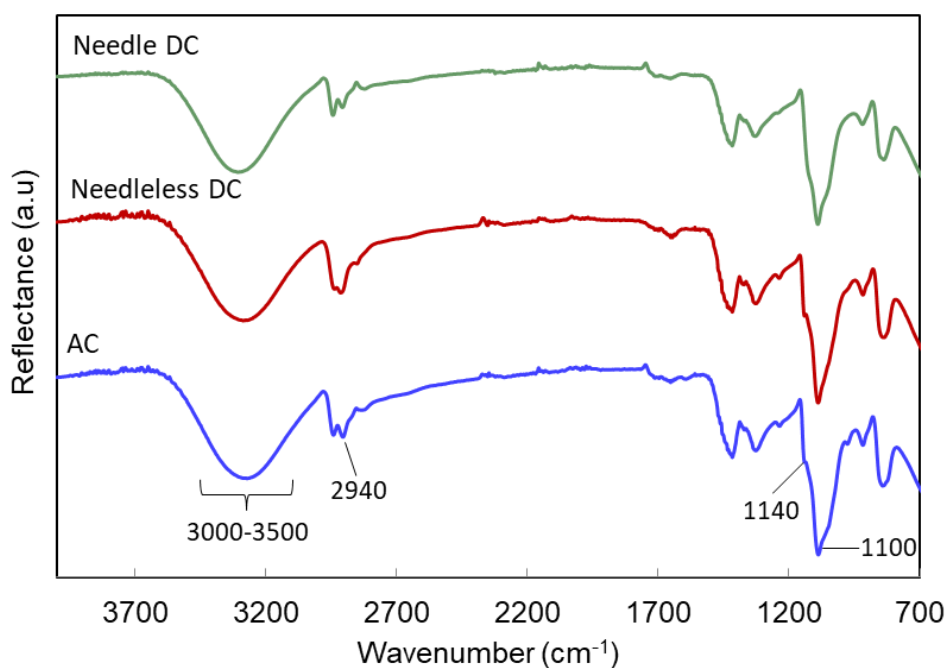
under convective flow, as there is no dependence on intrapore diffusion, a critical factor when developing materials for applications such as cell chromatography.



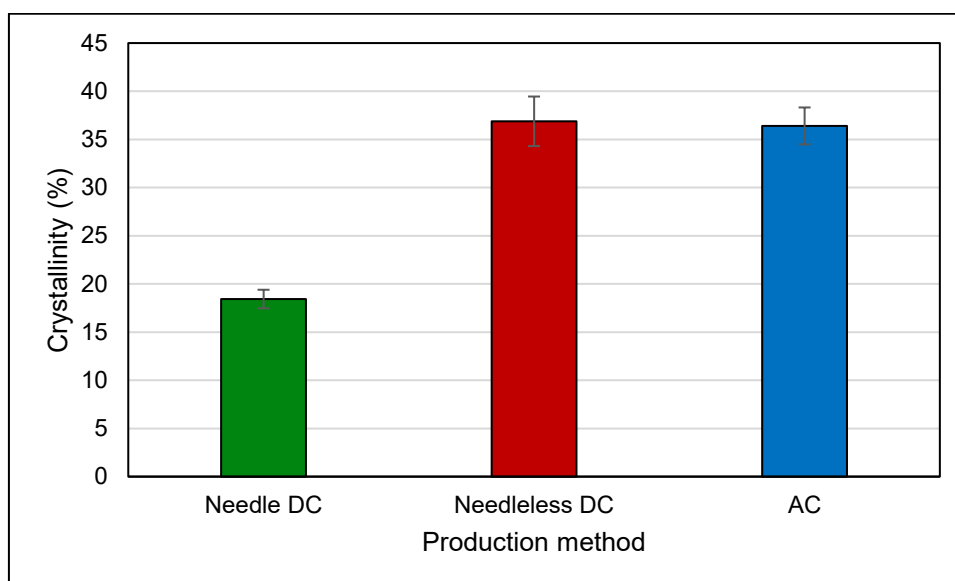
**Figure 2.12.** Histograms comparing fibre diameter distribution of untreated 99% hydrolysed PVA nanofibers by needle, needleless and AC electrospinning, created using SEMs from **Figure 2.8**, **Figure 2.9.b** and **Figure 2.11** respectively.

### 2.3.3.2 Chemical analysis

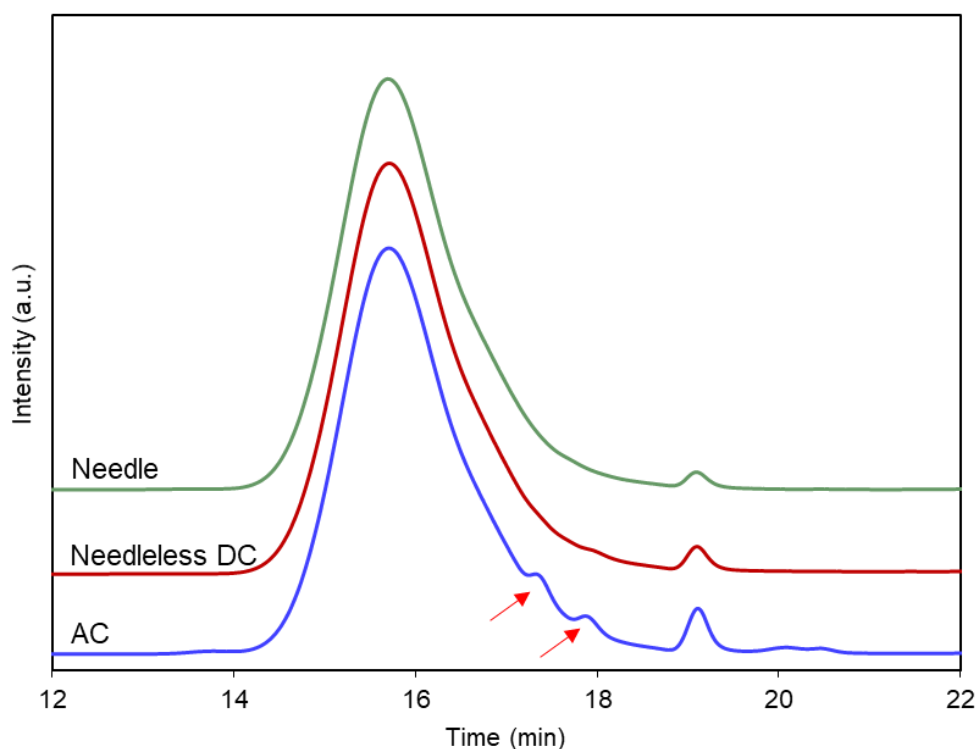
FT-IR spectra of untreated samples produced *via* the three different methods of electrospinning are compared in **Figure 2.13**. The overall chemical identity of the samples appears to be largely similar, with some small variances observed, particularly with respect to calculated crystallinity. There is some indication of small differences in the spectra around the  $980\text{ cm}^{-1}$  region, which could be attributed to C=C double bonds, and around the  $2900\text{-}3000\text{ cm}^{-1}$  which has been associated with CH bonds in methyl, methylene and methine groups. There is also a slight increase in the band at  $1144\text{ cm}^{-1}$ , linked to crystallinity, suggesting that fibres produced by the Nanospider™ and AC spinning possess a higher degree of crystallinity than those produced by needle electrospinning. To quantify this, equation 3 was used again to calculate percentage of crystallinity based on FT-IR absorbance data, as these supports more closely satisfy the criteria described by Tretinnikov and Zagorskaya (2012). Samples created by the needle spinning platform had crystallinity of 18.4%, compared to 36.9% and 36.4% for needleless and AC respectively (**Figure 2.14**). One possibility is that the higher applied voltages used in needleless and AC methods plays a role in polymer crystallisation during fibre formation (Lee et al., 2012). The voltage may also be responsible for some modification to the chemical structure, such as chain scission and formation of smaller species (Pathan *et al.*, 2015). These chemical differences were explored further with GPC and  $^1\text{H}$  NMR analysis.



**Figure 2.13.** FT-IR spectra of samples of 99% hydrolysed PVA produced by three methods of electrospinning: needle, needleless and AC.



**Figure 2.14.** Crystallinity for samples produced from 99% hydrolysed PVA by each method of electrospinning calculated using Eq. 3 and absorbance values from **Figure 2.13**. ( $n=3$ )

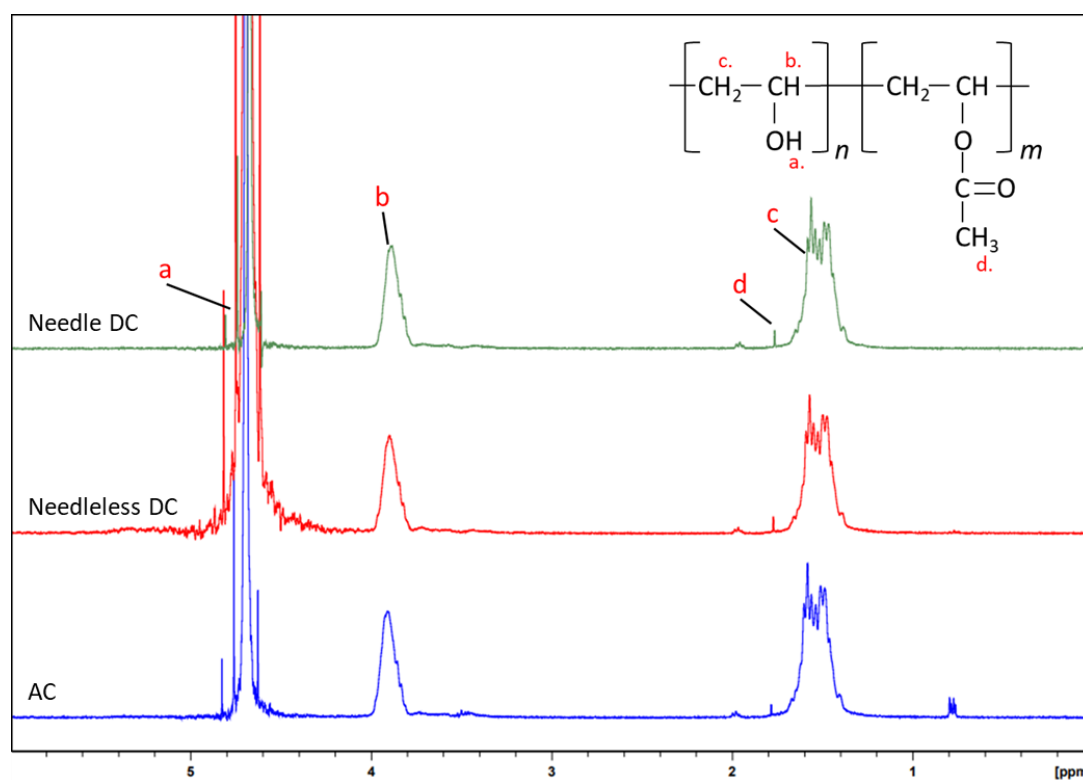


**Figure 2.15.** GPC traces of 99% hydrolysed PVA samples series produced by each method of spinning and re-dissolved post-electrospinning. The red arrows point at the potential smaller size species present in the AC sample.



Looking at the chromatograms (**Figure 2.15**), the primary peak starts to appear after 14 min and looks similar in all cases, which indicates that the different electrospinning methods did not alter the size of the polymer chains. A small change is observed in the AC spun sample suggesting the presence of smaller species flowing through the column at 17-18 min with a weaker signal intensity, as well as a very low intensity peak at 20-21 min.. This supports the idea that AC electrospinning may have some measurable effect on the chemical structure of PVA during the production of nanofibers, compared to DC based electrospinning.

Examination of the samples by  $^1\text{H}$  NMR was performed to further identify potential chemical changes resulting from the employment of the different production methods. The three spectra shown in **Figure 2.16**, are consistent with examples found in the literature (Budhlall et al., 2003, Moritani and Fujiwara, 1977, Taepaiboon et al., 2006, Vandervelden and Beulen, 1982), with the presence of a solvent residual peak caused by proton exchange overlapping the spectra at 4.79 ppm (Gottlieb *et al.*, 1997). There is significant similarity between samples created with the Nanospider™ and AC electrospinning, showing minor additional groups of peaks not observed in the sample from the needle-based electrospinning. A small triplet appears around 0.8 ppm for the Nanospider sample, and two overlapping doublets are found in the same region of the field in the AC spun samples. There is also a small, but not distinct variation at approximately 3.5 ppm on the AC spun sample.



**Figure 2.16.**  $^1\text{H}$  NMR spectra comparing samples of 99% hydrolysed PVA process by needle, needleless and AC electrospinning.

### 2.3.3.3 Method of production analysis

The non-woven mats created by each electrospinning method can be quite distinct in form. Samples from needle and needleless DC spinning are manufactured as sheets that are lightly adhered to a substrate, such as foil in needle-based methods, or a spunbond fabric in the Nanospider. In this configuration, the mats are easy to lift, transport and handle, and result in almost zero loss of material. In stark contrast, all samples produced in the AC equipment appear very similar to a loose sheet-insulation configuration, which can snag, stretch, and aggregate if not handled with extreme care (**Figure 2.17**). This characteristic, however, makes the materials somewhat malleable, and could offer unique benefits depending on the final application. Currently, the AC technology is still at a development phase even at laboratory scales, which poses barriers to its use for clinical applications. On the other hand, however, the higher effective pore size of the AC supports (as can be seen in **Figure 2.11** and implied by the greater fibre diameter from **Figure 2.12**) could be viewed as a major advantage in the processing of larger biomolecules, such as human cells, as it will allow their unimpeded passage and minimize mechanical entrapment. For most of the work described in this thesis, however, where suspended particulates, *i.e.* human erythrocytes, measure less than  $10\ \mu\text{m}$ , (Ward et al., 2018), supports with smaller fibre diameters produced by more mature technologies (e.g. needleless electrospinning) could also be utilised.



**Figure 2.17.** Photographs of PVA electrospun onto their respective substrates via (a) needle DC, (b) needleless DC, and (c) AC electrospinning.

Though it could be argued that there are benefits to the fibre morphology and overall structure of the mats produced by AC electrospinning, the technology is not yet developed as a production platform and is only being tested at the lab-scale for research purposes. When considering both scalability and the ability for easy adaptation into good manufacturing

practice (GMP), the commercial maturity of needle and needleless DC techniques, provides key advantages for both scale-up and scale-out potential, with large semi-industrial equipment already available on the market (e.g. the Elmarco NS 8S1600U, featuring 8 electrodes, each 1.6 m long; (Elmarco, 2020); or needle based methods featuring multi-emitter setups with upto 5000 needles (Bionicia, 2023), the design of these systems includes internal climate controls in a relatively closed system, whereas existing AC research typically does not feature such capabilities, which limits reproducibility.

Scalability potential was considered further by examining achieved productivities of the given solutions through each spinning method, with differences between the available platforms being properly accounted for and acknowledged. Using solutions of 99% hydrolysed PVA as described in section 2.2.2.2, needle-based DC electrospinning had a productivity of  $0.024 \text{ g} \cdot \text{h}^{-1}$  for single needle. This figure could theoretically be expanded for multi-emitter systems, though it would require validation, subject to access to such system. Elmarco's NS 1S500U platform, using needleless DC, produced  $2.519 \text{ g} \cdot \text{h}^{-1}$ , which is again subject to capacity for scale up within equipment already mentioned. Finally, the AC electrospinning platform was found to have productivities of  $0.815 \text{ g} \cdot \text{h}^{-1}$ , but this device has not yet been scaled beyond the described limits. Though this comparison is quite rough due to the fact that scaling up and scaling out is done in different manners for different platforms, it is worth being kept in consideration as a provisional insight into productivity of each system used.

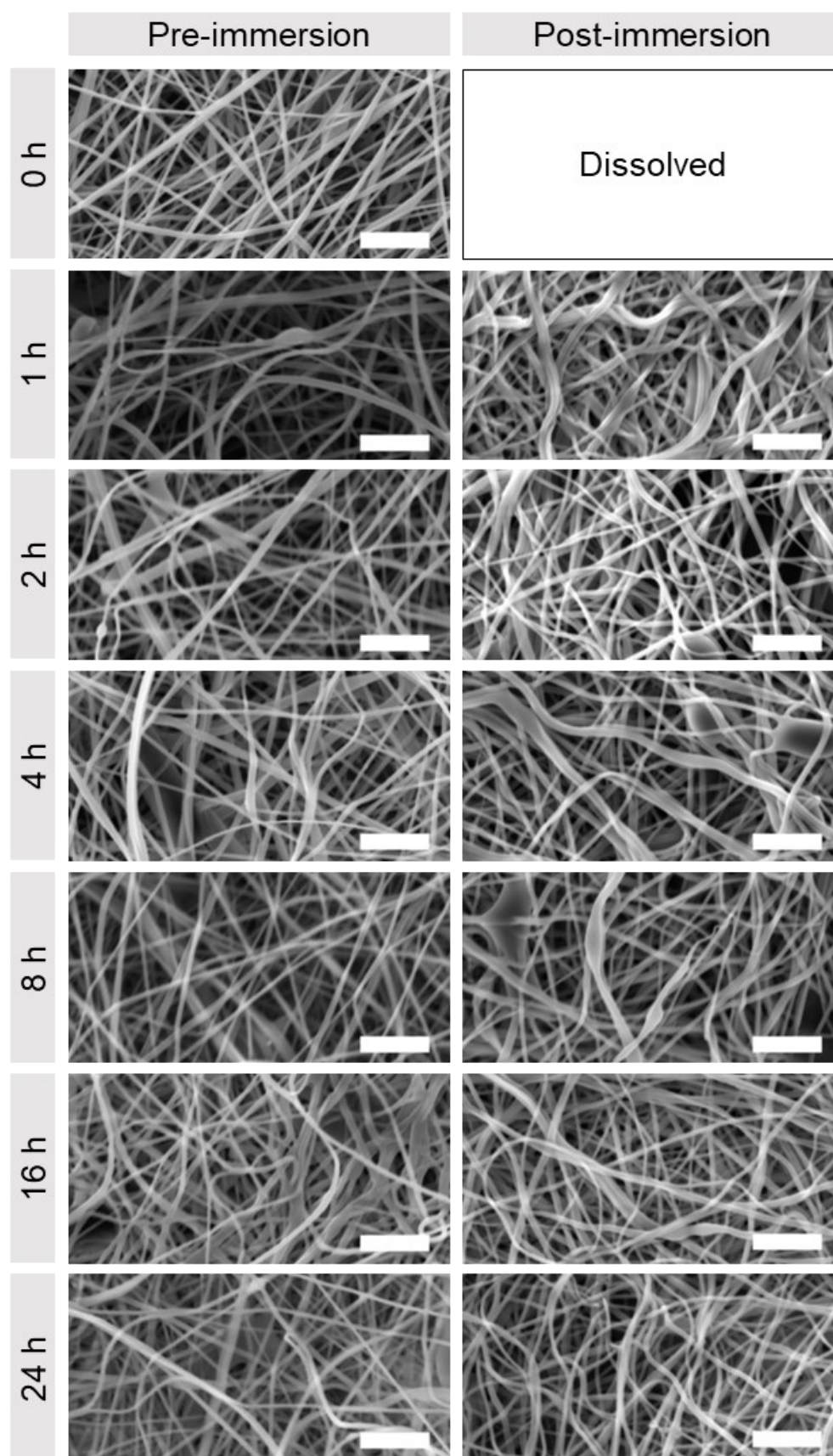
For subsequent work, given the lack of access to scalable needle-based electrospinning, combined with the low productivity and the fact that the materials produced by this method possessed the smallest average fibre diameter, needle DC was not carried forward for the extended characterisation of heat treated samples.

**Table 2.2.** Comparison of the material configurations and manufacturing considerations when needleless DC and AC platforms are used for the electrospinning of the PVA supports.

	<b>Needle DC</b>	<b>Needleless DC</b>	<b>AC</b>
Material format	Sheet/membrane configuration	Sheet/membrane configuration.	Loose fibres, akin to highly sparse sheet-insulation, but highly tuneable micro and macro structures.
Fibre and effective pore size	Smaller fibres with a tight fibre size distribution. Smaller effective pore size.	Smaller fibres with a tight fibre size distribution. Smaller effective pore size.	Larger fibres with a broad fibre size distribution. Larger effective pore size (Nelson et al., 2012).
Scalability	Mature technology, though predominantly employed in research applications. Scalable equipment available commercially with 100-1000s of needles.	Mature technology. Readily scalable (laboratory to high volume manufacturing). Highly reproducible.	Novel technology still under development.
Productivity	0.024 g·h <sup>-1</sup> ·needle <sup>-1</sup>	2.519 g·h <sup>-1</sup> within Elmarco, NS 1S500U	0.815 g·h <sup>-1</sup> based on AC setup at TUL.
GMP potential	Semi-industrial machinery and can be incorporated into a GMP process relatively easily when combined with environmental controls.	Semi-industrial machinery and can be incorporated into a GMP process relatively easily when combined with environmental controls.	Difficult to incorporate into a GMP process due to poor environmental controls in current set ups and subsequent variability of output.

### 2.3.4 Effects of extended heat treatment on 99% hydrolysed PVA

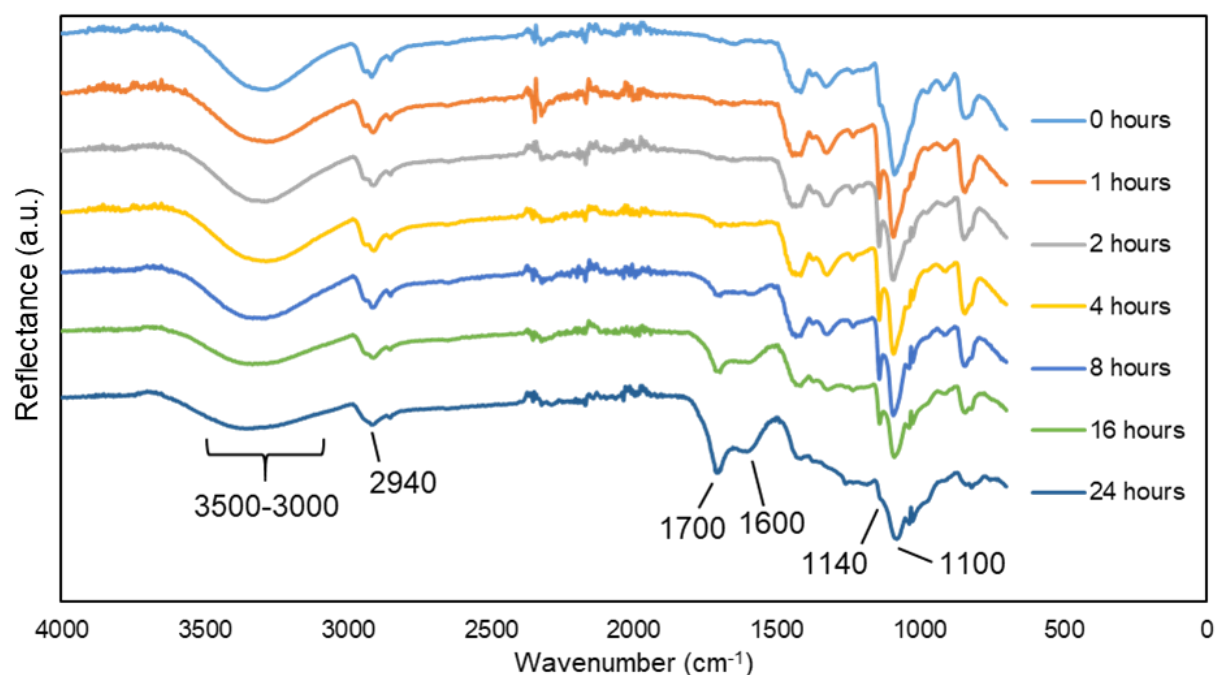
Following the promising results of the extended thermal treatment described in section 2.3.1.1 when applied to 88% hydrolysed PVA, an extended treatment duration of up to 24 h was carried out on nanofibrous samples produced by needleless electrospinning using 99% DH PVA. As before, samples were heat treated at 180 °C, to achieve physical crosslinking and therefore enhance their stability whilst in contact with water. **Figure 2.18** summarises SEM data prior to and after 24 h water immersion at 37 °C following the different curing times.



**Figure 2.18.** SEM images of heat treated samples (between 0 and 24 h) of 99% hydrolysed PVA nanofibers produced by needleless DC electrospinning before and after water immersion for 24 h at 37 °C. Scale bar: 5  $\mu$ m.

Unsurprisingly, the untreated PVA sample dissolved almost immediately, so no image could be obtained post water immersion. The samples treated for 1 h – and to a lesser extent 2 h – show a degree of swelling and clustering of fibres, leading to a visible reduction in effective pore size available for flow of large entities. The sample treated for 4 h displays little to no swelling, and much of the void space between fibres is still present. Finally, samples cured for 8 h or longer, appear to maintain their original morphology and effective pore structure, indicating that much shorter treatment durations are highly effective against preserving fibre morphology compared to samples produced from PVA with a lower degree of hydrolysis.

Prior to water immersion, samples were analysed by FT-IR to search for indications of chemical changes in the material arising from the treatment process and the spectra are presented in **Figure 2.19**. New bands appear at wavenumbers of  $1700\text{ cm}^{-1}$  and  $1600\text{ cm}^{-1}$ , which may indicate stretching of C=O and C=C bonds, respectively (Fleming and Williams, 2019). These signals become significant when heat treatment exceeded 8 h, and may be signs of increasing thermal degradation, which could be associated with a loss of some hydroxyl groups, as observed in the samples treated for 16 and 24 h. This closely matches behaviours observed in section 2.3.1.1, though in the case of 88% hydrolysed PVA the clarity of the signal is masked by the presence of the band from the C=O group in the more abundant acetate groups (See **Figure 2.19**).



**Figure 2.19.** FT-IR spectra of 99% hydrolysed PVA nanofibers produced by needleless DC electrospinning following heat treatment at  $180\text{ }^{\circ}\text{C}$ .

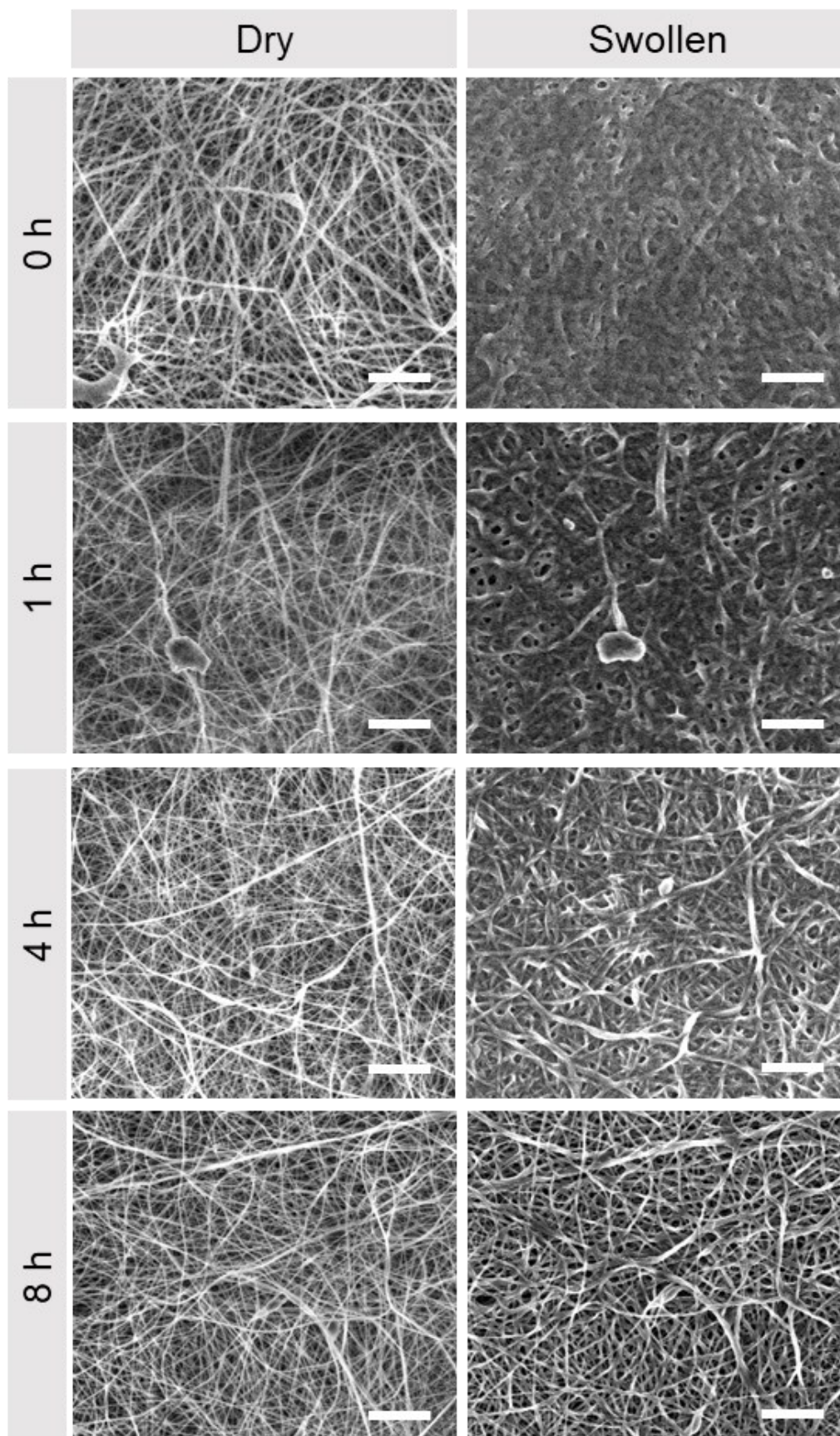
In regards to the crystallinity, a similar analysis to the one shown earlier in this chapter for the PVA with DH of 88% (see **Figure 2.6**), was carried out using equation 3, but given the limitations of the method, the results are included only in **appendix B**, with XRD analysis favoured of the more reliable method for measuring crystallinity (presented later on in **Figure 2.23** and discussed in section 2.3.5.2).

Samples that were heat treated for more than 8 h exhibited increased embrittling, in an analogous manner to the 88% DH samples, and the SEM images post immersion also confirmed that heat treatment for long time periods (> 8 h) offer no morphological benefit. It was therefore concluded that 8 h was the appropriate limit for heat treatment duration and used in the remaining experiments presented in this chapter.

### *2.3.5 Characterisation of thermally stabilised nanofibrous samples produced by and needleless DC and AC electrospinning.*

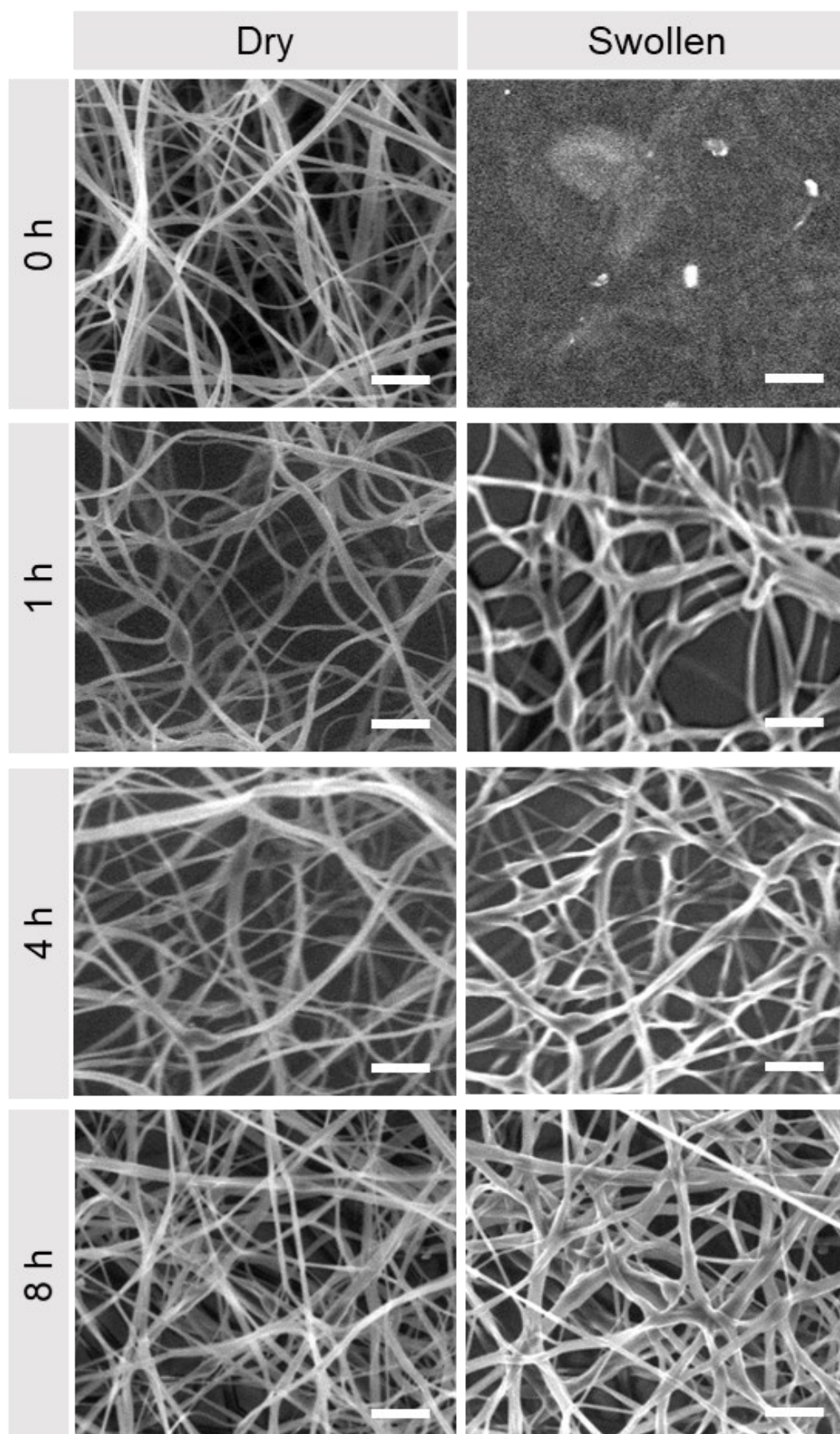
#### *2.3.5.1 In-situ swelling behaviour*

To provide greater insight into the *in situ* swelling behaviour of the non-woven mats, samples of 99% PVA produced by needleless DC and AC spinning and heat treated at 180 °C for durations ranging from 0 to 8 h, were analysed by ESEM to observe their morphology as they become saturated with condensing water vapour. Prior to contact with water, all materials possess a fibrous morphology with few defects present (left hand columns in **Figure 2.20** and **Figure 2.21**). Following condensation and subsequent evaporation, fibres not subjected to heat treatment were not able to retain their initial morphology (top right hand corner in **Figure 2.20** and **Figure 2.21**), though the degree of swelling and blending into an amorphous structure was less pronounced in the needleless DC samples (Swollen, 0 h, **Figure 2.20**) compared to that of the untreated AC spun samples (Swollen, 0 h, **Figure 2.21**). Heat treatments appear to have successfully preserved the morphology of the fibrous network for the needleless DC supports, although the 8 h duration seems to have the most significant effect (right hand side in **Figure 2.20**). This agrees with literature findings, which attribute the decrease in solubility to an increase in physical crosslinking as a result of closer packing of the polymer backbone and subsequent increase of hydrogen bonding arising from the curing process (Enayati et al., 2016, Mirafteb et al., 2014). Similarly, for AC spun samples, all heat treatment durations appear to have a positive effect on preservation of the morphology when saturated with water (right hand side in **Figure 2.21**).



**Figure 2.20.** ESEM images of electrospun PVA samples with 99% DH, produced by needleless DC electrospinning. Left: Samples prior to swelling. Right: Samples after swelling, immediately following surface moisture evaporation. Scale bar: 15  $\mu\text{m}$ .

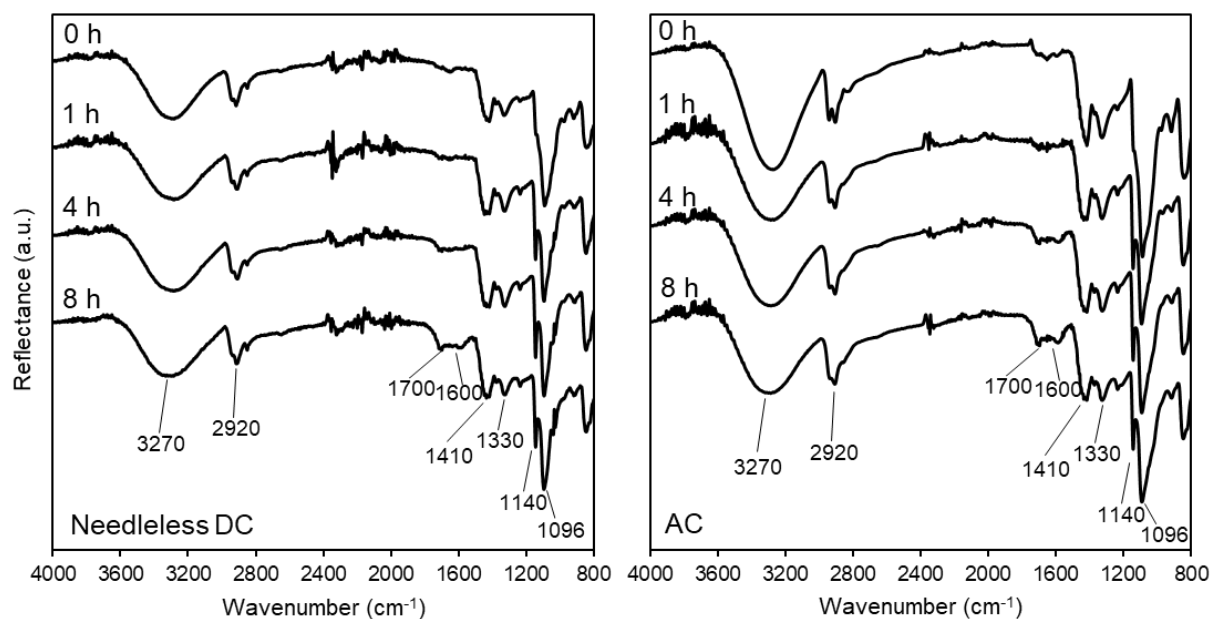




**Figure 2.21.** ESEM images of electrospun PVA samples with 99% DH, produced by AC electrospinning. Left: Samples prior to swelling. Right: Samples after swelling, immediately following surface moisture evaporation. Scale bar: 15  $\mu\text{m}$ .

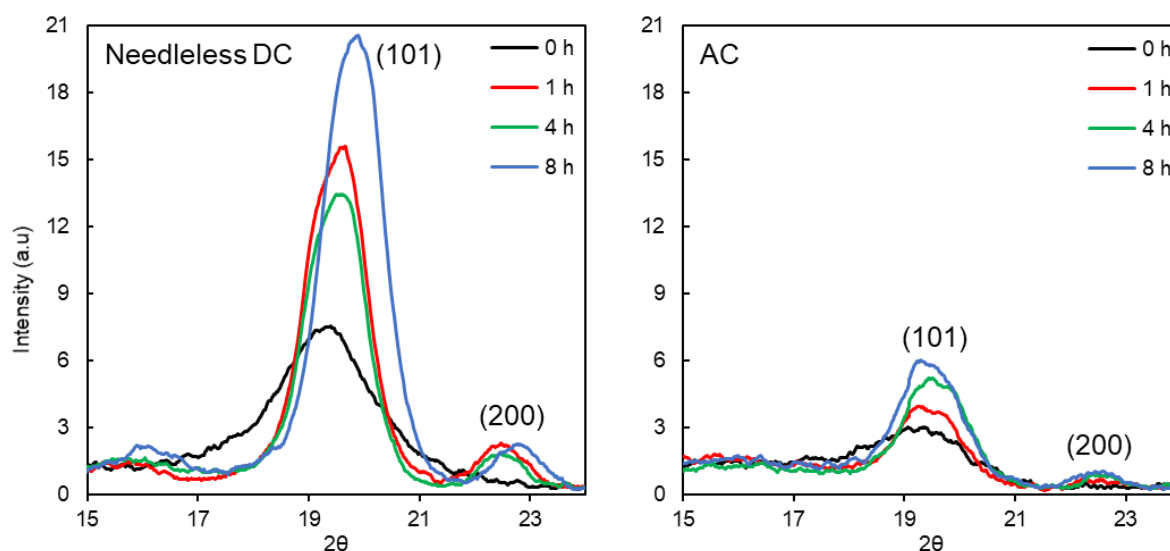
### 2.3.5.2 Chemical analysis

The FT-IR spectra of the non-woven fibres produced by the needleless DC and the AC equipment following different heat treatment durations are presented in **Figure 2.22**. As described previously (see section 2.3.1.1), characteristic peaks of the FT-IR spectra are associated with O-H stretching at  $3270\text{ cm}^{-1}$ , C-H stretching on the polymer backbone at  $2920\text{ cm}^{-1}$ , C-O stretching at  $1140\text{ cm}^{-1}$  (attributed to the crystalline phase of PVA), and O-H bending at  $1096\text{ cm}^{-1}$  (attributed to the amorphous phase) (Tretinnikov and Zagorskaya, 2012, Alhosseini et al., 2012, Jipa et al., 2012). The spectra show little difference between samples and their character is closely matched by spectra of both pristine and electrospun PVA samples with high degree of hydrolysis found in the literature (Tretinnikov and Zagorskaya, 2012, Alhosseini et al., 2012, Mansur et al., 2008). This, along with the effect of heat treatment on the materials is shown in **Figure 2.22**. All heat treatments of samples produced by DC and AC cause a significant increase in peak intensity around  $1140\text{ cm}^{-1}$ , indicating an increase in crystallinity. In AC electrospun mats, heat treatment of any duration caused a stepwise change in intensity around  $3270\text{ cm}^{-1}$ , which might indicate a reduction in O-H bonds, though a strong signal was still observed, indicating hydroxyl groups were still present in all samples, and therefore might represent a reduction in residual water content more significant than that in needleless DC samples. It is also possible that the reduction in this band, with the increase and maintenance of the signal strength around  $1140\text{ cm}^{-1}$ , may indicate that chemical crosslinking is occurring in the form of ether bonds, as C-O-C bonds share wavelengths with C-O stretching of alcohol groups. This could explain the extent of reduction in solubility and preservation of morphology observed in heat treated samples. Examples of intermolecular dehydration resulting in ether bonds have been found in literature, but are discussed as occurring through irradiation (Akhter et al., 1988, Petrova et al., 2005) or in the presence of acid vapour (Desai et al., 2020). Typically heat treatment is only described as promoting physical crosslinking, but it appears may play some role in ether bond formation also. Finally, more extensive heat treatments (4 and 8 h) begin to show clear signals around  $1600$  and  $1700\text{ cm}^{-1}$ , which are associated with formation of C=C and C=O bonds, respectively (Meszlényi and Körtvélyessy, 1999). This again is degradation due to thermolysis over time, resulting in chain scission and the formation of polyenes (Yang et al., 2012). This does not automatically render the samples unsuitable and is examined through cytotoxicity testing in section 2.3.5.4, but nevertheless demonstrates that selection of treatment duration might benefit from being kept at an appropriate minimum, such as 4 h, to preserve chemical properties as much as possible.



**Figure 2.22.** FT-IR Spectra of two sample series of 99% DH PVA produced by needleless DC (left) and AC (right) electrospinning with heat treatment time points indicated on the offset spectra.

In order to improve on the numerical methods used in earlier sections to quantify crystallinity from FT-IR data, XRD was employed to identify differences in crystal structure, or chain ordering, of each of the mats produced and by the thermal annealing process, with the (101) and (200) peaks indicated in **Figure 2.23** representing the reflections of monoclinic unit cell (Tretinnikov and Zagorskaya, 2012, Tang et al., 2015). Using equation 2, described in section 2.2.3.7, the untreated samples from DC and AC electrospinning had a degree of crystallinity of 48.68% and 34.64% respectively. The overall trend indicates increased crystallinity with extended thermal treatment duration, with the highest crystallinity found in samples treated for 8 h with 58.46% for DC spun samples and 39.68% for those produced by AC. This may be influenced by other factors including solvents used, differences in ambient production conditions, but also may be driven by the technology itself in the application of different current types. The lack of a grounded collector in AC electrospinning may result in samples with lower degrees of ordering, as crystallinity has been found to be influenced by strength of the attractive force between origin of the polymer solution and collector (Lee et al., 2012). This increase is associated with reduced swelling and solubility of PVA and could result in a reduction in material leaching and more stable morphology, corroborating the results presented in section 2.3.5.1.



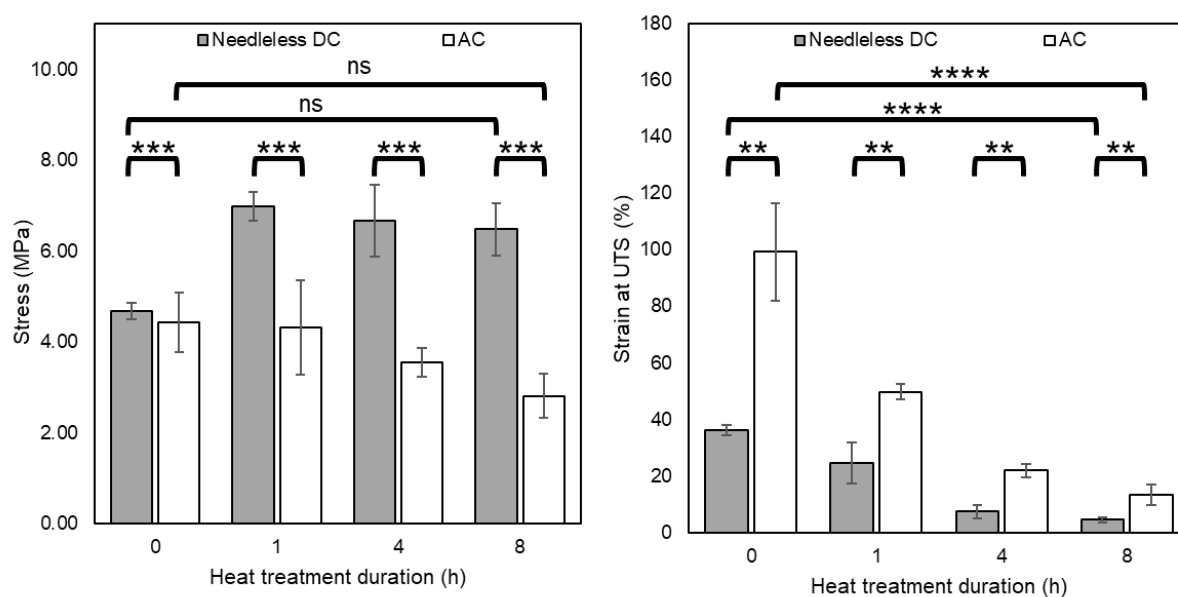
**Figure 2.23.** XRD spectra of 99% DH PVA materials produced by DC electrospinning (left) and AC electrospinning (right). Key: 0 h (black), 1 h (red), 4 h (green), and 8 h (blue).

### 2.3.5.3 Mechanical analysis

To quantify changes to the material with respect to handling properties and robustness for clinical application, mechanical testing experiments were carried out in the form of uniaxial tensile load testing. It is known that heat treatment can enhance crystallinity and lead to stronger supports, which was a pattern also broadly corroborated here, especially in the results relating to DC electrospinning (Lin et al., 2019). In the DC samples and following an initial increase in UTS of 49.1% after 1 h of treatment (4.68 MPa to 6.98 MPa), there was a steady reduction, dropping by 4.4% and then a further 2.8%, at 4 and 8 h respectively. This behaviour may be associated with enhanced crosslinking, both physical (Previously indicated by XRD results) and potentially chemical (see section 2.3.5.2), whereas a slow thermal degradation effect, which can result in some chain scission and formation of polyenes (Yang et al., 2012), would explain the reduction in UTS with increasing treatment duration. Conversely, with increasing heat treatment duration, each DC sample's UTS was achieved at lower and lower strain values. Comparison of both graphs shown in **Figure 2.24** indicate that untreated supports (0 h) as well as those treated for 1 h show signs of a typical strength-ductility trade off (Gao et al., 2020). The further reduction in ductility over the materials treated for 4 and 8 h (not associated with increases in strength, but rather a decrease) may also be attributed to a combined effect of reduced chain mobility through crosslinking, and an increasing degree of chain scission, which can also explain the excessive brittle behaviour in samples treated beyond this duration. With respect to samples produced *via* AC electrospinning, changes in UTS at various heat treatment durations, do not show the same

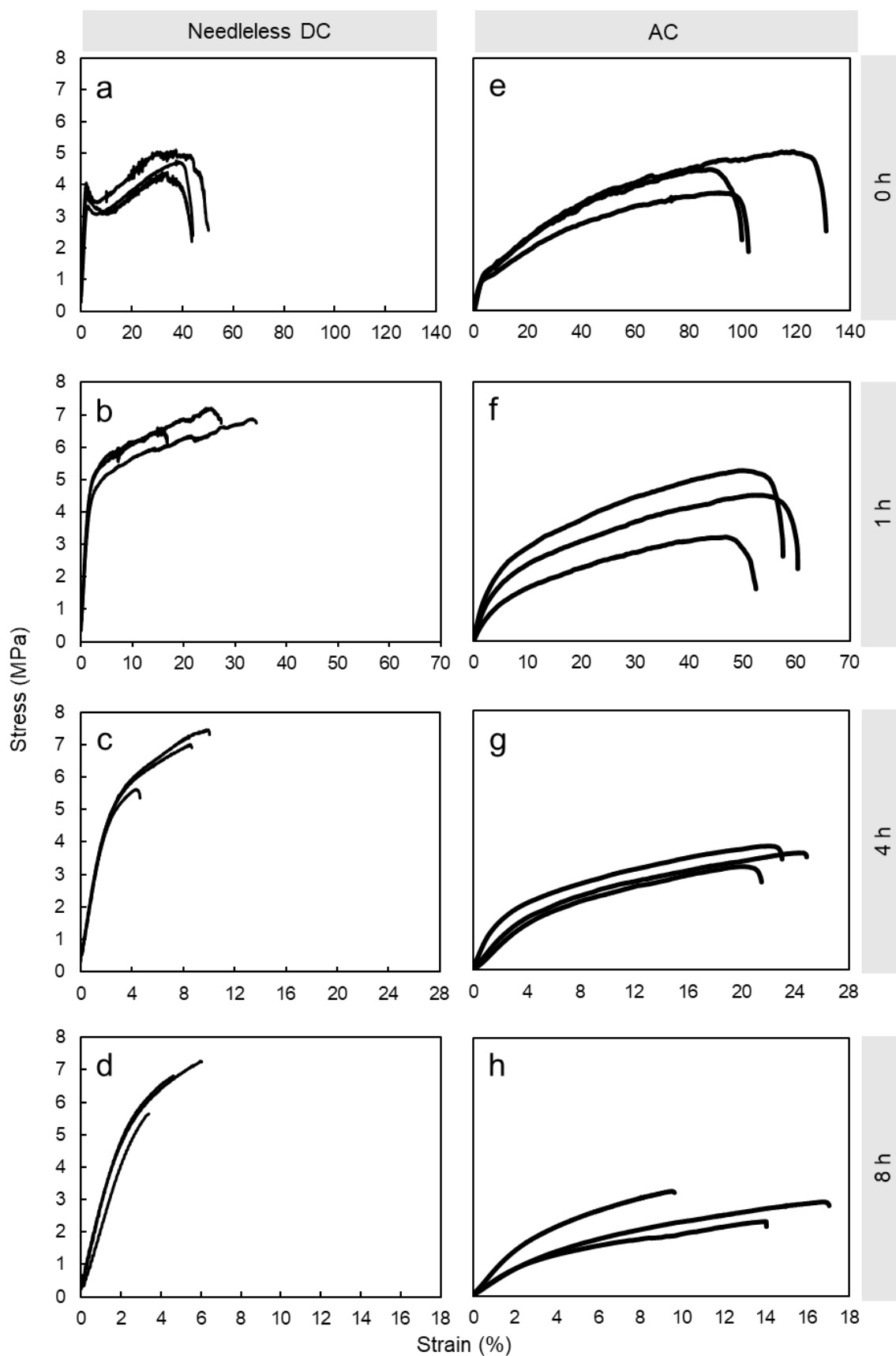
initial gain in material strength, but do follow the subsequent steady reduction after 4 and 8 h of heat treatment. Statistical analysis via a two-way anova test showed that overall, production method had a significant effect on material UTS ( $P < 0.0001$ ), whilst both production method and heat treatment duration had significant overall effects on strain at UTS ( $P < 0.0001$ ).

There are two proposed explanations for this behaviour, based on molecular and macro structures. The XRD data produced for AC spun materials indicated a less pronounced increase in crystallinity, when compared to those produced by DC. It is possibly therefore that the lack of an increase in UTS after 1 h of heat treatment is due to minimal enhancement of the crystallinity, but continued heat treatment still produced some steady degradation, which, as with the DC samples, is attributed to chain scission. Another possible mechanism which may explain this behaviour, or simultaneously contribute to it, could be due to the electrospinning process itself. AC electrospinning produces bundles of much shorter fibres which are intertwined and interconnected but not continuous, whereas DC spinning produces continuous – theoretically infinitely long – fibres. The failure mechanism could therefore be dictated by the inter-fibre friction and attractive forces between the collective fibres, rather than tensile properties of fibres themselves. If true, this may therefore act as a limiting factor to strength enhancement within materials produced by AC electrospinning. This theory would then be coupled with the stated pattern of thermal degradation, to describe the subsequent decrease in UTS at 4 and 8 h treatment duration. Though one or both of these factors could contribute to the observed behaviour, more work is required to better understand the underlying mechanism.



**Figure 2.24.** Tensile performance of PVA mats produced by DC and AC electrospinning following a range of heat treatment durations ( $n=3$ ). Key: DC (grey); AC (white).

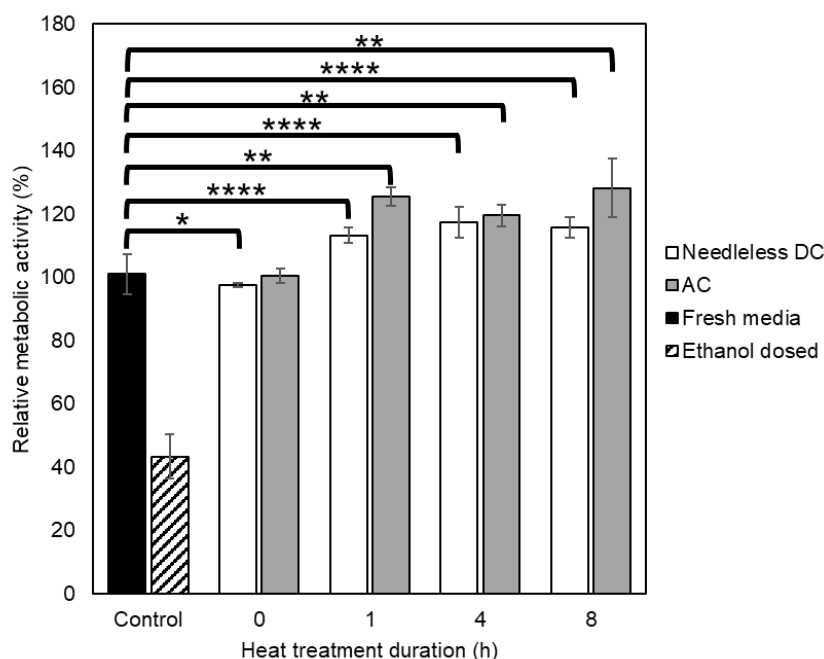
To convey the character of each material's behaviour, stress-strain curves for all samples are shown in **Figure 2.25**. Of all the samples, only the untreated ones produced by DC spinning exhibited a clear yield point, followed by strain softening, commonly associated with more ductile materials (Chen and Schweizer, 2011). This sample also features an elastic region, reaching much greater strain before its yield point. This was not observed in AC spun samples, which further highlights the fundamental difference in the material properties arising from the two production methods. Profiles of the heat treated samples demonstrate the tough and strong character usually associated with plastics, along with the increasing brittleness in both sample series, as a consequence of longer heat treatment duration.



**Figure 2.25.** Stress-strain graphs of PVA mats produced by AC and DC electrospinning under tensile load. Left column: Needleless DC samples heat treated for 0, 1, 4 and 8 h [a-d]. Right column: AC samples heat treated for 0, 1, 4 and 8 h [e-h].

## 2.3.5.4 Biological analysis

Cytotoxicity testing of the DC and AC spun membranes was carried out, to investigate the effects of the two electrospinning methods and heat treatment durations on the cytocompatibility of the otherwise highly biocompatible PVA (**Figure 2.26**). The extract method was chosen for these tests because it is the most adopted protocol for the *in vitro* cytotoxicity evaluation of medical devices, as it can be applied to a wide range of materials that may leach toxic substances from exposed surfaces (Baek et al., 2005). The extraction time used in this work was 24 h, which significantly exceeds the anticipated contact time (< 1 min) of the membranes with biological fluids when in use for blood salvage. The dissolved untreated mats had almost no effect on cell growth when compared to the fresh medium control sample, whilst medium conditioned with all other samples resulted in an increase in cell metabolic activity ranging between 13-17% for the needleless DC and 20-28% for the AC. Although there seemed to be no clear trend with respect to the duration of the heat treatment, statistical analysis suggested that both production method ( $P = 0.002$ ) and heat treatment ( $P < 0.0001$ ) played a significant roll in metabolic activity. Furthermore, the results are highly reproducible and confirm that any leachables from the potential dissolution of PVA have no cytotoxic effect under these conditions. This is a very promising result when considering the final application of the mats in cell-contacting medical devices, irrespective of production method and heat treatment duration.



**Figure 2.26.** Cytotoxicity of 99% DH PVA materials produced by DC and AC electrospinning following heat treatment between 0 and 8 h, using hMSCs measured with the CCK-8 assay. Key: Fresh medium control: black; Ethanol control: hatched; DC: grey; AC: black.



## 2.4 Conclusion

The effect of additive-free stabilisation by thermal treatment of PVA nanofibers (with DH of 88% and 99%) at 180 °C was successfully demonstrated in this chapter. Although this method has already been presented in the literature, longer durations were investigated and tested with non-woven materials produced using different electrospinning platforms. Due to its low productivity, the laboratory scale needle-based DC platform was employed in preliminary experiments to help identify parameters (*i.e.* polymer concentration and solvent) for the creation of bead-free nanofibers, which were then successfully transferred to needleless DC and AC electrospinning platforms with minimal modifications.

Using a series of characterisation methods (morphological, chemical, and biological), the extent of treatment duration on the behaviour of the non-woven supports as part of medical devices revealed that there is a trade-off between reducing PVA solubility in aqueous environments (and therefore preserving the highly desirable open fibrous structure) and maintaining ease of handling and desirable mechanical performance. Both needleless DC and AC electrospinning did not appear to impart a major change in Mw and structure, and neither did they produce cytotoxic leachables. The AC method however, enabled the creation of much larger diameter fibres, a characteristic that can be highly desirable in the processing of large biological entities such as human therapeutic cells.

## Chapter 3

# Cell flowthrough studies using thermally stabilised non-functionalised PVA nanofiber membranes

### 3.1 Introduction

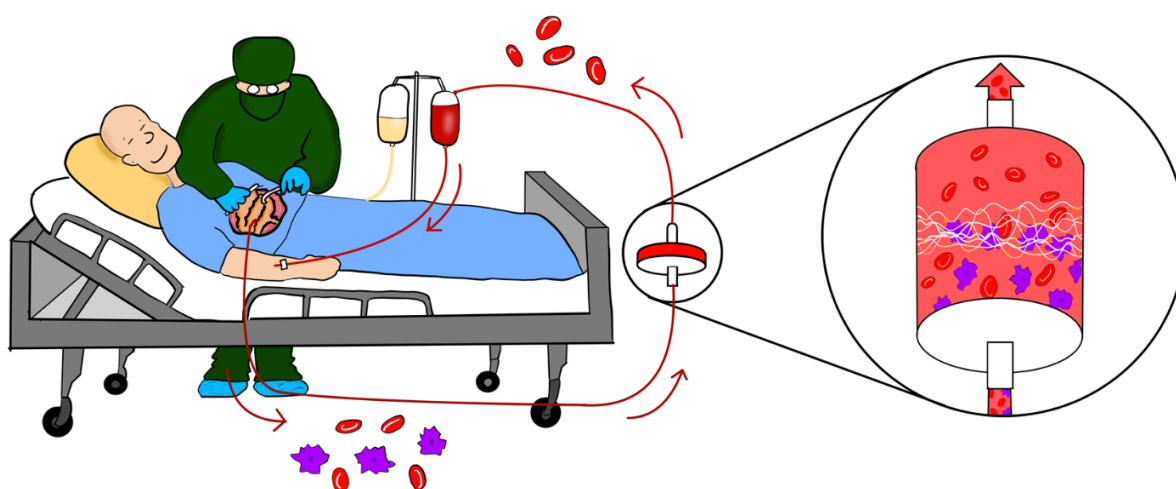
The blood loss associated with orthopaedic, cardiac, vascular, obstetrics and trauma surgeries often exceed 20% of a patient's estimated blood volume, and in cases of tumour surgeries, average losses of 2,180 mL have been reported (Shulman, 2000, Chen et al., 2013, Jaramillo et al., 2020). Despite the use of several techniques to minimize intra-operative blood loss, there is still a requirement for ABT within modern surgical practice, with approximately 1.4 million units issued each year in the UK (NHS, 2018, NHS, 2019, NHS, 2020). While ABT is used routinely as a life-sustaining and life-saving procedure, it is not without its own risks and complications (Chasse et al., 2016). Leading ABT-related causes of mortality include transfusion-related acute lung injury, haemolytic transfusion reactions, and transfusion-associated sepsis (Vamvakas and Blajchman, 2009). Based on the above safety concerns, as well as the increasing costs and ongoing variability of allogeneic blood supply, alternative solutions have been explored in the form of patient blood management (PBM) programs (Shander et al., 2013, Liumbruno et al., 2015, Sikorski et al., 2017, Frank et al., 2020). PBM can involve several practices, including preoperative autologous blood donation, red blood cell mass optimization, perioperative blood conservation and ICS, all of which are designed to reduce the need for ABT and associated post-operative complications (Shander et al., 2013, Sikorski et al., 2017, Spahn et al., 2013, Isbister, 2015, Zaw et al., 2017, Fischer et al., 2019).

ICS, or blood salvage, is a process by which the patient's shed blood is processed during surgery to recover and then return the red blood cells back to the patient. Most commercially available ICS devices are based on centrifugation, with one device using filtration (Sorin Group, 2013, Advancis Surgical, 2017, Haemonetics, 2019, Fresenius Kabi, 2020, JPAC, 2020). Whilst these separation methods can process blood quickly, they lack selectivity, and

subsequently, their use in oncological surgeries poses safety concerns, with Kumar and co-workers presenting data showing the inability of the existing cell salvage devices to remove CTCs from blood (Kumar et al., 2017). These facts create apprehension amongst clinicians, as the reinfusion of CTCs carries the risk of metastatic spread of a primary tumour and thus failure of otherwise curative operations. CTCs are rare cells [in the order of one CTC per  $10^6$  white blood cells and  $10^9$  red blood cells per mL of peripheral blood (Akpe et al., 2020)], and evidence suggests that intra-operative manipulation of a tumour during surgery can significantly increase their numbers in the blood stream (Miyazono et al., 2001, Marshall and King, 2016). Some publications have demonstrated successful removal, destruction, or otherwise reduction in metastatic capabilities of CTCs in salvage blood retrieved from patients undergoing primary tumour surgery, when the ICS devices were combined with leukodepletion filters (LDF) (Perseghin et al., 1997, Martin et al., 2005, Catling et al., 2008, Poli et al., 2008, Rajasekaran et al., 2021), whilst Waters and co-workers reported no difference in the recurrence rate of cancer between patients receiving ABT compared to those receiving salvage blood (Waters et al., 2012). Despite this, theoretical concern still persists within the oncological setting, with the Association of Anaesthetists recommending that the application of blood salvage in cancer surgery should be limited to case-by-case assessment and should require specific patient consent (Klein et al., 2018). Therefore, blood recovered by ICS is not commonly employed in instances of primary tumour surgeries outside of life-or-death situations.

A potential method of overcoming the safety issues associated with the processing of blood intraoperatively, involves the development of a device which can selectively remove tumour cells, whilst maintaining the high throughput of the existing cell salvage equipment. Chromatography is widely considered as the solution to all high-resolution separation problems within the bioprocessing industry and has been used routinely in this capacity since the 1950s (Curling, 2007). Amongst the different types of chromatography, immunoaffinity is the one with the highest specificity because it relies on antibody-antigen interaction, and has already been employed for lymphocyte enrichment using cell surface markers, in a similar principle to MACS (Mohr et al., 2018). Cell chromatography is still in its infancy however, with macroporous monoliths being the preferred stationary phase due to their reduced resistance to mass transfer (Dainiak et al., 2005, Kumar and Srivastava, 2010, González-González et al., 2017). Stacked membranes are another chromatographic format also utilized with convective flow configurations, and therefore identified as potential material for the separation of large biological entities, such as human cells (Gagnon, 2006). There are many different materials and configurations used for membrane chromatography supports and the reader is directed elsewhere for further details (Orr et al., 2013).

In this chapter, the thermally stabilised PVA nanofibers described in Chapter 2 are assessed for their ability to let through human cells, as a first step towards the development of a membrane chromatography platform. It is proposed that a high-throughput system, combined with immunoaffinity chromatography, has the potential to bring ICS to oncological surgery, with reduced risk to the patient (**Figure 3.1**). This work investigates the flowthrough capacity of unfunctionalised PVA membranes with different cell types and suspensions, *i.e.* neural blastoma cells as a cancer model, human erythrocytes, and sheep's blood, and looks at the effect of total cell number and concentration on the cell recovery.



**Figure 3.1.** Overview of the proposed cell salvage process. Blood is recovered from the patient during surgery and processed to remove tumour cells based on surface markers, before being returned to the patient. Image Copyright © 2022 Benjamin Dagès.

## 3.2 Materials and Methods

### 3.2.1 Materials

FBS, RPMI-1640 with L-Glutamine for cell culture were purchased from Merck KGAA (Darmstadt, Germany), whilst defibrinated sheep's blood was bought from TCS Biosciences Ltd. (Buckingham, UK). Cytiva Ficoll-Paque™ PLUS for RBC isolation was purchased from Fisher Scientific UK Ltd. (Loughborough, UK), and phosphate-buffered saline (PBS) for dilutions and suspensions was obtained from Scientific Laboratory Supplies Ltd. (Nottingham, UK). SH-SY5Y Neural blastoma cell line was purchased from European Collection of Authenticated Cell Culture (cat. no: 94030304) and modified for red fluorescence protein

expression according to George et al. (2018). Human blood was obtained from healthy donors pre-surgery by the Royal Orthopaedic Hospital.

### 3.2.2 Preparation of cell suspensions

#### 3.2.2.1 SH-SY5Y

SH-SY5Y neural blastoma cells were seeded at  $2 \times 10^4$  cells·cm<sup>-2</sup> in Corning T-75 cell culture flasks using cell growth medium comprised of RPMI-1640 combined with 10% FBS and cultivated at 37 °C and 5% CO<sub>2</sub> until confluent. After lifting and cell pellet preparation by centrifugation, the cells were resuspended in PBS, counted and diluted to a target concentration of  $10^7$  cells·mL<sup>-1</sup> by performing cell counts carried out using a Bright-Line haemocytometer (Sigma Aldrich, Gillingham, UK).

#### 3.2.2.2 Dilute defibrinated sheep's blood

Defibrinated sheep's blood was diluted using PBS to a concentration of  $8 \times 10^7$ , ascertained by cell counts, and then serially diluted to concentration of  $4 \times 10^7$ ,  $2 \times 10^7$ , and  $10^7$  cells·mL<sup>-1</sup>.

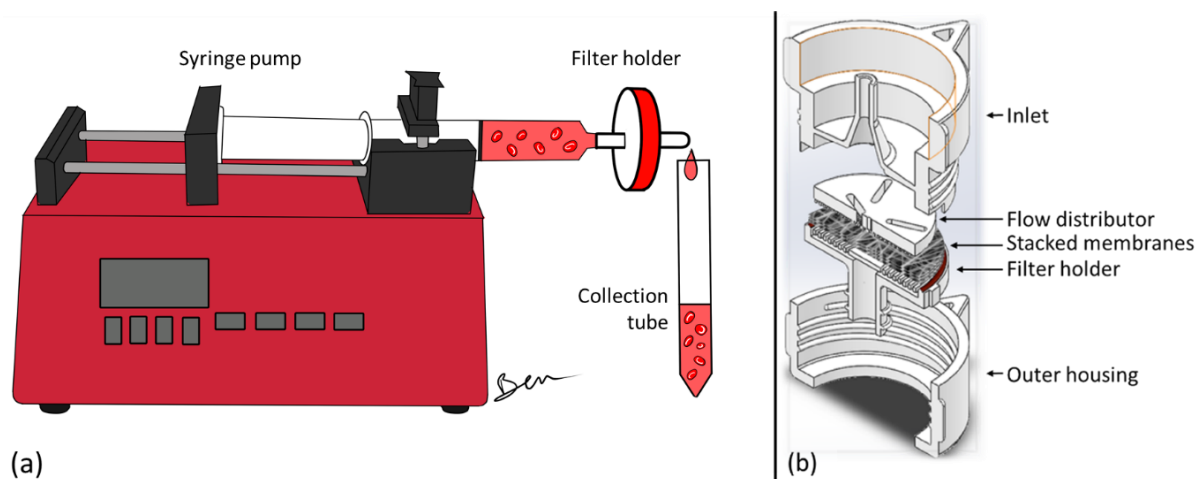
#### 3.2.2.3 Human erythrocytes

Human RBCs were isolated from whole human blood samples using Ficoll-Paque™ PLUS according to manufacturer's guidance, and serial dilutions prepared as for defibrinated sheep's blood.

#### 3.2.2.4 Flowthrough experimental set up

Cell permeation experiments were carried out using 25 mm Ø discs punched from 99% hydrolysed PVA nanofiber membranes (produced by electrospinning as described in the previous chapter) and were mounted in a Cole-Parmer™ filter holder (**Figure 3.2.b**). The filter holder was mounted into a syringe pump (AL-1800, WPI, Sarasota, FL, USA) and cell suspensions were passed through the membrane at a flow rate of 6 mL·min<sup>-1</sup>, followed by PBS wash steps under forward and reverse flow, with fractions being collected manually throughout each experiment, with brief pauses in flow between collections. Where utilised, accelerated wash steps were performed at 10× normal flow rate. For dilute cell suspensions, the total membrane thickness averaged 18 µm, resulting in a total bed volume of 8.8 µL and the collected cell fraction volume was 1 mL. Flowthrough experiments using undilute defibrinated sheep's blood used a membrane stack with an average cumulative thickness of

110  $\mu\text{m}$  (total bed volume of 54.0  $\mu\text{L}$ ) and collected fraction volume of 5 mL. Cell counts were carried out on all fractions.



**Figure 3.2.** (a): Illustrated setup of the flowthrough experiment. Flow of cell suspensions was achieved using a syringe pump under constant flow through a filter holder containing the electrospun membranes. Fractions were collected at the outlet of the filter holder. (b): Cross-section of the exploded filter holder assembly including the nanofiber membrane support. Image (a) Copyright © 2022 Benjamin Dagès

### 3.3 Results and Discussion

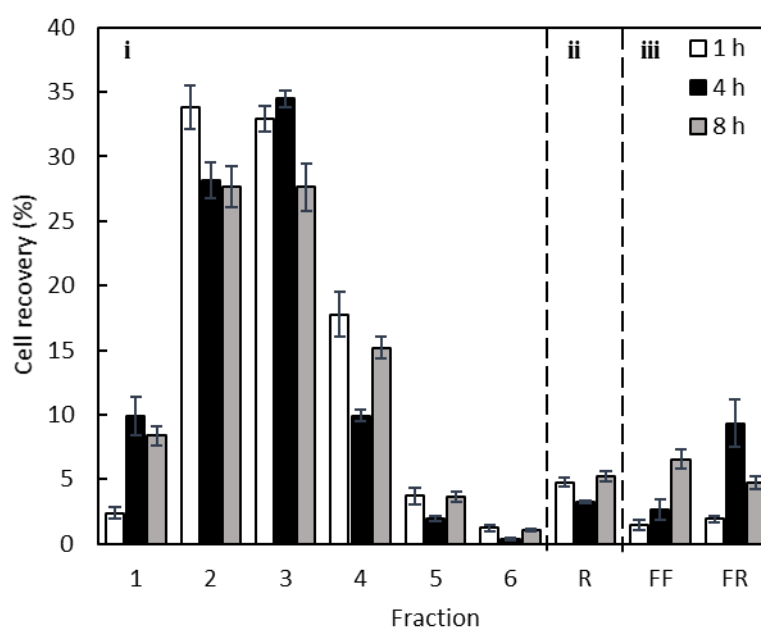
#### 3.3.1 Cell flowthrough studies using membranes produced by needleless DC electrospinning

Initial experiments with hMSCs (also used for the cytotoxicity testing described in section 2.3.5.4) showed that under the described conditions, the cells did not penetrate the membranes, most likely due to their large size (Average suspended diameter of 26.3  $\mu\text{m}$ ) and low cell concentration used<sup>1</sup>. The method and results of these experiments can be found in **appendix C**. A decision was therefore made to replace the hMSCs with SH-SY5Y neural blastoma cells, as these cells are a better representation of some populations of CTCs in terms of size (Mendelaar et al., 2021), and can be cultured at high concentrations (a fully confluent T-flask contains of 10 $\times$  more cells than hMSCs).

<sup>1</sup> The cell concentration used in these experiments was limited by the experimental conditions. The total number of hMSCs harvested from the fully confluent T-flasks was still low as a cell challenge for the flowthrough studies.

## 3.3.1.1 SH-SY5Y cell suspension of fixed concentration

The flowthrough performance of 99% hydrolysed PVA membranes heat treated for 1, 4 and 8 h was compared using SH-SY5Y cells. The flow rate of cell suspensions was held constant at  $6 \text{ mL}\cdot\text{min}^{-1}$  during cell challenges and wash steps, with very brief pauses between each collected fraction. This flowrate gives a superficial fluid velocity of  $0.02 \text{ cm}\cdot\text{s}^{-1}$ , which closely matches the flow velocities found in capillaries, therefore providing the minimum design base for operating conditions in a clinical setting.



**Figure 3.3.** Percentage of SH-SY5Y cells recovered per fraction following flowthrough experiments using heat treated 99% DH PVA materials produced by needleless DC electrospinning. Phase i: collected fractions representing initial cell challenge of  $4 \text{ mL}$  of suspension at  $10^7 \text{ cells}\cdot\text{mL}^{-1}$  ( $6 \text{ mL}\cdot\text{min}^{-1}$  flow rate), followed by PBS wash. Phase ii: PBS reverse wash fraction (fraction R). Phase iii: forward (fraction FF) and reverse (fraction FR) wash steps at  $60 \text{ mL}\cdot\text{min}^{-1}$ , used to purge loose cells from the system. (Phase i and ii fraction volume:  $1 \text{ mL}$ ; phase iii fraction volume:  $10 \text{ mL}$ ). Key: 1 h heat treated membranes (white); 4 h (black); 8 h (grey).

Freshly harvested SH-SY5Y neural blastoma cells were suspended in PBS at a concentration of  $10^7 \text{ cells}\cdot\text{mL}^{-1}$ , and  $4 \text{ mL}$  of this suspension was passed through the membrane, followed by washing steps with PBS (**Figure 3.3**). The cells collected in each fraction are shown as a percentage of total cells recovered. A consistent breakthrough effect was observed for all the membranes, with most cells being recovered in fractions 2 and 3. Cells recovered in phase ii (fraction ‘R’), suggest a small degree of caking on the filter, though cell counts indicate that this makes up for less than 6% of all recovered cells in all three experiments. Final wash steps at increased flow rates (phase iii) were intended to flush residual cells from the system. It

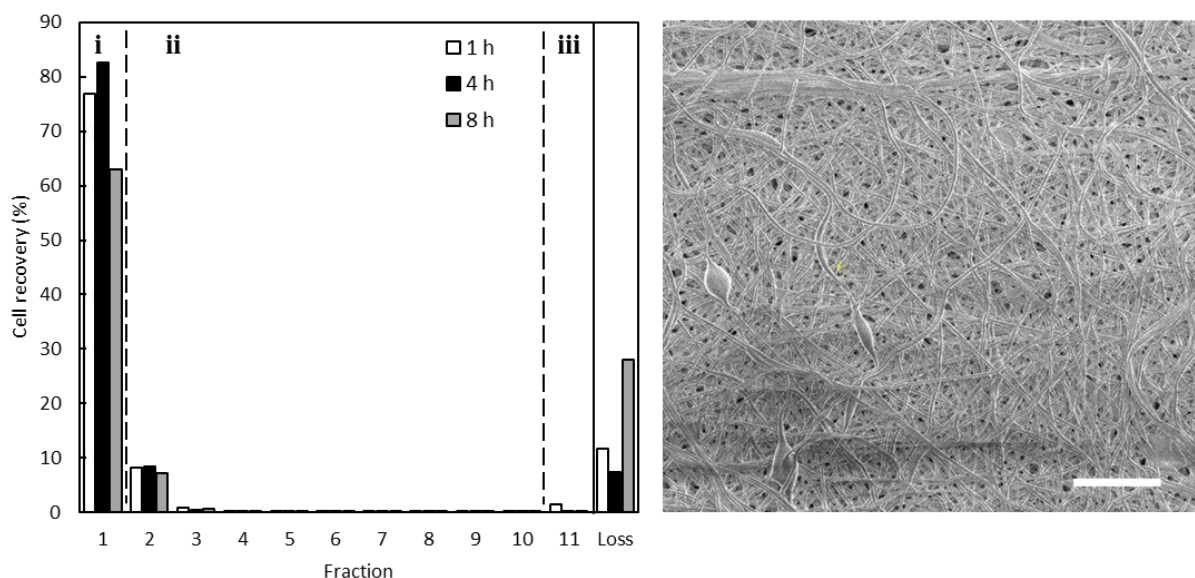
seems that most cells (> 75%) were able to pass freely through the membranes under normal operating conditions, despite the apparent tight packing of the nanofibers. The total combined cell recoveries from membranes treated for 1, 4 and 8 h were 78.55%, 77.93% and 83.08% respectively. This suggests that even after thorough flushing, the overall loss to the system is on average 20.15%. It was however unclear if this percentage would be consistent regardless of scale of the cell challenge, and whether it would ultimately lead to the clogging of the membrane.

### 3.3.1.2 Undiluted cell suspensions of defibrinated sheep's blood

To examine the membranes for evidence of caking, pure defibrinated sheep's blood (a screened mammalian blood product with coagulating components removed) was employed in a follow up cell permeation experiment. Defibrinated sheep's blood contains approximately  $10^{10}$  cells·mL<sup>-1</sup>, and such large cell numbers would help highlight any caking issues. The erythrocytes themselves have a similar morphology to human RBCs, with an average diameter of up to 4.5  $\mu$ m, compared to 7  $\mu$ m for human RBCs (Ward et al., 2018, Adili et al., 2016). In this instance, the challenge volume was 5 mL of undiluted blood, and all fractions collected were also 5 mL in volume. The percentage of cells recovered in each fraction is based on the number of cells in the initial feedstock and are shown in **Figure 3.4** (left hand side graph). Most cells were collected in the first two fractions (62.9%-81.7% in the first one and 7.2-8.3% in the second), whereas all other fractions contained no more than 0.8% of the initial cell challenge. Cumulative cell counts indicate that in total 88.4%, 92.7%, and 71.9% of cells were accounted for, from the non-woven mats that were heat treated for 1, 4 and 8 h, respectively. To find out if the cells seemingly lost in the system were physically trapped or non-specifically bound to the polymeric network, a representative membrane was immersed in formaldehyde (to fix any entrapped cells), lightly rinsed with PBS, and analysed by ESEM. The image from the 4 h heat treated sample (**Figure 3.4**, right hand side) shows no sign of entrapped RBCs or any other large entities. Although it seems possible that there could be flow restrictions through the small pore sizes observed in the ESEM image, the sheep RBCs are clearly able to migrate through the network. This is not surprising based on their morphology and function. Erythrocytes can travel through 3-5  $\mu$ m capillaries and 0.5-1  $\mu$ m splenic sinuses during their lifespan (Tomaiuolo, 2014, Brånemark and Lindström, 1963), because of their ability to undergo cellular deformation. This, combined with the added flexibility of the individual polymeric fibres, which allows them to also deform around the cells during flow, results in the unimpeded passage of RBCs through pores that are seemingly much smaller than the cells themselves. Given the absence of cells observed within the membrane, the apparent loss is considered a limitation of the traditional cell counting method, which is subject to human error



in both dilution and counting steps – a problem which is enhanced further when handling highly concentrated suspensions.



**Figure 3.4.** Left hand side: Recovery of defibrinated sheep's blood (left) following flowthrough experiments through heat treated 99% DH PVA materials produced by needleless DC electrospinning. Phase i: initial cell challenge with sheep's blood. Phase ii: PBS forward wash. Phase iii: PBS reverse wash. The percentage of cells unaccounted for at the end of each run is indicated in the right-hand column as 'Loss' (fraction volume: 5 mL). Key: 1 h heat treated membranes (white); 4 h (black); 8 h (grey). Right hand side: SEM image of a membrane treated for 4 h after flowthrough experiments and cell fixing (scale bar: 10  $\mu\text{m}$ ).

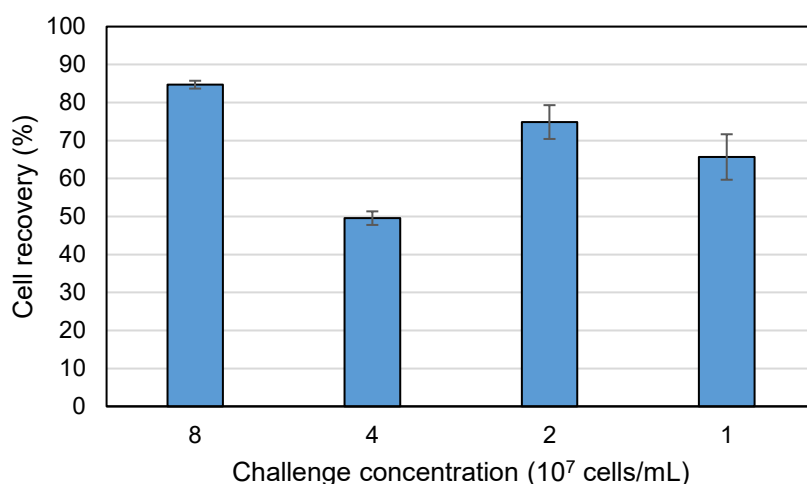
As no significant performance difference was observed between samples heat treated for differing durations, subsequent work was focused upon the samples heat treated for 4 h. It is proposed this material would be the most suitable for the suggested final application, as it apparently combines the benefits of good penetration by large biological entities shown here, along with minimising the degree of swelling in the presence of water above that seen in the 1 h treated sample, while still keeping treatment duration to a relative minimum – a factor which should not be overlooked when considering scaling up production for a potential medical device or material.

### 3.3.1.3 Dilute cell suspensions of defibrinated sheep's blood

Having established the ability of the membranes to facilitate the flowthrough of cell suspensions generally, the effect of the cell challenge concentration was explored by preparing serial dilutions of defibrinated sheep's blood, ranging from  $10^7$  to  $8 \times 10^7$  cells  $\cdot$  mL $^{-1}$ . These suspensions were applied to the 4 h heat treated membrane in largely the same manner

as for the SH-SY5Y cell suspensions, *i.e.* 4 mL of suspended cells (resulting in cumulative challenges of 32 down to  $4 \times 10^7$  cells), followed by 3 mL of PBS wash in normal forward flow, and 1 mL was under reverse flow conditions. The flow was paused briefly between the collection of each 1 mL to allow for exchanging eppendorfs.

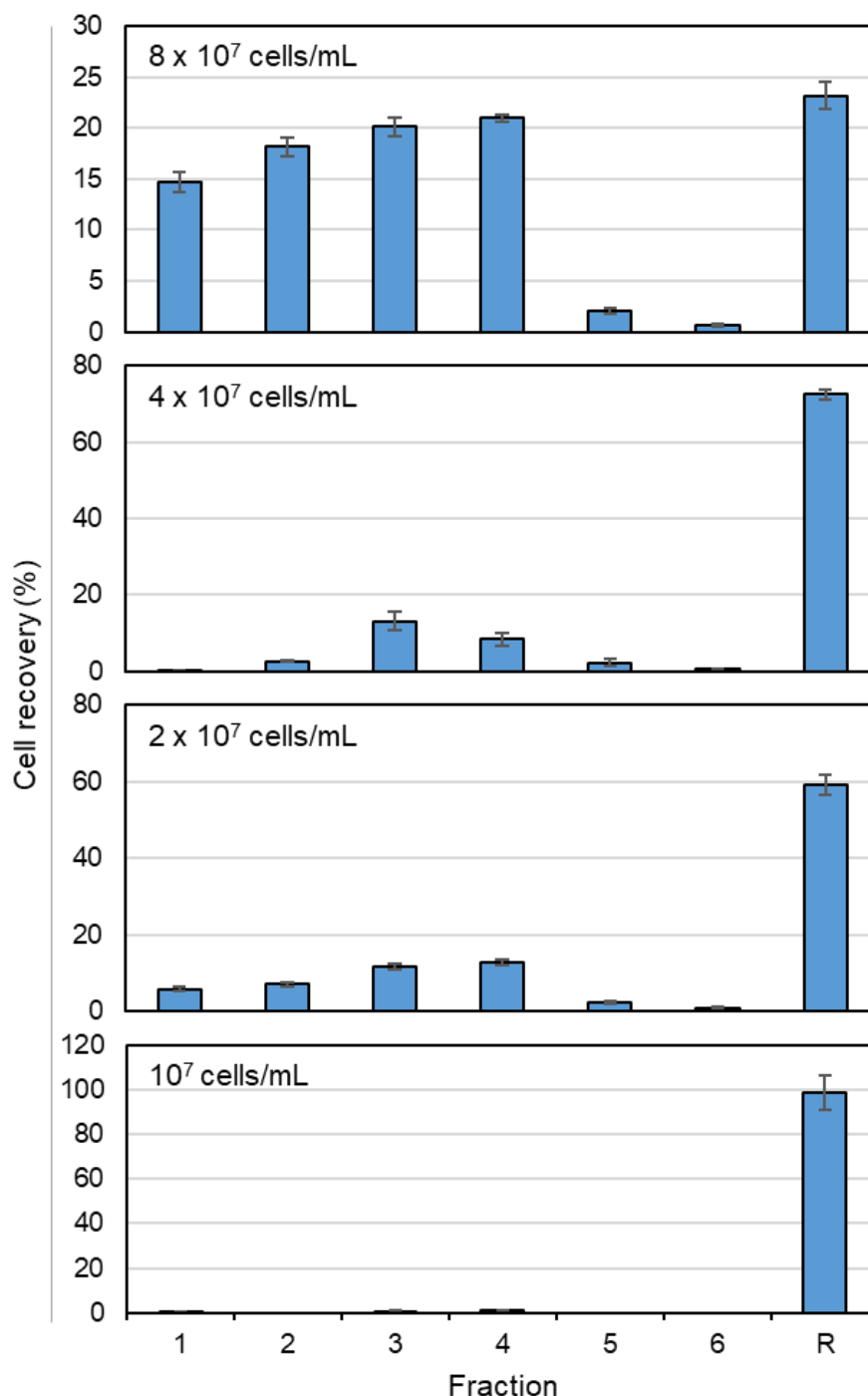
The total percentage of cells recovered across all fractions for each feedstock concentration ranged from 49.6% to 84.7% (**Figure 3.5**). Though a discrepancy was observed at  $4 \times 10^7$  cells·mL<sup>-1</sup>, there seems to be a trend in recovery which is mirrored by the concentration of cells applied to the membrane. This can be attributed to a constant minimal loss to the system, regardless of cell challenge concentration.



**Figure 3.5.** Total sheep blood cell recovery as a percentage of total cell challenge from flowthrough experiment with respect to cell challenge concentration after passing through 4 h heat treated 99% DH PVA materials produced by needleless DC electrospinning.

By examining the breakthrough pattern of the recovered cells per collected fraction, it can be seen that, at the lowest cell challenge concentration ( $10^7$  cells·mL<sup>-1</sup>) nearly all the recovered cells were counted in the reverse flow fraction, whereas as cell concentration increased to  $8 \times 10^7$  cells·mL<sup>-1</sup>, the percentage of cells recovered in the reverse flow fraction reduced from 98% to 23% (**Figure 3.6**). This matches the behaviour observed in the undiluted tests, where for all samples, < 2% of the recovered cells were accounted for in the reverse flow fraction. These results suggest that in the case of sheep erythrocytes, passage of the cells through the membrane is at least partly assisted by a physical interaction and flow of the suspended cells, and not exclusively by the suspension fluid. Interestingly, and although this is a similar behaviour to the SH-SY5Y cells, it is less pronounced for the equivalent cell concentrations

( $10^7$  cells·mL<sup>-1</sup>), since in the case of SH-SY5Ys, the cells encountered in the reverse flow fractions were < 10% of the total number of recovered cells, despite their larger size.

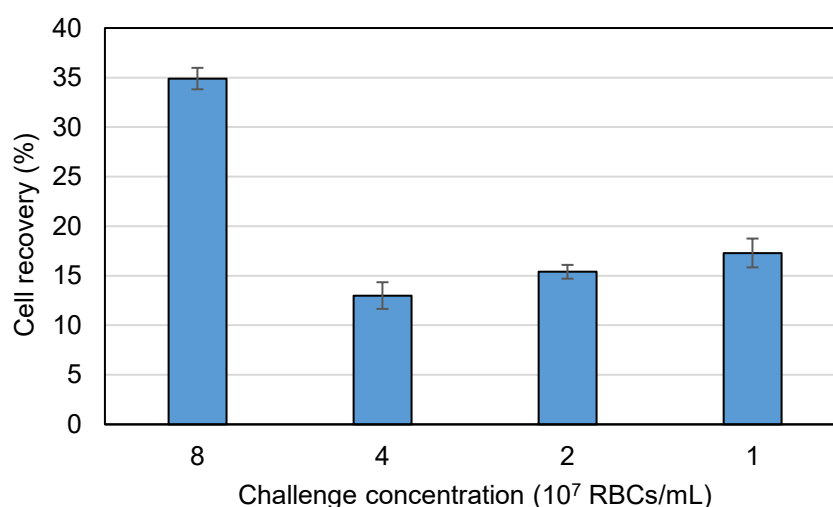


**Figure 3.6.** Percentage of the defibrinated sheep's bloodcells recovered per fraction following flowthrough experiments using 4 h heat treated 99% DH PVA materials produced by needleless DC electrospinning. Fraction 1-6 collected after 4 mL of suspension at the marked respective cell concentrations, followed by PBS wash and a final fraction (R) under reverse flow conditions. Flow rate of  $6 \text{ mL} \cdot \text{min}^{-1}$  used throughout, with 1 mL fraction volumes collected throughout, with brief 2-3 s pauses between each fraction to allow for swapping of collecting ependorf.

### 3.3.1.4 Dilute suspensions of human erythrocytes

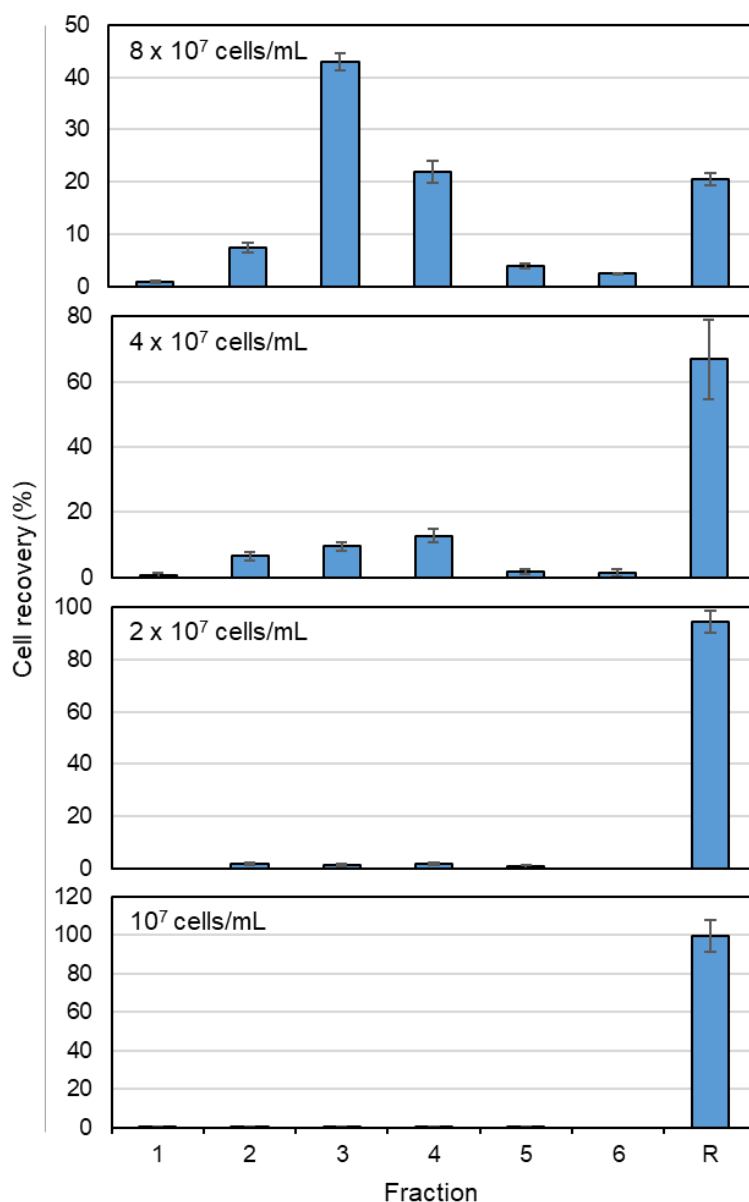
The intraoperative cell salvage device will be used with human blood and therefore the performance of the PVA membranes was subsequently tested with human cell samples. Human erythrocytes were isolated from whole donor blood using Ficoll-plaque PLUS according to the manufacturer's protocol, prepared in serial dilutions as for the defibrinated sheep's blood suspensions using PBS as a diluent, and pumped through the membranes using the same procedure as in section 3.2.2.4.

By comparison to the sheep's blood, recovery of human erythrocytes was substantially lower, ranging between 13.0% and 34.9% (**Figure 3.7**). The highest recovery was obtained when the highest concentration of cells ( $8 \times 10^7$  cells·mL<sup>-1</sup>) passed through the membrane, whilst there was little variance (an average of 15.1%,  $\pm$  2.1%) between all other cell challenges. These results are somewhat surprising, as human erythrocytes are larger than their sheep counterparts (7 vs 4.5  $\mu$ m respectively), but are smaller than the SH-SY5Y cells, which gave recoveries of  $\sim$ 78% at concentrations of  $10^7$  cells·mL<sup>-1</sup>. Furthermore, human RBCs are programmed to circulate around the body, and pass through narrow blood vessels (Tomaiuolo, 2014). A possible explanation can be offered by the unusual properties of red blood cells, such as their tendency for rouleaux formations, where cells form stacks and aggregates, though this is typically related to the presence of serum proteins such as fibrinogen (Wells et al., 1964, Rampling, 1998, Flormann et al., 2017). This could both obscure the accuracy of cell counts through formation of small stacks, but their grouping and subsequent ungrouping may also have some negative impact on the structural integrity of the cells, resulting in loss to haemolysis.



**Figure 3.7.** Total human erythrocyte recovery as a percentage of total cell challenge from flowthrough experiment with respect to cell challenge concentration after passing through 4 h heat treated 99% DH PVA materials produced by needleless DC electrospinning.

Analysis of the percentage of recovered cells per fraction, seen in **Figure 3.8**, shows similar behaviours to those found with the sheep's blood, with nearly 100% and 20% of the recovered cells being counted in the reverse flow fraction of the lowest ( $10^7$  cells $\cdot$ mL $^{-1}$ ) and the highest ( $8 \times 10^7$  cells $\cdot$ mL $^{-1}$ ) cell challenge concentrations, respectively.

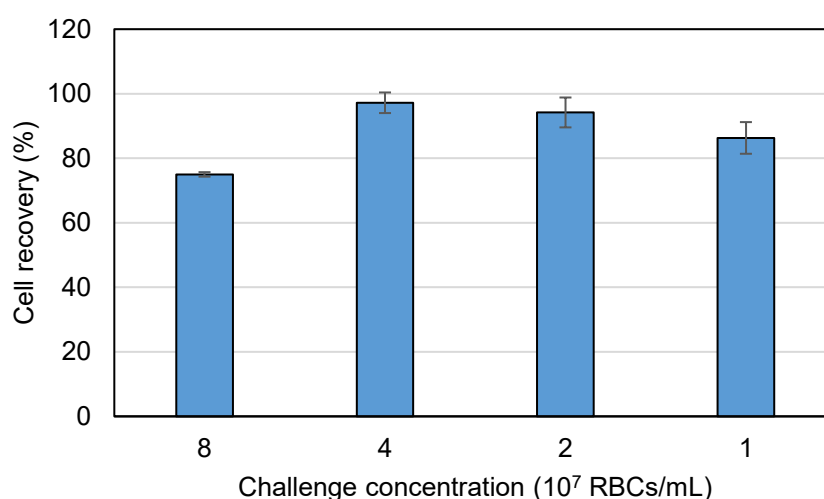


**Figure 3.8.** Percentage of human erythrocytes recovered per fraction following flowthrough experiments using 4 h heat treated 99% DH PVA materials produced by needleless DC electrospinning. Fraction 1-6 collected after 4 mL of suspension at the marked respective cell concentrations, followed by PBS wash and a final fraction (R) under reverse flow conditions. Flow rate of 6 mL $\cdot$ min $^{-1}$  used throughout, with 1 mL fraction volumes collected throughout, with brief 2-3 s pauses between each fraction to allow for swapping of collecting eppendorph.

### 3.3.2 Cell flowthrough studies using membranes produced by AC electrospinning

Considering the significant drop in cell recovery for human erythrocytes when passed through the membranes produced by needleless DC electrospinning, a series of cell challenge experiments were carried out with membranes produced by AC electrospinning with cell concentrations of 1, 2, 4 and  $8 \times 10^7$  cells·mL<sup>-1</sup>. In order to maintain consistency between the membranes, the AC non-woven support was produced from 99% hydrolysed PVA and heat treated for 4 h, and its average thickness was kept the same as the DC spun one (~18 µm).

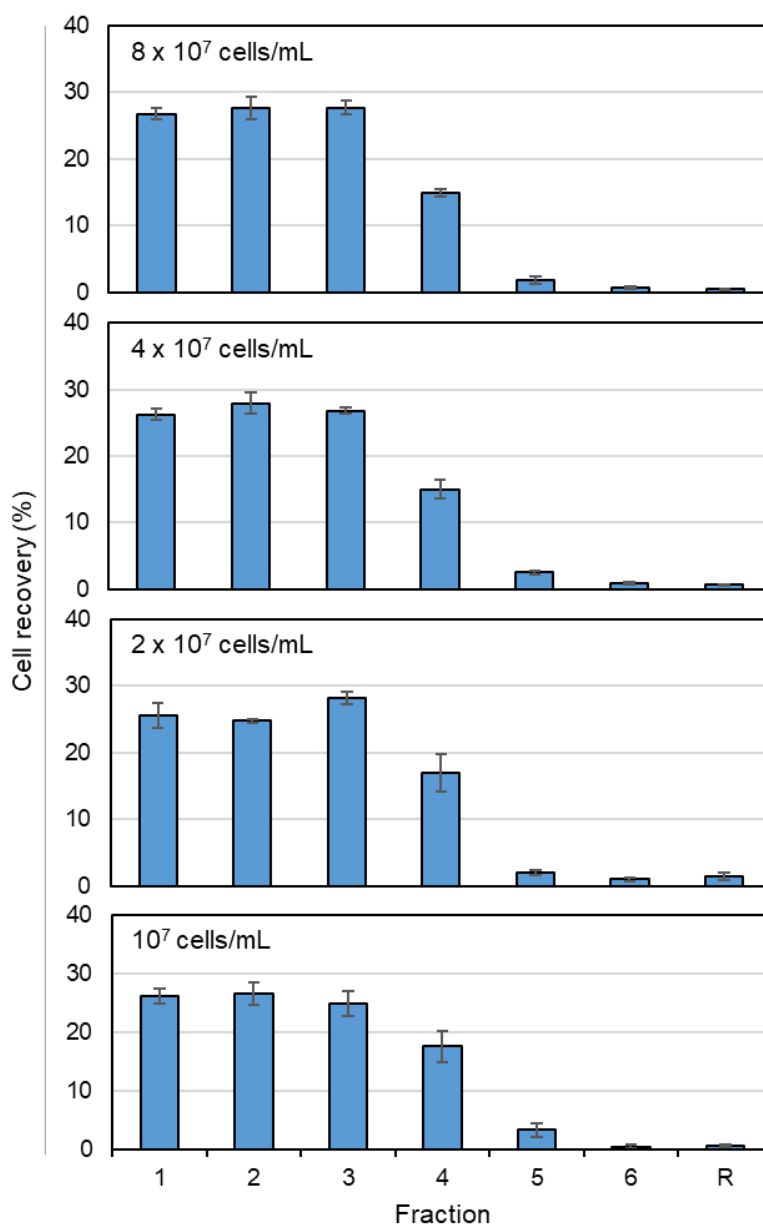
From the results presented in **Figure 3.9**, it can be seen that the cell recovery increased substantially for all cell concentrations, with numbers ranging between 75.0% and 97.2%. Unlike previous results, however, the greatest loss occurred with the highest cell concentration ( $8 \times 10^7$  cells·mL<sup>-1</sup>) with 25% of cells unaccounted for. Though there is no definitive trend, these increased recoveries could be attributed to the looser fibre structure, as well as the bigger pore sizes arising from the larger fibre diameters created by the AC electrospinning process, as opposed to the sheet like materials with tightly packed fibres produced by the needleless DC method.



**Figure 3.9.** Total erythrocyte recovery as a percentage of total cell challenge from flowthrough experiment with respect to cell challenge concentration after passing through 4 h heat treated 99% DH PVA materials produced by AC electrospinning.

The fraction-by-fraction recovery shown in **Figure 3.10** confirms an unimpeded flowthrough pattern, with cells predominantly being collected across the first 4 fractions, and nearly no cells

being recovered during the reverse wash step, which suggests that no caking or entrapment of cells occurs in the membrane under forward flow conditions. This very promising result demonstrates the significant potential benefit of using the AC electrospinning platform over needleless DC spinning, despite existing limitation on scalability of production and lack of maturity of technology.



**Figure 3.10.** Percentage of the human erythrocytes recovered per fraction following flowthrough experiments using 4 h heat treated 99% DH PVA materials produced by AC electrospinning. Fraction 1-6 collected after 4 mL of suspension at the marked respective cell concentrations, followed by PBS wash and a final fraction (R) under reverse flow conditions. Flow rate of  $6 \text{ mL} \cdot \text{min}^{-1}$  used throughout, with 1 mL fraction volumes collected throughout, with brief 2-3 s pauses between each fraction to allow for swapping of collecting endorph.

### 3.4 Conclusion

Flowthrough of cells through thermally stabilised nanofibrous PVA materials produced by DC electrospinning showed potential for the processing of large biological molecules. Cell size, type, concentration and total number had a substantial influence on final recoveries, although in all cases it was not possible to recover 100% of the cells that passed through the membranes. This could be caused by the experimental set up (e.g., filter holder, pump, etc.), cell counting method (manual instead of automatic) and in the case of erythrocytes, potential haemolysis. Human RBCs produced some unexpected results when processed through the small diameter, tightly packed DC electrospun membranes and further work is needed to improve their performance in a blood salvage context. Despite the limitations discussed in Chapter 2 with respect to scalability of production and maturity of the technology, AC electrospinning demonstrated great promise for processing human erythrocytes, as it was able to outperform its needleless DC counterpart significantly. Though no stated target recovery is given for existing blood salvage platforms or rules governing them, higher recovery percentages are of course preferable. This finding emphasises the potential of the AC platform and merits further research into materials produced by this method as cell processing membranes, especially when considered in the context of high-throughput situations, such as the proposed blood salvage application.



# Chapter 4

## Validation of flow behaviour through nanofibrous networks, and device design and prototyping

### 4.1 Introduction

Flow modelling using digital tools, such as discrete element modelling (DEM) and CFD, has been used either in isolation or coupled together to understand flow behaviours through packed beds (Zhao et al., 2012). Software, such as Structure Vision's DigiDEM suite, features tools employed for modelling flow in particle bed systems and simulating packed beds for porosity analysis (Caulkin et al., 2009, Fernengel et al., 2018), with results having been reported to be comparable to experimental data (Caulkin et al., 2008). The DigiDEM software in particular, has also been used to model flow through irregular beds (generated based on X-ray tomography), and could therefore be expanded to modelling flow through other non-traditional bed geometries, such as nanofibers (Menon et al., 2011). By rendering the nanofibrous bed as a digital volume, the modelled flow behaviour can be examined, in order to assess the likelihood of issues such as stagnation and flow channelling within the simulated 3D structure.

As well as the aforementioned flow simulations, consideration has also been given to the need for a housing of the nanofibrous membranes, with scales ranging from the bench top device used in Chapter 3, to a set-up capable of handling throughputs similar to those found in blood salvage (*i.e.*  $\sim 100 \text{ mL} \cdot \text{min}^{-1}$  or more). LDF are designed to reduce the presence of white blood cells and improve transfusion related complications. These LDF are routinely coupled with blood salvage devices during cancer surgeries, where prior consent has been agreed by patients (Klein et al., 2018), and can therefore be used as the design basis for device housing.

Additive manufacturing is the process of creating a solid three-dimensional object by building it one layer at a time and is commonly known as 3D printing (Molitch-Hou et al., 2018). Computer aided design (CAD) is routinely used along with 3D printing, for both production and

prototyping in a wide range of biomedical engineering applications, including manufacturing of medical prostheses, producing physical models for surgical planning and visualisation, and creating TE substrates (Lai et al., 2021). The greatest strength of additive manufacture techniques is their ability to quickly and cost-effectively generate singular bespoke parts (e.g., patient specific prosthetics), and enable the easy production of improved replacements. Even for small-to-moderate batch production, 3D printing can be economically viable due to reduced costs of tooling compared to processes such as injection moulding. Common forms of 3D printing use several different mechanisms, including fused deposition modelling (FDM), selective laser sintering (SLS), and stereolithography (SLA) (Shahrubudin et al., 2019). Of these, FDM and SLS both produce materials which are porous, without the requirement for additional post-processing, whilst SLA creates non-porous materials.

This chapter contains some preliminary work on the understanding of the flow within a prospective blood salvage device based on electrospun PVA membranes, through CFD modelling using the DigiDEM software suite. Furthermore, CAD is employed to provide an initial look at potential geometries for a device housing for the nanofibrous membranes and produce simple prototypes using SLA 3D printing.

## 4.2 Materials and Methods

### 4.2.1 Materials

Clear resin, white resin, and Tough 1500 resin for the 3D printing of the prototype filter holders were purchased from FormLabs (Sommerville, MA, USA).

### 4.2.2 DigiDEM - Investigation of flow through nanofibrous supports

#### 4.2.2.1 Generating pseudo-3D nanofibrous membranes

2D bitmap traces (dimensions: 400×400 pixels) were generated manually from the SEM images of nanofibers produced by needleless DC and AC electrospinning using Microsoft Paint 3D (version 6.1907.29027). The fibre diameter histograms from Chapter 2 (**Figure 2.12**) were used to mimic the ratio of diameters in the trace, *i.e.* for needleless DC traces 60 nm = 1 pixel, and for AC traces 100 nm = 1 pixel, thereby factoring in the relative fibre diameter frequencies into each trace, with a total of 100 fibres drawn per trace. This trace was then

used to generate an extruded membrane volume of a pseudo-3D nanofiber sheet using DigiUtility, with the extruded height set to 10 pixels<sup>1</sup>.

### 4.2.2.2 Generation of the packed bed

Once the membrane volumes were produced, they were imported into DigiPac and used to generate the starting structure using the 'rain' setting, allowing the individual volumes to be spawned at the top surface of the bed domain (dimensions: 500×500×500 pixels) in random locations across the bed to randomise the orientation and overlay of the materials. One volume was dropped every 10 steps for 100 volumes, followed by 100 steps of windup to allow for final settling and packing of the bed, totalling 1100 steps.

A core with dimensions 300×300×200 pixels was exported from DigiPac, and DigiDEM was used to embed this core into a solid external structure with dimensions 304×304×200 pixels, in order to generate the final bed for the simulation.

### 4.2.2.3 Flow simulation

DigiFlow operates based on a Lattice-Boltzmann Model (LBM) for flow simulation, and does not use physical units, so therefore some conversion is required. Flow velocities were given to be  $0.025 \text{ cm}\cdot\text{s}^{-1}$  with kinematic viscosity of blood considered to be  $2.65\times 10^{-6} \text{ m}^2\cdot\text{s}^{-1}$  (AntonPaarGmbH, 2023). Using the parity of Reynolds number in LBM and physical units, the relaxation value for the model was calculated to be 0.500016, applying a characteristic length of  $10^{-3}$ . Due to performance limitation in the software, initial flow velocity in the z-direction was set by assigning a body force (rather than velocity) of  $10^{-6}$  (LBM). Simulations were run for 3500 iterations, the maximum possible on the existing hardware, which was adequate time for the flow velocity to largely plateau (**Appendix D**).

## 4.2.3 Device design and prototyping

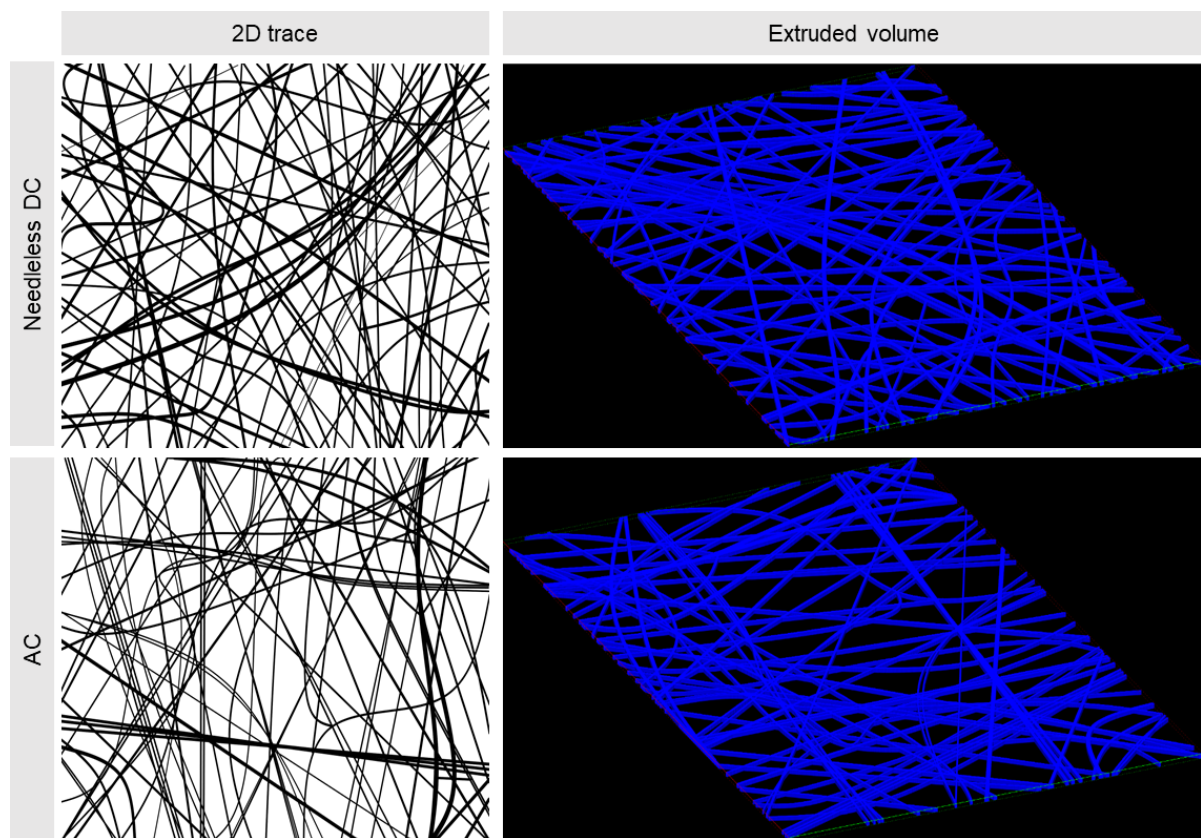
Device design iterations were created using SolidWorks 2021 (Dassault Systèmes SE, Vélizy-Villacoublay, France). These designs were 3D printed from three different resins using a Formlabs 3BL (Sommerville, MA, USA).

---

<sup>1</sup> This was selected with the purpose of rendering sheets from the trace where the 'fibres' are of approximately equal in depth and width, albeit with a cuboid cross-section, rather than cylindrical.

### 4.3 Results and Discussion

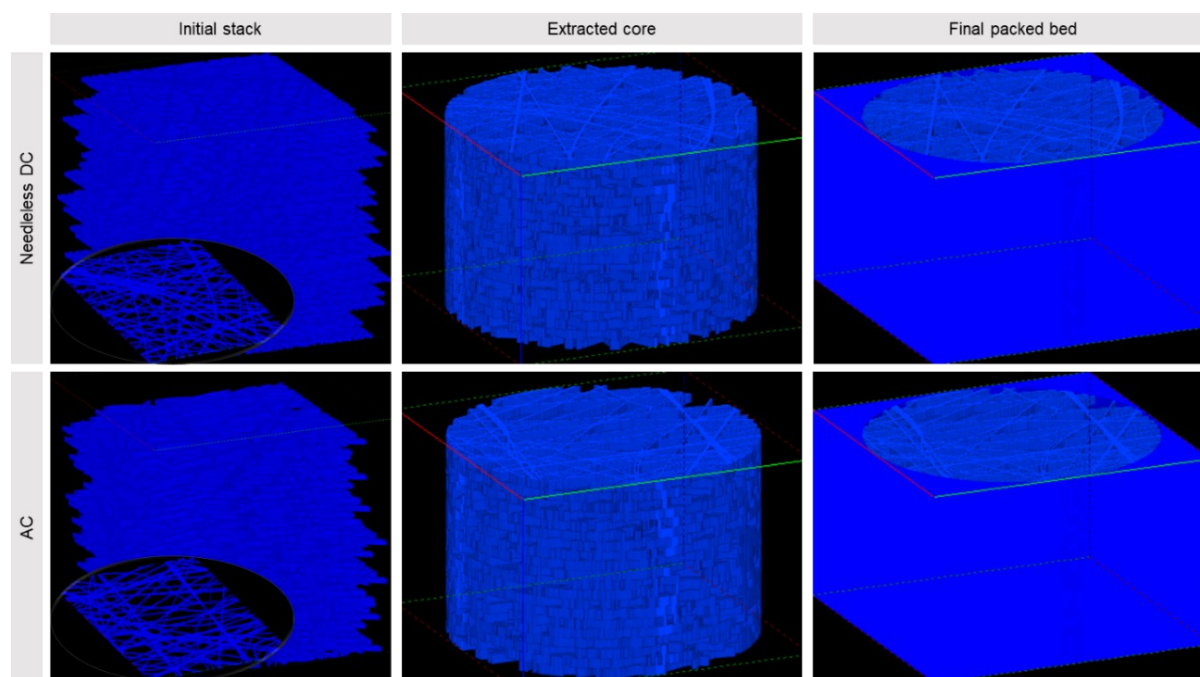
Formation of the fibrous bed was achieved by first creating a 2D trace based on SEMs of nanofibrous materials. The trace was then used to form an extruded volume, producing what was considered a pseudo-3D object, as shown in **Figure 4.1**. This is referred to as pseudo-3D as the ‘fibres’ which are modelled by the extrusion process do not have a cylindrical geometry, but rather have a cuboid cross-section. This limitation is unfortunately unavoidable within DigiDEM and will have an impact on the void space value calculated by the software and potentially on some of the flow characteristics in the simulation.



**Figure 4.1.** 2D bitmap traces of nanofibers produced by needleless DC and AC electrospinning and their corresponding extruded volumes.

A large, stacked tower of ‘fibres’ was subsequently created by randomly dropping the volumes within a slightly oversized bed (**Figure 4.2**). This prevented the direct overlay of fibres above each other in the same orientations as, and although particle collision is enabled within the software to facilitate rotation, it was not possible to randomise the rotation of the volume at the point it was spawned at the top layer of the volume. Each volume was therefore able to sit

upon the last with some random degree of offset in the x and y directions, but the lack of rotation was accepted as another limitation of the software and simulation. The core taken from this stack was encapsulated within an external solid volume to drive flow through the central core, producing the final packed object seen on the right in **Figure 4.2**, which acted as the stationary phase for the simulation.

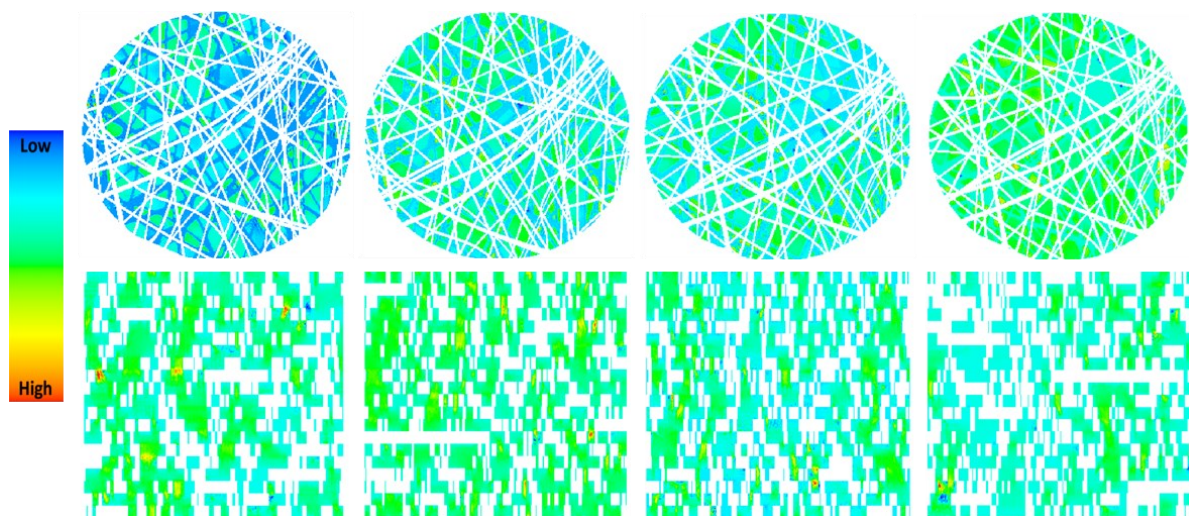


**Figure 4.2.** Stacks of extruded volumes produced from traces of needleless DC and AC electrospinning (left hand side), an extracted core of the initial stack (middle), and the final packed bed with the core encapsulated within a solid structure (right hand side).

At this point, the software offered a calculated porosity of 46.2% for the needleless DC samples, and 47.7% for the AC samples. This is in stark contrast with the measured porosities of the two samples (using the bulk density of the membranes and the density of PVA calculated as per Enayati et al., 2018b) which were found to be 84.9% and 94.2%, respectively. This can be attributed to the fact that the value produced by the software is for the total bed, and therefore is factoring in the structure encasing the core bed. Given the relative dimensions of  $300 \times 300 \times 200$  pixels for the core, and  $304 \times 304 \times 200$  pixels for the total bed, the maximum available void space in the core can be calculated to be 76.5%. Normalising for the given porosity against this, produces values of 60.4% and 62.4% for DC and AC samples respectively. The accuracy of these numbers was further improved by adjusting for the cross-section geometry of the fibres (and therefore volume) by a factor of 0.785 (the ratio of the area of a circle to the area of a square of equivalent diameter), resulting in a final adjusted volume

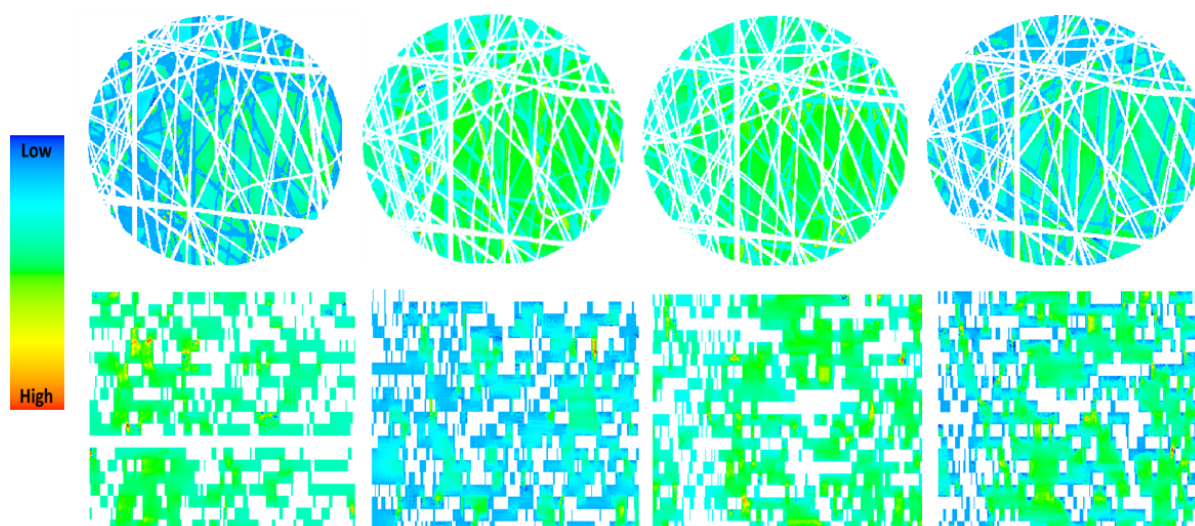
produced by the software of 68.9% for DC spun samples and 70.4% for AC spun samples. Although these values still fall substantially short of the measured porosity and could contribute to possible differences between real and simulated flow, it was considered beneficial to examine the flow through the materials, as it can nevertheless provide some insight into potential channelling and enable relative comparisons of flow behaviour between samples.

### 4.3.1 Flow simulation



**Figure 4.3.** Heat graphs indicating flow within the packed bed based on needleless DC electrospun nanofibers. Slices through Z-axis (top) taken at depths of 50, 100, 150, and 200 pixels. Slices through X-axis (bottom) taken at depths of 75, 150, 225 and 300 pixels.

Analysis of the flow through the final packed bed based on needleless DC fibres is shown in **Figure 4.3**, with several cross-sections corresponding to different bed depths. Broadly speaking, flow rates were distributed uniformly throughout the interstitial space, and though small spots of high flow rates can be identified, these did not represent significant areas of channelling with adjacent areas of dead flow, and flow speeds tended to occupy the middle range of velocities in the heat map.



**Figure 4.4.** Heat graphs indicating flow within the packed bed based on AC electrospun nanofibers. Slices through Z-axis (top) taken at depths of 50, 100, 150, and 200 pixels. Slices through X-axis (bottom) taken at depths of 75, 150, 225 and 300 pixels.

Similar results were found for the simulation of AC spun materials (**Figure 4.4**), though it was observed that the traces corresponding to clusters of fibres, led to a slight reduction in flow velocities, resulting in something slightly more reminiscent of channelling behaviour, albeit not substantial. This can also be considered as a limitation of the software and not necessarily representative of a real flow situation, based on the inability to rotate each extruded volume, which could result in areas of higher fibre density having greater overlap of 'fibres' in the simulation, and thus reducing flow. This issue could potentially be resolved and lead to improved simulation, by increasing the size of the trace, and the size of the bed used to generate the packed core, but unfortunately it would require substantially more powerful hardware, which was not available at the time of this work.

### 4.3.2 Device design

Having explored the flow behaviour via modelling of the nanofibrous membranes, some preliminary device design was attempted. 3D printing was utilised due to its flexibility to create bespoke design and prototype production. This provides great benefits for design iteration, specifically when using the SLA printing technique because of its high resolution and ability to produce non-porous materials.

The filter holder employed in Chapter 3 (shown in **Figure 4.5**) had a very small bed capacity, designed for use within the <1 mm thickness range, depending on the material. While this is adequate for laboratory testing, any cell processing application where throughput is important

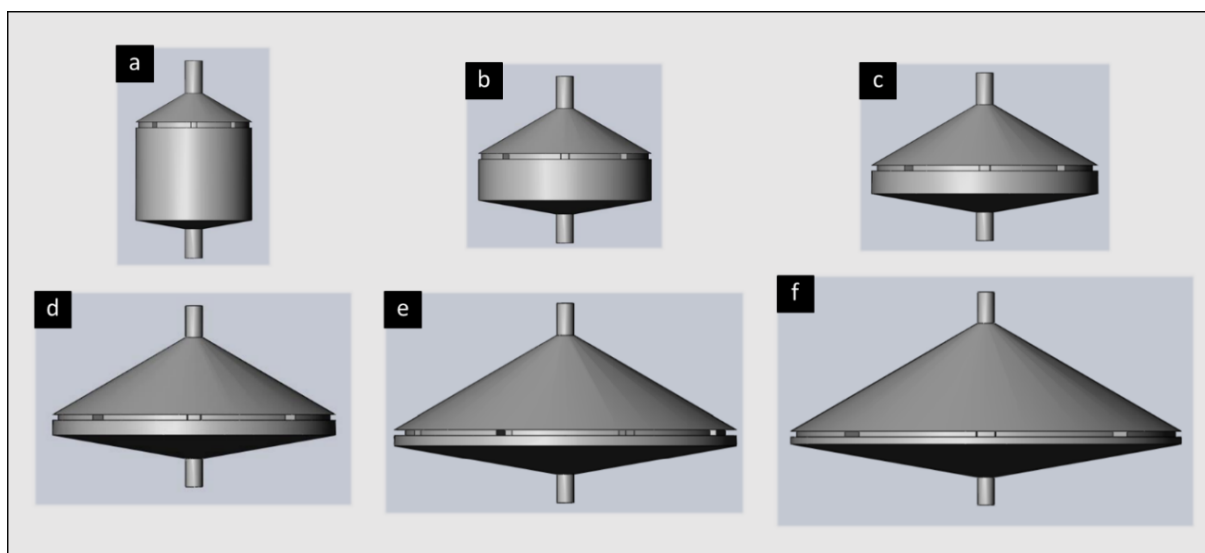
– such as blood salvage or small-scale bioprocessing – demands for higher flow capacity, as well as greater bed volume.



*Figure 4.5. Filter holder from Cole Parmer used for the flowthrough experiments in Chapter 3.*

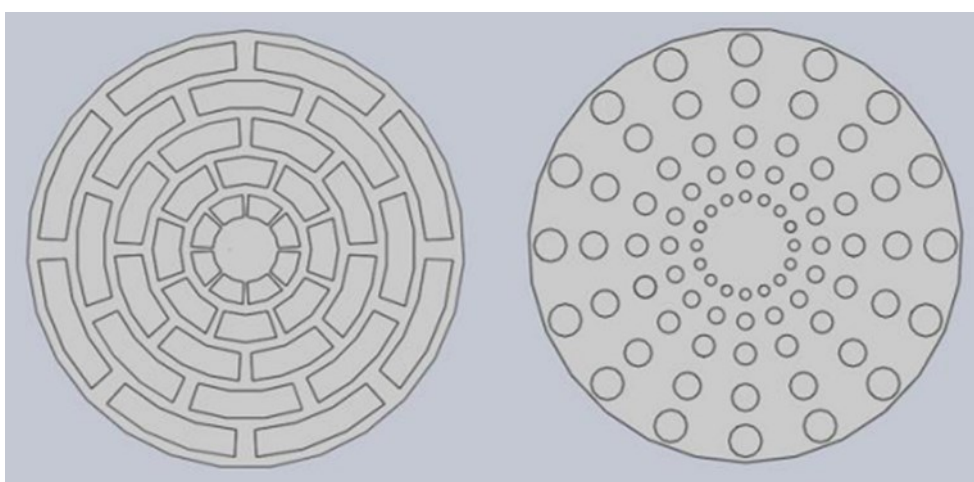
An LDF, commonly used in conjunction with intraoperative cell salvage, formed the basis of the design for the bed volume. Deconstruction of a LDF and measurement of the internal dimensions revealed that the filter material occupied a volume of approximately 5 mL. As the first step of the redesign of the filter holder, the diameter was changed (between 20 mm and 70 mm) while holding the bed volume constant, thereby allowing the bed height to vary accordingly. **Figure 4.6** shows the potential approximate geometries which would be produced (calculated bed depth of the narrowest design is ~4.0 mm, **Figure 4.6.a**, and the widest being ~0.3 mm, **Figure 4.6.f**). Theoretically, if flow is uniform, each design will result in equal bed contact time but offer different benefits and constraints, especially at the extremes of the geometries. Some theoretical issues proposed include greater difficulty in achieving good flow distribution for the wider diameter designs, whilst narrower diameter models could experience higher pressure drops when passing through a thicker bed of nanofibers. However, and without some form of validation, it is difficult to make a conclusive statement about which dimensions will produce the most optimal design. Though physical testing was outside of the scope of this work, this highlights a key benefit of additive manufacture, as prototypes for each size can be produced easily without the high tooling cost associated with methods such as injection moulding.





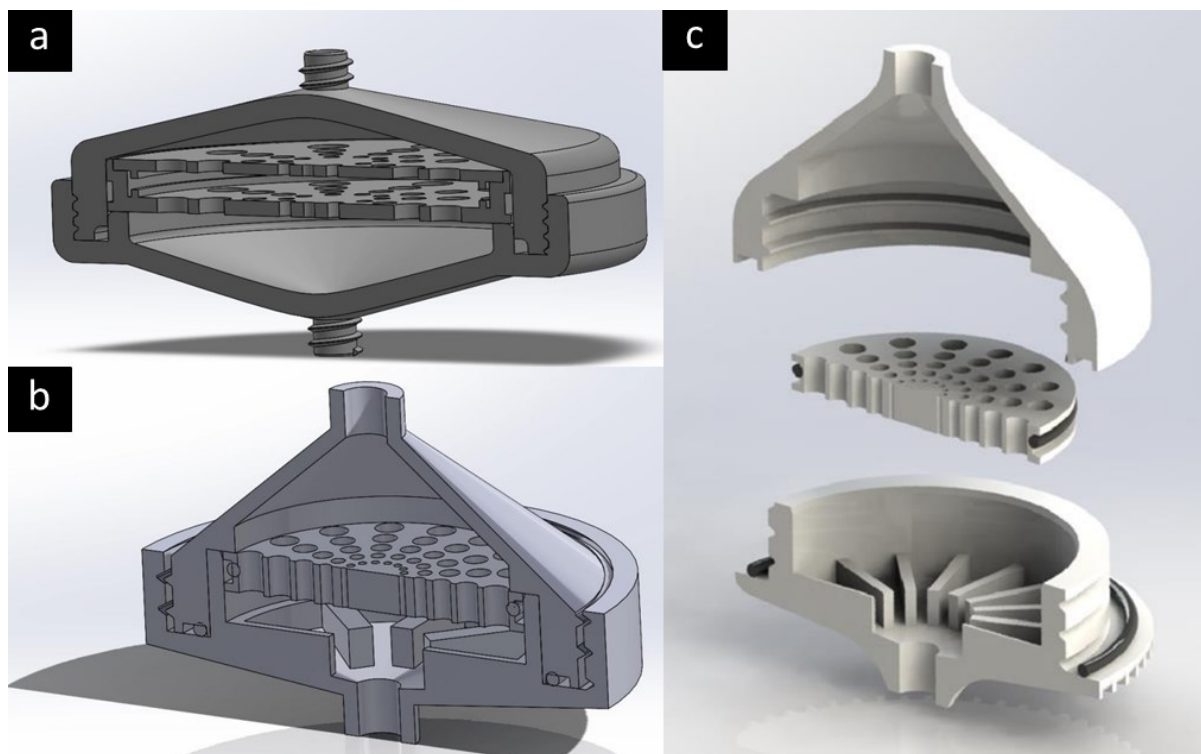
**Figure 4.6.** CAD generated sample models of filter holders with 5 mL fixed bed volume and varying diameters: (a) 20 mm, (b) 30 mm, (c) 40 mm, (d) 50 mm, (e) 60 mm, (f) 70 mm.

In order to proceed with this first attempt to create a prototype device, the 40 mm diameter filter holder was chosen for additional design considerations. The flow distribution is crucial to minimise channelling of liquids, and therefore the next step involved the production of some provisional flow distributor designs so that the printed prototype assembly can somewhat resemble a complete product. These place-holder designs are shown in **Figure 4.7**, though it is likely that much higher resolution design will be necessary, along with validation via CFD and empirical testing.



**Figure 4.7.** Provisional flow distributor designs, featuring off-set concentric cuts (left hand side) and circular cut-outs (right hand side).

First design iterations of the whole device using SolidWorks are presented in **Figure 4.8**. The assembly seen in **Figure 4.8.a** features a sandwich design, with the intention of encapsulating the filter holder within two flow distributors. This is based on the premise that the central filter unit could be produced and packed as single units, which can then be incorporated and exchanged within the device, reducing the need for disposal of the housing between filter changes after prolonged use. Though this approach could reduce waste, it is not strictly practical, as the risk of contamination within an otherwise sterile setting would be high. This is especially the case for blood salvage within an operating theatre, not to mention that the exchange of the internal components would be extremely messy and could introduce additional biohazards.



**Figure 4.8.** Initial design concepts and iterations for the 3D printed filter holder, created using SolidWorks.

**Figure 4.8.b** demonstrates an alternative iteration, without a separate internal assembly. This design supports the filter material upon the lower struts within the bed of the device, while the flow distributor is held in place, sandwiching the filter, by the upper section once screwed into place. This design introduced the O-rings required to ensure watertight seals at key locations to prevent leakage but lacked certain ergonomic benefits as it may be difficult to screw tight without clear points of purchase on the upper assembly component. The final and most recent

design iteration is depicted by **Figure 4.8.c**. This model has additional texturing and smoothing which should allow for improved handling properties and includes the addition of material supports at the base. **Figure 4.9** (left and middle) shows this design with the fewer support struts printed by SLA printing using FormLabs white and clear resins as sample materials, produced from materials which were readily available for print at short notice. The product shown on the right-hand side of **Figure 4.9**, has an increased number of support struts at the base and printed from Tough 1500 resin - a biocompatible resin certified for long term skin contact, though its safety for short term blood contact is not assured and further testing of this would be required.



*Figure 4.9. 3D printed prototypes of the third design iteration produced by SLA printing, produced using FormLabs White Resin (left hand side), Clear Resin (middle), and Tough 1500 Resin (right hand side).*

Considering the potential scale of production required for national or international supply as a blood salvage filter, 3D printing may not be the most suitable platform for production compared to injection moulding. However, during preliminary research, these designs and the associated production method will likely be very valuable from design prototyping all the way up to clinical trials.

## 4.4 Conclusion

Although DigiDEM enabled the digital reproduction of the packed fibre bed, discrepancies in 3D geometry, calculated porosity, and inability to properly randomise the orientation of the layers, left room for uncertainty as to how well these models match the real-world stationary phase of stacked non-woven membranes. Flow simulation suggested that there is no

substantial channelling or stagnation within the column, though some aspects of the simulation could likely be improved in future with access to greater computational power.

Through first stage designs, it was demonstrated that modelling and 3D printing can form a design basis for further development and exploration of the filter housing device. Undoubtedly this work is still in its infancy and further development, especially of flow distributors, is needed. This will include, exploring potential geometries, testing their performance in the laboratory, and validating appropriate biocompatible resins for SLA printing.

## Chapter 5

# Poly(vinyl alcohol) non-woven mats for tissue engineering applications

### 5.1 Introduction

TE is a field of research which combines the ingenuity and problem solving of engineering with the fields of medicine and biology, to develop substitute technologies and methods capable of maintaining, restoring, and enhancing tissue function, beyond what has been historically possible through more traditional or natural means. Commonly, TE utilises regenerative cell treatments (scaffold-free methods), and advanced biomaterials (scaffold-based methods), to enhance tissue recovery around a targeted defect site (Bakhshandeh et al., 2017). The materials developed for scaffold-based TE span a broad range of production methods, including solvent casting, 3D printing, freeze drying and electrospinning, to name a few (Rahmati et al., 2021, Pina et al., 2019). These can produce quite distinct material morphologies with differing properties, and while some properties, such as biocompatibility and capacity for diffusion of nutrients, are typically a ubiquitous requirement for all TE materials, others, such as mechanical strength and capacity for drug loading, can vary depending on application.

Among the many manufacturing techniques used, electrospinning has been explored extensively in TE, as it is simple, can easily produce nanofibers with tuneable sizes, and has the ability to control fibre orientation, with a high degree of reproducibility (Rahmati et al., 2021, Tan and Zhou, 2020, Bigdeli et al., 2013). The final fibrous morphology can frequently mimic the ECM, and therefore offers a good substrate for cell proliferation, while the highly interconnected pores allow for easy diffusion of nutrients. Fibres for TE have been produced from a range of materials, with some common examples including collagen, PCL, PLA, SF, and PVA (Lannutti et al., 2007, Tan and Zhou, 2020, Teixeira et al., 2020). Among others, PVA is highly desirable for biomedical applications, including bone, skin, vascular, and corneal

TE, as it is biocompatible, biodegradable and water soluble, and has good mechanical properties (Teixeira et al., 2020).

As a water-soluble polymer, PVA is highly hydrophilic which can be desirable for TE, however, depending upon the degree of hydrolysis and the Mw, the rate of dissolution can vary significantly. PVA nanofibers are routinely combined with chemical crosslinkers, such as GA or glyoxal, to further alter water solubility, but these chemicals are typically toxic, and the presence of any residual crosslinker may become problematic (Diez et al., 2022, Vashisth and Pruthi, 2016).

During TE applications, it can be highly desirable to match the rate of material degradation to the rate of healing, so the advantages of selecting PVA with a high degree of hydrolysis, which will prevent rapid dissolution of the fibres, are apparent. Furthermore, samples prepared in the absence of toxic crosslinkers are preferable, in order to minimise potential cytotoxic effects. Herein, we seek to apply the heat treatment conditions explored in Chapter 2 to two highly hydrolysed species of PVA nanofibers, namely 98% and 99%, and consider the physicochemical implications of the process in the context of TE. Material biocompatibility and haemocompatibility are also tested post heat treatment, to assess their potential use *in vivo*, as alternative 'greener' TE supports and delivery vehicles suitable for non-temperature sensitive species or substances.

## 5.2 Materials and Methods

### 5.2.1 Materials

PVA 'Mowiol 20-98' (98% hydrolysed, 125,000 Mw), PVA 'Mowiol 28-99' (99% hydrolysed, 145,000 Mw), and phosphate buffered saline (PBS, pH 7.4) were purchased from Sigma-Aldrich (Missouri, USA). Ethanol ( $\geq 99.8\%$ ) and GA (50%) were obtained from Fisher Scientific (Zurich, Switzerland). Composol PS solution for preservation of thrombocytes on thrombocyte rich solution (TRS) exposed samples was acquired from Fresenius Kabi (Bad Homburg, Germany). Mouse fibroblasts (3T3) for biocompatibility testing were purchased from ATCC (Virginia, USA) and cultured using DMEM, with 10% FBS, and Glutamine supplied by Biosera (Nuaille, France) and Penicillin-Streptomycin-Amphotericin B antibiotic mixture supplied by Lonza (Basel, Switzerland), with the assay carried out using CCK-8 was bought from Abcam (Cambridge, UK). Samples were sterilised using an Anprolene AN74i Ethylene-oxide cabinet (Anderson Sterilizers, North Caroline, USA). Human blood was collected from healthy patients

in vacutainers containing 0.129 M sodium citrate obtained from BD (New Jersey, USA). All chemicals were of analytical grade (unless otherwise stated) and used without further purification.

### *5.2.2 Production and stabilisation of electrospun materials*

Materials were produced using needleless DC electrospinning from solutions of 98% and 99% hydrolysed PVA as described in section 2.2.2.2.2. Briefly, 98% and 99% solutions were dissolved in 9:1 (w/w%) DI water to ethanol solvent at polymer concentrations of 10% and 8% respectively, and similarly subjected to heat treatments as per section 2.2.2.3, with samples being treated for 0, 1, 4, 8 and 16 h at 180 °C in a forced convection drying oven (SciQuip Oven-80 HT; Newtown, UK), before being allowed to cool at room temperature.

### *5.2.3 Analytical methods*

#### *5.2.3.1 Scanning electron microscopy*

As per section 2.2.3.1, SEM was used to examine the morphology of samples and measure the effect of heat treatment on fibre diameters. Samples were prepared for analysis by sputter-coating with gold using a Quorum (Q150R ES) sputter coater and then imaged using a Tescan Vega3 SB Easy Probe (Tescan, Brno, Czech Republic). Images were again analysed using ImageJ 1.52a software (NIH, USA).

#### *5.2.3.2 Fourier transform-infrared spectroscopy*

FT-IR was used as per section 2.2.3.2 using a Frontier Spectrometer (PerkinElmer Ltd., Waltham, MA, USA) combined with an ATR accessory (GladiATR; Pike Technologies, Madison, WI, USA), using a scan range from 4000  $\text{cm}^{-1}$  to 700  $\text{cm}^{-1}$  at a resolution of 4  $\text{cm}^{-1}$  for a total of 16 scans per measurement.

#### *5.2.3.3 X-ray diffraction*

Material crystallinity was evaluated as in section 2.2.3.7 using XRD on a Bruker D8 Advance diffractometer, equipped with a LynxeyePSD detector (Bruker, Billerica, MA, USA) and with  $\text{Cu K}\alpha_{1,2}$  radiation (40 kV and 40 mA), 0.02 mm  $\text{Ni K}\beta$  absorber, 5–50°  $2\theta$  range, a step scan of 0.02° with a sample rotation speed of 30 RPM. The degree of crystallinity was calculated using equation 2 (Originally found in section 2.2.3.7, but is restated below for convenience),

where  $\alpha$  is the degree of crystallinity,  $I_c$  is the sum of the intensity under the crystalline peaks, and  $I_a$  is the sum of the intensity under the amorphous sections of the spectra.

$$\alpha (\%) = \frac{I_c}{I_c + I_a} * 100 \quad (Eq. 2)$$

#### 5.2.3.4 Tensile testing

The mechanical properties of the mats were recorded using the same method as in section 2.2.3.8 by means of uniaxial tensile tests using an Instron 5965 (Instron, High Wycombe, Buckinghamshire, UK), equipped with a 50 N load cell, moving at a rate of 10 mm·min<sup>-1</sup>. Samples were prepared using a punch tool in a dumbbell shape (21  $\mu$ m average thickness, n=3) and continuously loaded until failure (defined as a 50% reduction from peak force). Stress-strain curves were obtained and mean averages of the UTS, and strain at UTS were calculated.

#### 5.2.3.5 Contact angle testing and film preparation

Contact angle testing was performed to examine changes to the hydrophilicity of the material, as a result of the duration of thermal treatment. Due to limitations of wicking behaviour with electrospun samples, 15 mm diameter disc films were prepared by filling a silicon mould with the same solutions used in the electrospinning process, and the moulds were left to form in a drying cabinet maintained at 25 °C for 2 days until they solidified. These films were then subjected to the same treatment durations of 1, 4, 8 and 16 h at 180 °C as the electrospun non-woven mats. Contact angle testing was performed using an Attension Theta Flux to carry out sessile drop testing and analysed using OneAttension software (Biolin Scientific, Gothenburg, Sweden). The liquid used was DI water, with a droplet volume of 5  $\mu$ L and recording duration of 10 s following liquid-sample contact.

#### 5.2.3.6 Biocompatibility testing

Samples were prepared as 13 mm diameter discs to match dimensions of the base of 24-well plates and sterilized by ethylene-oxide treatment in an Anprolene AN74i cabinet (Anderson Sterilizers, North Carolina, USA). Discs were then placed in the base of the well plates and held in place with cylindrical glass culture inserts to weight down the materials, and then seeded with 10<sup>4</sup> 3T3 murine fibroblasts per well at day 0. Plates were incubated at 37 °C in the presence of 5% CO<sub>2</sub>, and CCK-8 assays were carried out at days 1, 3 and 7. Cell culture media was composed of DMEM with the addition of 10% FBS, 1% glutamine and 1% antibiotic



(Penicillin-Streptomycin-Amphotericin B). For each time point measured, media from each well was aspirated and exchanged with 500  $\mu$ L of complete media containing 10% CCK-8, which was then incubated for 3 h, before final absorbance values were measured at 450 nm using a BioTek Synergy HTX (Agilent Technologies, Inc., Santa Clara, CA, USA) (n=4). After the final time point at day 7, cells were fixed with 2.5% GA solution in PBS for 30 min at 4 °C and imaged using SEM.

#### 5.2.3.7 Haemocompatibility – Collection and preparation of blood product solutions

Preparation of blood products for haemocompatibility testing was carried out according to (Horakova et al., 2018). Routinely, whole blood for haemolysis assays was collected from healthy donors in 4 mL BD vacutainers containing 0.129 M sodium citrate and then diluted with 5 mL PBS. Platelet poor plasma (PPP) was prepared for coagulation testing by centrifugation of 12 mL of whole blood (collected in three BD vacutainers containing 0.129 M sodium citrate) at 1500 g for 15 min. TRS for thrombogenicity testing was prepared by combining buffy coats collected from 4 blood donors after centrifugation using a deleucocytation filter (CompoStop Flex 3F T&B, Fresenius Kabi).

#### 5.2.3.8 Thrombogenicity

Thrombogenicity was tested by incubating the materials at 37 °C in the presence of TRS for 2 h and subsequently analysing each material using CCK-8 assay and SEM imaging. Nanofibrous mats were sterilized using ethylene-oxide, prepared in 6 mm discs, and placed in the wells of a 96 well plate. TRS (200  $\mu$ L) containing approximately  $7.85 \times 10^6$  thrombocytes, was placed in each well, and after 2 h of incubation, the TRS was aspirated, and the samples were washed twice with PBS. Materials for SEM analysis were fixed using 2.5% GA in PBS solution for 30 min at 4 °C, followed by rinsing with a series of graded ethanol solutions (60-100%). For thrombocyte viability testing, the materials were incubated for a further 4 days in Composol PS solution, before exchanging the culture solution for fresh Composol PS containing 10% CCK-8 for 3 h. Final absorbance values were measured at 450 nm using a Spark multimode microplate reader (Tecan, Männedorf, Switzerland) (n=10).

#### 5.2.3.9 Coagulation

The clotting time of PPP was measured after incubation with all electrospun materials, to determine the prothrombin time (PT) and activated partial thromboplastin time (APTT). Samples were prepared as 1 cm<sup>2</sup> square swatches, placed in test tubes and combined with

300  $\mu$ L PPP. For a negative control, PPP was incubated in the absence of any materials. Test tubes were incubated for 45 min at 37 °C before samples were removed from solution. Clotting time was measured using an automatic BCS XP analyser (Siemens, Munich, Germany) according to the manufacturer's instructions (n=5).

#### 5.2.3.10 Haemolysis

As for coagulation experiments, 1 cm<sup>2</sup> swatches were prepared from nanofibrous membranes which were then added to test tubes containing 10 mL of PBS. Negative and positive control tubes contained 10 mL of PBS and distilled water, respectively, in the absence of any materials. All samples were incubated at 37 °C for 30 min, prior to dosing with 200  $\mu$ L of anticoagulated dilute whole blood prepared earlier, and incubation for a further 60 min. The tubes were then centrifuged at 100 g for 5 min, the supernatant was aspirated from the container into well plates, and the absorbance was measured at 570 nm using a Spark multimode microplate reader (Tecan, Männedorf, Switzerland) (n=5, 2 measurements per sample).

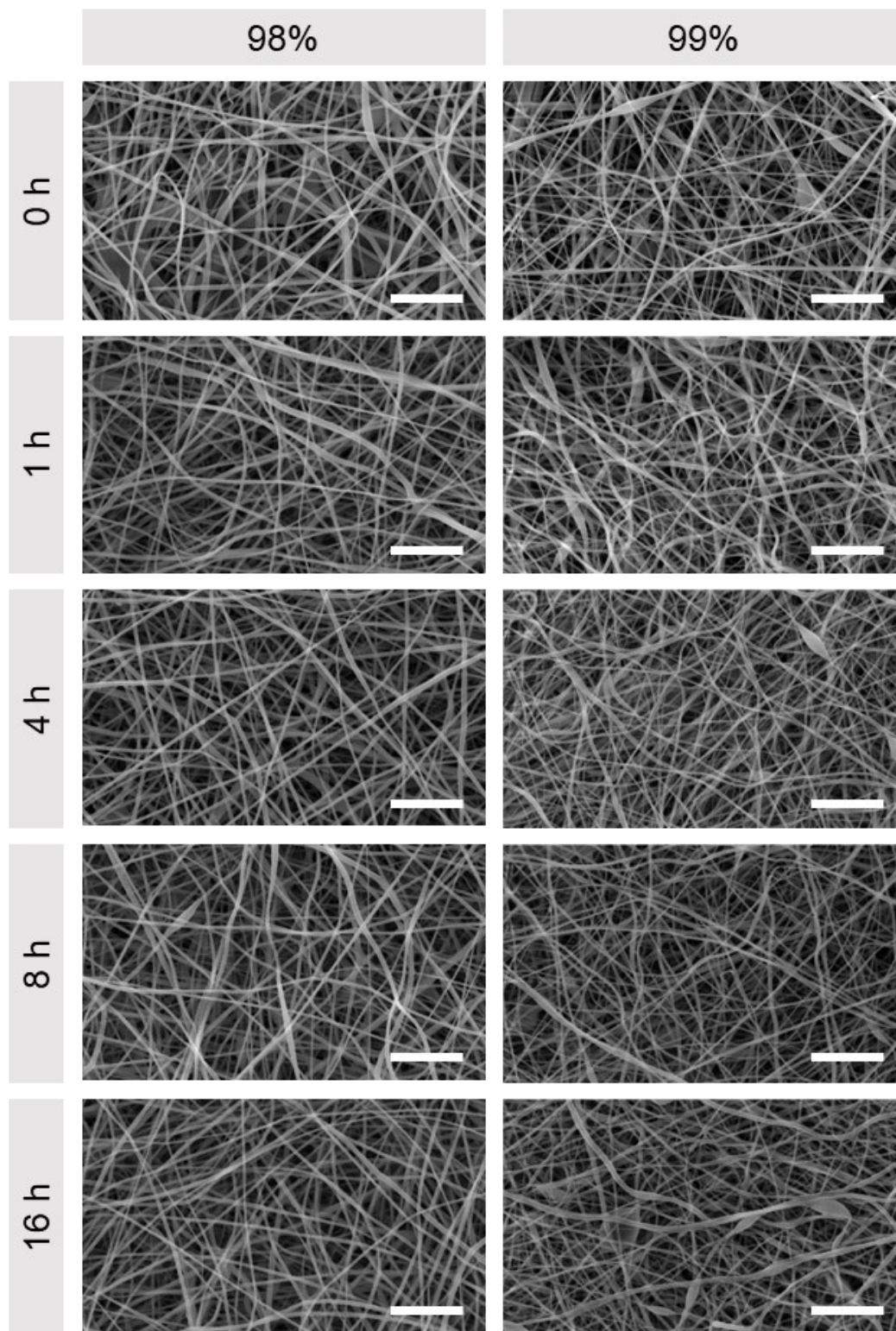
## 5.3 Results and Discussion

Nanofibrous non-woven supports were produced by needleless DC electrospinning using 98% and 99% hydrolysed PVA and thermally stabilised for up to 16 h at 180 °C. The supports were then compared to assess the effect of degree of hydrolysis and heat treatment duration on their potential use as biomaterials in TE applications. First, the samples were evaluated based on their morphological, physicochemical, and mechanical properties in a similar manner to that described in Chapter 2, before investigating their biocompatible and haemocompatible properties, which are essential for TE materials.

### *5.3.1 Morphological comparison of nanofibers produced from 98% and 99% hydrolysed PVA*

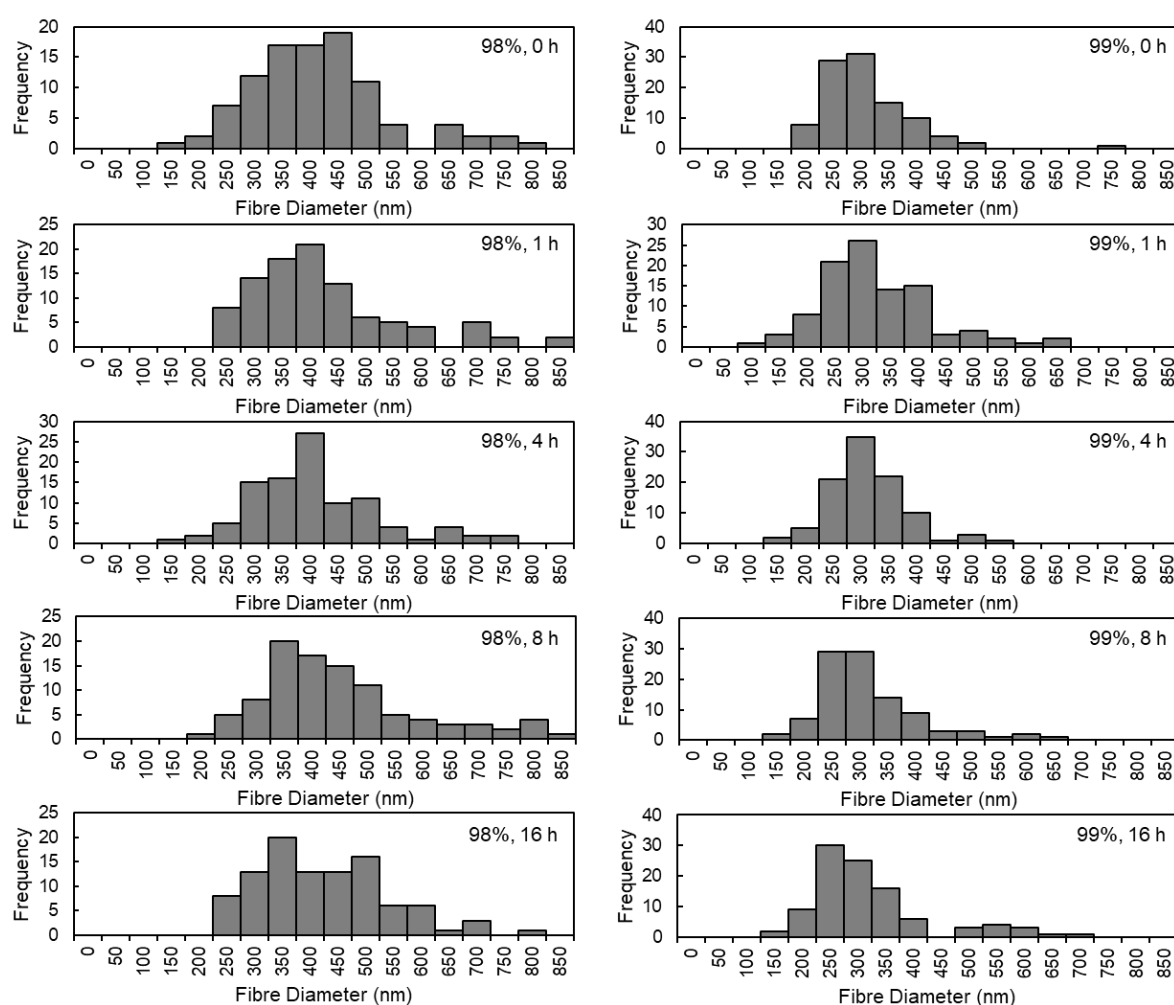
Morphological comparison was carried by imaging of the materials using SEM, to confirm that largely defect-free fibres are generated by the process. Based on the findings in Chapter 2, it was expected that neither the degree hydrolysis nor the duration of heat treatment should have any negative affect on fibre morphology and/or diameter. **Figure 5.1** shows SEM images of 98% and 99% hydrolysed PVA side-by-side for the respective heat treatment durations. It

is apparent that, when untreated, both materials present highly fibrous structures with few defects, which remains unchanged following heat treatment.



**Figure 5.1.** SEM images of 98% and 99% hydrolysed electrospun PVA following at 0, 1, 4, 8, 16 h of heat treatment at 180 °C. Scale bar: 10  $\mu$ m.

Fibre diameters were subsequently measured ( $n=100$ ) and histograms of this data are presented in **Figure 5.2**. For untreated samples, the average fibre diameter for 98% hydrolysed PVA samples was 399 nm, compared to 285 nm for the 99% hydrolysed sample. The average fibre diameter for 98% hydrolysed PVA across all heat treated samples measured was 406 nm, ranging from 383 nm (4 h) to 434 nm (8 h), whilst the average diameters for 99% samples was 291 nm, ranging from 285 nm (0 h) to 300 nm (1 h). While small differences do appear in average fibre diameter, the variance found here was small and suggests heat treatment may have only a limited effect on altering the morphology of the fibres. As well as demonstrating higher average fibre diameters, for all samples imaged, the range of fibre diameter distribution was greater for 98% hydrolysed PVA. In literature, the fibrous structure of electrospun materials (particularly when fibres are in the nanoscale) has been considered to mimic ECM and enhance cell proliferation *in vitro* (Cui et al., 2010, Lee and Arinzeh, 2011, Lin et al., 2020). This suggests that, based on morphology, all tested materials show promise for TE applications, particularly those produced from 99% DH PVA.



**Figure 5.2.** Histograms of fibre diameters for 98% and 99% DH PVA needleless electrospun mats heat treated for 0-16 h.

### 5.3.2 Physicochemical comparison of nanofibers produced from 98% and 99% hydrolysed PVA

#### 5.3.2.1 Fourier transform infrared spectroscopy

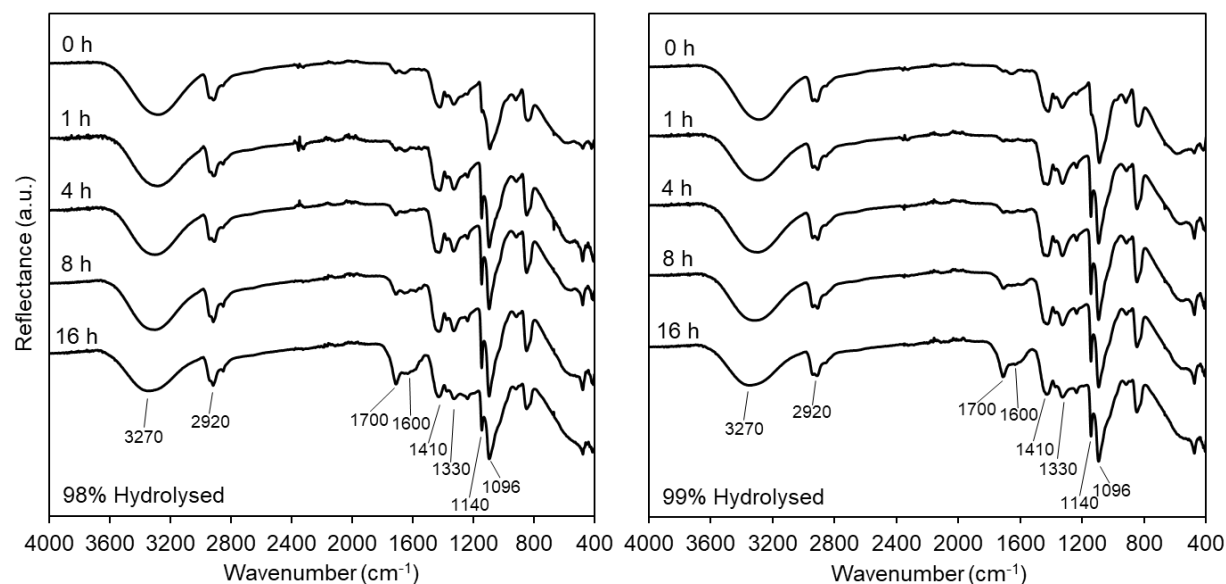
The key characteristic peaks of the FT-IR spectra of PVA were described in detail previously (Chapter 2), and **Table 5.1** briefly reiterates these key features.

**Table 5.1.** Summary recap of peaks identified in chapter 2 commonly associated with FT-IR spectrum of PVA.

Peak absorption (cm <sup>-1</sup> )	Group	Otherwise associated with
3000-3500	O-H stretching	
2900-2950	C-H stretching	
1710-1750	C=O stretching	
1600-1650	C=C stretching	
1410	C-H vibration	
1330	C-O vibration	
1140	C-O stretching	Crystalline phase of PVA
1096	O-H bending	Amorphous phase of PVA

Given the small difference of only 1% residual acetate groups between the hydrolysis percentage of the PVA samples, it was not anticipated that there would be any significant differences between untreated nanofibrous samples, which was confirmed by the 0 h spectra in **Figure 5.3**. Once again, heat treated samples of all durations produced increases in the absorption of the 1140 cm<sup>-1</sup> peak, attributed to a combination of C-O stretching, due to both increases in crystallinity and in prevalence of C-O-C bonds. This signal, along with the broad O-H signal at 3270 cm<sup>-1</sup>, see a slight reduction in absorbance in the samples treated for 16 h, which could be associated with reduced crystallinity (discussed further in the following XRD section). As described previously, as heat treatment progresses, the increase in peaks at 1600 and 1700 cm<sup>-1</sup> is most likely attributed to C=C and C=O bonds respectively, due to potential thermolysis (Meszlényi and Körtvélyessy, 1999, Yang et al., 2012). Further bio- and

haemocompatibility testing can indicate to what degree this degradation is tolerated in a TE context and is discussed in later sections.

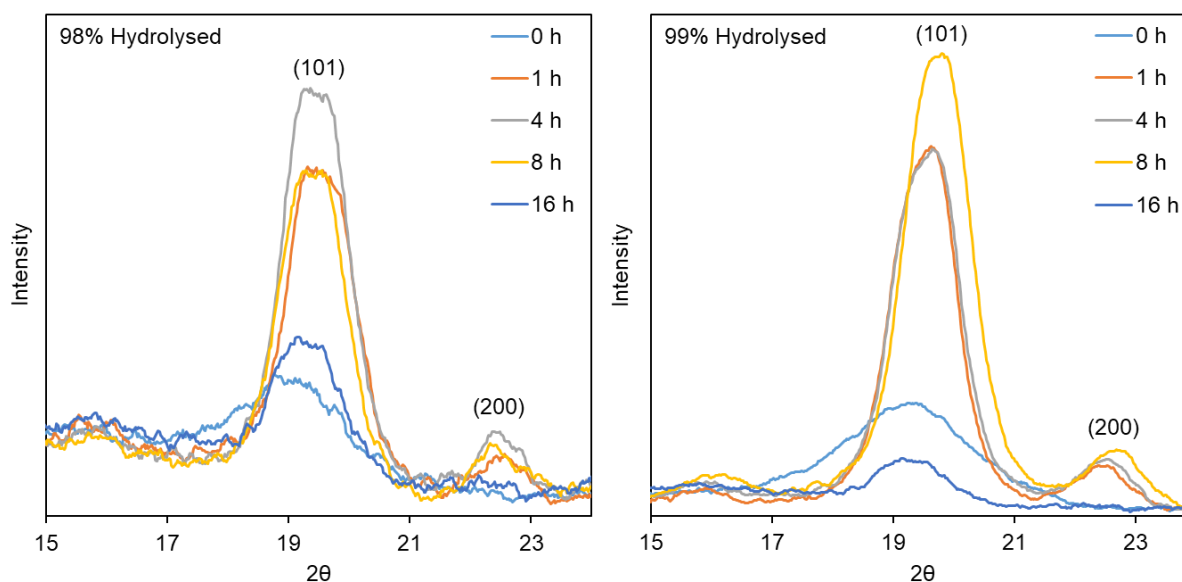


**Figure 5.3.** FT-IR Spectra of two sample series of 98% (left) and 99% (right) DH PVA produced by needleless electrospinning with heat treatment time points indicated on the offset spectra.

### 5.3.2.2 X-ray diffraction

All samples were analysed using XRD to compare their crystallinity, both in terms of differences between species of PVA, as well as arising from heat treatment duration. The monoclinic unit cell reflections shown at (101) and (200) suggest an increase in polymer chain ordering for samples treated for 1, 4 and 8 h in both species, followed by a sharp reduction at 16 h (Tretinnikov and Zagorskaya, 2012, Tang et al., 2015). Using the equation 2 again bears out this observation numerically, and as it can be seen in **Table 5.2**, crystallinity fell from 26.8% to 19.5% for 98% DH samples, and from 57.0% to 19.5% for 99% DH samples. This pattern approximately matches the one found earlier in 2.3.5.2 for like-for-like materials and extends it slightly with the 16 h treated materials. The samples produced from 99% DH PVA are consistently more crystalline than their 98% DH counterparts, and although this is not surprising, based on the reduction in steric effect produced by halving the residual acetate groups, it was more pronounced than expected. A possible explanation could be the limitation of applying this equation to materials, such as those made from polymers, which have only partial ordering but also are relatively thin in nature. This may well result in baseline signals (*i.e.* the area under the amorphous region of the spectra,  $I_a$ ) which is not strictly reliable.

Nevertheless, it may still be used cautiously, as a tool for relative comparison within a set of data, such as the heat treatment series presented here, to indicate the increase and subsequent decrease in crystallinity within each series separately.



**Figure 5.4.** XRD spectra of 98% (left) and 99% (right) DH PVA materials produced by DC electrospinning. Key: 0 h (light blue); 1 h (orange); 4 h (grey); 8 h (yellow); 16 h (dark blue).

**Table 5.2.** Crystallinity of nanofibrous samples after heat treatment calculated from XRD data.

Heat treatment duration (h)	Crystallinity	
	98% DH PVA	99% DH PVA
0	19.9	39.0
1	29.2	53.4
4	31.1	53.6
8	26.8	57.0
16	19.5	19.5

### 5.3.2.3 Tensile testing

Tensile load testing was carried out to assess the UTS and displacement at UTS of the nanofiber mats following heat treatment, and compare samples produced from PVA with

differing DH (**Figure 5.5**<sup>1</sup>). Samples produced from 99% DH PVA appeared significantly stronger than those created from 98% DH PVA ( $P = 0.0032$ ), with untreated samples having 62% greater UTS (4.68 MPa for 99% DH *c.f.* 2.88 MPa for 98% DH). This is most likely partly due to the reduced chain mobility as a result of fewer acetate groups and increased hydrogen bonding, and partly a result of differences in fibre morphology between samples. A similar trend was also observed within a polymer blend by Restrepo et al, where it was shown that PVA with higher degree of hydrolysis resulted in stronger materials (Restrepo et al., 2018). Strength differences in heat treated mats were 20-25% greater in the 99% DH sample than the equivalent 98% samples, with the exception of the 16 h treated sample which was ~36% weaker. Lower degree of hydrolysis samples (98%) achieved UTS of 5.82 (1 h), 5.33 (4 h), 5.23 (8 h), and 3.82 MPa (16 h) compared to UTS of 6.98, 6.67, 6.48, and 2.45 Mpa for the respective pairs from 99% hydrolysed PVA. This too is attributed to the lack of steric hindrance caused by a decrease of the large acetate groups in the 99% hydrolysed PVA, and the formation of strong hydrogen intramolecular bonds leading to increased ordering of the polymer chains and more effective chain packing. The results clearly demonstrate increased strength at the first treatment time point, caused by the enhanced crystallinity of PVA by the annealing process, followed by the steady reduction in material strength due to thermal degradation identified by FT-IR.

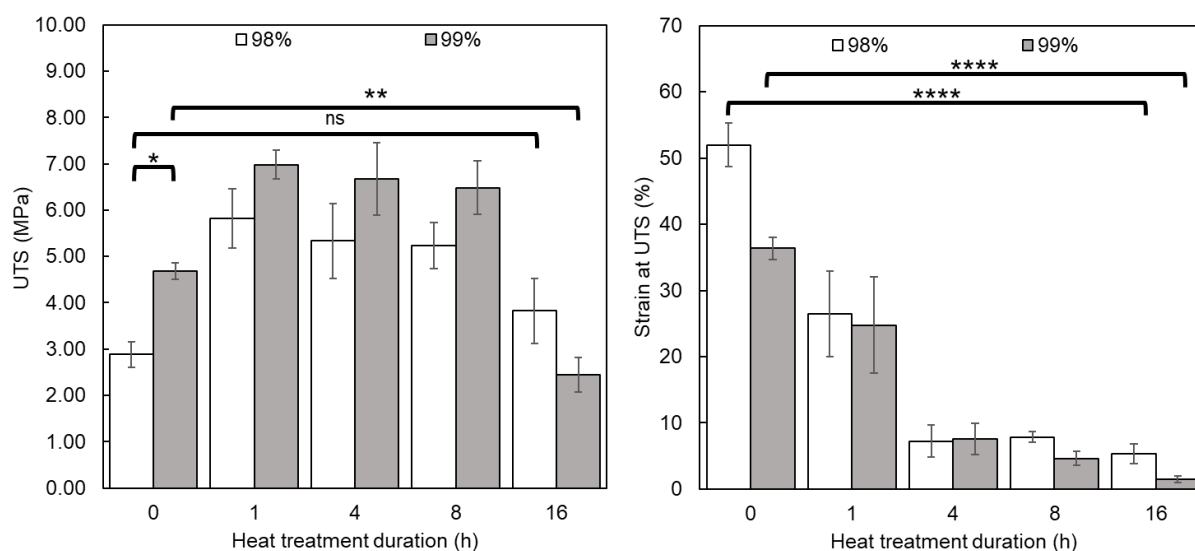
Conversely, and due to differences in chain mobility, untreated 98% DH samples tolerated strain at UTS which was on average 15.6% greater than the 99% DH untreated mats ( $P = 0.0144$ ), while treated versions of both sample series performed more similarly across all durations (average strain at UTS of 25.7%, 7.4%, 6.2%, and 3.4% for 1 h, 4 h, 8 h and 16 h treatments, respectively). Ultimately, both samples reduced in ductility with treatment duration, and became increasingly brittle, with duration playing a highly significant role in strain at UTS ( $P < 0.0001$ ) across all samples. This could be understood as a combination of increased chemical crosslinking of some chains, thereby reducing elastic properties, whilst also increasing in the extent of chain scission after 1 h, producing a progressively weaker material.

Mechanical properties are an important parameter in TE, and depending on the application, biomaterials can be subject to a range of mechanical stresses and load patterns. Therefore, it is not possible to point out which of the non-woven mats created in this work is better than the others in that respect, but we can conclude that this approach allows for better flexibility in the production of tailor-made biomimetic materials to suit a specific purpose.

---

<sup>1</sup> Please note that 99% data is duplicated from 99% DH, needleless DC data in Chapter 2 and combined with newly introduced data from 98% DH samples.





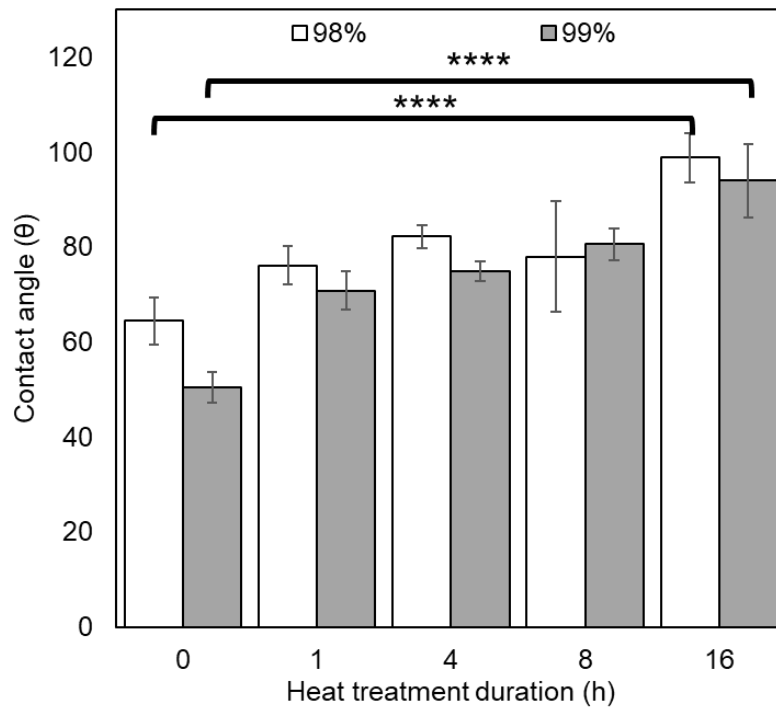
**Figure 5.5.** Tensile performance of samples produced from 98% and 99% hydrolysed PVA electrospun mats after thermal stabilisation. ( $n=3$ ). Key: 98% (white); 99% (grey).

### 5.3.2.4 Contact angle

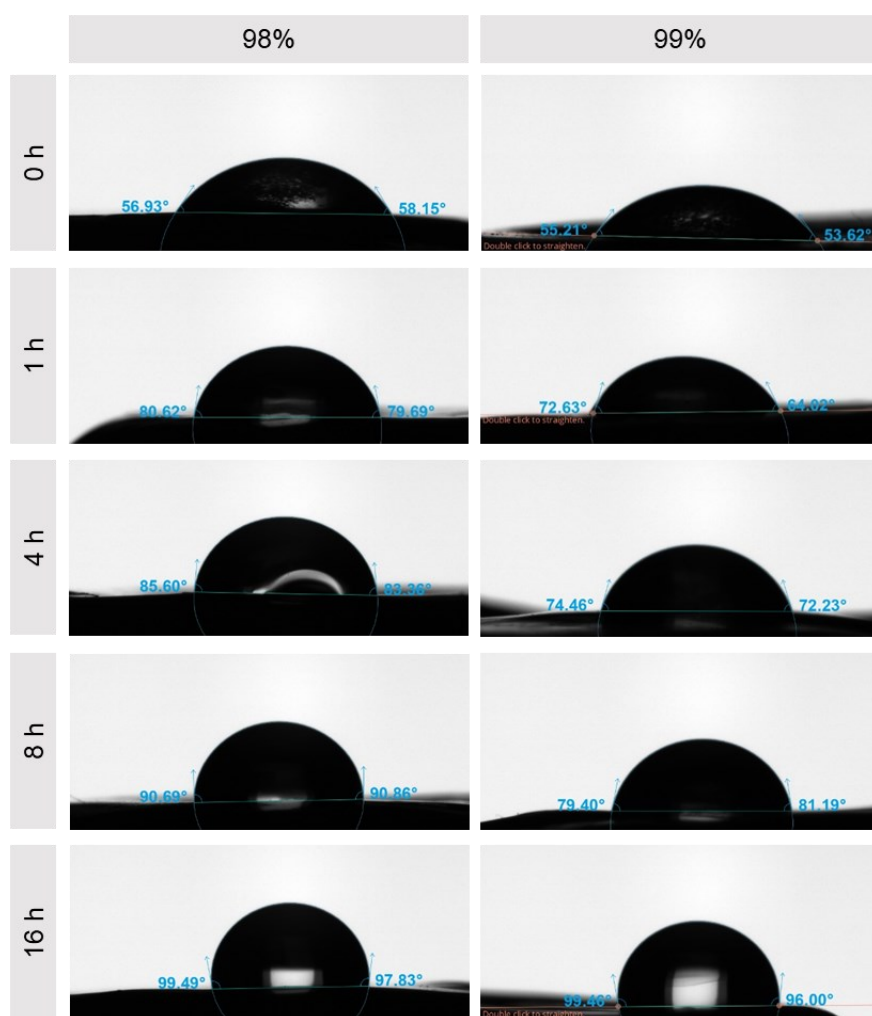
Initially, contact angle testing was carried out using PVA nanofibrous mats, but due to surface interactions between the water and the hydrophilic fibres, droplets on the surface of the material did not remain stable, but were drawn rapidly into the material and effectively dissipated. Therefore, films were created from the same solution to the one used in the electrospinning process for each material series, and heat treated at the same time points as with the nanofiber samples.

Sessile drop testing on these films indicated the contact angle of 98% DH PVA was generally higher than 99% counterparts ( $P = 0.0288$ ), as shown in **Figure 5.6**, with corresponding optical images in **Figure 5.7**. This trend is reflected in literature, where PVA with higher DH produces lower contact angles with water – a trend which appears to persist post heat treatment, suggesting hydroxyl groups remain more abundant in the 99% DH PVA films even after annealing (Zuo et al., 2013). Untreated films produced contact angles of  $64.45^\circ$  (98% DH) and  $50.52^\circ$  (99% DH), demonstrating their hydrophilic character, with contact angle steadily rising until the materials develop increasing hydrophobic character ( $> 90^\circ$ ) in the samples treated for 16 h (with values of  $98.84^\circ$  and  $93.98^\circ$ , for 98% and 99% DH respectively), reflecting the significant role of treatment duration on contact angle ( $P < 0.0001$ ). This is in-line with expectations based on FT-IR results and the formation of polyenes due to thermolysis. In some instances, such as some blood contacting materials, increased hydrophobicity may be desirable for TE applications, where a mixture of hydrophobic and

hydrophilic domains can improve compatibility, reducing protein adsorption and effects on coagulation (Menzies and Jones, 2010).



**Figure 5.6.** Sessile drop contact angle data for films produced from 98% and 99% hydrolysed PVA after thermal stabilisation. ( $n=3$ ). Key: 98% (white); 99% (grey).

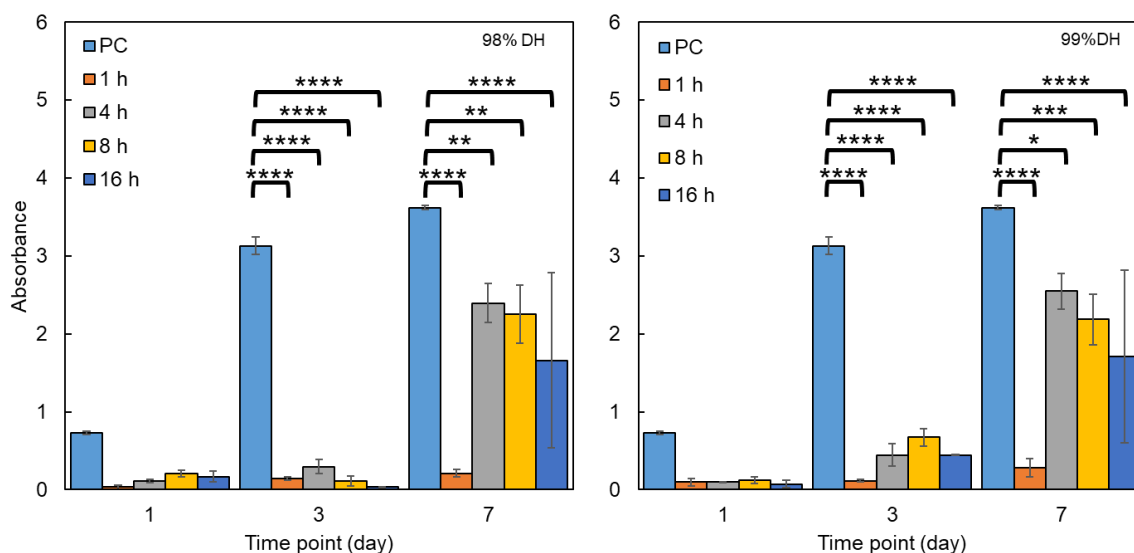


**Figure 5.7.** Representative images from sessile drop contact angle testing of films produced from 98% and 99% hydrolysed PVA films after thermal stabilisation.

### 5.3.3 Biological assessment and comparison of nanofibers produced from 98% and 99% hydrolysed PVA

#### 5.3.3.1 Biocompatibility

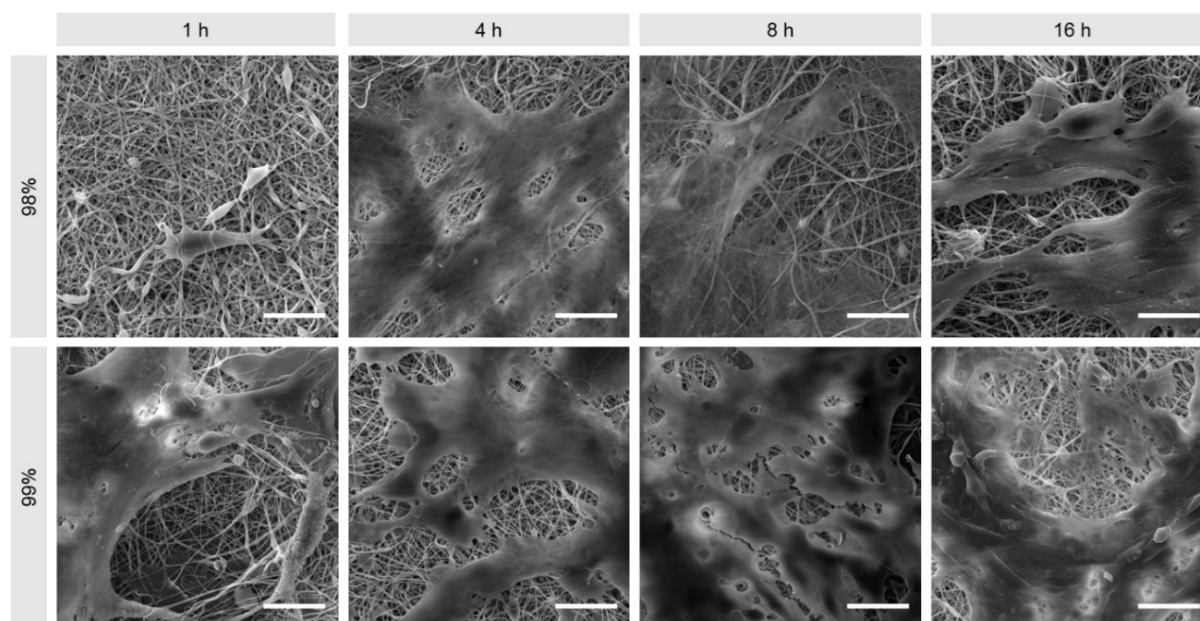
Biocompatibility tests were conducted by cultivating 3T3 mouse fibroblasts directly on the electrospun scaffolds and performing CCK-8 assays to assess cell viability. Cells were seeded ( $10^4$  cells·well<sup>-1</sup>) in 24 well plates on day 0, and cell viability assays were performed at 1, 3 and 7 days, measuring absorbance at 450 nm using a microplate reader (**Figure 5.8**). Untreated samples were excluded from the analysis as they dissolved immediately on contact with cell culture media. At day 1, there was no notable difference in absorbance between wells containing nanofibrous mats, though the positive control in the empty well plate had much greater cell viability, indicating good adherence and early proliferation.



**Figure 5.8.** Cell viability results of 98% (left) and 99% (right) PVA nanofibrous mats after heat treatment at time points of 1, 3 and 7 days after seeding, with absorbance measured at 450 nm. Key: Positive control/PC – Well plate plastic (light blue); 1 h (orange); 4 h (grey); 8 h (yellow); 16 h (dark blue). ( $n=4$ )

At day 3, some proliferation had begun to occur on both sample series. For the samples made from 98% DH PVA, the greatest absorbance was found in the sample that was treated for 4 h, whilst in the case of the 99% DH PVA, this occurred for the 8 h treated sample. At day 7, 1 h heat treated materials had achieved little proliferation for both sample series, whilst all other materials showed significant cell proliferation, with 4 h having the greatest average proliferation for both grades of PVA, and gradual decrease for each heat treatment duration thereafter. Notably, samples treated for 16 h began to exhibit poor wettability, which resulted in highly variable results, as is indicated by the significant error bars on the graphs.

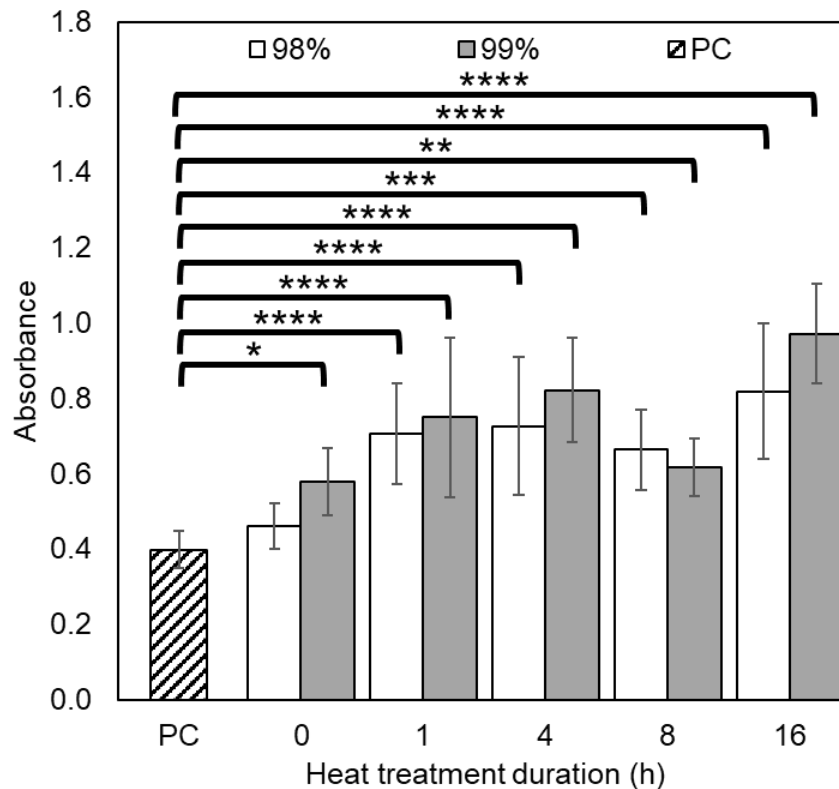
To better visualise the differences in cell adhesion and proliferation, day 7 samples had their cells fixed using GA and were imaged by SEM (**Figure 5.9**). Samples treated for 4 and 8 h exhibit a relatively smooth cell monolayer with somewhat uniform coverage, whilst the samples treated for 16 h tend to form clusters of cells which did not spread evenly along the surface of the mats, further supporting the idea that 8 hours is a reasonable limit of heat treatment duration for tissue engineering applications, and 4 hours treatment duration may be most suitable more generally.



**Figure 5.9.** Representative SEM images of 3T3 cells on 98% and 99% DH PVA mats produced by electrospinning 7 days after cell seeding. Scale bar: 20  $\mu\text{m}$ .

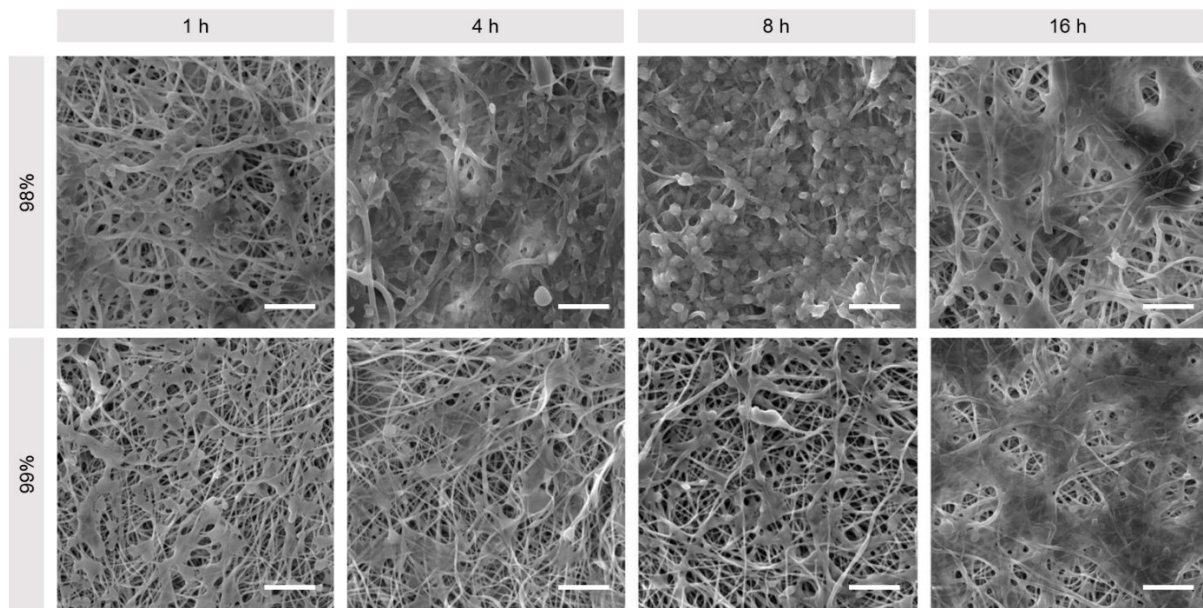
### 5.3.3.2 Thrombogenicity

Materials were exposed to TRS for 2 h, rinsed and then measured for thrombogenicity using a CCK-8 assay, wherein viability corresponds to rate of platelet activation. **Figure 5.10** shows that all samples had an increase in thrombogenicity relative to the positive control, though this effect was less pronounced in the untreated and 8 h treated samples. Overall, however, it appears to be a positive trend correlating thrombogenicity and heat treatment duration for both materials ( $P < 0.0001$ ), whilst DH played a lesser but still significant role in extent of thrombogenicity ( $P = 0.0108$ ). Given that in general the fibrous structure of electrospun materials is a thrombogenic factor, the stabilising effect of heat treatment on the material morphology predictably increased thrombogenicity, with the exception of the samples treated for 8 h, which appear to have paradoxical effect which is difficult to explain (Horakova et al., 2018). Conversely, it is suggested that the lack of thermal stabilisation is the reason for lower thrombogenicity in untreated samples, as the fibrous structure would not be preserved, due to dissolution and formation of a hydrogel, and therefore not be able to act as a thrombogenic factor.



**Figure 5.10.** Cell viability results of thrombocyte activity on 98% and 99% DH PVA mats following heat treatment and 2 h exposure to TRS, with absorbance measured at 450 nm. Key: Positive control/PC – well plate plastic (cross-hatched); 98% (white); 99% (grey).

Examination of the materials under SEM (**Figure 5.11**) reveals the presence of activated platelets on all samples, largely forming a smooth later and bridging between fibres. In the case of the 8 h treated samples, the thrombocytes seem to be less spread out, withdrawn and potentially detaching or inadequately attached, appearing as more spherical structures on the surface of the fibres.

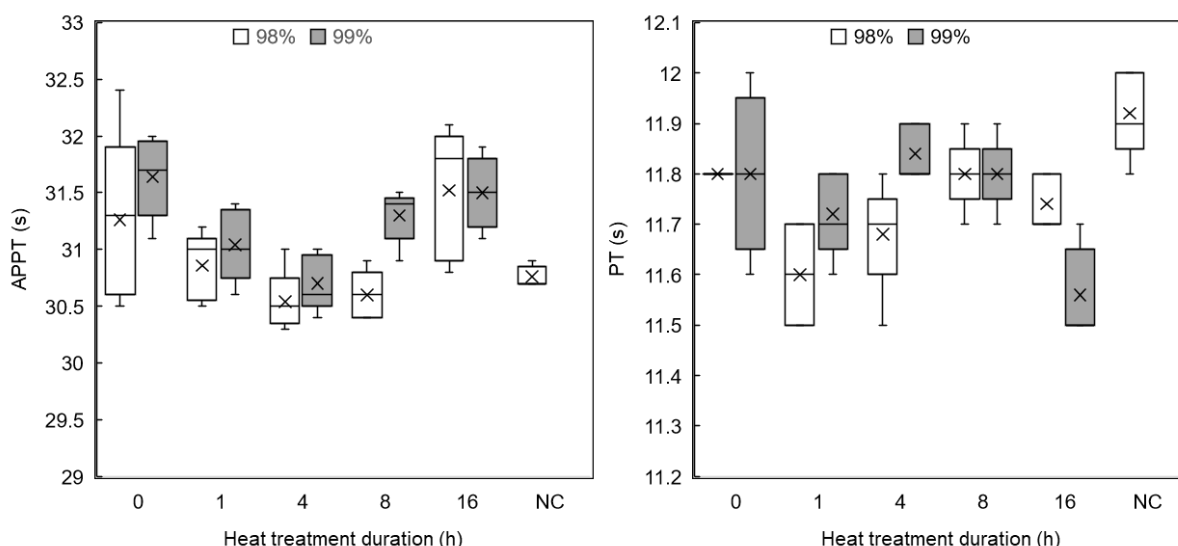


**Figure 5.11.** Representative SEM images of activated platelets on 98% and 99% DH PVA mats produced by needleless electrospinning. Scale bar: 10  $\mu\text{m}$ .

### 5.3.3.3 Coagulation

Adsorption of proteins from blood plasma to the material surface can cause changes in rate of coagulation. The APTT (intrinsic pathway) and PT (extrinsic pathway) were performed, to test if the materials have any anticoagulation effect or cause accelerated coagulation, with the normal bounds being 23-35 s for APTT and 10-15 s for PT (Horakova et al., 2018). Clinical plasma in the absence of any materials was used as a test control.

The APTT test, shown in **Figure 5.12** (left hand side), demonstrated that samples produced from 99% DH PVA tended to have slight anticoagulation effects compared to 98% DH samples, but on average all samples were  $\leq 3\%$  above the negative control. Conversely, the PT test (**Figure 5.12**, right hand side) showed that on average all materials from both sample series had a minor accelerating effect on coagulation time, but once again the difference was  $\leq 3\%$ . Though all samples exhibited some deviation from the control, the deviation was not considered to be substantial in a clinical context (Miller et al., 2012). This suggests materials may be potentially suitable in a blood contacting environment, subject to haemolysis results, but indicates a neutral result with respect to wound dressings, where accelerated coagulation is desirable as the first step of wound healing (Rembe et al., 2015).



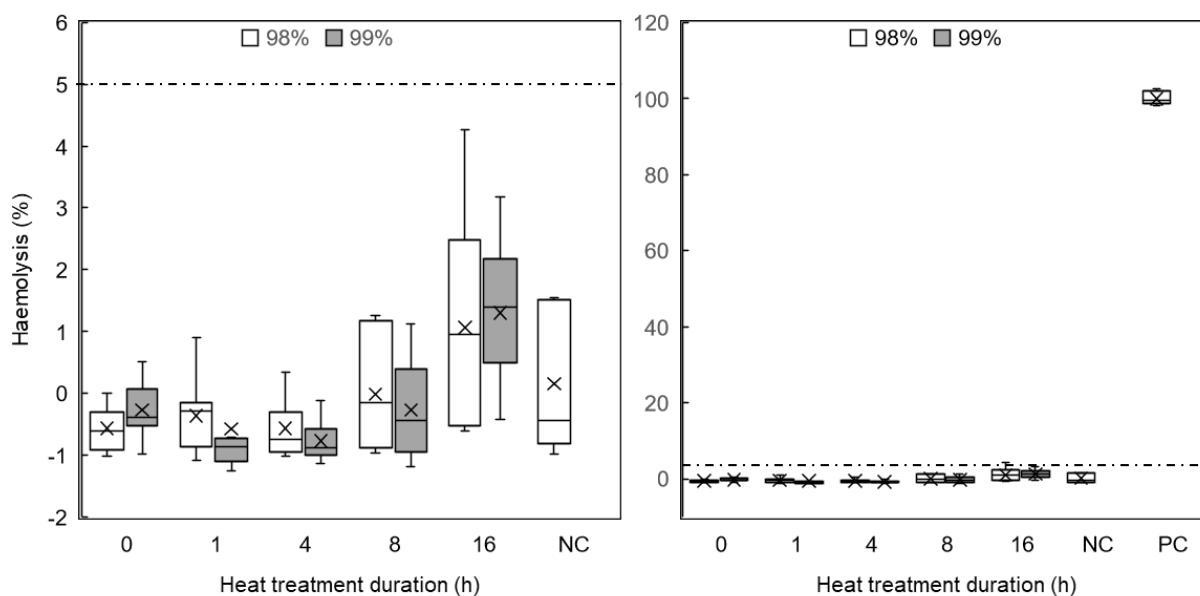
**Figure 5.12.** Box and whisker plots of APTT (left) and PT (right) coagulation tests of nanofibrous mats produced from 98% and 99% hydrolysed PVA after heat treatment. Key: 98% (white); 99% (grey). Control/NC – PPP in isolation ( $n=5$ ).

#### 5.3.3.4 Haemolysis

Haemolysis can be caused when interaction between erythrocytes and a given material may lead to damage to the red blood cell membrane, resulting in leakage of haemoglobin into solution and potentially eliciting entire disintegration of the cells. Haemolysis absorbance values, measured at 570 nm, can be normalised against positive controls (erythrocytes in contact with distilled water), in order to plot haemolysis as a percentage rather than as absorbance values. Haemolysis testing is governed by ISO 10993-4:2017, which states that blood contacting medical devices should not exhibit > 5% haemolysis.

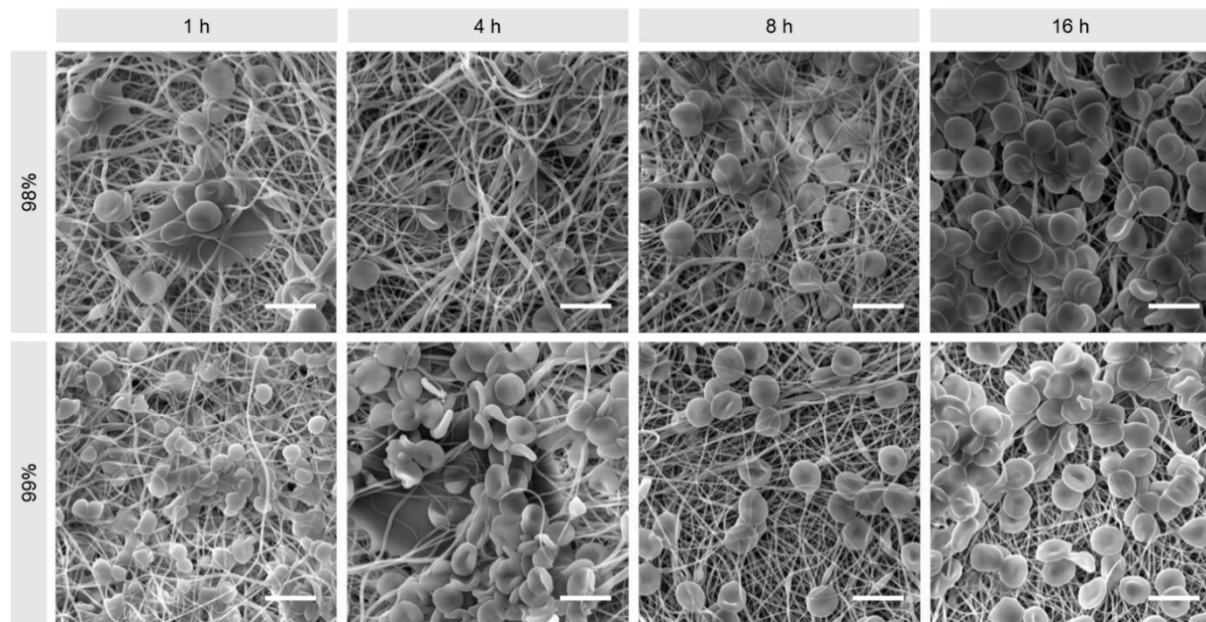
**Figure 5.13** shows haemolysis results for 98% and 99% DH PVA electrospun materials after heat treatment, along with positive and negative controls. Average haemolysis values were almost equal for both DH of PVA at equivalent heat treatment durations, showing a gradual increase as the treatment duration progressed. All materials, other than those subject to 16 h of heat treatment, had lower average haemolysis values than the negative control (erythrocytes in PBS), and even those at 16 h did not exceed the 5% threshold of haemolysis laid out by the governing standard (indicated by the dashed line), though did begin to exhibit greater variability in data, consistent with biocompatibility results previously presented (section 5.3.3.1). This suggests that the materials fall within the haemocompatibility requirements for haemolysis for implantable devices, and is therefore promising for these materials as potential tissue engineering scaffolds (Horakova et al., 2018).





**Figure 5.13.** Haemolysis percentage of red blood cells after incubation in the presence of nanofibrous materials. Absorbance measured at 570 nm measures haemoglobin released in the solution after centrifugation to sediment erythrocytes. Absorbance value for controls were measured by using distilled water (PC) and PBS (NC) and then all values were normalised against the positive control. The left graph excludes PC to allow focusing on the area of interest, while the right graph has the PC included. Dashed line indicates 5% haemolysis. Key: 98% (white); 99% (grey). (n=5)

**Figure 5.14** shows SEM images of erythrocytes fixed upon the nanofibrous materials. The untreated samples are not included because they dissolved, and it was not possible to recover them from the solution following the assay. Where haemolysis has occurred, it is typically expected to observe evidence of crenation of the cells due to membrane damage. However, crenated or otherwise damaged cells were not evident on any samples, regardless of PVA species or heat treatment duration, which is a very encouraging result for many TE applications.



**Figure 5.14.** SEM images of nanofibrous materials produced by needlesh electrospinning after fixing of red blood cells. Scale bar: 10  $\mu\text{m}$ .

## 5.4 Conclusion

Electrospinning PVA with differing DH followed by heat treatment at durations between 1 and 16 h, has the potential to create almost bead-free non-woven nanofibrous supports, with properties that can be tailor made for various TE applications. The DH influences fibre diameter, and the heat treatment process at 180 °C produces some chemical changes which have implications on the hydrophilicity of the sample, as demonstrated by contact angle measurements. Biocompatibility testing of all materials revealed a bell-shaped behaviour between 1 and 16 h of heat treatment duration, with 4 h corresponding to the greatest cell proliferation after 7 days. The haemocompatibility assay indicated that while neither degree of hydrolysis nor treatment duration had a notable effect on coagulation time or haemolysis when in contact with blood, some thrombogenic effect was observed for samples treated for 1, 4 and 16 h. Combined, the results suggest that PVA electrospun materials thermally stabilised for upward of 4 h show promise for TE applications, with the possible exception of situations involving long term blood contact, such as vascular TE, where thrombin formation is a concern.

# Chapter 6

## Conclusions and Future work

### 6.1 Conclusions

The goal of this thesis was to explore crosslinker-free, thermally stabilised PVA nanofibers produced by electrospinning as potential water-stable biomaterials in cell processing and tissue engineering. The work sought to establish what the reasonable limits of treatment duration of heating at 180 °C for highly hydrolysed PVA nanofibers were and explore these limits in the context of materials produced by scalable needleless DC (Nanospider™) and AC electrospinning platforms, by comparison to the more commonly used needle-based approaches. The research then aimed to examine materials produced on said platforms and observe the ability of the heat treatments to stabilise the fibre morphology in aqueous environments. This could be used as a basis to identify which platform and treatment duration was most suitable for situation-specific biomedical applications, with scalable production in mind. The two primary contexts of interest included blood and cell processing, and tissue engineering, where the additional factor of degree of hydrolysis was also examined, with the objective of studying if a cross-linker free approach to morphological stabilisation could meet the requirements of both biomedical applications.

Comparing nanofibrous materials produced from 99% DH PVA using the scalable electrospinning platforms of needleless DC and AC electrospinning showed a number of key differences relating to the production technology which were discussed within this work. These included variations in:

- Macroscopic configurations
- Mechanical properties
- Productivity

The macroscopic structure of materials produced by each platform were distinct, with needleless DC producing membrane/sheet like structures, compared to much looser,

insulation like nanofibrous material produced *via* AC electrospinning. This fact introduces additional factors to consider when selecting a suitable production platform, such as how critical is handling of material, and what is the desired density of the material fibres? Though AC electrospinning produces materials which are difficult to handle, the nature of the novel 'collectorless' (i.e., no charged/grounded collector is required) electrospinning allows for creative approaches to material collection based on mechanical methods, resulting in a great potential for variability and creativity in the macroscopic structures. These variances also resulted in clear differences in mechanical properties, especially with respect to capacity for strain, with AC spun fibres typically having strain at UTS of 2-3x that of the needleless DC counterpart. Finally, while both platforms have capacity for scalability, the AC spinning technology is still in its infancy, whilst needleless DC electrospinning has commercial products readily available on the market. Thus, for now, it is beneficial to defer to the use of the DC needleless spinning platforms wherever suitable, if scalability of production is a chief concern. However, AC electrospinning clearly has potential to form a specific product niche, and further development of electrodes and collection techniques may yield highly promising structures for many applications in the future.

Chemical, morphological, and biological analysis were carried out to compare differences in the materials produced on each platform. Perhaps most critically, morphological analysis indicated that AC spun fibres had over twice the average fibre diameter to their DC counterparts, with a much broader distribution of fibre diameters. This, combined with the macroscopic structure of AC spun materials, highlights the distinct properties of the platform, and may yield materials suited for filtration, or perhaps even as 3D scaffolds for bioengineering. However, it was also found that both needleless DC and AC electrospinning appeared to introduce minor chemical changes to the materials, which may pose barriers to adoption with respect to gaining regulatory approval if the additional species cannot be properly identified and deemed safe. Nevertheless, following cytotoxicity assays there was no evidence of cytotoxic effect resulting from indirect contact with the electrospun samples produced *via* either platform. This result was considered promising, though clearly species identification and assessment may require revisiting if any candidate materials were to progress towards clinical applications.

Heat treatment was shown to successfully stabilise the morphology all the PVA nanofibers produced in this work, however materials showed signs of thermal degradation with increasing heat treatment, which became problematic at greater durations due to embrittling behaviour and clear chemical breakdown shown *via* FT-IR. Based on this, a limit of heat treatment duration was provisionally proposed at 8 hours. *In-situ* saturation analysis by ESEM indicated good retention of the fibrous morphology for heat treated samples produced on all

W. J. A. Homer, PhD Thesis, Aston University, 2023

electrospinning platforms, while total loss of structure was observed for the untreated samples. This finding clearly showed that crosslinker-free stabilisation of PVA nanofibers was possible depending purely on heat treatment at 180 °C, with materials treated for 4-8 hours able to retain much of their pre-saturation morphology.

Based on the logic of readiness for scalability, the decision was used initially to select the needleless DC production platform for all blood and cell flowthrough work. The membranes produced by needleless DC electrospinning and subject to heat treatment were investigated for cell processing using a range of cell populations, including neural blastoma cells as a cancer model cell, and sheep and human RBCs. It was found that cell recovery varied substantially, depending on size and properties of each cell type, as well as the concentration of the cell challenge. This included higher than expected recovery of neural blastoma, and (in places) lower than expected recovery of human RBCs. Given the larger size of neural blastoma cells in suspension this result was unexpected, as RBCs, whilst not only smaller, are better adapted for flow through constricted spaces. This suggests there may be unexplained factors in the behaviour of cross-membrane flow of cells which has not yet been identified. Nevertheless, it was shown that some degree of penetration of all cell populations was possible in a stacked membrane configuration under convective flow, which at least demonstrates suitable proof of concept to explore nanofibrous structures produced by needleless DC electrospinning as a large biomolecule processing substrate.

The observed lower than expected recover of human RBCs compared to other cell populations formed a cause for concern, so a decision was made to reintroduce AC spun materials, with the expectation that the looser structure might result in less impedance to free passage of cells. This improved cell recoveries substantially, and therefore emphasising a strong potential use-case for the application of AC spun materials over its DC counterparts in applications such as blood salvage, providing functionalisation of the material is possible to form a chromatography support. This demonstrates just one potential use of currently underutilised AC electrospinning platform, where the material performance exceeded that those produced via needleless DC electrospinning, due to the creation of larger fibre diameters and the unique production process resulting in a looser macrostructure. Furthermore, development of a specialised collection process for AC spun fibres has the potential to yield bespoke structures, such as loose cottonwool-like materials, composite yarns or even coreless, unwound nanofiber yarns, which may be able to be adapted and optimised for cell processing applications, and it is suggested that further research and collaborations in this area may be warranted.

As exploration of the true flow behaviours within the DC and AC spun material is not feasible, some attempts were carried out to use simulation packages to better understand the flow behaviours. Using CFD tools, a more detailed investigation into flow through both types of nanofibrous network were conducted to explore the presence of channelling within the bed structure. Simulations were established based on stacked 'sheets' of nanofibrous membranes dropped into a packing column before flow simulation was carried out. Several limitations of the model itself were identified and discussed, including inaccuracies in support geometries of the model, improper randomisation, and the lack of particles (i.e., proxies for cells in suspension) simulated in the model. Allowing for these limitations, the model suggested that flow through the simulated non-woven fibre beds is well distributed, with no evidence of channelling or restricted flow. However, ultimately there are limitations of the design of the software, due to the overly simplistic modelling which was used. Though future software does intend to allow for the simulation of fluids containing rigid particles, it is anticipated that this will require substantial increases in processing requirements and would need much more powerful computers than those which were readily available at this time of this research. Furthermore, this would not resolve the still simplistic nature of the simulation containing only rigid particles, rather than readily deformable biomolecules such as RBCs. Subsequently, though CFD modelling may be used as a slight confirmation that uniform flow is clearly possible within the structures, extrapolation of these conclusions to the real world use of these materials in blood salvage should be considered too to be largely speculative.

Briefly, this research included preliminary design considerations which were explored for the housing of stacked beds of nanofibers in a blood salvage context, and SLA 3D printing was used to create initial prototypes. Though the designs were simple provisional test prints, and the designed model series was a simple demonstration of potential housing dimensions, broadly it is proposed that utilisation of the rapid prototyping capacity of 3D printing may be useful in the design of novel configurations for blood salvage devices, as well as for experimentation with ideal bed depth for electrospun materials.

Finally, research was carried out to compare the performance of nanofibers produced via needleless DC spinning from 98% DH PVA and 99% DH PVA, which was considered largely in the context of tissue engineering. For this chapter, heat treatment durations were extended once more to 16 h, with the intention of demonstrating a declining performance with excessive thermal exposure. Biological assays suggested that all the materials were largely bio- and haemocompatible, though all samples exhibited elevated thrombogenicity as a function of heat treatment duration – a similar correlation to that observed with contact angle measurements. The ability to tune hydrophilicity, while maintaining good wettability could prove useful for a number of applications, where bespoke properties can be bestowed upon the PVA nanofibers,

W. J. A. Homer, PhD Thesis, Aston University, 2023

depending on the desired use, without rendering the materials cytotoxic. Notably, biocompatibility assays indicated that materials treated for 4 h had the best cell proliferation after 7 days, whilst treatment durations beyond that began to exhibit highly variable behaviour, and reproducibility clearly declined. Increasing treatment duration also correlated with slight increases in haemolysis, though these results were within tolerable limits, and do not automatically indicate a cause concern, but should be considered holistically in combination with other compatibility results depending on any given potential application beyond that discussed here. This chapter built upon the biological work from chapter 2, and clearly demonstrated that these materials may have applications outside of the initially conceived use-case of blood salvage which was the first proposed application of interest in this project.

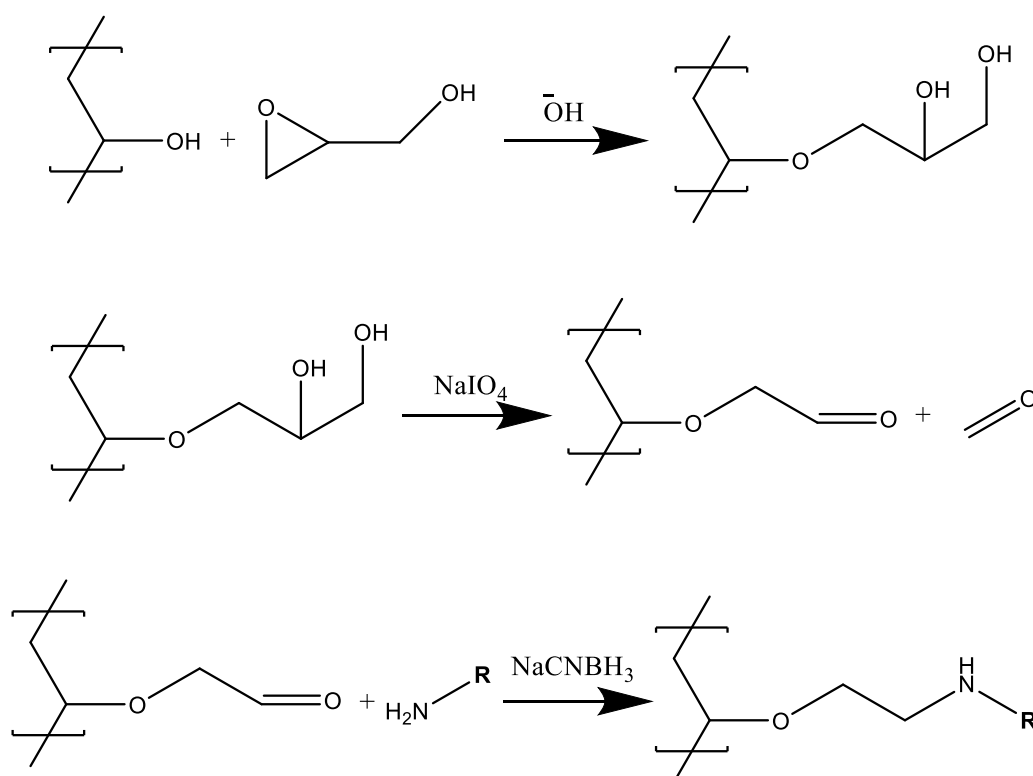
Ultimately, this work demonstrates the potential of crosslinker-free PVA nanofibers as non-gelating biomaterials and suggests that within many applications the de facto use of such additives may warrant reconsidering, as it unnecessarily introduces cytotoxic agents into the production process. In many cases, 4 h of treatment at 180 °C appears to be an optimum duration, with treatments beyond this resulting in trade-offs in strength or reduced biocompatibility with little-to-no additional stabilisation to fibre morphology. Furthermore, the use of AC electrospinning to produce these materials may offer many benefits distinct to the technology, most notably as a method of creating new and interesting biomaterials with unique macrostructures made from nanofibers.

## 6.2 Future work

Four distinct areas of potential future work can be clearly identified following the outcomes of this research.

The next step following the results presented in Chapter 3, would seek to explore these materials in cell separation through the functionalisation of the nanofibers. The immobilization of antibody ligands to the fibre surface would result in the formation of an immunoaffinity membrane, capable of highly selective binding of cells based on surface markers. This targeted removal of specific cell sub-population from a mixture based on antibody-antigen interactions is the critical next step in progressing these materials towards use in blood salvage, as well as more generally in bioprocessing of cells. It is possible this could be achieved through utilisation of avidin-biotin conjugates, previously demonstrated by Šutar, (2015) on dextran coated beads, using the reaction sequence shown in **Figure 6.1**, which allows for the immobilisation of amine containing species (in this instance, the protein avidin)

to hydroxyl containing supports (Hermanson et al., 1992). The nanofibers could then be functionalised using CTC specific biotinylated antibodies for the target absorbance of these sub-populations. However, it should be noted that these chemicals are highly toxic, and use of such a process might compromise biocompatibility of the material and would therefore require rigorous examination.



**Figure 6.1.** Reaction pathway for the modification of hydroxyl containing supports with proteins as a route for functionalisation (Hermanson et al., 1992).

Another area of investigation would be the incorporation of heat-tolerant bioactive components, such as bioactive glass for accelerated healing, metal nanoparticles for antimicrobial applications, or thermally stable drugs for controlled drug release. These components could be combined prior to electrospinning, and exposed to the annealing process, without effecting their biological application, but encapsulating them within a more stable nanofiber structure. An example application of this might be the incorporation of bioactive glass particles to nanofiber membranes, so as to form a tape for bone tissue engineering (Wang et al., 2022a), which offers the benefit of securing the bioactive glass where it needs to be during the healing process, compared to bioactive glass containing pastes which are free to move and diffuse.



Given the relative immaturity of the AC electrospinning technology, there is tremendous breadth of opportunity for transposition of established compositions from DC electrospinning to this alternative platform. Existing material compositions may benefit from different, more 3D, macrostructures, such as utilisation of polymer blends or incorporation of other bioactive molecules, such as pharmaceuticals, into loosely packed fibres or nanofiber yarns. Furthermore, upcoming developments in AC electrospinning emitter geometry and technology will likely yield interesting new applications not previously considered possible by using DC techniques. One example could be the employment of AC spun aligned fibres in neural tissue engineering, where DC based systems have produced aligned fibres able to act as guides for neural cells (Kim et al., 2016). The loose structure of the AC materials has the potential to create 3D configurations for greater cell penetration, while retaining a similar guiding effect. Alternatively, the formation of loosely packed fibres could be utilised as a superior analogue than conventionally spun nanofibers for mimicking ECM of the trabecular meshwork of the eye, which is a complex, multi-layered structure (Crouch et al., 2021). AC electrospinning does not behave in the same reproducible way as DC methods, so the field would also likely benefit from a robust replication study of common blends or composites, to provide better insight into some of the limitations of the platform and explore possible approaches to reliably modify DC spun solutions to be suitable for AC spinning.

Finally, more work could be carried out to develop device housing for convective flow cell processing materials, using 3D printing from haemocompatible resins. As already mentioned in Chapter 4, housing geometry could be optimised to maximise material contact time with low pressure drops and well distributed flow. Live encapsulation of materials during printing is possible using FDM 3D printing and could yield devices that feature self-contained substrates, which can then be functionalised and sterilised in post-processing. These approaches could be applied not only to nanofibers in stacked membranes, but other potential bed materials such as cryogels, which are also suitable for convective flow processing (Gagnon, 2006). It is possible that in the instance of cryogels, they could be formed *in-situ* within the device, creating a highly porous bed already built into the device. This utilisation of 3D printing for production of the device housing is the work set to be carried out in the next stage of research and is already underway in our laboratories.

# References

- ADELNIA, H., ENSANDOOST, R., MOONSHI, S. S., GAVGANI, J. N., VASAFI, E. I. & TA, H. T. 2022. Freeze/thawed polyvinyl alcohol hydrogels: Present, past and future. *European Polymer Journal*, 164.
- ADILI, N., MELIZI, M. & BELABBAS, H. 2016. Species determination using the red blood cells morphometry in domestic animals. *Veterinary World*, 9, 960-963.
- ADVANCIS SURGICAL 2017. HemoSep: Cell saver for all blood components. Nottinghamshire: England.
- AGARWAL, S., WENDORFF, J. H. & GREINER, A. 2008. Use of electrospinning technique for biomedical applications. *Polymer*, 49, 5603-5621.
- AGRAWAL, S., RANJAN, R., LAL, B., RAHMAN, A., SINGH, S. P., SELVARATNAM, T. & NAWAZ, T. 2021. Synthesis and Water Treatment Applications of Nanofibers by Electrospinning. *Processes*, 9.
- AKHTER, S., ALLAN, K., BUCHANAN, D., COOK, J. A., CAMPION, A. & WHITE, J. M. 1988. XPS AND IR STUDY OF X-RAY-INDUCED DEGRADATION OF PVA POLYMER FILM. *Applied Surface Science*, 35, 241-258.
- AKPE, V., KIM, T. H., BROWN, C. L. & COCK, I. E. 2020. Circulating tumour cells: a broad perspective. *Journal of the Royal Society Interface*, 17.
- AL-JBOUR, N. D., BEG, M. D., GIMBUN, J. & ALAM, A. 2019. An Overview of Chitosan Nanofibers and their Applications in the Drug Delivery Process. *Current Drug Delivery*, 16, 272-294.
- ALHOSSEINI, S. N., MOZTARZADEH, F., MOZAFARI, M., ASGARI, S., DODEL, M., SAMADIKUCHAKSARAEI, A., KARGOZAR, S. & JALALI, N. 2012. Synthesis and characterization of electrospun polyvinyl alcohol nanofibrous scaffolds modified by blending with chitosan for neural tissue engineering. *International Journal of Nanomedicine*, 7, 25-34.
- AMARAL, K. F., ROGERO, M. M., FOCK, R. A., BORELLI, P. & GAVINI, G. 2007. Cytotoxicity analysis of EDTA and citric acid applied on murine resident macrophages culture. *International Endodontic Journal*, 40, 338-343.
- AMARIEI, N., MANEA, L. R., BERTEA, A. P., BERTEA, A. & POPA, A. 2017. The Influence of Polymer Solution on the Properties of Electrospun 3D Nanostructures. International Conference on Innovative Research (ICIR Euroinvent), May 25-26 2017 Iasi, ROMANIA.
- ANGAMMANA, C. J. & JAYARAM, S. H. 2011. Analysis of the Effects of Solution Conductivity on Electrospinning Process and Fiber Morphology. *Ieee Transactions on Industry Applications*, 47, 1109-1117.
- ANTABY, E., KLINKHAMMER, K. & SABANTINA, L. 2021. Electrospinning of Chitosan for Antibacterial Applications-Current Trends. *Applied Sciences-Basel*, 11.
- ANTONPAARGMBH. 2023. *Viscosity of Whole Blood* [Online]. Available: <https://wiki.anton-paar.com/uk-en/whole-blood/> [Accessed].
- ARULDASS, S., MATHIVANAN, V., MOHAMED, A. R. & TYE, C. T. 2019. Factors affecting hydrolysis of polyvinyl acetate to polyvinyl alcohol. *Journal of Environmental Chemical Engineering*, 7.
- ASHRAF, R., SOFI, H. S., MALIK, A., BEIGH, M. A., HAMID, R. & SHEIKH, F. A. 2019. Recent Trends in the Fabrication of Starch Nanofibers: Electrospinning and Non-electrospinning Routes and Their Applications in Biotechnology. *Applied Biochemistry and Biotechnology*, 187, 47-74.

- AZARI, A., GOLCHIN, A., MAYMAND, M. M., MANSOURI, F. & ARDESHIRYLAJIMI, A. 2022. Electrospun Polycaprolactone Nanofibers: Current Research and Applications in Biomedical Application. *Advanced Pharmaceutical Bulletin*, 12, 658-672.
- BACHS-HERRERA, A., YOUSEFZADE, O., DEL VALLE, L. J. & PUIGGALI, J. 2021. Melt Electrospinning of Polymers: Blends, Nanocomposites, Additives and Applications. *Applied Sciences-Basel*, 11.
- BAEK, H. S., YOO, J. Y., RAH, D. K., HAN, D. W., LEE, D. H., KWON, O. H. & PARK, J. C. 2005. Evaluation of the extraction method for the cytotoxicity testing of latex gloves. *Yonsei Medical Journal*, 46, 579-583.
- BAKER, M. I., WALSH, S. P., SCHWARTZ, Z. & BOYAN, B. D. 2012. A review of polyvinyl alcohol and its uses in cartilage and orthopedic applications. *Journal of Biomedical Materials Research Part B-Applied Biomaterials*, 100B, 1451-1457.
- BAKSHANDEH, B., ZARRINTAJ, P., OFTADEH, M. O., KERAMATI, F., FOULADIHA, H., SOHRABI-JAHROMI, S. & ZIRAKSAZ, Z. 2017. Tissue engineering; strategies, tissues, and biomaterials. *Biotechnology and Genetic Engineering Reviews*, Vol 33, Issue 2, 33, 144-172.
- BAUMGARTEN, P. K. 1971. Electrostatic spinning of acrylic microfibers. *Journal of Colloid and Interface Science*, 36, 71.
- BECKMANCOULTER 2017. MoFlo Astrios, MoFlo Astrios EQ, and MoFlo Astrios EQS Instructions for Use. Switzerland: Beckman Coulter Eurocentre.
- BELBEOCH, C., LEJEUNE, J., VROMAN, P. & SALAUN, F. 2021. Silkworm and spider silk electrospinning: a review. *Environmental Chemistry Letters*, 19, 1737-1763.
- BHUSHANI, J. A. & ANANDHARAMAKRISHNAN, C. 2014. Electrospinning and electrospaying techniques: Potential food based applications. *Trends in Food Science & Technology*, 38, 21-33.
- BIGDELI, A. K., LYER, S., DETSCH, R., BOCCACCINI, A. R., BEIER, J. P., KNESER, U., HORCH, R. E. & ARKUDAS, A. 2013. Nanotechnologies in tissue engineering. *Nanotechnology Reviews*, 2, 411-425.
- BIONICIA. 2023. *Fluidnatek HT* [Online]. Available: <https://www.nanoscience.com/products/electrospinning-equipment/fluidnatek-ht/> [Accessed 16th March 2023].
- BIRANJE, S., MADIWALE, P. & ADIVAREKAR, R. V. 2019. Porous electrospun Casein/PVA nanofibrous mat for its potential application as wound dressing material. *Journal of Porous Materials*, 26, 29-40.
- BOYLE, G., KUFFEL, A., PARMAR, K., GIBSON, K., SMITH, M., GREHAN, A., HUNT, B. J. & CHAMBERS, D. J. 2019. A comparison of haemostatic biomarkers during low-risk patients undergoing cardiopulmonary bypass using either conventional centrifugal cell salvage or the HemoSep device. *Perfusion-Uk*, 34, 76-83.
- BOYS, C. V. 1887. On the Production, Properties, and some suggested Uses of the Finest Threads. *Proceedings of the Physical Society of London*, 9, 8.
- BRANDSLUND, I., RASMUSSEN, J. M., FISKER, D. & SVEHAG, S. E. 1982. Separation of human peripheral-blood monocytes on continuous density gradients of polyvinylpyrrolidone-coated silica-gel (Percoll). *Journal of Immunological Methods*, 48, 199-211.
- BREN, K. L., EISENBERG, R. & GRAY, H. B. 2015. Discovery of the magnetic behavior of hemoglobin: A beginning of bioinorganic chemistry. *Proceedings of the National Academy of Sciences of the United States of America*, 112, 13123-13127.

- BRÅNEMARK, P. & LINDSTRÖM, J. 1963. Shape of circulating blood corpuscles. *Biorheology*, 1, 139-142.
- BUDHLALL, B. M., LANDFESTER, K., SUDOL, E. D., DIMONIE, V. L., KLEIN, A. & EL-AASSER, M. S. 2003. Characterization of partially hydrolyzed poly(vinyl alcohol). Effect of poly(vinyl alcohol) molecular architecture on aqueous phase conformation. *Macromolecules*, 36, 9477-9484.
- CALABRÒ, V., BASILE, A., BASILE, A. & NUNES, S. P. 2011. 1 - Fundamental membrane processes, science and engineering. *Advanced Membrane Science and Technology for Sustainable Energy and Environmental Applications*. Woodhead Publishing.
- CAN-HERRERA, L. A., OLIVA, A. I., DZUL-CERVANTES, M. A. A., PACHECO-SALAZAR, O. F. & CERVANTES-UC, J. M. 2021. Morphological and Mechanical Properties of Electrospun Polycaprolactone Scaffolds: Effect of Applied Voltage. *Polymers*, 13.
- CATLING, S., WILLIAMS, S., FREITES, O., REES, M., DAVIES, C. & HOPKINS, L. 2008. Use of a leucocyte filter to remove tumour cells from intra-operative cell salvage blood. *Anaesthesia*, 63, 1332-1338.
- CAULKIN, R., JIA, X., XU, C., FAIRWEATHER, M., WILLIAMS, R. A., STITT, H., NIJEMEISLAND, M., AFERKA, S., CRINE, M., LEONARD, A., TOYE, D. & MARCHOT, P. 2009. Simulations of Structures in Packed Columns and Validation by X-ray Tomography. *Industrial & Engineering Chemistry Research*, 48, 202-213.
- CAULKIN, R., JIA, X. D., FAIRWEATHER, M. & WILLIAMS, R. A. 2008. Lattice approaches to packed column simulations. *Particuology*, 6, 404-411.
- CAY, A., AKCAKOCA KUMBASAR, E. P. & AKDUMAN, C. 2015. EFFECTS OF SOLVENT MIXTURES ON THE MORPHOLOGY OF ELECTROSPUN THERMOPLASTIC POLYURETHANE NANOFIBRES. *Tekstil Ve Konfeksiyon*, 25, 38-46.
- CHASSE, M., MCINTYRE, L., ENGLISH, S. W., TINMOUTH, A., KNOLL, G., WOLFE, D., WILSON, K., SHEHATA, N., FORSTER, A., VAN WALRAVEN, C. & FERGUSON, D. A. 2016. Effect of Blood Donor Characteristics on Transfusion Outcomes: A Systematic Review and Meta-Analysis. *Transfusion Medicine Reviews*, 30, 69-80.
- CHEE, B. S., DE LIMA, G. G., DE LIMA, T. A. M., SEBA, V., LEMARQUIS, C., PEREIRA, B. L., BANDEIRA, M., CAO, Z. & NUGENT, M. 2021. Effect of thermal annealing on a bilayer polyvinyl alcohol/polyacrylic acid electrospun hydrogel nanofibres loaded with doxorubicin and clarithromycin for a synergism effect against osteosarcoma cells. *Materials Today Chemistry*, 22.
- CHEN, K., LI, Y. H., LI, Y. B., PAN, W. S. & TAN, G. X. 2023. Silk Fibroin Combined with Electrospinning as a Promising Strategy for Tissue Regeneration. *Macromolecular Bioscience*, 23.
- CHEN, K. & SCHWEIZER, K. S. 2011. Theory of Yielding, Strain Softening, and Steady Plastic Flow in Polymer Glasses under Constant Strain Rate Deformation. *Macromolecules*, 44, 3988-4000.
- CHEN, M. X., GAO, S., WANG, P., LI, Y., GUO, W. M., ZHANG, Y., WANG, M. J., XIAO, T. G., ZHANG, Z. Z., ZHANG, X. L., JING, X. G., LI, X., LIU, S. Y., GUO, Q. Y. & XI, T. F. 2018. The application of electrospinning used in meniscus tissue engineering. *Journal of Biomaterials Science-Polymer Edition*, 29, 461-475.
- CHEN, Y., TAI, B. C., NAYAK, D., KUMAR, N., CHUA, K. H., LIM, J. W., GOY, R. W. L. & WONG, H. K. 2013. Blood loss in spinal tumour surgery and surgery for metastatic spinal disease A META-ANALYSIS. *Bone & Joint Journal*, 95B, 683-688.
- CHENG, J., JUN, Y., QIN, J. H. & LEE, S. H. 2017. Electrospinning versus microfluidic spinning of functional fibers for biomedical applications. *Biomaterials*, 114, 121-143.

- CHONG, S. F., SMITH, A. A. A. & ZELIKIN, A. N. 2013. Microstructured, Functional PVA Hydrogels through Bioconjugation with Oligopeptides under Physiological Conditions. *Small*, 9, 942-950.
- CHOUDHURY, N., SHUKLA, A., SAMPATH, S. & PITCHUMANI, S. 2006. Cross-Linked Polymer Hydrogel Electrolytes for Electrochemical Capacitors. *Journal of The Electrochemical Society - J ELECTROCHEM SOC*, 153.
- COELHO, S. C., ESTEVINHO, B. N. & ROCHA, F. 2022. Recent Advances in Water-Soluble Vitamins Delivery Systems Prepared by Mechanical Processes (Electrospinning and Spray-Drying Techniques) for Food and Nutraceuticals Applications-A Review. *Foods*, 11.
- COOLEY, J. F. 1902. Apparatus for electrically dispersing fluids. Google Patents.
- COSKUN, O. 2016. Separation techniques: Chromatography. *Northern clinics of Istanbul*, 3, 156-160.
- COWIE, J. M. G. & ARRIGHI, V. 2008. *Polymers : chemistry and physics of modern materials*, CRC.
- CROUCH, D. J., SHERIDAN, C. M., D'SA, R. A., WILLOUGHBY, C. E. & BOSWORTH, L. A. 2021. Exploiting biomaterial approaches to manufacture an artificial trabecular meshwork: A progress report. *Biomaterials and Biosystems*, 1, 100011.
- CUI, W. G., ZHOU, Y. & CHANG, J. 2010. Electrospun nanofibrous materials for tissue engineering and drug delivery. *Science and Technology of Advanced Materials*, 11.
- CURLING, J. 2007. *Process Chromatography: Five Decades of Innovation* [Online]. BioPharmInternational.com: BioPharm International. [Accessed 11th of August 2021].
- DAGUR, P. K. & MCCOY, J. P., JR. 2015. Collection, Storage, and Preparation of Human Blood Cells. *Current protocols in cytometry*, 73, 5.1.1-5.1.16.
- DAI, Y. Q., LIU, W. Y., FORMO, E., SUN, Y. M. & XIA, Y. N. 2011. Ceramic nanofibers fabricated by electrospinning and their applications in catalysis, environmental science, and energy technology. *Polymers for Advanced Technologies*, 22, 326-338.
- DAINIAK, M. B., PLIEVA, F. M., GALAEV, I. Y., HATTI-KAUL, R. & MATTIASSON, B. 2005. Cell chromatography: Separation of different microbial cells using IMAC supermacroporous monolithic columns. *Biotechnology Progress*, 21, 644-649.
- DARBASIZADEH, B., FATAHI, Y., FEYZI-BARNAJI, B., ARABI, M., MOTASADIZADEH, H., FARHADNEJAD, H., MORAFFAH, F. & RABIEE, N. 2019. Crosslinked-polyvinyl alcohol-carboxymethyl cellulose/ZnO nanocomposite fibrous mats containing erythromycin (PVA-CMC/ZnO-EM): Fabrication, characterization and in-vitro release and anti-bacterial properties. *International Journal of Biological Macromolecules*, 141, 1137-1146.
- DE CASTRO, K. C., SILVA, E. K., CAMPOS, M. G. N. & MEI, L. H. I. 2022. Hyaluronic Acid/Polyvinyl Alcohol Electrospun Nanofiber Membranes Loaded with Plantago Major Extract for Smart Wound Dressings. *Acs Applied Nano Materials*, 5, 12616-12625.
- DEITZEL, J. M., KLEINMEYER, J. D., HIRVONEN, J. K. & TAN, N. C. B. 2001. Controlled deposition of electrospun poly(ethylene oxide) fibers. *Polymer*, 42, 8163-8170.
- DEJOB, L., TOURY, B., TADIER, S., GREMILLARD, L., GAILLARD, C. & SALLES, V. 2021. Electrospinning of in situ synthesized silica-based and calcium phosphate bioceramics for applications in bone tissue engineering: A review. *Acta Biomaterialia*, 123, 123-153.
- DEMIR, M. M., YILGOR, I., YILGOR, E. & ERMAN, B. 2002. Electrospinning of polyurethane fibers. *Polymer*, 43, 3303-3309.
- DESAI, S. D., KUNDU, I., SWAMY, N. P., CRULL, G. B., PAN, D. H., ZHAO, J. S., SHAH, R. P., VENKATESH, C., VIG, B., VARIA, S. A., BADAWY, S. I. F., DESIKAN, S. & BHUTANI, H. 2020. Cross-linking of

- poly (vinyl alcohol) films under acidic and thermal stress. *European Journal of Pharmaceutical Sciences*, 152.
- DIEZ, B., HOMER, W. J. A., LESLIE, L. J., KYRIAKOU, G., ROSAL, R., TOPHAM, P. D. & THEODOSIOU, E. 2022. Chemically cross-linked poly(vinyl alcohol) electrospun fibrous mats as wound dressing materials. *Journal of Chemical Technology and Biotechnology*, 97, 620-632.
- DO NASCIMENTO, F. C., DE AGUIAR, L. C. V., COSTA, L. A. T., FERNANDES, M. T., MARASSI, R. J., GOMES, A. D. & DE CASTRO, J. A. 2021. Formulation and characterization of crosslinked polyvinyl alcohol (PVA) membranes: effects of the crosslinking agents. *Polymer Bulletin*, 78, 917-929.
- DONG, Z. X., KENNEDY, S. J. & WU, Y. Q. 2011. Electrospinning materials for energy-related applications and devices. *Journal of Power Sources*, 196, 4886-4904.
- DOPKE, C., GROTHE, T., STEBLINSKI, P., KLOCKER, M., SABANTINA, L., KOSMALSKA, D., BLACHOWICZ, T. & EHRMANN, A. 2019. Magnetic Nanofiber Mats for Data Storage and Transfer. *Nanomaterials*, 9.
- DOSHI, J. & RENEKER, D. H. 1995. ELECTROSPINNING PROCESS AND APPLICATIONS OF ELECTROSPUN FIBERS. *Journal of Electrostatics*, 35, 151-160.
- DOU, Y. B., ZHANG, W. J. & KAISER, A. 2020. Electrospinning of Metal-Organic Frameworks for Energy and Environmental Applications. *Advanced Science*, 7.
- DOWNEY, R. F. 2017. Complete blood count reference ranges from a rural Haitian ambulatory care clinic. *Laboratory Medicine*, 48, E24-E29.
- DROSOU, C. G., KROKIDA, M. K. & BILIADERIS, C. G. 2017. Encapsulation of bioactive compounds through electrospinning/electrospraying and spray drying: A comparative assessment of food-related applications. *Drying Technology*, 35, 139-162.
- EL-OKAILY, M. S., EL-RAFEI, A. M., BASHA, M., GHANI, N. T. A., EL-SAYED, M. M. H., BHAUMIK, A. & MOSTAFA, A. A. 2021. Efficient drug delivery vehicles of environmentally benign nano-fibers comprising bioactive glass/chitosan/polyvinyl alcohol composites. *International Journal of Biological Macromolecules*, 182, 1582-1589.
- ELMARCO. 2020. *NS 8S1600U: Scalable industrial production line* [Online]. Available: <https://www.elmarco.com/production-lines/ns-8s1600u> [Accessed 4th of April 2020].
- ENAYATI, M. S., BEHZAD, T., SAJKIEWICZ, P., BAGHERI, R., GHASEMI-MOBARAKEH, L., ŁOJKOWSKI, W., PAHLEVANNESHAN, Z. & AHMADI, M. 2016. Crystallinity study of electrospun poly (vinyl alcohol) nanofibers: effect of electrospinning, filler incorporation, and heat treatment. *Iranian Polymer Journal*, 25, 647-659.
- ENAYATI, M. S., BEHZAD, T., SAJKIEWICZ, P., RAFIENIA, M., BAGHERI, R., GHASEMI-MOBARAKEH, L., KOLBUK, D., PAHLEVANNESHAN, Z. & BONAKDAR, S. H. 2018a. Development of electrospun poly (vinyl alcohol)-based bionanocomposite scaffolds for bone tissue engineering. *Journal of Biomedical Materials Research Part A*, 106, 1111-1120.
- ENAYATI, M. S., BEHZAD, T., SAJKIEWICZ, P. L., BAGHERI, R., GHASEMI-MOBARAKEH, L. & PIERINI, F. 2018b. Theoretical and experimental study of the stiffness of electrospun composites of poly(vinyl alcohol), cellulose nanofibers, and nanohydroxy apatite. *Cellulose*, 25, 65-75.
- ERBEN, J., KALOUS, T. & CHVOJKA, J. 2020. ac Bubble Electrospinning Technology for Preparation of Nanofibrous Mats. *Acs Omega*, 5, 8268-8271.
- ESENTURK, I., ERDAL, M. S. & GUNGOR, S. 2016. Electrospinning method to produce drug-loaded nanofibers for topical/ transdermal drug delivery applications. *Istanbul Journal of Pharmacy*, 46, 49-68.

- FARAGHAT, S. A., HOETTGES, K. F., STEINBACH, M. K., VAN DER VEEN, D. R., BRACKENBURY, W. J., HENSLEE, E. A., LABEED, F. H. & HUGHES, M. P. 2017. High-throughput, low-loss, low-cost, and label-free cell separation using electrophysiology-activated cell enrichment. *Proceedings of the National Academy of Sciences of the United States of America*, 114, 4591-4596.
- FARKAS, B., BALOGH, A., CSELKO, R., MOLNAR, K., FARKAS, A., BORBAS, E., MAROSI, G. & NAGY, Z. K. 2019. Corona alternating current electrospinning: A combined approach for increasing the productivity of electrospinning. *International Journal of Pharmaceutics*, 561, 219-227.
- FARKAS, B., BALOGH, A., FARKAS, A., MAROSI, G. & NAGY, Z. K. 2020. Frequency and waveform dependence of alternating current electrospinning and their uses for drug dissolution enhancement. *International Journal of Pharmaceutics*, 586.
- FAROKHI, M., MOTTAGHITALAB, F., FATAHI, Y., KHADEMHOSEINI, A. & KAPLAN, D. L. 2018. Overview of Silk Fibroin Use in Wound Dressings. *Trends in Biotechnology*, 36, 907-922.
- FAROKHI, M., MOTTAGHITALAB, F., REIS, R. L., RAMAKRISHNA, S. & KUNDU, S. C. 2020. Functionalized silk fibroin nanofibers as drug carriers: Advantages and challenges. *Journal of Controlled Release*, 321, 324-347.
- FERNENGEL, J., VON SECKENDORFF, J. & HINRICHSEN, O. 2018. Influence of Cylinder-to-Particle Diameter Ratio and Filling Speed on Bed Porosity of Random Packed Beds of Spheres. 28th European Symposium on Computer-Aided Process Engineering (ESCAPE), Jun 10-13 2018 Graz, AUSTRIA. 97-102.
- FILOVA, E., BLANQUER, A., KNITLOVA, J., PLENCNER, M., JENCOVA, V., KOPRIVOVA, B., LISNENKO, M., KOSTAKOVA, E. K., PROCHAZKOVA, R. & BACAKOVA, L. 2021. The Effect of the Controlled Release of Platelet Lysate from PVA Nanomats on Keratinocytes, Endothelial Cells and Fibroblasts. *Nanomaterials*, 11.
- FISCHER, D., NEB, H., CHOORAPOIKAYIL, S., ZACHAROWSKI, K. & MEYBOHM, P. 2019. Red blood cell transfusion and its alternatives in oncologic surgery-A critical evaluation. *Crit Rev Oncol Hematol*, 134, 1-9.
- FLEMING, I. & WILLIAMS, D. 2019. Infrared and Raman Spectra. *Spectroscopic Methods in Organic Chemistry*. Cham: Springer International Publishing.
- FLORMANN, D., AOUANE, O., KAESTNER, L., RULOFF, C., MISBAH, C., PODGORSKI, T. & WAGNER, C. 2017. The buckling instability of aggregating red blood cells. *Scientific Reports*, 7.
- FRANK, S. M., SIKORSKI, R. A., KONIG, G., TSILIMIGRAS, D. I., HARTMANN, J., POPOVSKY, M. A., PAWLIK, T. M. & WATERS, J. H. 2020. Clinical Utility of Autologous Salvaged Blood: a Review. *Journal of Gastrointestinal Surgery*, 24, 464-472.
- GAAZ, T. S., SULONG, A. B., AKHTAR, M. N., KADHUM, A. A. H., MOHAMAD, A. B. & AL-AMIERY, A. A. 2015. Properties and Applications of Polyvinyl Alcohol, Halloysite Nanotubes and Their Nanocomposites. *Molecules*, 20, 22833-22847.
- GAGNON, P. 2006. Monoliths seen to revitalize bioseparations - New research will broaden the range of applications. *Genetic Engineering News*, 26.
- GAO, Y. F., ZHANG, W., SHI, P. J., REN, W. L. & ZHONG, Y. B. 2020. A mechanistic interpretation of the strength-ductility trade-off and synergy in lamellar microstructures. *Materials Today Advances*, 8.
- GARKAL, A., KULKARNI, D., MUSALE, S., MEHTA, T. & GIRAM, P. 2021. Electrospinning nanofiber technology: a multifaceted paradigm in biomedical applications. *New Journal of Chemistry*, 45, 21508-21533.

- GEORGE, J. H., NAGEL, D., WALLER, S., HILL, E., PARRI, H. R., COLEMAN, M. D., CUI, Z. F. & YE, H. 2018. A closer look at neuron interaction with track-etched microporous membranes. *Scientific Reports*, 8.
- GHADERPOUR, A., HOSEINKHANI, Z., YARANI, R., MOHAMMADIANI, S., AMIRI, F. & MANSOURI, K. 2021. Altering the characterization of nanofibers by changing the electrospinning parameters and their application in tissue engineering, drug delivery, and gene delivery systems. *Polymers for Advanced Technologies*, 32, 1924-1950.
- GHARAEI, R., TRONCI, G., DAVIES, R. P. W., GOUGH, C., ALAZRAGI, R., GOSWAMI, P. & RUSSELL, S. J. 2016. A structurally self-assembled peptide nano-architecture by one-step electrospinning. *Journal of Materials Chemistry B*, 4, 5475-5485.
- GHORBANI, F., REITER, T., LIVERANI, L., SCHUBERT, D. W., BOCCACCINI, A. R. & ROETHER, J. A. 2023. Progress on Electrospun Composite Fibers Incorporating Bioactive Glass: An Overview. *Advanced Engineering Materials*.
- GOLBA, B., KALAOGLU-ALTAN, O. I., SANYAL, R. & SANYAL, A. 2022. Hydrophilic Cross-Linked Polymeric Nanofibers Using Electrospinning: Imparting Aqueous Stability to Enable Biomedical Applications. *Acs Applied Polymer Materials*, 4, 1-17.
- GONG, X., YANG, J. L., JIANG, Y. L. & MU, S. C. 2014. Application of Electrospinning Technique in Power Lithium-Ion Batteries. *Progress in Chemistry*, 26, 41-47.
- GONZÁLEZ-GONZÁLEZ, M., GONZÁLEZ-VALDEZ, J., MAYOLO-DELOISA, K. & RITO-PALOMARES, M. 2017. Monolithic chromatography: insights and practical perspectives. *Journal of Chemical Technology & Biotechnology*, 92, 9-13.
- GOTTLIEB, H. E., KOTLYAR, V. & NUDELMAN, A. 1997. NMR chemical shifts of common laboratory solvents as trace impurities. *Journal of Organic Chemistry*, 62, 7512-7515.
- GUNAYDIN, S. & GOURLAY, T. 2013. Novel ultrafiltration technique for blood conservation in cardiac operations. *Annals of Thoracic Surgery*, 95, 2148-2151.
- GUNAYDIN, S., ROBERTSON, C., BUDAK, A. B. & GOURLAY, T. 2018. Comparative evaluation of blood salvage techniques in patients undergoing cardiac surgery with cardiopulmonary bypass. *Perfusion-Uk*, 33, 105-109.
- GUPTA, S., RAWAT, S., ARORA, V., KOTTARATH, S. K., DINDA, A. K., VAISHNAV, P. K., NAYAK, B. & MOHANTY, S. 2018. An improvised one-step sucrose cushion ultracentrifugation method for exosome isolation from culture supernatants of mesenchymal stem cells. *Stem Cell Research & Therapy*, 9.
- HAEMONETICS 2019. Cell Saver® 5+ Brochure. Massachusetts: USA.
- HAIDER, A., HAIDER, S. & KANG, I.-K. 2018a. A comprehensive review summarizing the effect of electrospinning parameters and potential applications of nanofibers in biomedical and biotechnology. *Arabian Journal of Chemistry*, 11, 1165-1188.
- HAIDER, A., HAIDER, S. & KANG, I. K. 2018b. A comprehensive review summarizing the effect of electrospinning parameters and potential applications of nanofibers in biomedical and biotechnology. *Arabian Journal of Chemistry*, 11, 1165-1188.
- HALAUI, R., ZUSSMAN, E., KHALFIN, R., SEMIAT, R. & COHEN, Y. 2017. Polymeric microtubes for water filtration by co-axial electrospinning technique. *Polymers for Advanced Technologies*, 28, 570-582.
- HALIMA, N. B. 2016. Poly(vinyl alcohol): review of its promising applications and insights into biodegradation. *Rsc Advances*, 6, 39823-39832.



- HALLENSLEBEN, M. L., FUSS, R. & MUMMY, F. 2015. Polyvinyl Compounds, Others. *Ullmann's Encyclopedia of Industrial Chemistry*.
- HAN, D. & STECKL, A. J. 2013. Triaxial Electrospun Nanofiber Membranes for Controlled Dual Release of Functional Molecules. *Acs Applied Materials & Interfaces*, 5, 8241-8245.
- HAN, J. Q., WANG, S. W., ZHU, S. L., HUANG, C. B., YUE, Y. Y., MEI, C. T., XU, X. W. & XIA, C. L. 2019. Electrospun Core-Shell Nanofibrous Membranes with Nanocellulose-Stabilized Carbon Nanotubes for Use as High-Performance Flexible Supercapacitor Electrodes with Enhanced Water Resistance, Thermal Stability, and Mechanical Toughness. *Acs Applied Materials & Interfaces*, 11, 44624-44635.
- HAN, K. H., LANDERS, J. P., FRAZIER, A. B. & IEEE 2003. Continuous paramagnetophoretic microseparator for blood cells. *Boston Transducers'03: Digest of Technical Papers, Vols 1 and 2*, 1229-1232.
- HARTATIEK, YUDYANTO, WURIANTIKA, M. I., UTOMO, J., NURHUDA, M., MASRUROH & SANTJOJO, D. 2021. Nanostructure, porosity and tensile strength of PVA/Hydroxyapatite composite nanofiber for bone tissue engineering. 7th International Conference of Advanced Materials Science and Technology (ICAMST), Sep 25-26 2019 Bandung, INDONESIA. 3203-3206.
- HASSAN, C. M. & PEPPAS, N. A. 2000. Structure and applications of poly(vinyl alcohol) hydrogels produced by conventional crosslinking or by freezing/thawing methods. *Biopolymers/Pva Hydrogels/Anionic Polymerisation Nanocomposites*, 153, 37-65.
- HDIDAR, M., CHOUIKHI, S., FATTOUM, A. & AROUS, M. 2017. Effect of hydrolysis degree and mass molecular weight on the structure and properties of PVA films. *Ionics*, 23, 3125-3135.
- HEDAYATI, H. R., KHORASANI, M., AHMADI, M. & BALLARD, N. 2022. Preparation of well-defined Poly(Vinyl alcohol) by hydrolysis of Poly(Vinyl acetate) synthesized by RAFT suspension polymerization. *Polymer*, 246.
- HEILINGOETTER, A., SMITH, S., MALHOTRA, P., JOHNSON, J. & CHIANG, T. 2021. Applications of Electrospinning for Tissue Engineering in Otolaryngology. *Annals of Otolaryngology and Laryngology*, 130, 395-404.
- HEMAMALINI, T. & DEV, V. R. G. 2018. Comprehensive review on electrospinning of starch polymer for biomedical applications. *International Journal of Biological Macromolecules*, 106, 712-718.
- HENRIQUES, C., VIDINHA, R., BOTEQUIM, D., BORGES, J. P. & SILVA, J. 2009. A Systematic Study of Solution and Processing Parameters on Nanofiber Morphology Using a New Electrospinning Apparatus. *Journal of Nanoscience and Nanotechnology*, 9, 3535-3545.
- HERMANSON, G. T., MALLIA, A. K. & SMITH, P. K. 1992. *Immobilized Affinity Ligand Techniques*, Academic Press.
- HERRMANN, W. O. W., HAEHNEL. 1924. *Process for the preparation of polymerized vinyl alcohol and its derivatives*. United States patent application.
- HOGAN, M., NEEDHAM, A., ORTMANN, E., BOTTRILL, F., COLLIER, T. J., BESSER, M. W. & KLEIN, A. A. 2015. Haemoconcentration of residual cardiopulmonary bypass blood using Hemosep (R): a randomised controlled trial. *Anaesthesia*, 70, 563-570.
- HONG, J., YEO, M., YANG, G. H. & KIM, G. 2019. Cell-Electrospinning and Its Application for Tissue Engineering. *International Journal of Molecular Sciences*, 20.
- HORAKOVA, J., MIKES, P., SAMAN, A., SVARCOVA, T., JENCOVA, V., SUCHY, T., HECZKOVA, B., JAKUBKOVA, S., JIROUSOVA, J. & PROCHAZKOVA, R. 2018. Comprehensive assessment of electrospun scaffolds hemocompatibility. *Materials Science & Engineering C-Materials for Biological Applications*, 82, 330-335.

- HU, X. L., LIU, S., ZHOU, G. Y., HUANG, Y. B., XIE, Z. G. & JING, X. B. 2014. Electrospinning of polymeric nanofibers for drug delivery applications. *Journal of Controlled Release*, 185, 12-21.
- ICOGLU, H. I. & OGULATA, R. T. 2017. EFFECT OF AMBIENT PARAMETERS ON MORPHOLOGY OF ELECTROSPUN POLY (TRIMETHYLENE TEREPHTHALATE) (PTT) FIBERS. *Tekstil Ve Konfeksiyon*, 27, 215-223.
- ISBISTER, J. P. 2015. The three-pillar matrix of patient blood management. *State of the Art Presentations 33rd International Congress of the International Society of Blood Transfusion, in Conjunction with the 33rd Congress of the Ksbt and 2014 Congress of the Korean Hematology Societies, Vol 10, No S1, 10*, 286-294.
- JADBABAEI, S., KOLAHDOOZAN, M., NAEIMI, F. & EBADI-DEHAGHANI, H. 2021. Preparation and characterization of sodium alginate-PVA polymeric scaffolds by electrospinning method for skin tissue engineering applications. *Rsc Advances*, 11, 30674-30688.
- JAFARI, M., BANIASADI, H., REZVANPOUR, A. & LOTFI, M. 2021. Fabrication and characterisation of a wound dressing composed of polyvinyl alcohol and quince seed mucilage. *Journal of Wound Care*, 30, XIII-XIIX.
- JARAMILLO, S., MONTANE-MUNTANE, M., GAMBUS, P. L., CAPITAN, D., NAVARRO-RIPOLL, R. & BLASI, A. 2020. Perioperative blood loss: estimation of blood volume loss or haemoglobin mass loss? *Blood Transfusion*, 18, 20-29.
- JARBRINK, K., NI, G., SONNERGREN, H., SCHMIDTCHEN, A., PANG, C., BAJPAI, R. & CAR, J. 2016. Prevalence and incidence of chronic wounds and related complications: a protocol for a systematic review. *Systematic Reviews*, 5.
- JATOI, A. W., OGASAWARA, H., KIM, I. S. & NI, Q. Q. 2019. Polyvinyl alcohol nanofiber based three phase wound dressings for sustained wound healing applications. *Materials Letters*, 241, 168-171.
- JIA, Y. F., YANG, C. Y., CHEN, X. Y., XUE, W. Q., HUTCHINS-CRAWFORD, H. J., YU, Q. Q., TOPHAM, P. D. & WANG, L. G. 2021. A review on electrospun magnetic nanomaterials: methods, properties and applications. *Journal of Materials Chemistry C*, 9, 9042-9082.
- JIAN, S. J., ZHU, J., JIANG, S. H., CHEN, S. L., FANG, H., SONG, Y. H., DUAN, G. G., ZHANG, Y. F. & HOU, H. Q. 2018. Nanofibers with diameter below one nanometer from electrospinning. *Rsc Advances*, 8, 4794-4802.
- JIPA, I. M., STROESCU, M., STOICA-GUZUN, A., DOBRE, T., JINGA, S. & ZAHARESCU, T. 2012. Effect of gamma irradiation on biopolymer composite films of poly(vinyl alcohol) and bacterial cellulose. *Nuclear Instruments & Methods in Physics Research Section B-Beam Interactions with Materials and Atoms*, 278, 82-87.
- JOSEPH, J., PATEL, R. M., WENHAM, A. & SMITH, J. R. 2018. Biomedical applications of polyurethane materials and coatings. *Transactions of the Institute of Metal Finishing*, 96, 121-129.
- JPAC. 2020. *Information on ICS Equipment* [Online]. JPAC. Available: <Go to WoS>://WOS:000319335400053 [Accessed 04/02/20 2020].
- JUNG, J. & HAN, K. H. 2008. Lateral-driven continuous magnetophoretic separation of blood cells. *Applied Physics Letters*, 93.
- FRESENIUS KABI. 2020. *CATSmart: Procedures* [Online]. Available: <https://www.fresenius-kabi.com/in/products/catsmart> [Accessed April 16th 2020].
- KAILASA, S., REDDY, M. S. B., MAURYA, M. R., RANI, B. G., RAO, K. V. & SADASIVUNI, K. K. 2021. Electrospun Nanofibers: Materials, Synthesis Parameters, and Their Role in Sensing Applications. *Macromolecular Materials and Engineering*, 306.

- KALANTARI, K., AFIFI, A. M., JAHANGIRIAN, H. & WEBSTER, T. J. 2019. Biomedical applications of chitosan electrospun nanofibers as a green polymer - Review. *Carbohydrate Polymers*, 207, 588-600.
- KALOUS, T., HOLEC, P., JIRKOVEC, R., LUKAS, D. & CHVOJKA, J. 2021. Improved spinnability of PA 6 solutions using AC electrospinning. *Materials Letters*, 283.
- KAMOUN, E. A., CHEN, X., ELDIN, M. S. M. & KENAWY, E. R. S. 2015. Crosslinked poly(vinyl alcohol) hydrogels for wound dressing applications: A review of remarkably blended polymers. *Arabian Journal of Chemistry*, 8, 1-14.
- KANMAZ, D., TOPRAKCI, H. A. K., TOPRAKCI, O. & OLMEZ, H. 2018. Electrospun polylactic acid based nanofibers for biomedical applications. *Material Science Research India (Online)*, 15, 224-240.
- KESSICK, R., FENN, J. & TEPPER, G. 2004. The use of AC potentials in electro spraying and electrospinning processes. *Polymer*, 45, 2981-2984.
- KIM, G., CHO, Y. S. & KIM, W. D. 2006. Stability analysis for multi jets electrospinning process modified with a cylindrical electrode. *European Polymer Journal*, 42, 2031-2038.
- KIM, J. I., HWANG, T. I., AGUILAR, L. E., PARK, C. H. & KIM, C. S. 2016. A Controlled Design of Aligned and Random Nanofibers for 3D Bi-functionalized Nerve Conduits Fabricated via a Novel Electrospinning Set-up. *Scientific Reports*, 6.
- KIM, S. J., LEE, C. K. & KIM, S. I. 2005. Effect of ionic salts on the processing of poly(2acrylamido-2-methyl-1-propane sulfonic acid) nanofibers. *Journal of Applied Polymer Science*, 96, 1388-1393.
- KISHAN, A. P. & COSGRIFF-HERNANDEZ, E. M. 2017. Recent advancements in electrospinning design for tissue engineering applications: A review. *Journal of Biomedical Materials Research Part A*, 105, 2892-2905.
- KLEIN, A. A., BAILEY, C. R., CHARLTON, A. J., EVANS, E., GUCKIAN-FISHER, M., MCCROSSAN, R., NIMMO, A. F., PAYNE, S., SHREEVE, K., SMITH, J. & TORELLA, F. 2018. Association of Anaesthetists guidelines: cell salvage for peri-operative blood conservation 2018. *Anaesthesia*, 73, 1141-1150.
- KO, F. K. & YANG, H. J. 2008. Functional Nanofibre: enabling materials for the next generation SMART textiles. *Textile Bioengineering and Informatics Symposium Proceedings, Vols 1 and 2*, 1-12.
- KOCIS, L., POKORNY, P., LUKAS, D., MIKES, P., CHVOJKA, J., KOSTAKOVA, E., BERAN, J., BILEK, M., VALTERA, J., AMLER, E., BUZGO, M. & MICKOVA, A. 2018. *Method for production of polymeric nanofibers by spinning of solution or melt of polymer in electric field, and a linear formation from polymeric nanofibers prepared by this method*. 13824581.6.
- KONG, B. & MI, S. L. 2016. Electrospun Scaffolds for Corneal Tissue Engineering: A Review. *Materials*, 9.
- KOSKI, A., YIM, K. & SHIVKUMAR, S. 2004. Effect of molecular weight on fibrous PVA produced by electrospinning. *Materials Letters*, 58, 493-497.
- KUDO, K., ISHIDA, J., SYUU, G., SEKINE, Y. & IKEDA-FUKAZAWA, T. 2014. Structural changes of water in poly(vinyl alcohol) hydrogel during dehydration. *Journal of Chemical Physics*, 140.
- KUMAR, A. & HAN, S. S. 2017. PVA-based hydrogels for tissue engineering: A review. *International Journal of Polymeric Materials and Polymeric Biomaterials*, 66, 159-182.
- KUMAR, A. & SRIVASTAVA, A. 2010. Cell separation using cryogel-based affinity chromatography. *Nature Protocols*, 5, 1737-1747.

- KUMAR, N., ZAW, A. S., KANTHARAJANNA, S. B., KHOO, B. L., LIM, C. T. & THIERY, J. P. 2017. Metastatic efficiency of tumour cells can be impaired by intraoperative cell salvage process: truth or conjecture? *Transfus Med*, 27 Suppl 5, 327-334.
- KUMAR, R. G. & RAJAN, T. P. 2022. A Review on Electrospinning of Natural Bio Herbs Blended with Polyvinyl Alcohol Nanofibres for Biomedical Applications. *Journal of Natural Fibers*, 19, 11984-12003.
- KUMAR, R. K. & LYKKE, A. W. J. 1984. Cell-Separation - A Review. *Pathology*, 16, 53-62.
- LAI, J. H., WANG, C. & WANG, M. 2021. 3D printing in biomedical engineering: Processes, materials, and applications. *Applied Physics Reviews*, 8.
- LANNUTTI, J., RENEKER, D., MA, T., TOMASKO, D. & FARSON, D. F. 2007. Electrospinning for tissue engineering scaffolds. *Materials Science & Engineering C-Biomimetic and Supramolecular Systems*, 27, 504-509.
- LEE, H., PARK, B. & KIM, H. 2012. Crystallinity and Diameter Changes of Electrospun Fiber for Different Processing Conditions and Collection Areas. *Textile Science and Engineering*, 49.
- LEE, Y. S. & ARINZEH, T. L. 2011. Electrospun Nanofibrous Materials for Neural Tissue Engineering. *Polymers*, 3, 413-426.
- LEMURSKI, E. G., JAHANGIRIAN, H., DASHTI, M., KHAJEHALI, E., SHARAFINIA, S., RAFIEE-MOGHADDAM, R. & WEBSTER, T. J. 2021. Antimicrobial Double-Layer Wound Dressing Based on Chitosan/Polyvinyl Alcohol/Copper: In vitro and in vivo Assessment. *International Journal of Nanomedicine*, 16, 223-235.
- LI, A., HAN, Z. Z., LI, Z. Y., LI, J. F., LI, X. L. & ZHANG, Z. C. 2021a. A PTHrP-2 loaded adhesive cellulose acetate nanofiber mat as wound dressing accelerates wound healing. *Materials & Design*, 212.
- LI, H. H., CHEN, X., LU, W. P., WANG, J., XU, Y. S. & GUO, Y. C. 2021b. Application of Electrospinning in Antibacterial Field. *Nanomaterials*, 11.
- LIN, S. T., LIU, X. Y., LIU, J., YUK, H., LOH, H. C., PARADA, G. A., SETTENS, C., SONG, J., MASIC, A., MCKINLEY, G. H. & ZHAO, X. H. 2019. Anti-fatigue-fracture hydrogels. *Science Advances*, 5.
- LIN, W. M., CHEN, M., QU, T., LI, J. D. & MAN, Y. 2020. Three-dimensional electrospun nanofibrous scaffolds for bone tissue engineering. *Journal of Biomedical Materials Research Part B-Applied Biomaterials*, 108, 1311-1321.
- LIU, D. P., SHI, Q. Q., JIN, S., SHAO, Y. L. & HUANG, J. 2019a. Self-assembled core-shell structured organic nanofibers fabricated by single-nozzle electrospinning for highly sensitive ammonia sensors. *Infomat*, 1, 525-532.
- LIU, H. F., DING, X. L., ZHOU, G., LI, P., WEI, X. & FAN, Y. B. 2013. Electrospinning of Nanofibers for Tissue Engineering Applications. *Journal of Nanomaterials*, 2013.
- LIU, M. M., CAI, N., CHAN, V. & YU, F. Q. 2019b. Development and Applications of MOFs Derivative One-Dimensional Nanofibers via Electrospinning: A Mini-Review. *Nanomaterials*, 9.
- LIU, W. J., HUANG, C. & JIN, X. Y. 2015. Electrospinning of Grooved Polystyrene Fibers: Effect of Solvent Systems. *Nanoscale Research Letters*, 10.
- LIU, Y., HE, J. H. & YU, J. Y. 2008. Bubble-Electrospinning: A Novel Method for Making Nanofibers. International Symposium on Nonlinear Dynamics, Oct 2007 DongHua Univ, Shanghai, PEOPLES R CHINA.
- LIU, Y., LIU, L., WANG, Z., ZHENG, G. S., CHEN, Q. M. & LUO, E. 2018. Application of Electrospinning Strategy on Cartilage Tissue Engineering. *Current Stem Cell Research & Therapy*, 13, 526-532.

- LIUMBRUNO, G. M., VAGLIO, S., GRAZZINI, G., SPAHN, D. R. & BIANCOFIORE, G. 2015. Patient blood management: a fresh look at a fresh approach to blood transfusion. *Minerva Anestesiologica*, 81, 1127-1137.
- LUO, C. J., STOYANOV, S. D., STRIDE, E., PELAN, E. & EDIRISINGHE, M. 2012. Electrospinning versus fibre production methods: from specifics to technological convergence. *Chemical Society Reviews*, 41, 4708-4735.
- LURAGHI, A., PERI, F. & MORONI, L. 2021. Electrospinning for drug delivery applications: A review. *Journal of Controlled Release*, 334, 463-484.
- LYU, C. X., ZHAO, P., XIE, J., DONG, S. Y., LIU, J. W., RAO, C. C. & FU, J. Z. 2021. Electrospinning of Nanofibrous Membrane and Its Applications in Air Filtration: A Review. *Nanomaterials*, 11.
- MADALOSSO, H. B., MACHADO, R., HOTZA, D. & MARANGONI, C. 2021. Membrane Surface Modification by Electrospinning, Coating, and Plasma for Membrane Distillation Applications: A State-of-the-Art Review. *Advanced Engineering Materials*, 23.
- MAILLEY, D., HEBRAUD, A. & SCHLATTER, G. 2021. A Review on the Impact of Humidity during Electrospinning: From the Nanofiber Structure Engineering to the Applications. *Macromolecular Materials and Engineering*, 306.
- MANSUR, H. S., SADAHIRA, C. M., SOUZA, A. N. & MANSUR, A. A. P. 2008. FTIR spectroscopy characterization of poly (vinyl alcohol) hydrogel with different hydrolysis degree and chemically crosslinked with glutaraldehyde. *Materials Science & Engineering C-Biomimetic and Supramolecular Systems*, 28, 539-548.
- MARSHALL, J. R. & KING, M. R. 2016. Surgical intervention and circulating tumor cell count: a commentary. *Translational Cancer Research*, 5, S126-S128.
- MARTIN, R. C. G., WELLHAUSEN, S. R., MOEHLE, D. A., MARTIN, A. W. & MCMASTERS, K. M. 2005. Evaluation of intraoperative autotransfusion filtration for hepatectomy and pancreatectomy. *Annals of Surgical Oncology*, 12, 1017-1024.
- MATABOLA, K. P. & MOUTLOALI, R. M. 2013. The influence of electrospinning parameters on the morphology and diameter of poly(vinylidene fluoride) nanofibers- effect of sodium chloride. *Journal of Materials Science*, 48, 5475-5482.
- MCCLELLAN, P. & LANDIS, W. J. 2016. Recent Applications of Coaxial and Emulsion Electrospinning Methods in the Field of Tissue Engineering. *BioResearch Open Access*, 5, 212-227.
- MEGELSKI, S., STEPHENS, J. S., CHASE, D. B. & RABOLT, J. F. 2002. Micro- and nanostructured surface morphology on electrospun polymer fibers. *Macromolecules*, 35, 8456-8466.
- MEJIA, M. L., MONCADA, M. E., OSSA-OROZCO, C. P. & IEEE. 2021. Poly (vinyl alcohol)/Silk Fibroin/Ag NPs composite nanofibers for bone tissue engineering. 43rd Annual International Conference of the IEEE-Engineering-in-Medicine-and-Biology-Society (IEEE EMBC), Nov 01-05 2021 Electr Network. 1176-1180.
- MELVILLE, D., PAUL, F. & ROATH, S. 1975. Direct Magnetic Separation of Red-Cells from Whole-Blood. *Nature*, 255, 706-706.
- MENDELAAR, P. A. J., KRAAN, J., VAN, M., ZEUNE, L. L., TERSTAPPEN, L., OOMEN-DE HOOP, E., MARTENS, J. W. M. & SLEIJFER, S. 2021. Defining the dimensions of circulating tumor cells in a large series of breast, prostate, colon, and bladder cancer patients. *Molecular Oncology*, 15, 116-125.
- MENON, M., YUAN, Q., JIA, X., DOUGILL, A. J., HOON, S. R., THOMAS, A. D. & WILLIAMS, R. A. 2011. Assessment of physical and hydrological properties of biological soil crusts using X-ray microtomography and modeling. *Journal of Hydrology*, 397, 47-54.

- MENZIES, K. L. & JONES, L. 2010. The Impact of Contact Angle on the Biocompatibility of Biomaterials. *Optometry and Vision Science*, 87, 387-399.
- MERCANTE, L. A., SCAGION, V. P., MIGLIORINI, F. L., MATTOSO, L. H. C. & CORREA, D. S. 2017. Electrospinning-based (bio)sensors for food and agricultural applications: A review. *Trends in Analytical Chemistry*, 91, 91-103.
- MESZLÉNYI, G. & KÖRTVÉLYESSY, G. 1999. Direct determination of vinyl acetate content of ethylene-vinyl acetate copolymers in thick films by infrared spectroscopy. *Polymer Testing*, 18, 551-557.
- MIAO, J. J., MIYAUCHI, M., SIMMONS, T. J., DORDICK, J. S. & LINHARDT, R. J. 2010. Electrospinning of Nanomaterials and Applications in Electronic Components and Devices. *Journal of Nanoscience and Nanotechnology*, 10, 5507-5519.
- MIGONNEY, V. 2014. History of Biomaterials. *Biomaterials*.
- MILLER, C. H., PLATT, S. J., RICE, A. S., KELLY, F., SOUCIE, J. M. & HEMOPHILIA INHIBITOR RES STUDY, I. 2012. Validation of Nijmegen-Bethesda assay modifications to allow inhibitor measurement during replacement therapy and facilitate inhibitor surveillance. *Journal of Thrombosis and Haemostasis*, 10, 1055-1061.
- MILTENYI, S., MULLER, W., WEICHEL, W. & RADBRUCH, A. 1990. High-gradient magnetic cell-separation with MACS. *Cytometry*, 11, 231-238.
- MIRAFTAB, M., SAIFULLAH, A. N. & ÇAY, A. 2014. Physical stabilisation of electrospun poly(vinyl alcohol) nanofibres: comparative study on methanol and heat-based crosslinking. *Journal of Materials Science*, 50, 1943-1957.
- MIYAZONO, F., NATSUGOE, S., TAKAO, S., TOKUDA, K., KIJIMA, F., ARIDOME, K., HOKITA, S., BABA, M., EIZURU, Y. & AIKOU, T. 2001. Surgical maneuvers enhance molecular detection of circulating tumor cells during gastric cancer surgery. *Annals of Surgery*, 233, 189-194.
- MOHAMMADI, M. A., HOSSEINI, S. M. & YOUSEFI, M. 2020. Application of electrospinning technique in development of intelligent food packaging: A short review of recent trends. *Food Science & Nutrition*, 8, 4656-4665.
- MOHAMMADI, S., RAMAKRISHNA, S., LAURENT, S., SHOKRGOZAR, M. A., SEMNANI, D., SADEGHI, D., BONAKDAR, S. & AKBARI, M. 2019. Fabrication of Nanofibrous PVA/Alginate-Sulfate Substrates for Growth Factor Delivery. *Journal of Biomedical Materials Research Part A*, 107, 403-413.
- MOHR, F., PRZIBILLA, S., LEONHARDT, F., STEMBERGER, C., DREHER, S., MULLER, T. R., FRASSLE, S. P., SCHMIDT, G. P., KIENE, M. L., STADLER, H. & BUSCH, D. H. 2018. Efficient immunoaffinity chromatography of lymphocytes directly from whole blood. *Scientific Reports*, 8.
- MOLDAY, R. S., YEN, S. P. S. & REMBAUM, A. 1977. Application of Magnetic Microspheres in Labelling and Separation of Cells. *Nature*, 268, 437-438.
- MOLITCH-HOU, M., ZHANG, J. & JUNG, Y.-G. 2018. 1 - Overview of additive manufacturing process. *Additive Manufacturing*. Butterworth-Heinemann.
- MORGAN, E. F., UNNIKRISSANAN, G. U. & HUSSEIN, A. I. 2018. Bone Mechanical Properties in Healthy and Diseased States. *Annual Review of Biomedical Engineering*, Vol 20, 20, 119-143.
- MORIKAWA, K., VASHISTH, A., GRIMME, C. J., GREEN, M. J. & NARAGHI, M. 2019. Wire Melt Electrospinning of Thin Polymeric Fibers via Strong Electrostatic Field Gradients. *Macromolecular Materials and Engineering*, 304.
- MORITANI, T. & FUJIWARA, Y. 1977. C-13-NMR and H-1-NMR investigations of sequence distribution in vinyl alcohol vinyl acetate copolymers. *Macromolecules*, 10, 532-535.

- MORTIMER, C. J. & WRIGHT, C. J. 2017. The fabrication of iron oxide nanoparticle-nanofiber composites by electrospinning and their applications in tissue engineering. *Biotechnology Journal*, 12.
- MOTTAGHITALAB, F., FAROKHI, M., MOTTAGHITALAB, V., ZIABARI, M., DIVSALAR, A. & SHOKRGOZAR, M. A. 2011. Enhancement of neural cell lines proliferation using nano-structured chitosan/poly(vinyl alcohol) scaffolds conjugated with nerve growth factor. *Carbohydrate Polymers*, 86, 526-535.
- MULHOLLAND, E. J. 2020. Electrospun Biomaterials in the Treatment and Prevention of Scars in Skin Wound Healing. *Frontiers in Bioengineering and Biotechnology*, 8.
- MUNTEANU, B. S. & VASILE, C. 2021. Encapsulation of Natural Bioactive Compounds by Electrospinning-Applications in Food Storage and Safety. *Polymers*, 13.
- MUPPALANENI, S. 2013. Polyvinyl Alcohol in Medicine and Pharmacy: A Perspective. *Journal of Developing Drugs*, 02.
- MURTHA-LEMEKHOVA, A., FUCHS, J., RITSCHER, E. & HOFFMANN, K. 2022. Effect of Autotransfusion in HCC Surgery on Survival and Recurrence: A Systematic Review and Meta-Analysis. *Cancers*, 14.
- MUTHUKRISHNAN, L. 2022. An overview on electrospinning and its advancement toward hard and soft tissue engineering applications. *Colloid and Polymer Science*, 300, 875-901.
- NANGARE, S., JADHAV, N., GHAGARE, P. & MUTHANE, T. 2020. Pharmaceutical applications of electrospinning. *Annales Pharmaceutiques Francaises*, 78, 1-11.
- NARAYANAN, K. B., PARK, G. T. & HAN, S. S. 2020. Electrospun poly(vinyl alcohol)/reduced graphene oxide nanofibrous scaffolds for skin tissue engineering. *Colloids and Surfaces B-Biointerfaces*, 191.
- NATARAJ, D., REDDY, R. & REDDY, N. 2020. Crosslinking electrospun poly (vinyl) alcohol fibers with citric acid to impart aqueous stability for medical applications. *European Polymer Journal*, 124.
- NAWAZ, A. & HUMMELGEN, I. A. 2019. Poly(vinyl alcohol) gate dielectric in organic field-effect transistors. *Journal of Materials Science-Materials in Electronics*, 30, 5299-5326.
- NELSON, T., KEITH, J., LI, B.-B., STOCUM, D. & LI, J. 2012. Electrospun composite polycaprolactone scaffolds for optimized tissue regeneration. *Proceedings of the Institution of Mechanical Engineers, Part N: Journal of Nanoengineering and Nanosystems*, 226, 111-121.
- NGUYEN, L. T. B., NGUYEN, T. H., HUYNH, C. K., LEE, B. T. & YE, H. 2020. Composite Nano-fiber Mats Consisting of Biphasic Calcium Phosphate Loaded Polyvinyl Alcohol-Gelatin for Bone Tissue Engineering. 7th International Conference on the Development of Biomedical Engineering, Jun 27-29 2018 Ho Chi Minh City, VIETNAM. 301-305.
- NGUYEN, T. D. & LEE, J. S. 2022. Electrospinning-Based Carbon Nanofibers for Energy and Sensor Applications. *Applied Sciences-Basel*, 12.
- NIAZI, S. K. 2016. *Disposable bioprocessing systems*, CRC press.
- NIU, H. T. & LIN, T. 2012. Fiber Generators in Needleless Electrospinning. *Journal of Nanomaterials*, 2012.
- OKADA, Y., KAWANOBE, W., HAYAKAWA, N., TSUBOKURA, S., CHUJO, R., FUJIMATSU, H., TAKIZAWA, T. & HIRAI, T. 2011. Whitening of polyvinyl alcohol used as restoration material for Shohekiga. *Polymer Journal*, 43, 74-77.
- OLI, S. 2022. *Metal plate fused to 2,000-year-old Peruvian warrior's skull proof of early surgery* [Online]. National Post. Available: <https://nationalpost.com/news/world/metal-plate-fused->
- W. J. A. Homer, PhD Thesis, Aston University, 2023

[on-2000-year-old-peruvian-warriors-skull-is-earliest-evidence-of-surgery](#) [Accessed 20th March 2023].

- ORR, V., ZHONG, L., MOO-YOUNG, M. & CHOU, C. P. 2013. Recent advances in bioprocessing application of membrane chromatography. *Biotechnol Adv*, 31, 450-65.
- OSEI-BIMPONG, A., MCLEAN, R., BHONDA, E. & LEWIS, S. M. 2012. The use of the white cell count and haemoglobin in combination as an effective screen to predict the normality of the full blood count. *International Journal of Laboratory Hematology*, 34, 91-97.
- OWEN, C. S. 1978. High gradient magnetic separation of erythrocytes. *Biophysical journal*, 22, 171-178.
- PANT, B., PARK, M. & PARK, S. J. 2019. Drug Delivery Applications of Core-Sheath Nanofibers Prepared by Coaxial Electrospinning: A Review. *Pharmaceutics*, 11.
- PARK, J.-C., ITO, T., KIM, K.-O., KIM, K.-W., KIM, B.-S., KHIL, M.-S., KIM, H.-Y. & KIM, I.-S. 2010. Electrospun poly(vinyl alcohol) nanofibers: effects of degree of hydrolysis and enhanced water stability. *Polymer Journal*, 42, 273-276.
- PARK, J. Y. & LEE, I. H. 2010. Relative Humidity Effect on the Preparation of Porous Electrospun Polystyrene Fibers. *Journal of Nanoscience and Nanotechnology*, 10, 3473-3477.
- PARTHENIADIS, I., NIKOLAKAKIS, I., LAIDMAE, I. & HEINAMAKI, J. 2020. A Mini-Review: Needleless Electrospinning of Nanofibers for Pharmaceutical and Biomedical Applications. *Processes*, 8.
- PATEL, P. R. & GUNDLOORI, R. V. N. 2023. A review on electrospun nanofibers for multiple biomedical applications. *Polymers for Advanced Technologies*, 34, 44-63.
- PATHAN, S. G., FITZGERALD, L. M., ALI, S. M., DAMRAUER, S. M., BIDE, M. J., NELSON, D. W., FERRAN, C., PHANEUF, T. M. & PHANEUF, M. D. 2015. Cytotoxicity associated with electrospun polyvinyl alcohol. *Journal of Biomedical Materials Research Part B-Applied Biomaterials*, 103, 1652-1662.
- PAULING, L. & CORYELL, C. D. 1936. The magnetic properties and structure of the Hhemochromogens and related substances. *Proceedings of the National Academy of Sciences of the United States of America*, 22, 159-163.
- PELIPENKO, J., KRISTL, J., JANKOVIC, B., BAUMGARTNER, S. & KOCBEK, P. 2013. The impact of relative humidity during electrospinning on the morphology and mechanical properties of nanofibers. *International Journal of Pharmaceutics*, 456, 125-134.
- PENG, Z. & KONG, L. X. 2007. A thermal degradation mechanism of polyvinyl alcohol/silica nanocomposites. *Polymer Degradation and Stability*, 92, 1061-1071.
- PEPPAS, N. A. 1975. Turbidimetric studies of aqueous poly(vinyl alcohol) solutions. *Die Makromolekulare Chemie*, 176, 3433-3440.
- PEREAO, O. K., BODE-ALUKO, C., NDAYAMBAJE, G., FATOBA, O. & PETRIK, L. F. 2017. Electrospinning: Polymer Nanofibre Adsorbent Applications for Metal Ion Removal. *Journal of Polymers and the Environment*, 25, 1175-1189.
- PERSEGHIN, P., VIGANO, M., ROCCO, G., DELLAPONA, C., BUSCEMI, A. & RIZZI, A. 1997. Effectiveness of leukocyte filters in reducing tumor cell contamination after intraoperative blood salvage in lung cancer patients. *Vox Sanguinis*, 72, 221-224.
- PETROVA, N. V., EVTUSHENKO, A. M., CHIKHACHEVA, I. P., ZUBOV, V. P. & KUBRAKOVA, I. V. 2005. Effect of microwave irradiation on the cross-linking of polyvinyl alcohol. *Russian Journal of Applied Chemistry*, 78, 1158-1161.



- PHAM, Q. P., SHARMA, U. & MIKOS, A. G. 2006. Electrospinning of polymeric nanofibers for tissue engineering applications: A review. *Tissue Engineering*, 12, 1197-1211.
- PILLAI, M. M., GOPINATHAN, J., INDUMATHI, B., MANJOOSHA, Y. R., SAHANAND, K. S., RAI, B. K. D., SELVAKUMAR, R. & BHATTACHARYYA, A. 2016. Silk-PVA Hybrid Nanofibrous Scaffolds for Enhanced Primary Human Meniscal Cell Proliferation. *Journal of Membrane Biology*, 249, 813-822.
- PINA, S., RIBEIRO, V. P., MARQUES, C. F., MAIA, F. R., SILVA, T. H., REIS, R. L. & OLIVEIRA, J. M. 2019. Scaffolding Strategies for Tissue Engineering and Regenerative Medicine Applications. *Materials*, 12.
- PING, Z. H., NGUYEN, Q. T., CHEN, S. M., ZHOU, J. Q. & DING, Y. D. 2001. States of water in different hydrophilic polymers - DSC and FTIR studies. *Polymer*, 42, 8461-8467.
- PLIEVA, F. M., KARLSSON, M., AGUILAR, M. R., GOMEZ, D., MIKHALOVSKY, S., GALAEV, I. Y. & MATTIASSON, B. 2006. Pore structure of macroporous monolithic cryogels prepared from poly(vinyl alcohol). *Journal of Applied Polymer Science*, 100, 1057-1066.
- POLI, M., CAMARGO, A., VILLA, L., MOURA, R., COLELLA, R. & DEHEINZELIN, D. 2008. Intraoperative autologous blood recovery in prostate cancer surgery: in vivo validation using a tumour marker. *Vox Sanguinis*, 95, 308-312.
- RAGHUPRASAD, P. K. 1982. A Rapid Simple Method of Basophil Purification By Density Centrifugation On Percoll. *Journal of Immunology*, 129, 2128-2133.
- RAHMATI, M., MILLS, D. K., URBANSKA, A. M., SAEB, M. R., VENUGOPAL, J. R., RAMAKRISHNA, S. & MOZAFARI, M. 2021. Electrospinning for tissue engineering applications. *Progress in Materials Science*, 117.
- RAJASEKARAN, R. B., PALMER, A. J. R., WHITWELL, D., COSKER, T. D. A., PIGOTT, D., ZSOLT, O., BOOTH, R., GIBBONS, M., CARR, A. & COLLABORATORS 2021. The role of intraoperative cell salvage for musculoskeletal sarcoma surgery. *Journal of Bone Oncology*, 30.
- RAMAKRISHNA, S., FUJIHARA, K., TEO, E., TEIK-CHENG, L. & MA, Z. 2005. *An Introduction To Electrospinning And Nanofibers*.
- RAMPLING, R. W. 1999. Rouleaux formation; its causes and consequences. Conference on Cardiovascular Flow Modelling and Measurement with Application to Clinical Medicine, Sep 1998 Univ Salford, Salford, England. 183-193.
- RASOULI, R., BARHOUM, A., BECHELANY, M. & DUFRESNE, A. 2019. Nanofibers for Biomedical and Healthcare Applications. *Macromolecular Bioscience*, 19.
- RAVANDI, S. A. H., SADRJAHANI, M., VALIPOURI, A., DABIRIAN, F. & KO, F. K. 2022. Recently developed electrospinning methods: a review. *Textile Research Journal*.
- RAY, S. S., CHEN, S. S., LI, C. W., NGUYEN, N. C. & NGUYEN, H. T. 2016. A comprehensive review: electrospinning technique for fabrication and surface modification of membranes for water treatment application. *Rsc Advances*, 6, 85495-85514.
- REISE, M., KRANZ, S., GUELLMAR, A., WYRWA, R., ROSENBAUM, T., WEISSER, J., JURKE, A., SCHNABELRAUCH, M., HEYDER, M., WATTS, D. C. & SIGUSCH, B. W. 2023. Coaxial electrospun nanofibers as drug delivery system for local treatment of periodontitis. *Dental Materials*, 39, 132-139.
- REMBE, J. D., BÖHM, J. K., FROMM-DORNIEDEN, C., SCHÄFER, N., MAEGELE, M., FRÖHLICH, M. & STUERMER, E. K. 2015. Comparison of hemostatic dressings for superficial wounds using a new spectrophotometric coagulation assay. *Journal of Translational Medicine*, 13.

- REPANAS, A., ANDRIOPOULOU, S. & GLASMACHER, B. 2016. The significance of electrospinning as a method to create fibrous scaffolds for biomedical engineering and drug delivery applications. *Journal of Drug Delivery Science and Technology*, 31, 137-146.
- GRAND VIEW RESEARCH. 2022. *Biomaterials Market Size, Share & Trends Analysis Report By Product (Natural, Metallic, Polymer), By Application (Cardiovascular, Orthopedics, Plastic Surgery), By Region, And Segment Forecasts, 2022 - 2030* [Online]. Available: <https://www.grandviewresearch.com/industry-analysis/biomaterials-industry> [Accessed 20th March 2023].
- STRAITS RESEARCH. 2021. *Nanofibers Market Share, Demand, Growth Forecast to 2030* [Online]. Available: <https://straitsresearch.com/report/nanofibers-market> [Accessed 17th March 2023].
- RESTREPO, I., MEDINA, C., MERUANE, V., AKBARI-FAKHRABADI, A., FLORES, P. & RODRIGUEZ-LLAMAZARES, S. 2018. The effect of molecular weight and hydrolysis degree of poly(vinyl alcohol)(PVA) on the thermal and mechanical properties of poly(lactic acid)/PVA blends. *Polimeros-Ciencia E Tecnologia*, 28, 169-177.
- REZAEI, A., NASIRPOUR, A. & FATHI, M. 2015. Application of Cellulosic Nanofibers in Food Science Using Electrospinning and Its Potential Risk. *Comprehensive Reviews in Food Science and Food Safety*, 14, 269-284.
- ROY, S., KUDDANNAYA, S., DAS, T., LEE, H. Y., LIM, J., HU, X., YOONA, Y. C. & KIM, J. 2017. A novel approach for fabricating highly tunable and fluffy bioinspired 3D poly(vinyl alcohol) (PVA) fiber scaffolds. *Nanoscale*, 9, 7081-7093.
- SAKINA, R. & ALI, M. 2014. An Appraisal of the Efficacy and Effectiveness of Nanoscaffolds Developed by Different Techniques for Bone Tissue Engineering Applications: Electrospinning A Paradigm Shift. *Advances in Polymer Technology*, 33.
- SALAZAR-BRANN, S. A., PATINO-HERRERA, R., NAVARRETE-DAMIAN, J. & LOUVIER-HERNANDEZ, J. F. 2021. Electrospinning of chitosan from different acid solutions. *Aims Bioengineering*, 8, 112-129.
- SAMBUDI, N. S., SATHYAMURTHY, M., LEE, G. M. & PARK, S. B. 2015. Electrospun chitosan/poly(vinyl alcohol) reinforced with CaCO<sub>3</sub> nanoparticles with enhanced mechanical properties and biocompatibility for cartilage tissue engineering. *Composites Science and Technology*, 106, 76-84.
- SAPALIDIS, A. A. 2020. Porous Polyvinyl Alcohol Membranes: Preparation Methods and Applications. *Symmetry-Basel*, 12.
- SARBATLY, R., KRISHNAIAH, D. & KAMIN, Z. 2016. A review of polymer nanofibres by electrospinning and their application in oil-water separation for cleaning up marine oil spills. *Marine Pollution Bulletin*, 106, 8-16.
- SARKAR, S., DEEVI, S. & TEPPER, G. 2007. Biased AC electrospinning of aligned polymer nanofibers. *Macromolecular Rapid Communications*, 28, 1034-1039.
- SATOH, K. 2021. Poly(vinyl alcohol) (PVA). *Encyclopedia of Polymeric Nanomaterials*. Berlin, Heidelberg: Springer Berlin Heidelberg.
- SAXENA, S. K. 2003. Polyvinyl Alcohol (PVA).
- SAYED, M. M., MOUSA, H. M., EL-AASSAR, M. R., EL-DEEB, N. M., GHAZALY, N. M., DEWIDAR, M. M. & ABDAL-HAY, A. 2019. Enhancing mechanical and biodegradation properties of polyvinyl alcohol/silk fibroin nanofibers composite patches for Cardiac Tissue Engineering. *Materials Letters*, 255.

- SCHIFFMAN, J. D. & DIEP, E. 2023. Electrospinning Living Bacteria: A Review of Applications from Agriculture to Health Care. *Acs Applied Bio Materials*.
- SCHROEDER, J. T. & BIENEMAN, A. P. 2016. Isolation of human basophils. *Current protocols in immunology*, 112, 7.24.1-7.24.8.
- SEAL, S. H. 1964. A sieve for the isolation of cancer cells and other large cells from the blood. *Cancer*, 17, 637-642.
- SEN, S., BAL, T. & RAJORA, A. D. 2022. Green nanofiber mat from HLM-PVA-Pectin (Hibiscus leaves mucilage-polyvinyl alcohol-pectin) polymeric blend using electrospinning technique as a novel material in wound-healing process. *Applied Nanoscience*, 12, 237-250.
- SERIO, F., DA CRUZ, A. F., CHANDRA, A., NOBILE, C., ROSSI, G. R., D'AMONE, E., GIGLI, G., DEL MERCATO, L. L. & DE OLIVEIRA, C. C. 2021. Electrospun polyvinyl-alcohol/gum arabic nanofibers: Biomimetic platform for in vitro cell growth and cancer nanomedicine delivery. *International Journal of Biological Macromolecules*, 188, 764-773.
- NHS. 2018. NHS Blood and Transplant annual report and accounts: 2017 to 2018. *In: NHSBT (ed.)*. UK: Her Majesty's Stationery Office.
- NHS. 2019. NHS Blood and Transplant annual report and accounts: 2018 to 2019. *In: NHSBT (ed.)*. UK: Her Majesty's Stationery Office.
- NHS. 2020. NHS Blood and Transplant annual report and accounts: 2019 to 2020. *In: NHSBT (ed.)*. UK: Her Majesty's Stationery Office.
- SHABANNEJAD, M., NOURBAKHS, M. S., SALATI, A. & BAHRAMI, Z. 2020. Fabrication and Characterization of Electrospun Scaffold Based on Polycaprolactone-Aloe vera and Polyvinyl Alcohol for Skin Tissue Engineering. *Fibers and Polymers*, 21, 1694-1703.
- SHAHRUBUDIN, N., LEE, T. C. & RAMLAN, R. 2019. An Overview on 3D Printing Technology: Technological, Materials, and Applications. *2nd International Conference on Sustainable Materials Processing and Manufacturing (Smpm 2019)*, 35, 1286-1296.
- SHANDER, A., HOFMANN, A., ISBISTER, J. & VAN AKEN, H. 2013. Patient blood management – The new frontier. *Best Practice & Research Clinical Anaesthesiology*, 27, 5-10.
- SHANKHWAR, N., KUMAR, M., MANDAL, B. B., ROBI, P. S. & SRINIVASAN, A. 2016. Electrospun polyvinyl alcohol-polyvinyl pyrrolidone nanofibrous membranes for interactive wound dressing application. *Journal of Biomaterials Science-Polymer Edition*, 27, 247-262.
- SHULMAN, G. 2000. Quality of processed blood for autotransfusion. *The Journal of extra-corporeal technology*, 32, 11-9.
- SIKORSKI, R. A., RIZKALLA, N. A., YANG, W. W. & FRANK, S. M. 2017. Autologous blood salvage in the era of patient blood management. *Vox Sanguinis*, 112, 499-510.
- SIVAN, M., MADHESWARAN, D., VALTERA, J., KOSTAKOVA, E. K. & LUKAS, D. 2022. Alternating current electrospinning: The impacts of various high-voltage signal shapes and frequencies on the spinnability and productivity of polycaprolactone nanofibers. *Materials & Design*, 213.
- SORINGROUP 2013. The eXtraordinarily innovative, intuitive and powerful ATS system.
- SOUCEK, J., VALTERA, J., KALOUS, T. & LTD, T. 2018. ELECTRODE FOR CONTINUOUS PRODUCTION OF COMPOSITE NANOFIBER MATERIAL USING AC-ELECTROSPINNING METHOD. *9th International Conference on Nanomaterials - Research & Application (Nanocon 2017)*, 378-383.
- SPAHN, D. R., SHANDER, A. & HOFMANN, A. 2013. The chiasm: Transfusion practice versus patient blood management. *Best Practice & Research Clinical Anaesthesiology*, 27, 37-42.

- SPURNY, K. R. 1996. Nikolai Albertowich Fuchs (1895-1982) aerosol scientist and humanist - Memories on the occasion of his 100th birthday. *Journal of Aerosol Science*, 27, 833-852.
- SRISUK, P., BISHI, D. K., BERTI, F. V., SILVA, C. J. R., KWON, I., CORRELO, V. M. & REIS, R. L. 2018. Eumelanin Nanoparticle-Incorporated Polyvinyl Alcohol Nanofibrous Composite as an Electroconductive Scaffold for Skeletal Muscle Tissue Engineering. *Acs Applied Bio Materials*, 1, 1893-1905.
- STEMCELL TECHNOLOGIES 2017. Frequencies of Cell Types in Human Peripheral Blood. 4 ed. Canada.
- SU, Z. Q., DING, J. W. & WEI, G. 2014. Electrospinning: a facile technique for fabricating polymeric nanofibers doped with carbon nanotubes and metallic nanoparticles for sensor applications. *Rsc Advances*, 4, 52598-52610.
- SUBRAHMANYA, T. M., BIN ARSHAD, A., LIN, P. T., WIDAKDO, J., MAKARI, H. K., AUSTRIA, H. F. M., HU, C. C., LAI, J. Y. & HUNG, W. S. 2021. A review of recent progress in polymeric electrospun nanofiber membranes in addressing safe water global issues. *Rsc Advances*, 11, 9638-9663.
- SUN, F. B., SUN, X. D., WANG, H. T., LI, C. X., ZHAO, Y., TIAN, J. J. & LIN, Y. H. 2022. Application of 3D-Printed, PLGA-Based Scaffolds in Bone Tissue Engineering. *International Journal of Molecular Sciences*, 23.
- SUPAPHOL, P. & CHUANGCHOTE, S. 2008. On the electrospinning of poly(vinyl alcohol) nanofiber mats: A revisit. *Journal of Applied Polymer Science*, 108, 969-978.
- SUPAPHOL, P., SUWANTONG, O., SANGSANOH, P., SRINIVASAN, S., JAYAKUMAR, R. & NAIR, S. V. 2012. Electrospinning of Biocompatible Polymers and Their Potentials in Biomedical Applications. In: JAYAKUMAR, R. & NAIR, S. V. (eds.) *Biomedical Applications of Polymeric Nanofibers*.
- SURENDRAN, G. & SHERJE, A. P. 2022. Cellulose nanofibers and composites: An insight into basics and biomedical applications. *Journal of Drug Delivery Science and Technology*, 75.
- SUTERMASTER, B. A. & DARLING, E. M. 2019. Considerations for high-yield, high-throughput cell enrichment: fluorescence versus magnetic sorting. *Scientific Reports*, 9.
- TAEPAIBOON, P., RUNGSARDTHONG, U. & SUPAPHOL, P. 2006. Drug-loaded electrospun mats of poly(vinyl alcohol) fibres and their release characteristics of four model drugs. *Nanotechnology*, 17, 2317-2329.
- TAKAYASU, M., KELLAND, D. R. & MINERVINI, J. V. 2000. Continuous magnetic separation of blood components from whole blood. *Ieee Transactions on Applied Superconductivity*, 10, 927-930.
- TAN, G. Z. & ZHOU, Y. G. 2020. Electrospinning of biomimetic fibrous scaffolds for tissue engineering: a review. *International Journal of Polymeric Materials and Polymeric Biomaterials*, 69, 947-960.
- TAN, S. M., TEOH, X. Y., LE HWANG, J., KHONG, Z. P., SEJARE, R., ALMASHHADANI, A. Q., ABOU ASSI, R. & CHAN, S. Y. 2022. Electrospinning and its potential in fabricating pharmaceutical dosage form. *Journal of Drug Delivery Science and Technology*, 76.
- TAN, Z. K., WANG, H. J., GAO, X. K., LIU, T. & TAN, Y. J. 2016. Composite vascular grafts with high cell infiltration by co-electrospinning. *Materials Science & Engineering C-Materials for Biological Applications*, 67, 369-377.
- TANG, C., SAQUING, C. D., HARDING, J. R. & KHAN, S. A. 2010. In Situ Cross-Linking of Electrospun Poly(vinyl alcohol) Nanofibers. *Macromolecules*, 43, 630-637.
- TANG, C. M., TIAN, Y. H. & HSU, S. H. 2015. Poly(vinyl alcohol) Nanocomposites Reinforced with Bamboo Charcoal Nanoparticles: Mineralization Behavior and Characterization. *Materials*, 8, 4895-4911.

- TAYLOR, G. I. 1964. Disintegration of water drops in an electric field. *Proceedings of the Royal Society of London. Series A. Mathematical and Physical Sciences*, 280, 383-397.
- TEIXEIRA, M. A., AMORIM, M. T. P. & FELGUEIRAS, H. P. 2020. Poly(Vinyl Alcohol)-Based Nanofibrous Electrospun Scaffolds for Tissue Engineering Applications. *Polymers*, 12.
- THOMAS, L. V. & NAIR, P. D. 2019. An electrospun citric acid modified polyvinyl alcohol scaffold for vascular tissue engineering. *Journal of Bioactive and Compatible Polymers*, 34, 263-279.
- THOMSON, L., MCDOWALL, D., MARSHALL, L., MARSHALL, O., NG, H., HOMER, W. J. A., GHOSH, D., LIU, W. L., SQUIRES, A. M., THEODOSIOU, E., TOPHAM, P. D., SERPELL, L. C., POOLE, R. J., SEDDON, A. & ADAMS, D. J. 2022. Transferring Micellar Changes to Bulk Properties via Tunable Self-Assembly and Hierarchical Ordering. *Acs Nano*, 16, 20497-20509.
- TOMAIUOLO, G. 2014. Biomechanical properties of red blood cells in health and disease towards microfluidics. *Biomicrofluidics*, 8.
- TOMLINSON, M. J., TOMLINSON, S., YANG, X. B. & KIRKHAM, J. 2013. Cell separation: Terminology and practical considerations. *Journal of tissue engineering*, 4.
- TOPUZ, F. & UYAR, T. 2019. Electrospinning of Cyclodextrin Functional Nanofibers for Drug Delivery Applications. *Pharmaceutics*, 11.
- TORRES-MARTINEZ, E. J., BRAVO, J. M. C., MEDINA, A. S., GONZALEZ, G. L. P. & GOMEZ, L. J. V. 2018. A Summary of Electrospun Nanofibers as Drug Delivery System: Drugs Loaded and Biopolymers Used as Matrices. *Current Drug Delivery*, 15, 1360-1374.
- TRETINNIKOV, O. N. & ZAGORSKAYA, S. A. 2012. Determination of the degree of crystallinity of poly(vinyl alcohol) by FT-IR spectroscopy. *Journal of Applied Spectroscopy*, 79, 521-526.
- TRUDICOVA, M., ZAHRAKKA, J., SEDLACEK, P., PEKAR, M. & LTD, T. 2021. CONTROLLING THE INTERNAL MICROSTRUCTURE AND PROPERTIES OF PHYSICALLY CROSS-LINKED PVA HYDROGELS BY THE RATE OF FREEZING. *12th International Conference on Nanomaterials - Research & Application (Nanocon 2020)*, 547-552.
- TUCKER, N., STANGER, J. J., STAIGER, M. P., RAZZAQ, H. & HOFMAN, K. 2012. The history of the science and technology of electrospinning from 1600 to 1995. *Journal of Engineered Fibers and Fabrics*, 7, 63-73.
- URA, D. P. & STACHEWICZ, U. 2022. The Significance of Electrical Polarity in Electrospinning: A Nanoscale Approach for the Enhancement of the Polymer Fibers' Properties. *Macromolecular Materials and Engineering*, 307.
- VAMVAKAS, E. C. & BLAJCHMAN, M. A. 2009. Transfusion-related mortality: the ongoing risks of allogeneic blood transfusion and the available strategies for their prevention. *Blood*, 113, 3406-3417.
- VAN DER BRUGGEN, B. & LUIS, P. 2018. Chapter 2 - Microfiltration, ultrafiltration, nanofiltration, reverse osmosis, and forward osmosis. *Fundamental Modelling of Membrane Systems*. Elsevier.
- VANDERVELDEN, G. & BEULEN, J. 1982. 300-MHz H-1-NMR and 25-MHz C-13 NMR investigations of sequence distributions in vinyl alcohol cinyl-avetate copolymers. *Macromolecules*, 15, 1071-1075.
- VASHISTH, P. & PRUTHI, V. 2016. Synthesis and characterization of crosslinked gellan/PVA nanofibers for tissue engineering application. *Materials Science & Engineering C-Materials for Biological Applications*, 67, 304-312.

- VASS, P., SZAB, E., DOMOKOS, A., HIRSCH, E., GALATA, D., FARKAS, B., DEMUTH, B., ANDERSEN, S. K., VIGH, T., VERRECK, G., MAROSI, G. & NAGY, Z. K. 2020. Scale-up of electrospinning technology: Applications in the pharmaceutical industry. *Wiley Interdisciplinary Reviews-Nanomedicine and Nanobiotechnology*, 12.
- VAZQUEZ, G., ALVAREZ, E. & NAVAZA, J. M. 1995. Surface-tension of alcohol plus water from 20-degrees-C to 50-degrees-C. *Journal of Chemical and Engineering Data*, 40, 611-614.
- VEERAMUTHU, L., VENKATESAN, M., LIANG, F. C., BENAS, J. S., CHO, C. J., CHEN, C. W., ZHOU, Y., LEE, R. H. & KUO, C. C. 2020. Conjugated Copolymers through Electrospinning Synthetic Strategies and Their Versatile Applications in Sensing Environmental Toxicants, pH, Temperature, and Humidity. *Polymers*, 12.
- VELLAYAPPAN, M. V., VENUGOPAL, J. R., RAMAKRISHNA, S., RAY, S., ISMAIL, A. F., MANDAL, M., MANIKANDAN, A., SEAL, S. & JAGANATHAN, S. K. 2016. Electrospinning applications from diagnosis to treatment of diabetes. *Rsc Advances*, 6, 83638-83655.
- WADE, R. J. & BURDICK, J. A. 2014. Advances in nanofibrous scaffolds for biomedical applications: From electrospinning to self-assembly. *Nano Today*, 9, 722-742.
- WAHYUDIONO, MURAKAMI, K., MACHMUDAH, S., SASAKI, M. & GOTO, M. 2012. Production of nanofibers by electrospinning under pressurized CO<sub>2</sub>. *High Pressure Research*, 32, 54-59.
- WALDROP, K., WYCISK, R. & PINTAURO, P. N. 2020. Application of electrospinning for the fabrication of proton -exchange membrane fuel cell electrodes. *Current Opinion in Electrochemistry*, 21, 257-264.
- WANG, J. F., XU, H. J., HUO, Y. P., WANG, Y. T. & DONG, M. D. 2020a. Progress of electrospray and electrospinning in energy applications. *Nanotechnology*, 31.
- WANG, L., YANG, G. R., PENG, S. J., WANG, J. N., YAN, W. & RAMAKRISHNA, S. 2020b. One-dimensional nanomaterials toward electrochemical sodium-ion storage applications via electrospinning. *Energy Storage Materials*, 25, 443-476.
- WANG, L., ZHANG, G. Q., HE, X. H., CUI, Y. D., LASHARI, N. U. R., GUO, D. G. & ZHENG, J. 2022a. In vitro biocompatibility and mechanical properties of bone adhesive tape composite based on poly(butyl fumarate)/poly(propylene fumarate)-diacrylate networks. *Journal of the Mechanical Behavior of Biomedical Materials*, 126.
- WANG, M. H., BAI, J. Z., SHAO, K., TANG, W. W., ZHAO, X. L., LIN, D. H., HUANG, S., CHEN, C., DING, Z. & YE, J. Y. 2021. Poly(vinyl alcohol) Hydrogels: The Old and New Functional Materials. *International Journal of Polymer Science*, 2021.
- WANG, S. X., YAP, C. C., HE, J. T., CHEN, C., WONG, S. Y. & LI, X. 2016. Electrospinning: a facile technique for fabricating functional nanofibers for environmental applications. *Nanotechnology Reviews*, 5, 51-73.
- WANG, Y. M., LU, S. M., ZHENG, J. Y. & LIANG, L. G. 2022b. Advances in Latest Application Status, Challenges, and Future Development Direction of Electrospinning Technology in the Biomedical. *Journal of Nanomaterials*, 2022.
- WARD, J. M., CHERIAN, S., LINDEN, M. A., TREUTING, P. M., DINTZIS, S. M. & MONTINE, K. S. 2018. 19 - Hematopoietic and Lymphoid Tissues. *Comparative Anatomy and Histology (Second Edition)*. San Diego: Academic Press.
- WATERS, J. H., YAZER, M., CHEN, Y. F. & KLOKE, J. 2012. Blood salvage and cancer surgery: a meta-analysis of available studies. *Transfusion*, 52, 2167-2173.

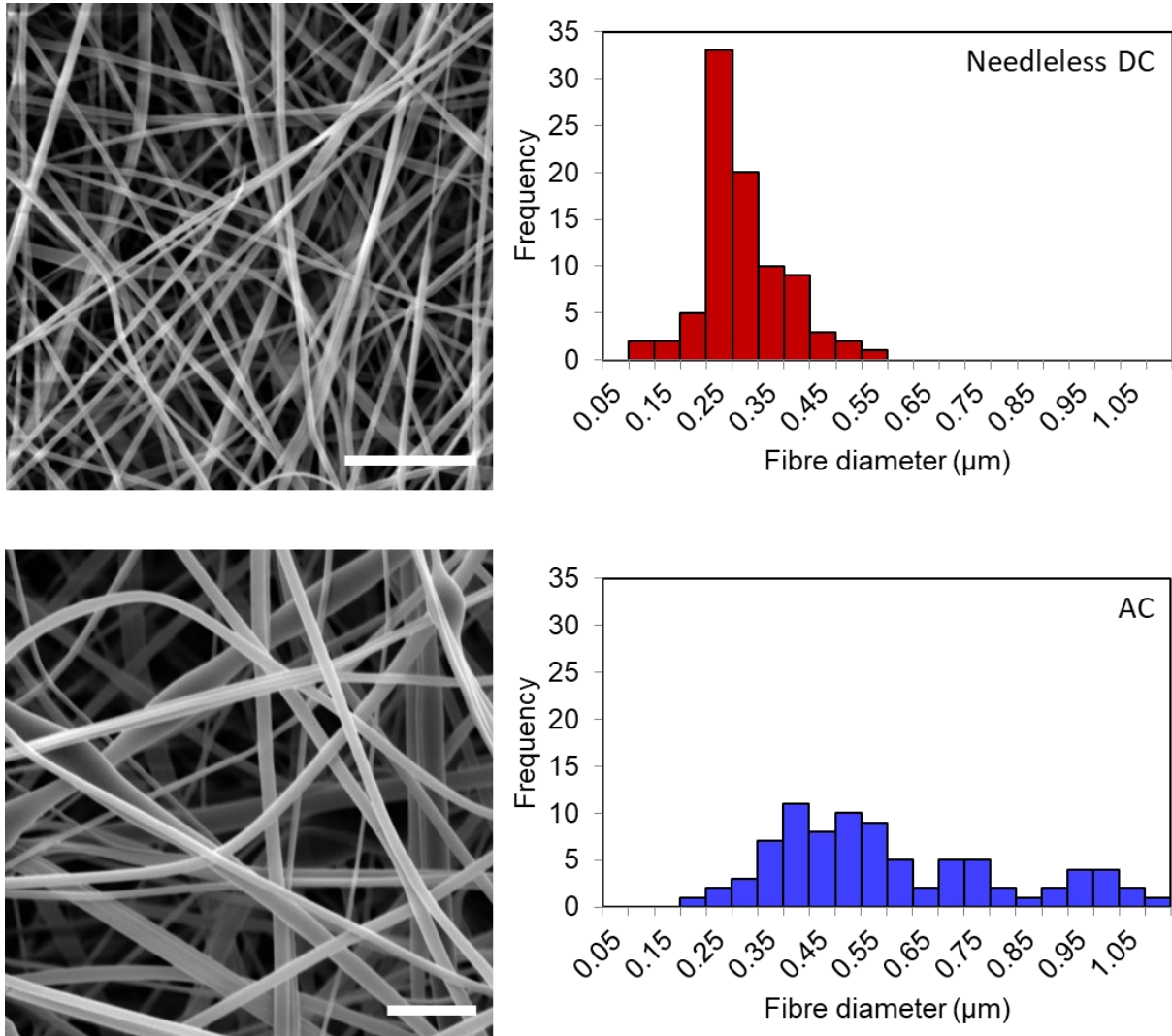
- WELLS, R. E., GAWRONSKI, T. H., COX, P. J. & PERERA, R. D. 1964. Influence of fibrinogen on flow properties of erythrocyte suspensions. *American Journal of Physiology-Legacy Content*, 207, 1035-1040.
- WIJANARKO, T. A. W., KUSUMAATMAJA, A., CHOTIMAH, ROTO & TRIYANA, K. 2016. Effect of heat treatment on morphology and crystallinity of electrospun Poly(vinyl alcohol) nanofibers.
- WILEY, V. C. H. 2016. Ullmann's Polymers and Plastics. *Ullmann's Polymers and Plastics - Products and Processes, 4 Volume Set*. John Wiley & Sons.
- WROBLEWSKA-KREPSZTUL, J., RYDZKOWSKI, T., MICHALSKA-POZOGA, I. & THAKUR, V. K. 2019. Biopolymers for Biomedical and Pharmaceutical Applications: Recent Advances and Overview of Alginate Electrospinning. *Nanomaterials*, 9.
- WU, H., PAN, W., LIN, D. D. & LI, H. P. 2012. Electrospinning of ceramic nanofibers: Fabrication, assembly and applications. *Journal of Advanced Ceramics*, 1, 2-23.
- WU, M. X., OUYANG, Y. S., WANG, Z. Y., ZHANG, R., HUANG, P. H., CHEN, C. Y., LI, H., LI, P., QUINN, D., DAO, M., SURESH, S., SADOVSKY, Y. & HUANG, T. J. 2017. Isolation of exosomes from whole blood by integrating acoustics and microfluidics. *Proceedings of the National Academy of Sciences of the United States of America*, 114, 10584-10589.
- WYPYCH, G. 2022. *Handbook of polymers. [electronic resource]*, ChemTec Publishing.
- XIA, S. H., TENG, S. H. & WANG, P. 2018. Synthesis of bioactive polyvinyl alcohol/silica hybrid fibers for bone regeneration. *Materials Letters*, 213, 181-184.
- XUE, J. J., WU, T., DAI, Y. Q. & XIA, Y. N. 2019. Electrospinning and Electrospun Nanofibers: Methods, Materials, and Applications. *Chemical Reviews*, 119, 5298-5415.
- YAN, E. Y., CAO, M. L., WANG, Y. W., HAO, X. Y., PEI, S. C., GAO, J. W., WANG, Y., ZHANG, Z. F. & ZHANG, D. Q. 2016. Gold nanorods contained polyvinyl alcohol/chitosan nanofiber matrix for cell imaging and drug delivery. *Materials Science & Engineering C-Materials for Biological Applications*, 58, 1090-1097.
- YAN, E. Y., JIANG, J. Y., YANG, X. Y., FAN, L. Q., WANG, Y. W., AN, Q. L., ZHANG, Z. Y., LU, B. R., WANG, D. Y. & ZHANG, D. Q. 2020. pH-sensitive core-shell electrospun nanofibers based on polyvinyl alcohol/polycaprolactone as a potential drug delivery system for the chemotherapy against cervical cancer. *Journal of Drug Delivery Science and Technology*, 55.
- YAN, Y. & KELLIE, G. 2016. 2 - Developments in fibers for technical nonwovens. *Advances in Technical Nonwovens*. Woodhead Publishing.
- YANG, C. Q., SHAO, Q., HAN, Y. L., LIU, Q. X., HE, L., SUN, Q. & RUAN, S. C. 2021. Fibers by Electrospinning and Their Emerging Applications in Bone Tissue Engineering. *Applied Sciences-Basel*, 11.
- YANG, G. Z., LI, H. P., YANG, J. H., WAN, J. & YU, D. G. 2017. Influence of Working Temperature on The Formation of Electrospun Polymer Nanofibers. *Nanoscale Research Letters*, 12.
- YANG, H. G., XU, S. B., JIANG, L. & DAN, Y. 2012. Thermal decomposition behavior of poly (vinyl alcohol) with different hydroxyl content. *Journal of Macromolecular Science Part B-Physics*, 51, 464-480.
- YANG, X., ZHU, Z., LIU, Q. & CHEN, X. 2008. Thermal and rheological properties of poly(vinyl alcohol) and water-soluble chitosan hydrogels prepared by a combination of  $\gamma$ -ray irradiation and freeze thawing. *Journal of Applied Polymer Science*, 109, 3825-3830.

- YAO, L., HAAS, T. W., GUISEPPI-ELIE, A., BOWLIN, G. L., SIMPSON, D. G. & WNEK, G. E. 2003. Electrospinning and stabilization of fully hydrolyzed poly(vinyl alcohol) fibers. *Chemistry of Materials*, 15, 1860-1864.
- YAO, M. R., SUN, F. F., NIE, J. Y., YANG, Q. L., WU, W. & ZHAO, F. Y. 2023. Electrospinning in Food Safety Detection: Diverse Nanofibers Promote Sensing Applications. *Food Reviews International*.
- YERRA, A. & DADALA, M. M. 2022. Silk fibroin electrospun nanofiber blends with antibiotics and polyvinyl alcohol for burn wound healing. *Journal of Applied Polymer Science*, 139.
- ZANDER, N. E. 2013. Hierarchically Structured Electrospun Fibers. *Polymers*, 5, 19-44.
- ZAW, A. S., KANTHARAJANNA, S. B., MAHARAJAN, K., TAN, B., SAPARAMADU, A. A. & KUMAR, N. 2017. Metastatic spine tumor surgery: does perioperative blood transfusion influence postoperative complications? *Transfusion*, 57, 2790-2798.
- ZHANG, B. L., LIU, H., DONG, J. Z., LIU, S. M. & IOP. 2019. Effect of temperature and mole fraction on viscosity and thermal conductivity of water and ethanol mixture. 3rd International Conference on Energy Engineering and Environmental Protection (EEEE), Nov 19-21 2018a Sanya, PEOPLES R CHINA.
- ZHANG, C., FENG, F. Q. & ZHANG, H. 2018b. Emulsion electrospinning: Fundamentals, food applications and prospects. *Trends in Food Science & Technology*, 80, 175-186.
- ZHANG, M. F., ZHAO, X. N., ZHANG, G. H., WEI, G. & SU, Z. Q. 2017. Electrospinning design of functional nanostructures for biosensor applications. *Journal of Materials Chemistry B*, 5, 1699-1711.
- ZHANG, X., HAN, L. B., SUN, Q. H., XIA, W. L., ZHOU, Q. F., ZHANG, Z. Z. & SONG, X. F. 2020. Controlled release of resveratrol and xanthohumol via coaxial electrospinning fibers. *Journal of Biomaterials Science-Polymer Edition*, 31, 456-471.
- ZHANG, X., SHI, X. T., GAUTROT, J. E. & PEIJS, T. 2021. Nanoengineered electrospun fibers and their biomedical applications: a review. *Nanocomposites*, 7, 1-34.
- ZHAO, W., LIU, W. L., LI, J. J., LIN, X. & WANG, Y. 2015. Preparation of animal polysaccharides nanofibers by electrospinning and their potential biomedical applications. *Journal of Biomedical Materials Research Part A*, 103, 807-818.
- ZHAO, X., MONTGOMERY, T., LU, P., ZHANG, S. J. & ASME 2012. FLOW SIMULATIONS IN PACKED BEDS BY A COUPLED DEM AND CFD APPROACH. *Proceedings of the Asme Fluids Engineering Division Summer Meeting, 2012, Vol 1, Pts a and B, Symposia*, 685-694.
- ZHAO, X. H., NIU, Y. N., MI, C. H., GONG, H. L., YANG, X. Y., CHENG, J. S. Y., ZHOU, Z. Q., LIU, J. X., PENG, X. L. & WEI, D. X. 2021. Electrospinning nanofibers of microbial polyhydroxyalkanoates for applications in medical tissue engineering. *Journal of Polymer Science*, 59, 1994-2013.
- ZHONG, H. L., HUANG, J., WU, J. & DU, J. H. 2022. Electrospinning nanofibers to 1D, 2D, and 3D scaffolds and their biomedical applications. *Nano Research*, 15, 787-804.
- ZONG, X. H., KIM, K., FANG, D. F., RAN, S. F., HSIAO, B. S. & CHU, B. 2002. Structure and process relationship of electrospun bioabsorbable nanofiber membranes. *Polymer*, 43, 4403-4412.
- ZUO, B., HU, Y. Y., LU, X. L., ZHANG, S. X., FAN, H. & WANG, X. P. 2013. Surface Properties of Poly(vinyl alcohol) Films Dominated by Spontaneous Adsorption of Ethanol and Governed by Hydrogen Bonding. *Journal of Physical Chemistry C*, 117, 3396-3406.
- ŠUTAR, T. 2015. *New formats for affinity selection of human therapeutic cells*. PhD Thesis, Loughborough University.

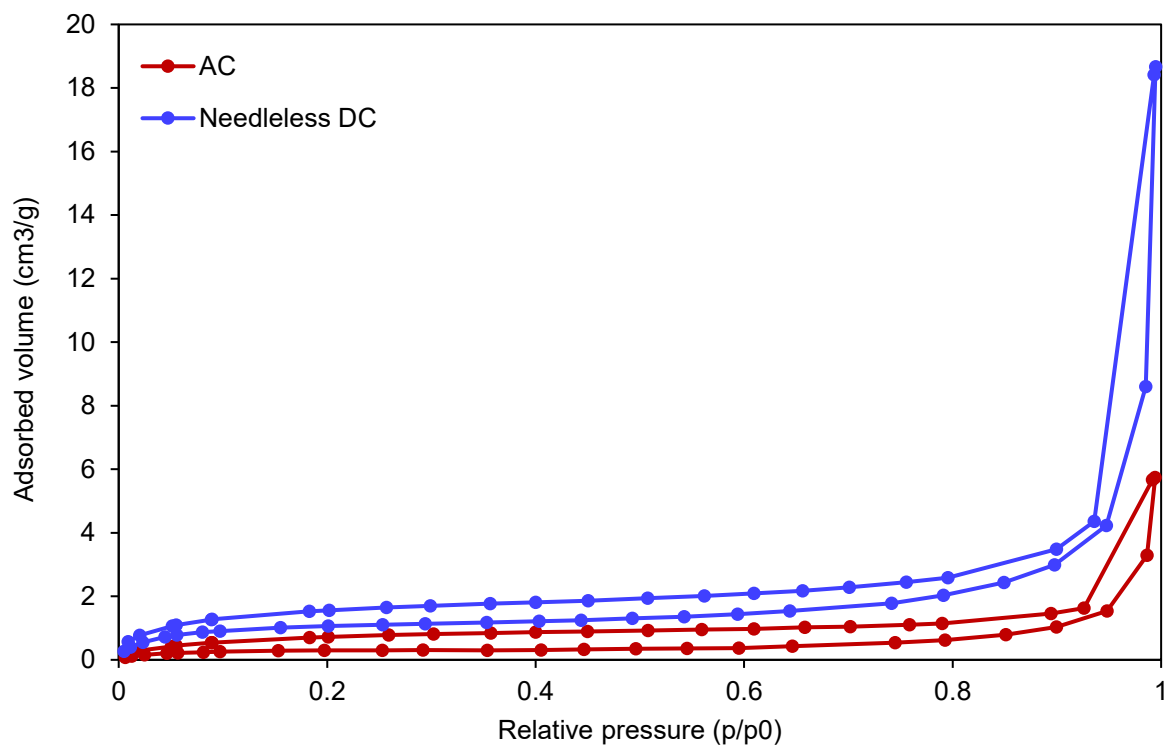


# Appendices

## Appendix A – Nitrogen porosimetry



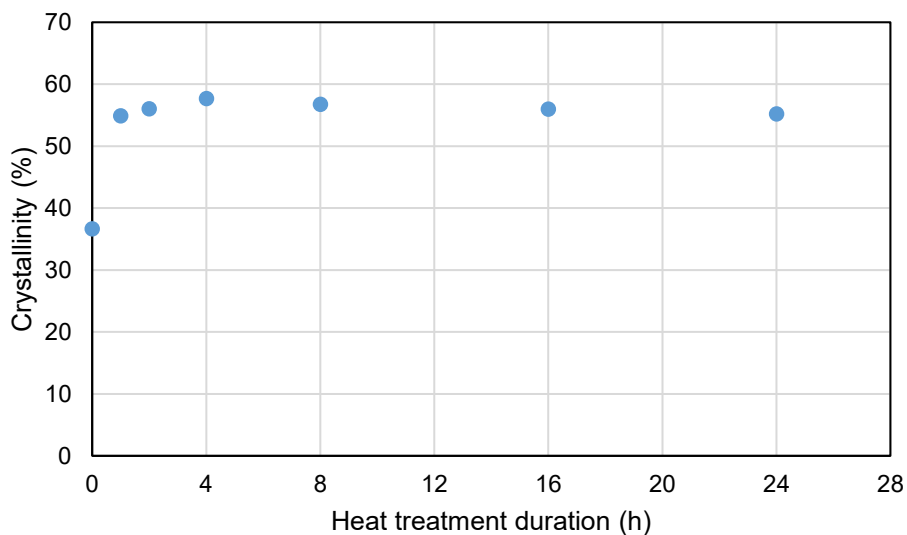
**Figure A.1.** SEM and Histogram for Needleless DC and AC spun PVA nanofibers analysed by  $N_2$  porosimetry. Average fibre diameters were calculated to be 271 nm ( $n=87$ ) and 554 nm ( $n=84$ ). Scale bar: 5  $\mu\text{m}$ .



**Figure A.2.** Porosimetry adsorption graph for 99% DH PVA produced by AC (red) and needleless DC (blue) electrospinning.

## Appendix B - FT-IR of 99% hydrolysed PVA produced by needle electrospinning

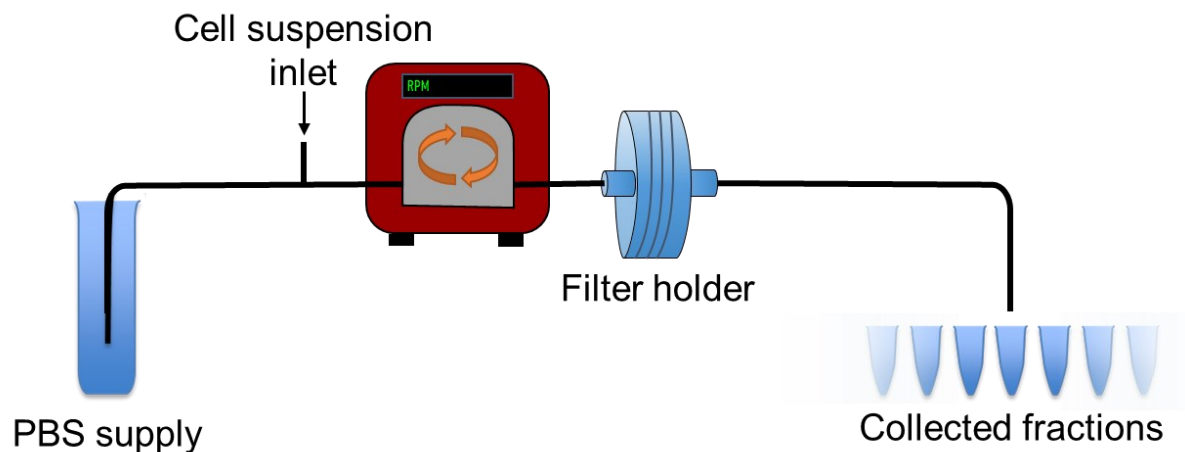
As with previous analysis, the ratios of the absorbance, at bands  $1094\text{ cm}^{-1}$  and  $1144\text{ cm}^{-1}$  (this time with the latter more clearly visible in the spectra) were used to infer crystallinity using (Tretinnikov and Zagorskaya, 2012) correlation in equation 3 (see **Figure B.3**). Like the samples produced using 88% DH PVA (**Figure 2.6**), an increase in crystallinity is implied for all samples undergoing heat treatment, from 36.7% for the untreated sample to 54.9-57.7% for the range of treated ones. Though this implies an increase in crystallinity for treated samples, it still lies outside of the typical application of the given equation due to the higher treatment temperature and should be interpreted with caution.



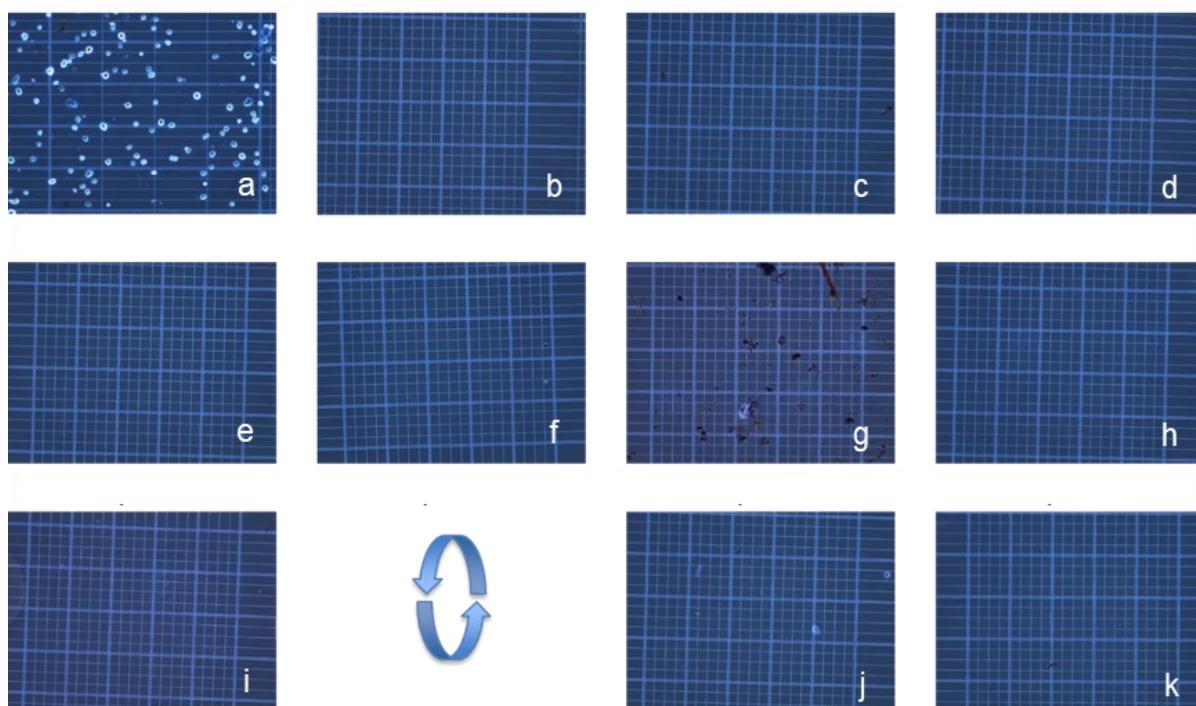
**Figure B.1.** Crystallinity (%) vs heat treatment duration graph for samples of needleless DC spun 99% DH PVA calculated using Eq. 2 and absorbance values from FT-IR data shown in **Figure 2.19**.

## Appendix C - Flowthrough of hMSCs using PVA non-woven membranes created by needleless DC electrospinning

hMSCs were expanded until confluent and subsequently prepared in a suspension of  $10^6$  cells·mL<sup>-1</sup> in PBS. 2 mL of this suspension was challenged to nanofiber membranes made from 99% DH PVA and heat treated at 180 °C, using a peristaltic pump at a flow rate of 10 mL·min<sup>-1</sup> followed by PBS to wash in both forward and reverse flow configurations (setup shown in **Figure C.1**). Collected fractions were examined using an optical microscope (**Figure C.2**), and it was found cells did not successfully pass through the membrane. It was deduced this was likely due to a combination of the large size of hMSCs in suspensions ( $26.3\ \mu\text{m}$ ,  $\pm 8.4$ ), as well as the relatively small cell challenge concentration. Subsequently, a change to a smaller cell type was proposed, namely SH-SY5Ys neural blastomas, as these cells have a smaller diameter in suspension ( $12.3\ \mu\text{m}$ ,  $\pm 1.5$ ), better reflecting some populations of CTCs (Mendelaar et al., 2021). Furthermore, confluent cell culture flasks of SH-SY5Y cells contain in the order of 10× more cells per flasks and are therefore more easily scaled for greater cell challenges.

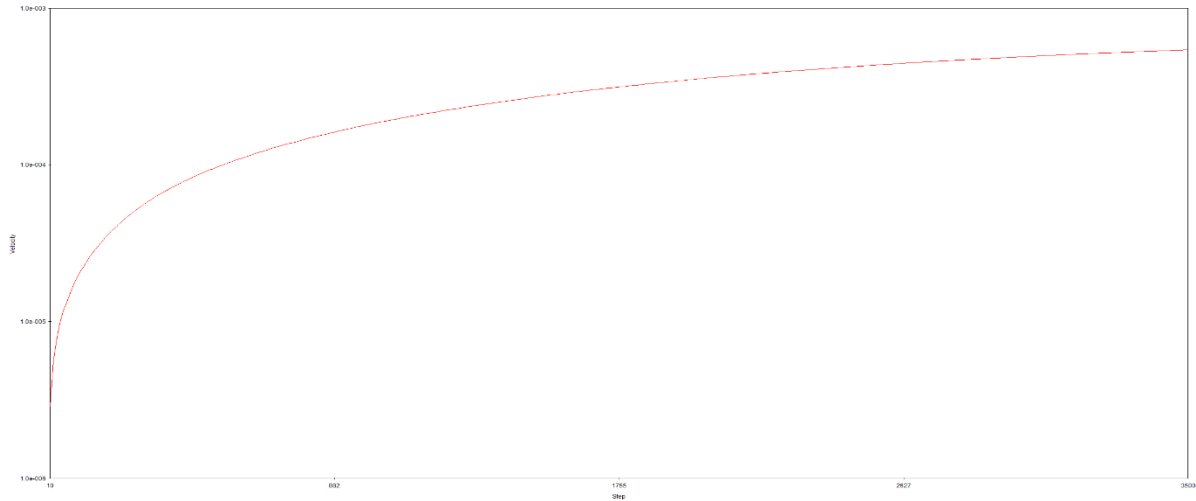


**Figure C.1.** Setup for hMSC flowthrough experiment. Suspended cells were loaded manually into the system via a side inlet, and then the pump was activated flowing the 2 mL suspension through the membrane whilst drawing PBS from the supply falcon tube. Forward flow (8 fraction) and reverse flow (2 fractions) were collected. Fraction volume = 0.75 mL

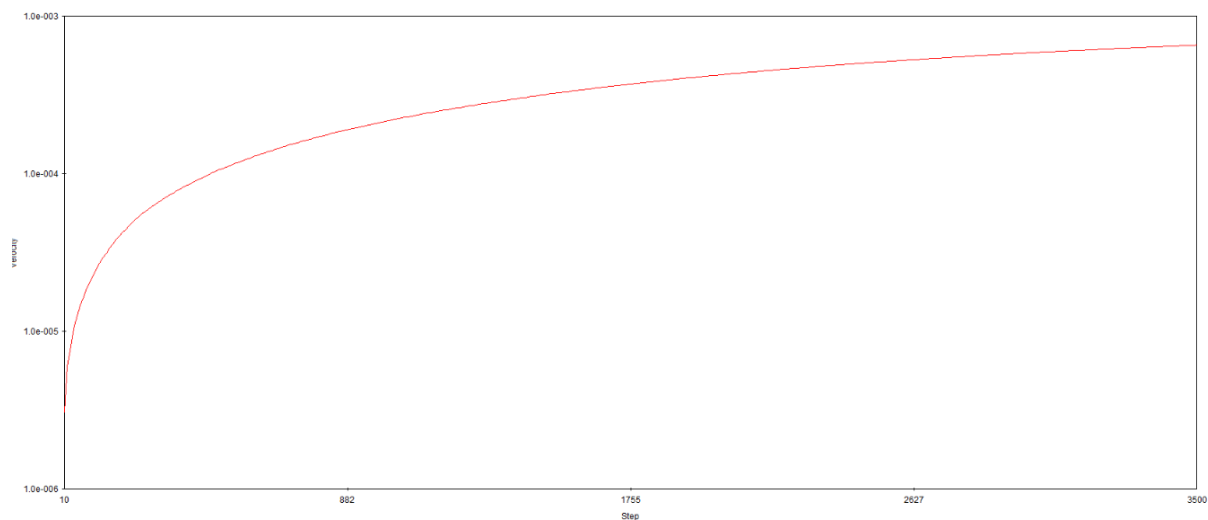


**Figure C.2.** Optical microscope images of fractions collected during the hMSC flowthrough experiments, mixed 1:1 with trypan blue. (a) Image of cells taken during cell counts, prior to flowthrough. (b-i) forward flow fractions, prior to reversal of the filter holder. (j-k) reverse flow fractions.

## Appendix D – Velocity profile during flow simulation through nanofiber packed beds



**Figure D.1.** Velocity vs step graph for simulated flow through untreated nanofiber beds produced by Nanospider™. Steps shown from 0 to 3500 showing full duration of the simulation, demonstrating plateauing of overall flow velocity as the simulation progressed.



**Figure D.1.** Velocity vs step graph for simulated flow through untreated nanofiber beds produced by AC electrospinning. Steps shown from 0 to 3500 showing full duration of the simulation, demonstrating plateauing of overall flow velocity as the simulation progressed.